THESIS

INVESTIGATION OF MINERAL BENTONITE BARRIERS OPTIMIZED FOR HYDRAULIC COMPATIBILITY AND SHEAR STRENGTH

Submitted by

Samuel Robert Jacob

Department of Civil and Environmental Engineering

In partial fulfillment of the requirements

For the Degree of Master of Science

Colorado State University

Fort Collins, Colorado

Fall 2024

Master's Committee:

Advisor: Joseph Scalia IV

Christopher Bareither

William Sanford

ABSTRACT

INVESTIGATION OF MINERAL BENTONITE BARRIERS OPTIMIZED FOR HYDRAULIC COMPATIBILITY AND SHEAR STRENGTH

Liners are a foundation tool of environmental geotechnics. Modern liners are constructed using natural and polymeric materials with low hydraulic conductivity (*k*), often at the expense of having low shear strength. These liners are often subject to high stresses on the order of hundreds to thousands of kPa which can lead to decreased performance over time and failure of the liner in shear. This research investigates mineral-bentonite mixtures in the context of high-stress liner applications. Mixtures containing varying amounts of sand, bentonite, and rock flour were created in the laboratory. Hydraulic conductivity of specimens was measured using flexible wall permeameters in accordance with ASTM D7100 using either de-ionized (DI) water, 10 mM, or 500 mM $CaCl_2$ solutions. Specimens were removed from permeameters once *k* termination criteria were met and subsequently tested in direct shear at either 35 kPa or 825 kPa effective stress to obtain peak (φ'_{peak}) and ultimate (φ'_u) friction angles. Mixtures generally achieved a final *k* of 10^{-9} m/s with bentonite contents of 4.5% and 8% when permeated with DI water and 10 mM $CaCl_2$ solutions, respectively. Adding rock flour to mixtures containing bentonite lowered final equilibrium *k* but rock flour was not suitable as a complete replacement for bentonite. At 35 kPa effective stress, shear strength increased until approximately 15% equivalent fines, whereas shear strength was relatively constant at 825 kPa with increasing equivalent fines from 0-15%. At 825 kPa, shear strength substantially dropped at equivalent fines greater than 15%, which is the approximate percentage of fines that the sand matrix began to lose grain-grain contact due to the displacement by fines. The results from this study highlight that while low *k* and high φ' can be

achieved, even at high effective stresses, care and precision during design and construction of a mineral-bentonite barrier is required to ensure that all design criteria are met.

ACKNOWLEDGEMENTS

To begin, I would like to thank my advisor Dr. Joeseph Scalia for all his support during this project and for giving me the freedom to pursue this research how I wanted. Without his guidance, I would never have been able to do this research. I would also like to thank Dr. Christopher Bareither for his input on the strength portions of this project, whose insight was invaluable in assisting me in data analysis of direct shear data. Thank you to Dr. William Sanford for serving on my graduate committee.

I owe great gratitude to previous professors and advisors from my time as an undergraduate student at Bucknell University. Particularly, special thanks are required to acknowledge the impact that Dr. Michael Malusis and Dr. Carl Kirby had on my development as a student. Each of them has had a profound influence on my understanding of geoenvironmental engineering and on my interest in research, and I could not be more thankful.

I would like to thank every single one of my colleagues, past and present, who has been a part of the Geoenvironmental Lab during my time at Colorado State University. Each one of them has played a role, whether big or small, in helping me develop not only as a student, but also as a person throughout the last three years. Thank you to Emily and Abhishek, Esther and Kendall, and Heath and Justin, for spending way too much time with me and always being there when I needed it most, whether in the office, around Fort Collins, or in the mountains.

Lastly, and most importantly, I would like to thank my mom, dad, and brother for the endless support that they have given me throughout this project. I think it is fair to say that there is absolutely no way that I would be where I am at today without them, and I will be forever thankful for all they have done for me.

TABLE OF CONTENTS

LIST OF FIGURES

1. INTRODUCTION

The lining of containment facilities is critical in preventing potential contaminants from escaping into the environment. A liner is constructed using materials with a low hydraulic conductivity (k) to leachate so that advective transport is limited. Typically, a liner is required to maintain a k less than 10^{-9} m/s. Below this k, diffusive transport dominates advective transport. Some of the most used liner types are geosynthetic clay liners (GCLs), geomembranes, and sand-bentonite mixtures. Liners are used in various containment applications, including municipal solid waste and hazardous waste landfills, industrial by-products like coal combustion residuals, radioactive waste, and certain mining and mine waste applications.

Common uses for liners in mining and mine waste include heap leach pads, tailings impoundments, waste rock dumps, and process solution ponds (Lupo & Morrison, 2007). A barrier is required in heap leach and process solution ponds to retain pregnant solution containing high concentrations of valuable metals, and in tailings impoundments and waste rock piles, a liner is sometimes needed to prevent the contamination of surface and groundwater. In both cases, these facilities are often designed to heights over 100 meters, resulting in stresses on the liner that are on the scale of hundreds or even thousands of kPa. At these high loads, these liners also need to have adequate shear strength to prevent shear failure. In addition, mine waste facilities are often built in stages spread out across the life of the mine. Mine operations dictate how mine waste facilities are constructed and can change over time, resulting in uncertainty in the final design of these facilities. Uncertainty in the final height of mine waste facilities makes predictions of long-term stresses on liners difficult.

1.1.1 GCLs

GCLs are composed of a layer of sodium bentonite (or sodium activated bentonite) that is typically placed between a top and bottom geotextile (Koerner, 2012). To ensure the geotextiles remain bonded to the bentonite, GCLs are often reinforced with needle-punched fibers, which provide resistance to internal shear. GCLs are constructed off-site and shipped to where they are needed. Ease of installation of GCLs makes GCLs an attractive option for a liner. GCLs do not have the longevity concerns regarding *k* that geomembranes can exhibit because their hydraulic properties are determined by minerals that are stable relative to anthropogenically created compounds such as plastics.

1.1.1.1 Hydraulic Conductivity and Chemical Compatibility

Montmorillonite, the primary mineral in bentonite, has a low *k* to water ($\leq 10^{-10}$ m/s). Montmorillonite has a high specific surface area (800 m^2/g) (Mitchell & Soga, 2005). When hydrated with water, montmorillonite will swell and push platelets away from each other. In addition, isomorphous substitution in montmorillonite causes high net negative surface charges. The high specific surface area and the high net negative surface of montmorillonite result in many adsorbed cations to the mineral surface layer. Hydration of these adsorbed cations and the mineral surface yields a layer of bound water (that does not participate in flow) that limits available pathways for fluid flow (Mitchell & Soga, 2005). As a result, hydrated montmorillonite has a low *k* to water and is what causes GCLs to have a low *k* when permeated with low ionic strength (*I)* solutions.

When a permeant solution has a high concentration of cations, a high cation valence, or both, a decrease in the adsorbed water layer thickness will occur (Shackelford et al., 2000). A

thinner adsorbed layer will allow larger pathways for fluid flow and increase hydraulic conductivity. Higher *k* values in GCLs when permeated with high *I* solutions is well documented in the literature. (Kolstad et al., 2004; Lee et al., 2005; Lee & Shackelford, 2005b; Petrov & Rowe, 1997; Shackelford et al., 2000, 2010). A GCL thus may be deemed "incompatible" with a particular non-standard liquid when the GCL's *k* is higher when permeated with the non-standard liquid than when permeated with tap or deionized (DI) water.

1.1.1.2 Shear Strength

To keep the geotextiles together and increase internal shear strength, most GCLs are reinforced by needle-punching fibers. In unreinforced GCLs, the shear strength is governed solely by the shear strength of the bentonite clay (Eid & Stark, 1997). Because bentonite has a residual friction angle of 5-10 degrees, unreinforced GCLs have low internal shear strength and cannot be placed on slopes (Mitchell & Soga, 2005). In reinforced GCLs, the internal shear strength is largely a result of the tensile strength of the needle-punched fiber reinforcement (Stark & Eid, 1996). Friction angles larger than 60 degrees have been measured due to the tensile strength of the fiber reinforcement (Zanzinger & Alexiew, 2000; Zanzinger & Saathoff, 2012).

The reinforcing fibers in GCLs have finite strength that can eventually fail. Needle-punching fibers behave plastically because they come from bundles of the non-woven top geotextile. Plastic materials creep when subjected to sustained loads. At high strains, creep failure in GCLs can occur due to pullout or rupture of the reinforcing fibers, leading to rapid increase in horizontal displacement (Ghazizadeh & Bareither, 2016; Zanzinger & Saathoff, 2012). Higher creep stress ratios also result in faster time to failure in GCLs (Zanzinger & Saathoff, 2012). In general, adding more fiber bundles in a GCL increases strength, as the shear load taken by each

bundle is reduced. But there is a tradeoff. Uneven cation exchange along needle-punching bundles can occur in a GCL during the initial hydration phase, decreasing swell around the bundles (Scalia & Benson, 2010b). The fibers can then act as conduits for fluid flow, resulting in an increased *k* in the GCL (Bareither et al., 2017).

1.1.2 Sand Bentonite

Sand-bentonite mixtures are one type of barrier used in hydraulic containment applications. Unlike a GCL, where the entire barrier is brought in from off site, sand-bentonite liners are conventionally constructed by mixing local sand (or tailings) with imported bentonite. Sand-bentonite has traditionally been used when there is insufficient locally natural clay on or near-site to make a compacted clay liner. Sand-bentonite mixtures have been used in various containment applications, including liners for sewage lagoons (Chapuis et al., 1992; Sharma & Kozicki, 1988) radioactive waste disposal (Komine & Ogata, 1999), and waste rock piles (Hojka et al., 2019). The mixing process for sand-bentonite barriers can either be done using a rototiller or in a pug-mill to attain homogeneity (Alston et al., 1997; Chapuis et al., 1992; Haug et al., 1988). Water can be added either during or after the mixing process. The mixture is then compacted to meet engineering requirements. Lowering the amount of void space limits the size of pathways for fluid flow.

1.1.2.1 Hydraulic Conductivity and Chemical Compatibility

The *k* of sand-bentonite mixtures is controlled by the percentage of bentonite added to the mixture. In general, as bentonite content increases, *k* decreases, up to a threshold (e.g. Abichou et al., 2002; Chapuis, 2002; Chapuis et al., 1992; Kenney et al., 1992). At low (1-2% by mass) bentonite percentages, there is not enough bentonite to block large pathways for fluid flow. Pores are progressively clogged as more bentonite is introduced (Abichou et al., 2002). At high enough

bentonite percentages, all large pathways for fluid flow are eliminated, so increases in bentonite lead to little changes in *k*. The percentage of bentonite when small changes in *k* are observed with increasing bentonite varies but generally falls between 5-15% (Abichou et al., 2002; Chalermyanont & Arrykul, 2005; Chapuis, 2002; Stern & Shackelford, 1998).

Like GCLs, sand-bentonite mixtures are susceptible to chemical incompatibility with certain permeant liquids. Gipson (1985) studied the effects that a pH = 2.2 acid liquor solution obtained from a phosphogypsum field had on silty sand-bentonite mixtures. For samples containing 7.5, 10, and 15% bentonite, *k* increased approximately 7, 13, and 41 times, respectively. Stern & Shackelford (1998) found that for a sand amended with 10% attapulgite clay and 10% bentonite, *k* increases 150 times when permeated with a 0.5 M $CaCl_2$ solution compared to tap water. In addition, when increasing the percentage of attapulgite clay in the sand-bentonite mixture, there was an improved resistance to an increase in *k* when permeating with higher *I* solutions. This is due to the relatively inert behavior of attapulgite compared to the bentonite. However, the mixture containing the highest percent of bentonite (20%) still had the lowest *k* (Stern & Shackelford, 1998). Mishra et al. (2009) measured the *k* and free swell index of basalt soil (12% clay by mass) and bentonite mixtures using NaCl and $CaCl_2$ solutions and found increases in *k* with increasing permeant concentrations. In general, *k* increased about one order of magnitude for each specimen when increasing permeant concentration from 0 to 0.1 N $CaCl_2$. Increasing permeant concentration from 0 to 1 N caused an approximately 20-30 times increase in *k*.

1.1.2.2 Shear Strength

Sand mixtures amended with bentonite tend to have lower friction angles than sand alone (Chalermyanont & Arrykul, 2005; Gueddouda et al., 2008; Tiwari & Marui, 2003). The residual

friction angle of hydrated sodium bentonite ranges from 5-10 degrees (Mitchell & Soga, 2005). As the percentage of bentonite increases in a sand-bentonite mixture the pore space between sand grains is reduced. At a certain point, the bentonite volume exceeds the sand porosity, and begins to make up the matrix of the mixture resulting in a lowering of the contact area between sand grains. Tiwari & Marui (2003) found that adding 20% bentonite to Toyoura sand lowered the residual friction angle from 29.7 degrees to 19.6 degrees, and at 40% bentonite the residual friction angle dropped to 5.6 degrees. Similarly, Chalermyanont and Arrykul (2005) found that adding a bentonite content of 7% to sand lowers the friction angle from 49 degrees to 22 degrees. However, at lower bentonite contents the bentonite may improve strength. Mollins et al. (1999) found that sand mixtures with 5-10% bentonite have higher peak friction angles than similar mixtures with 0 and 20% bentonite, suggesting that there is not a direct correlation between decreasing shear strength with increased bentonite content.

Changing the pore fluid of sand-bentonite mixtures can also alter the shear strength of bentonite. Zhang et al. (2016) measured the shear strength of sand-bentonite mixtures with 50% bentonite hydrated at varying concentrations of NaCl and found that the shear strength at an effective stress of 1600 kPa increased from about 300 kPa using distilled water to greater than 1000 kPa using 2 M NaCl. Xiang et al. (2021) found that the friction angle of sand-bentonite mixtures amended with 30% bentonite increased from 23° to 37° when samples were saturated with distilled water and 0.5 M NaCl, respectively. These increases in strength have largely been attributed to the shrinkage of the diffuse double layer in montmorillonite. A smaller diffuse double layer causes an increase in the surface roughness and flocculation of clay platelets, increasing strength. At the same time, *e* of the bentonite is decreased which allows greater interaction between sand grains. However, Zhang et al. (2016) and Xiang et al. (2021) only looked at sand-bentonite

mixtures at bentonite contents greater than 30 percent. The increased swell in lower *I* solutions could improve shear strength of mixtures at lower bentonite contents by filling voids with mineral solids rather than free water.

1.1.3 Geomembranes

Geomembranes consist of thin polymeric sheets that have very low (10^{-12} to 10^{-15} m/s) water-vapor transmission permeability (Koerner, 2012). Geomembrane liners are constructed by rolling out panels of the geomembrane and welding the seams together. Despite having virtually zero permeability to liquid and vapor when fully intact, geomembranes are susceptible to leaking due to tearing and punctures.

Geomembranes will become increasingly brittle over time due to long-term degradation (Koerner, 2012). Certain chemicals that are incompatible with the plastics used in geomembranes can also cause reactions that will weaken the geomembrane and lower the internal shear strength. This is particularly important when the chemistry of the permeant liquid might change over time due to unknown synergistic effects of multi-component liquids. High temperatures can also decrease the service time of geomembranes (Rowe, 2005). Temperatures can exceed 50 °C at the bottom of heap leach facilities which will lead to shorter service life times of geomembranes (Thiel & Smith, 2004). Geomembranes may not be an effective barrier for mine waste over the long-term because due to the inevitability that the plastics used will degrade. In addition to internal shear strength concerns, the shear resistance between the geomembrane and a GCL in a composite system, or the geomembrane and the surrounding soil, will often be weaker than the internal shear strength of the geomembrane itself (Koutsourais et al., 1991; Daniel et al., 1998; Triplett & Fox, 2001; Thielmann et al., 2013; Ghazizadeh & Bareither, 2019). Because mine waste is required to

be stored in perpetuity, mineral barriers with relatively stable *k* and shear strength over time make for better liners than geomembranes.

1.2 Research Motivation

1.2.1 Objectives

Due to the previously described shortcomings of GCLs and geomembranes, the goal of this study is to explore the possibility of designing a mineral barrier that has a low hydraulic conductivity while maintaining a high shear strength. The barrier needs to be potentially compatible with various *I* chemical solutions. The shear strength of the barrier should be derived from mineral strength rather than plastics such that high shear strengths are achieved in high stress applications such as mining heap leach and waste rock piles. The barrier should be resilient such that the shear strength does not decrease, and *k* does not increase, substantially with time.

Few studies have simultaneously evaluated both *k* and shear strength of sand-bentonite mixtures. Chalermyanont & Arrykul (2005) compared the shear strength and hydraulic conductivity of sand-bentonite mixtures up to 9% bentonite. Gueddouda et al., (2008) examined the hydraulic conductivity and shear strength of sand-bentonite mixtures up to 15% bentonite content. Both of these studies did not test elevated *I* solutions (DI water and unspecified for Chalermyanont & Arrykul (2005) and Gueddouda et al., (2008), respectively). In addition, neither study uses a flexible-wall permeameter to measure hydraulic conductivity or measured the shear strength of permeated (viz. cation exchanged) specimens.

The present study provides an in-depth analysis of the relationship between hydraulic conductivity and shear strength of mineral-bentonite mixtures. A unique data set is produced by measuring the shear strength of specimens that have previously undergone permeability testing.

The addition of rock flour as an intermediate grain-sized soil between sand and bentonite also differentiates the present study compared to other studies that only use sand-bentonite. Rock flour acts as a silt-sized pore filler in the mineral-bentonite system that is inert compared to bentonite alone. By decreasing the percentage of bentonite with an increase in rock flour, my hypothesis is that the mineral-bentonite barrier will be less susceptible to chemical desiccation, resulting in a barrier with improved chemical compatibility.

1.2.2 Natural Analogs For Barriers

To build a mineral barrier with low hydraulic conductivity and high shear strength that will not suffer performance loss over time, natural analogs can be used to identify characteristics that are indicative of such a barrier. One of the most widespread soils that meet the above requirements is glacial till. While tills can range from matrix to clast dominated, tills are often poorly sorted with particle sizes ranging from boulder to silt and clay size particles. The wide range of particle sizes allows pores of varying size to be occupied. Tills also are often heavily overconsolidated due to the induced stresses from advancing/retreating ice sheets. The compression that tills undergo can result in void ratios (e) as low as 0.20 in some cases (Easterbrook, 1964). Low e limit the available flowpaths in tills, lowering k. Hydraulic conductivities in tills are often lower than 10^{-9} m/s and can be as low as 10^{-12} m/s as long as the soil is not fractured (Clark, 2018). Because tills have a low k from small void ratios, tills lack the chemical compatibility issues that mineral-bentonite barriers exhibit with high ionic strength solutions. Rather than relying on a high-swelling mineral (namely montmorillonite) like bentonite, which is susceptible to chemical desiccation, the minerals in tills are generally more inert and thus k does not drastically increase with an increase

in *I*. The angle of internal friction in tills can also be high, greater than 35 degrees (Cao et al., 2015; Clark, 2018).

1.3 Conceptual Model

A conceptual model for the intended barrier system is shown in Figure 1. In Figure 1a, only a sand grain matrix is present**.** Relatively large diameter flowpaths exist due to large pores and provide little resistance to flow. Shear strength is determined by the properties of the sand matrix. Silt-sized particles are added to Figure 1b, filling void space. The addition of silt-sized grains make flowpaths smaller and more tortuous, lowering *k*. Shear strength will be greater than a sand matrix alone due to the increase in contacts between all grains and a decrease in void space. In Figure 1c, bentonite clay is added to further fill pore space. This addition of bentonite further lowers *k*. There is still full contact between sand grains at this percentage of bentonite and the shear strength is still governed by sand-sand, sand-silt, and silt-silt interactions. In this case, the bentonite provides a slight increase in shear strength because the bentonite particles provide more shearing resistance than void space alone while not displacing contacts between the coarser particles. Figure 1c is most representative of a clast-supported glacial till where coarse particles still maintain contact with one another. The difference between Figure 1c and a glacial till is the bentonite providing the elimination of large pores in Figure 1c, whereas large pores are reduced in a till by compression under large normal stresses. If too much bentonite is added, grain-to-grain contact of the sand matrix is lost (Figure 1d). Shear strength will then be governed by a combination of sand-silt-clay interactions rather than just sand-to-sand contact, resulting in a lower shear strength. As more bentonite is added, shear strength is decreased until the shear strength is equivalent to that of hydrated bentonite, and disparate sand grains float isolated in hydrated clay.

Figure 2 shows the effect of a high *I* solution on the swell of bentonite and the resulting *k* in a mineral-bentonite barrier. In Figure 2a, the permeant is a low *I* solution, such as DI water. Bentonite maintains full swell which limits the size of macropores. Intra-aggregate flow dominates in this system which results in a low *k*. In Figure 2b, the swell of bentonite has been reduced due to a high *I* permeant solution. Bentonite becomes more flocculated in the high *I* solution, increasing the size and number of macropores. While an increase in contacts between coarser grains will occur in this scenario, *k* is also greatly increased because of the larger pathways for fluid flow.

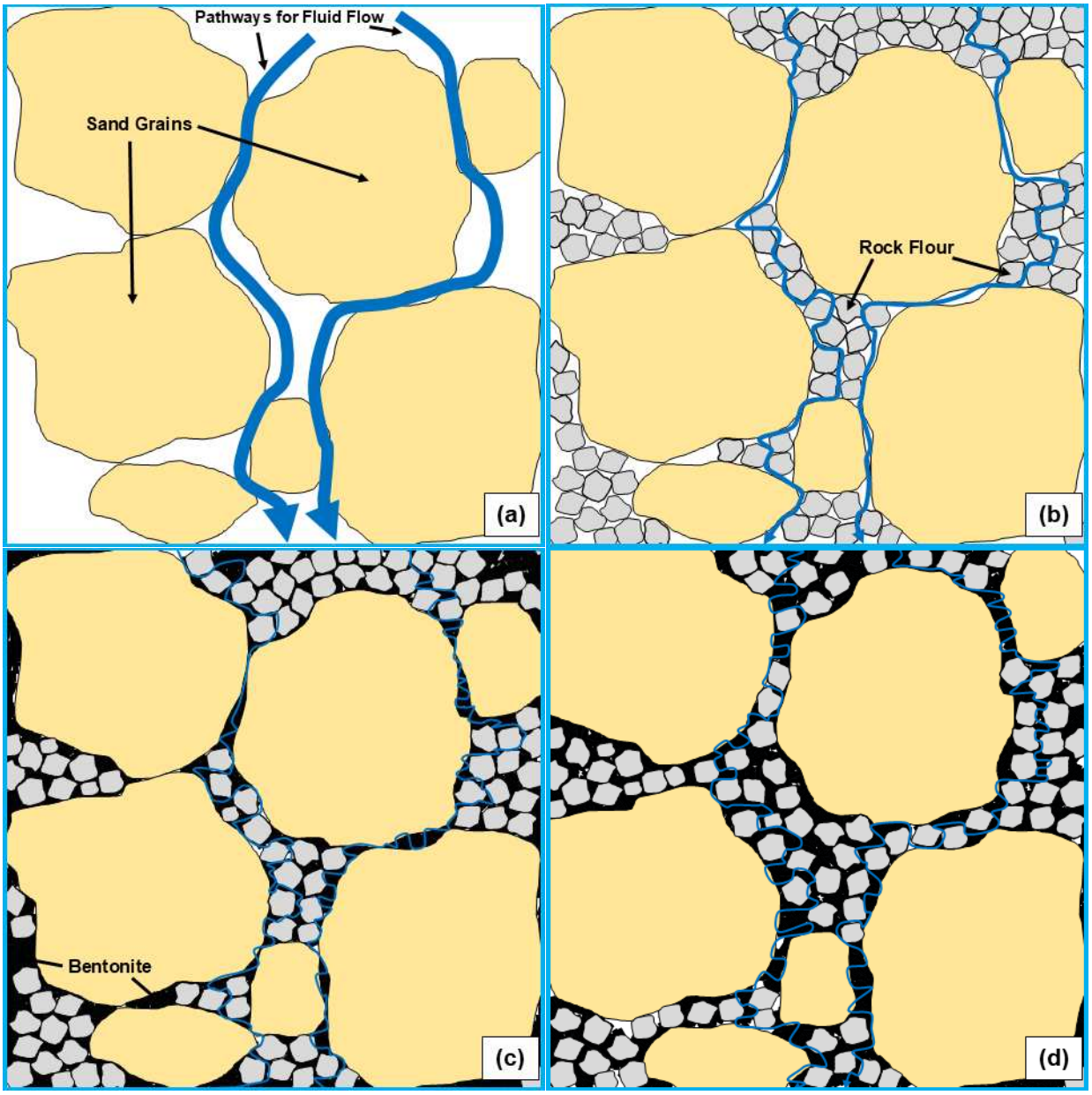

Figure 1. Conceptual model of the intended barrier system. The color of each grain indicates its type, with tan being sand, gray being silt/ rock flour, and black being bentonite clay. Blue arrows show a generalized model for fluid flow with the thickness of the arrow indicating how much flow can move through each flowpath. (a) Barrier when only a sand-grain matrix is present with large pathways for fluid flow; (b) Silt-sized particles are added to sand-grain matrix to reduce average pore size; (c) Bentonite is added to further reduce pore size while still maintaining contact between coarse-grained sand- and silt-sized particles; (d) Bentonite is added in excess of available pore space in coarse-grained matrix, reducing contact between coarse-grained particles by displacing sand- and silt-sized clasts.

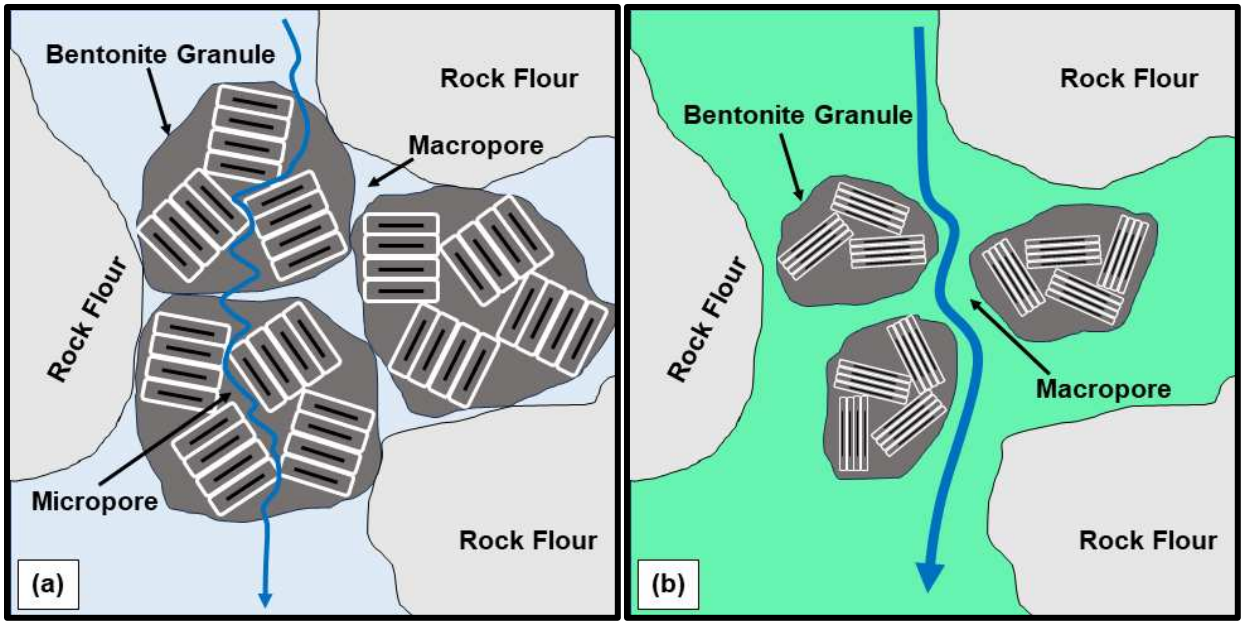

Figure 2. Conceptual model showing the effects of (a) a low *I* permeant solution and (b) a high *I* permeant solution on *k* of a mineral-bentonite barrier. Blue arrows show a generalized model for fluid flow with the thickness of the arrow indicating how much flow can move through each flowpath. The size of the bentonite tactoids are depicted as much larger than actual scale for legibility.

2. MATERIALS AND METHODS

2.1 Sand

The grain size curve for the sand used in this study is shown in Figure 3. The test sand was created by combining 50% by mass of a well-graded sand and a poorly-graded sand. The combined mixture classifies as SP based on the USCS classification system (*ASTM D2487-17*) and is quartz-dominated.

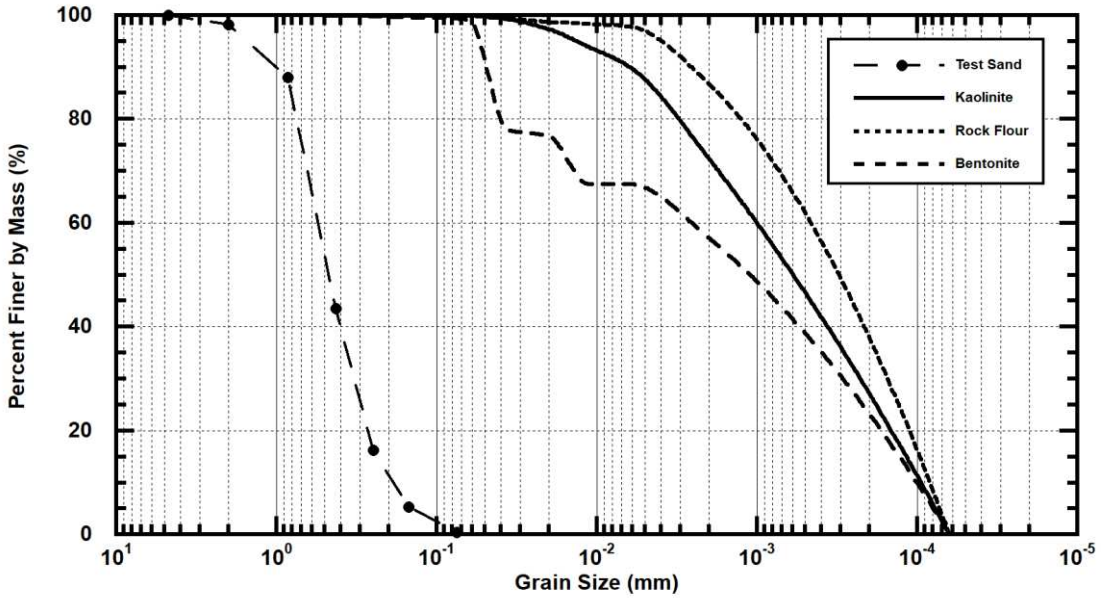

Figure 3. Grain size curve for mineral solids used in sand-bentonite mixtures. The sand grain size curve for sand was obtained using a mechanical sieve, and the kaolinite, rock flour, and bentonite grain size curves were obtained using a laser hydrometer.

The minimum void ratio (max dry density) and maximum (min dry density) void ratios (e_{min} and e_{max}) of the sand were calculated according to ASTM D4253-16 and D4254-16. Dry density (γ_d) is defined as the mass of solids divided by the total volume of specimen. From these tests, e_{min} and e_{max} are 0.49 and 0.76, respectively.

2.2 Bentonite

Bentonite used in this study is GCL-grade, powdered sodium bentonite (CETCO, Hoffman Estates, IL). The bentonite is the same as which is used in Sample-Lord (2015), however the bentonite in that study was in a granular rather than powdered form (SP gradation). The specific gravity is 2.71 and the bentonite contains greater than 90% montmorillonite. The plastic limit and liquid limit are 46 and 502, respectively (ASTM D4318-17), and the cation exchange capacity is 78.3 cmol/kg. The grain size distribution for bentonite was measured using a PARIO laser hydrometer (Meter Group, Pullman, Washington, USA) which is shown in Figure 3.

2.3 Rock Flour and Kaolinite

Rock flour in the form of silica powder was used in this study (U.S Silica, Maryland, USA). Kaolin primarily consisting of kaolinite was also used (Thiele Kaolin Company, Georgia, USA). Grain size distributions were measured using a PARIO laser hydrometer (Meter Group, Pullman, Washington, USA) (Figure 3).

2.4 Swell Tests

Swell tests were conducted on bentonite, rock flour, and kaolinite. Dry specimens of approximately one millimeter in thickness were placed in an oedometer. Specimens were confined with filter paper and porous stones to allow drainage. A stress of 20 kPa was applied using the oedometer. This stress condition is expected to be exceeded in the field for materials being used as a liner but may represent conditions during initial operations. In this way, the 20 kPa stress provides a "worst-case scenario" for sand-grain displacement by fine-grained materials that occurs when constructing a barrier. Specimens were then hydrated using either deionized (DI) water or a 10 mM $CaCl_2$ solution. Once changes in height ceased, specimens were removed from the

oedometer, and water content was measured. The volume taken up per gram of solid was calculated using weight-volume relationships. Results from the swell tests are shown in Figure 4. In DI water, kaolinite and rock flour had very small changes in volume, swelling very little to a value of 1.1 cm^3/g, whereas bentonite swelled to 2.4 cm^3/g. At 10 mM $CaCl_2$, kaolinite had slight decrease in volume, whereas rock flour observed a small increase in volume. Bentonite had less of an increase in swell at 10 mM $CaCl_2$ compared to DI water with a final hydrated value of 2.1 cm^3/g.

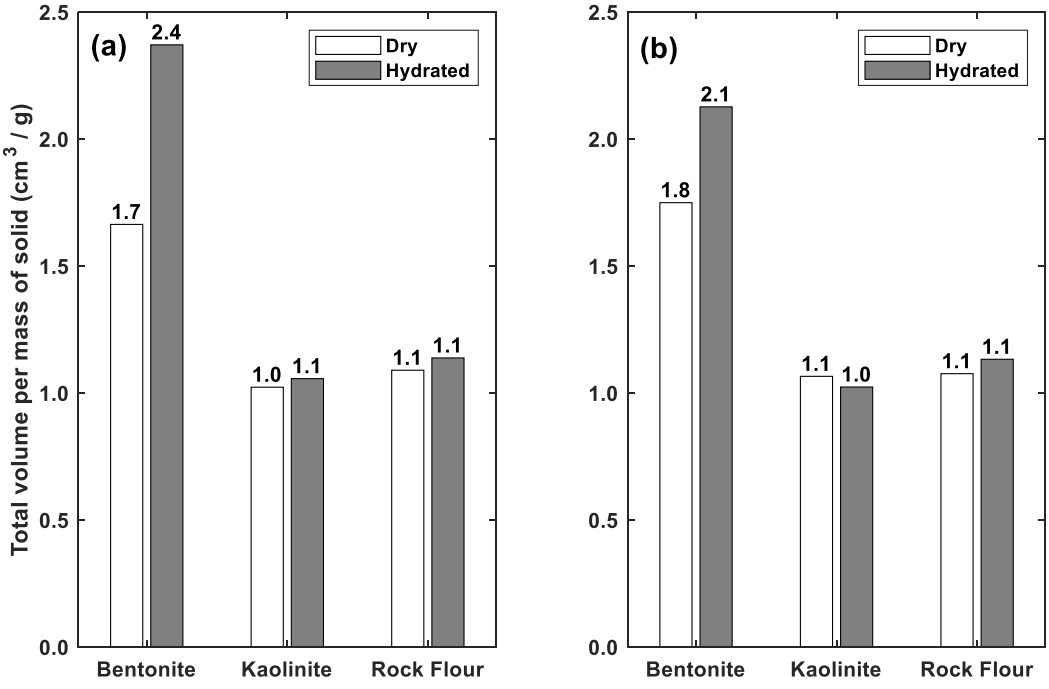

Figure 4. Swell test results for kaolinite, rock flour, and powdered sodium bentonite in (a) DI water and (b) 10 mM $CaCl_2$ solution.

2.5 Mixture Process

Sand-bentonite mixtures were prepared by combining sand with differing amounts of rock flour, kaolinite, and bentonite. Air dry solids were first combined using either a spoon or a kitchen mixer. DI water was then added and mixed with the solids until homogenized (approximately 10 minutes). Previous studies have shown that final *k* is independent of if water is added to the mixture

before bentonite as long as sufficient mixing is achieved (Kenney et al., 1992). The mixture was then compacted in a 15.24 cm diameter Proctor mold using a modified Proctor hammer. Each specimen was compacted in 5 separate lifts using 25 blows per lift, resulting in an energy of about 25,000 lbf-ft/ft^3. This energy is approximately half of modified Proctor energy and double standard Proctor energy. An extruder was used to separate the compacted specimens from the mold. Specimens were then cut in half horizontally with a wire saw to permeate with either DI water, 10 mM $CaCl_2$, or 500 $CaCl_2$ solution. Each specimen was approximately 6 cm in height and 15.24 cm in diameter. In instances when a DI water and a 10 mM $CaCl_2$ specimen were obtained from the same mixture, the DI water sample was always taken from the bottom and the 10 mM $CaCl_2$ specimen from the top of the Proctor mold specimen.

Due to the low *k* of bentonite to DI water, six specimens were made using a different process than above (see Table 1 for specimen info). These specimens each had above 10% bentonite by dry mass and would have required an extended duration to reach hydraulic equilibrium. To allow hydration before shear strength testing, specimens were compacted in 10.16 cm diameter Proctor molds and subsequently placed in a permeameter. To achieve the same amount of compaction energy as the 15.24 cm specimens, 10.16 cm specimens were compacted in 5 lifts with 11 blows per lift using a modified Proctor hammer. The permeameters were then connected to pressure panels with a confining pressure of 41.2 kPa, headwater pressure of 10.3 kPa, and tailwater pressure of 3.4 kPa. These pressures allow for an average effective stress of approximately 34 kPa on the specimens. Headwater and tailwater valves remained open to allow hydration using DI water. Specimens were allowed to hydrate for at least 30 days.

Each mixture had a target percentage of pores filled by either rock flour, kaolinite, or bentonite. The amounts of sand, rock flour, kaolinite, and bentonite added were determined by

using the calculated sand e_{min} of 0.49. The available pore space in the modified proctor mold is known assuming the sand attained this *e* after compacting. Using standard Proctor energy, *e* at maximum dry density is approximately 0.51, indicating that this assumption is reasonable for sand-rock flour-bentonite mixtures compacted using a higher energy. A specified percentage of the pores could then be filled by either rock flour, kaolinite, or bentonite. For example, at an *e* of 0.49, the sand would occupy 1424 cm^3 in the modified proctor mold (volume of mold equal to 2124 cm^3) leaving 701 cm^3 available pore space. To achieve 100% of the pores filled with bentonite, 296 grams need to be added (296 g × 2.37 cm^3/g = 701 cm^3).

The amount of water added to each mixture was determined by calculating the remaining available pore space in the sand matrix after the volume of bentonite, kaolinite, and rock flour was known. In the 100% pores occupied by bentonite example, the volume of 296 g of bentonite is 109 cm^3 based on a specific gravity of 2.71. The remaining pore space is equal to 701 cm^3 – 109 cm^3 = 592 cm^3 of water. Thus, 592 g of water is added.

The swell with DI water was used to calculate the pore space occupied in each mixture by sand additives, as each specimen was initially mixed with DI water. However, because some specimens were permeated with 10 mM $CaCl_2$ solution, this led to the pore space in some bentonite-containing specimens not being fully filled due to chemical dehydration.

2.6 Liquids

All specimens were initially mixed using DI water. DI water and target calcium chloride solutions of 10 and 500 mM $CaCl_2$ were used to permeate specimens during hydraulic conductivity testing. Calcium chloride solutions were prepared by mixing $CaCl_2$*$2H_2O$ salt (Alfa Aesasr, Ward Hill, MA) with DI water in 2L batches. Electrical conductivities (EC) of the liquids were measured

using an Orion Conductivity Cell (Orion 013005MD, Waltham, MA). The electrical conductivity of the DI water, the 10 mM, and 500 mM $CaCL_2$ solution are 9.96×10^{-4}, 2.206, and 86.43 mS/cm, respectively. The *I* of 10 mM $CaCl_2$ (0.03 M) and 500 mM $CaCl_2$ (1.5 M) span the range of *I* of typical mining process solutions (Ghazizadeh et al., 2018).

2.7 Hydraulic Conductivity Testing

Specimens were placed in a 15.24 cm diameter flexible wall permeameter following extraction from the modified proctor mold. A cell pressure of 35 kPa was applied using a panel board (M100000 Standard Panel and M116000 Standard Add-Panel, Trautwein, Houston, TX). Specimens were hydrated for 48 hours before permeation, and tests were conducted in accordance with ASTM D7100 using a falling headwater, constant tailwater setup, with the caveat that no backpressure was applied (e.g., Kolstad et al., 2004; Lee & Shackelford, 2005; Meer & Benson, 2007; Scalia et al., 2014). Either DI water, 10 mM $CaCl_2$ solution, or 500 mM $CaCl_2$ solution was used as the permeant liquid.

For tests that exhibited a sufficiently high *k* such that the inflow burette would run out of permeant within 24 hours ($k \approx 1\times10^{-9}$ m/s), specimens were allowed to permeate a maximum of once per day (PVF ≈ 0.1 for 60 mm specimens) to allow adequate time for cation exchange to occur. Although cation exchange is generally accepted as a rapid process, the replacement of monovalent cations for divalent cations is also diffusion limited (Jo et al., 2006; Essington, 2021). Cation exchange can only happen once a cation is present at the exchange site. In montmorillonite, the majority of exchange sites are located in the hydrated interlayer of the mineral (Mitchell & Soga, 2005). Diffusion of cations into the interlayer can be a slow process depending on the concentration of the permeant solution due to the low diffusion coefficient of montmorillonite.

High k tests using GCLs and sand-bentonite mixtures can appear to be at chemical equilibrium if run continuously because the permeant has not had enough time to diffuse into the exchange sites of the bentonite. In this case, the influent concentration of the permeant will be largely the same as the effluent. Adequate time is needed to ensure cation exchange has been completed between the bentonite and the permeant liquid.

An average hydraulic gradient of less than 30 was maintained for all tests per ASTM D7100-11. ASTM D7100-11 recommends a hydraulic gradient of ≤ 20 for soils exhibiting a $k > 10^{-9}$ m/s because large gradients might inadvertently affect k during testing. Although many specimens had a $k > 10^{-9}$ m/s, the primary purpose of this study was to find the approximate range of mixtures that could potentially achieve a hydraulic conductivity of 10^{-9} m/s or less. In this case, the changes in effective stress across a specimen due to the hydraulic gradient are not expected to change the hydraulic conductivity by multiple orders of magnitude, so all tests were run at the same hydraulic gradient. Thus, k values may not be accurate for specimens with $k > 10^{-9}$ m/s.

Tests were performed on specimens until the termination criteria specified in ASTM D7100-11 were met. That is, for at least four measurements, (1) the ratio of inflow to outflow must be between 0.75 and 1.25 and (2) k is steady and there is no obvious upward or downward trend in k. In addition, tests using either 10 or 500 mM $CaCl_2$ solution were permeated until (1) a minimum of two pore volumes passed through the specimen and (2) the inflow to outflow ratio of electrical conductivity, EC_{in}/EC_{out}, was 1.00 ± 0.10.

2.8 Direct Shear Testing

After k termination criteria were met, 15.24 cm diameter specimens were removed from permeameters and prepared for direct shear testing. A 6.35 cm cutting ring was used to vertically

cut sub-samples that would fit in a circular direct shear box and trimmed to a height of approximately 23 mm. Samples were then inundated using the same permeant liquid used during *k* testing to prevent desiccation while undergoing shear.

ASTM D3080-98 requires specimens to be sheared at such a rate that no excess pore pressures exist at failure. The standard recommends that:

$$t_f = 50t_{50}$$

where t_f is the time to failure in the specimen and t_{50} is the time required to reach 50% consolidation under the applied load. Primary consolidation under the applied load was recorded using a digital acquisition system. The t_{50} for each specimen was then determined using the logarithm-of-time method.

Shearing rate is determined as (ASTM D3080-98):

$$d_r = \frac{d_f}{t_f}$$

where d_f is the estimated horizontal displacement at failure and d_r is the displacement rate. A d_f = 12mm for normally or lightly consolidated specimens was used. The minimum displacement rate was then calculated for each test.

Each specimen exhibited a t_{50} value of a few seconds. Using the equations above, d_r would be approximately 5-10 mm/min with a t_{50} value in this range. Instead, and conservatively, a shearing rate of d_r = 0.25 mm/min was used for all specimens. A shearing rate of d_r = 0.25 mm/min is expected to provide a factor of safety of approximately = 10 in preventing excess pore water pressures from developing during shear.

The load sensors used to measure shear force during testing have a 2.22 kN capacity. The maximum shear stress able to be measured from each sensor is calculated as follows using the Mohr-Coulomb failure criterion:

$$\tau_f = \sigma \tan(\phi')$$

Cohesion is assumed to be zero because specimens were normally consolidated and fully saturated. The shear stress on the failure plane at failure, τ_f, is calculated as follows:

$$\tau_f = \frac{F_f}{A}$$

where F_f is the shear force at failure on the failure plane and A is the area of the specimen at failure. In this study, a constant A = 31.68 cm^2 was used. Although the shear area will decrease with increasing deformation, assuming the area remains constant is a conservative assumption. From this, the maximum shear stress for the test apparatus can be calculated:

$$\tau_f = \frac{2.22\ kN}{31.68\ cm^2} = 703\ kPa$$

Assuming a theoretical maximum effective stress friction angle φ´ of 38 degrees based on sands with similar grain size and particle roundness to the sand used in this study (Bareither et al., 2008), the maximum normal stress that can be applied is:

$$703\ kPa = \sigma_{max} \tan(38°)$$

$$903\ kPa = \sigma_{max}$$

From the information above, direct shear tests were run at 35 kPa and 825 kPa to examine the widest range possible of shear behavior. The 35 kPa stress is equivalent to the cell pressure that was applied during hydraulic conductivity testing. Considering a safety factor of 1.1, 825 kPa

was used to obtain specimen shear strength at the highest possible stress with the available equipment. High-stress shear strength is important in this study due to the intended high-stress environment application of these barriers.

Data points were collected every 5 seconds during shearing. A 20-point moving average was used to normalize scatter. For specimens that dilated during shear, some tests exhibited contraction after reaching a critical state. Ultimate strengths were chosen before this occurred.

2.9 Naming Convention

Each test was given an identification based on the mixture constituents and the permeant liquid. The first set of letters and numbers indicate the percent bentonite (B), rock flour (R), and kaolinite (K) by dry mass percentage. The actual percentages were rounded to the nearest whole number for simplicity (see Table 1 for true values). The next number specifies the $CaCl_2$ concentration in mM, with 0 being DI water. The final letter indicates whether the specimen was hand-mixed using a spoon (H) or automatically mixed with a kitchen mixer (A). If multiple tests were run using the same mixture at the same concentration, a "dup" is added to the naming convention identifying that the test is a duplicate. An example showing the naming convention for a specific test is shown in Figure 5.

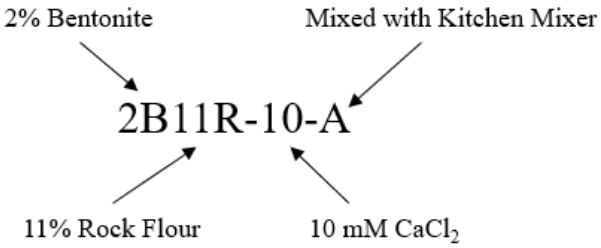

Figure 5. Example test identification labeling convention.

Table 1. Specimen properties during mixing.

Test ID	Permeant Liquid	% Bentonite by Dry Mass	% Kaolinite by Dry Mass	% Rock Flour by Dry Mass	% Fines by dry Mass	Target % Sand Pores Filled*	Water Content (g/g)	γ_d (g/cm3)	Mixing Method
7B-0-H	DI Water	7.26	0	0	7.26	100	0.146	1.85	Spoon
7B-10-H	10 mM CaCl2	7.26	0	0	7.26	100	0.146	1.65	Spoon
15K-0-H	DI Water	0	14.90	0	14.90	100	0.101	2.01	Spoon
15K-10-H	10 mM CaCl2	0	14.90	0	14.90	100	0.101	1.89	Spoon
14R-0-H	DI Water	0	0	14.00	14.00	100	0.107	1.86	Spoon
14R-10-H	10 mM CaCl2	0	0	14.00	14.00	100	0.107	1.97	Spoon
4B-0-H	DI Water	3.77	0	0	3.77	50	0.165	1.71	Spoon
4B-10-H	10 mM CaCl2	3.77	0	0	3.77	50	0.165	1.64	Spoon
4B7R-0-H	DI Water	3.50	0	7.27	10.77	100	0.126	1.90	Spoon
4B7R-10-H	10 mM CaCl2	3.50	0	7.27	10.77	100	0.126	1.78	Spoon
2B11R-0-H	DI Water	1.72	0	10.70	12.42	100	0.116	1.92	Spoon
2B11R-10-H	10 mM CaCl2	1.72	0	10.70	12.42	100	0.116	1.83	Spoon
5B4R-0-H	DI Water	5.34	0	3.70	9.04	100	0.136	2.01	Spoon
5B4R-10-H	10 mM CaCl2	5.34	0	3.70	9.04	100	0.136	1.78	Spoon
2B11R-0-A	DI Water	1.72	0	10.70	12.42	100	0.116	1.86	Mixer
2B11R-10-A	10 mM CaCl2	1.72	0	10.70	12.42	100	0.116	1.97	Mixer
4B7R-0-A	DI Water	3.50	0	7.27	10.77	100	0.126	1.84	Mixer
4B7R-10-A	10 mM CaCl2	3.50	0	7.27	10.77	100	0.126	1.82	Mixer
5B4R-0-A	DI Water	5.34	0	3.70	9.04	100	0.136	1.80	Mixer
5B4R-10-A	10 mM CaCl2	5.34	0	3.70	9.04	100	0.136	1.70	Mixer
8B-10-A	10 mM CaCl2	8.02	0	0	8.02	111	0.142	1.72	Mixer
10B-500-A	500 mM CaCl2	10.00	0	0	10.00	142	0.131	1.74	Mixer
15B-500-A	500 mM CaCl2	15.00	0	0	15.00	225	0.131	1.82	Mixer
15B-0-A	DI Water	15.00	0	0	15.00	225	0.131	1.81	Mixer
15B-0-dup-A	DI Water	15.00	0	0	15.00	225	0.131	1.85	Mixer
20B-0-A	DI Water	20.00	0	0	20.00	319	0.147	1.75	Mixer
20B-0-dup-A	DI Water	20.00	0	0	20.00	319	0.147	1.79	Mixer
30B-0-A	DI Water	30.00	0	0	30.00	548	0.138	1.81	Mixer
30B-0-dup-A	DI Water	30.00	0	0	30.00	548	0.138	1.80	Mixer

*The target percentage of sand pores filled is based on the swell characteristics measured using DI water. At 7.26% bentonite, the sand pores are assumed to be 100% filled.

3. RESULTS AND DISCUSSION

3.1 Hydraulic Conductivity

Exemplar plots of *k* versus pore volumes of flow for three specimens are shown in Figure 6, with all plots being shown in Appendix C. In general, tests exhibited a decrease in *k* with increasing pore volumes of flow. This effect is more apparent in specimens containing higher bentonite contents and has been observed in other studies (e.g. Stern & Shackelford, 1998). The swell of bentonite will increase as more water permeates through the specimen which in turn lowers *k*. Some tests experienced a gradual increase in *k* over time after the initial decrease (e.g. specimen 4B7R-10-H, Figure 6). Increased *k* over time has been observed by others and results from slow divalent-for-monovalent cation exchange (Lee & Shackelford, 2005b).

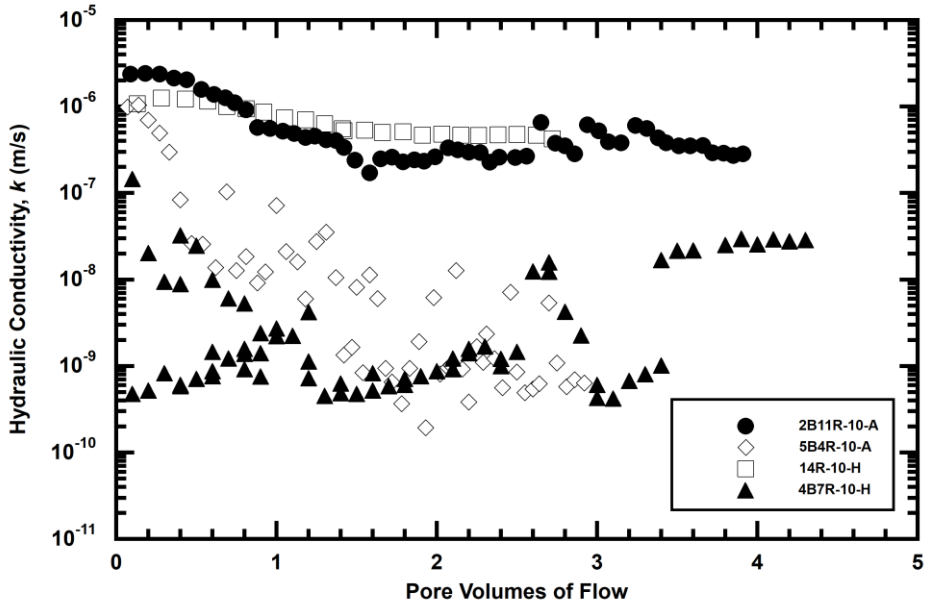

Figure 6. Hydraulic conductivity versus pore volumes of flow for four specimens.

Some tests experienced large changes in *k* between single measurements, as shown in specimen 5B4R-10-A in Figure 6. This trend happened most often for specimens with *k* of

approximately 10^{-9} m/s. The most likely cause for these fluctuations is effective stress changes in the specimen. As mentioned in the Materials and Methods section, specimens with high *k* were only permeated a maximum of once per day to allow for cation exchange to occur before meeting termination criteria. During permeation, the effective stress at the effluent side of the specimen would be greater than the influent due to differences in hydraulic head. After permeating, the tailwater would be closed to prevent permeation while the headwater remained open. The effective stress would slowly equilibrate in the specimen during this time. The constant changes in effective stress in specimens with low hydraulic conductivities might have resulted in measurable changes in *k* between measurements. This behavior is also reported in Scalia (2012). For specimens with high *k*, the effective stress between the top and bottom of the specimen equilibrated quickly enough such that the stress difference did not affect *k*.

The equilibrium *k* values for each test are shown in Figure 7. Tests 15K-0-H and 14R-0-H show similar *k* at 1.1×10^{-7} m/s and 1.7×10^{-7} m/s, respectively. Similarly, Tests 15K-10-H and 14R-10-H have *k* of 6.1×10^{-7} m/s and 4.6×10^{-7} m/s, respectively. The similarities between the *k* achieved using either rock flour or kaolinite are to be expected due to the similar grain sizes of each material. No additional mixtures using kaolinite were included in the study due to the similar hydraulic properties between rock flour and kaolinite to lessen the number of experimental combinations.

Some tests with zero bentonite using 10 mM $CaCl_2$ have higher *k* than the same mixture using DI water (i.e. 15K-10-H compared to 15K-0-H and 14R-10-H compared to 14R-0-H). The *k* ratios of 10 mM $CaCl_2$ to DI water are 5.5 and 2.7 for kaolinite and rock flour, respectively, where the *k* ratio of 10 mM $CaCl_2$ to DI water is the final equilibrium *k* of a mixture permeated using 10 mM $CaCl_2$ divided by the same mixture permeated with DI water. Although the swell is slightly greater in DI water than $CaCl_2$ solution for both kaolinite and rock flour, this could be

attributed to the $CaCl_2$ specimens being taken from the top of the Proctor mold. In almost all cases, DI water specimens have greater initial γ_d than 10 mM $CaCl_2$ specimens created from the same mixture (Table 1).

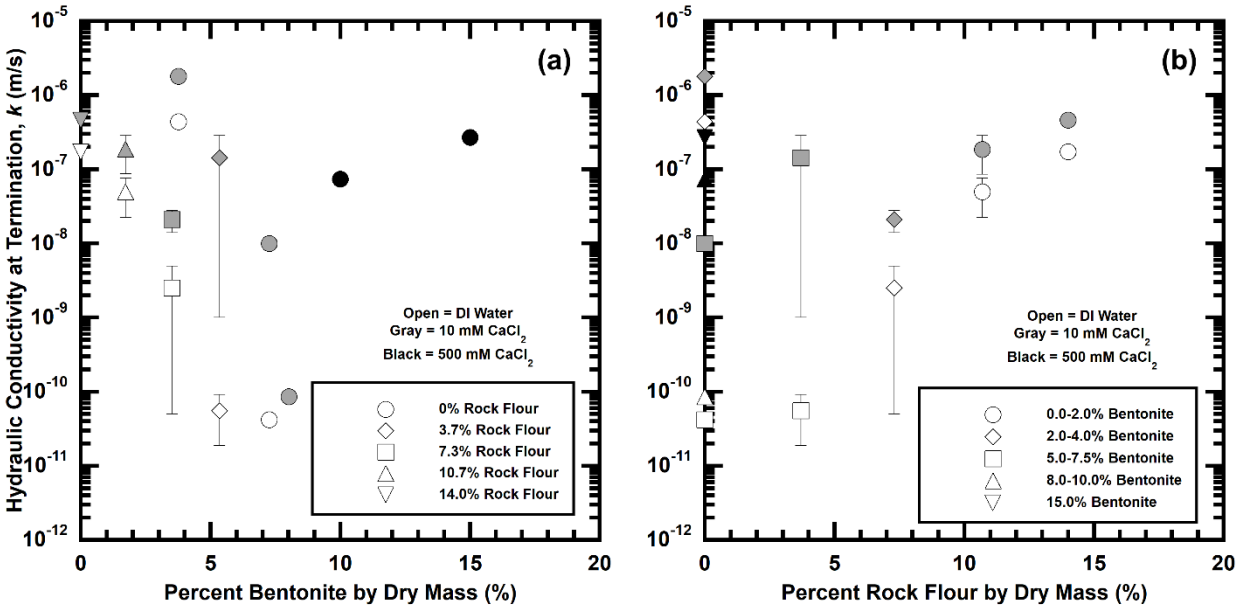

Figure 7. Final hydraulic conductivity versus (a) percent bentonite by dry mass and (b) percent rock flour by dry mass. Error bars are used to show the range of *k* values if (1) duplicates were made between tests (i.e. 8B-10-A and 8B-10-dup-A) or (2) two separate mixing methods were used for the same specimen constituents (i.e. 4B7R-10-H and 4B-7R-10-A). This is indicated in the legend because the amount of rock flour differs between each test.

3.1.1 Effect of Increasing Bentonite Content

Also shown in Figure 7, as bentonite percentage increases, *k* generally decreases. This is consistent for both DI water and 10 mM $CaCl_2$. To obtain a *k* of 10^{-9} m/s, the mixtures need approximately 4.5% bentonite for DI water and 8% bentonite for 10 mM $CaCl_2$. These percentages fall between the approximate amount of bentonite needed to obtain a *k* of 10^{-9} m/s while permeating with tap water, which has been reported as 6% (Abichou et al., 2002). Standard tap water has an EC that falls between that of DI water and 10 mM $CaCl_2$ (Scalia & Benson, 2010a).

Specimens only using rock flour as an amendment to sand (14R-0-H and 14R-10-H) do not achieve a k of 10^{-9} m/s or less. This is consistent with Stern and Shackelford (1998) who showed a 15% attapulgite amendment to yield a k of 3.9×10^{-7} m/s using a tap water solution. Attapulgite and rock flour provide similar hydraulic behavior when combined with sand because both are relatively inert fine-grained fillers.

Test 15B-500-A has a slightly higher k than test 10B-500-A (2.7×10^{-7} vs 7.4×10^{-7} m/s). Studies have shown that the difference in swell index in bentonite is less at high concentrations of $CaCl_2$ than at low concentrations. For example, Lee and Shackelford (2005) show that the decrease in swell in a high-quality bentonite from 10 mM to 100 mM $CaCl_2$ is about 21 to 8 mL/2g, whereas the decrease from 100 mM to 500 mM $CaCl_2$ is only from 8 to 6 mL/2g. This suggests that at higher concentrations of $CaCl_2$ bentonite reaches a lower limit for swell. While a lower k is still expected for test 15B-500-A than for test 10B-500-A, the effects of bentonite swell at 500 mM $CaCl_2$ is lessened. In addition, as described by Abichou et al. (2002), once a certain percentage of bentonite is added to a mixture, all large flow paths are eliminated if homogeneity is maintained. Adding additional bentonite will not substantially decrease k if these large flowpaths are already clogged.

3.1.2 Kitchen Mixer vs. Spoon Mixing

Specimens in this study were created either by hand mixing with a spoon or automatically mixing with a kitchen mixer to evaluate the role of mixing. Some tests were duplicates except for the mixing method (i.e. 4B7R-0-H and 4B7R-0-A). A comparison between the final hydraulic conductivities from each of these tests is shown in Figure 8.

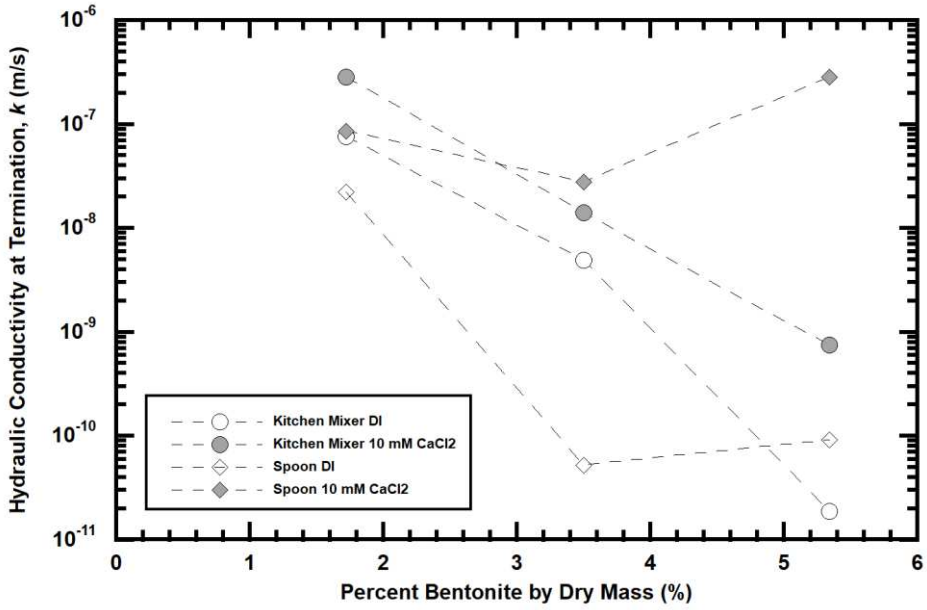

Figure 8. Hydraulic conductivity versus bentonite percent by dry mass for three different mixture combinations. The specimens were made by either mixing manually with a spoon or automatically with a kitchen mixer. Dashed lines are used to better display trends in the data.

In general, as bentonite percentage increases there was a greater variability in equilibrium *k*, although the maximum bentonite percentage tested was only 5.3%. At 1.7% bentonite, the greatest difference in *k* between two specimens with the same mixture proportions is 2B11R-0-A being 3.4 times greater than 2B11R-0-A. The difference in k for 5B4R-10-H and 5B4R-10-A is greater than two orders of magnitude. At higher bentonite percentages, ensuring that the mixture is homogeneous and that the bentonite is distributed evenly becomes increasingly difficult. Mollins et al. (1996) reported that the highest measured *k* is 3 times greater than the lowest *k* at 5% bentonite sand-bentonite mixtures (4 specimens), 13 times greater at 10% bentonite (12 specimens), and 30 times greater at 20% bentonite (9 specimens). In the field for large scale liner projects, ensuring a homogeneous distribution of bentonite is crucial so that the number of large pathways for fluid flow is limited. However, this homogeneity will be increasingly difficult to achieve with greater bentonite percentages.

3.1.3 Effect of $CaCl_2$

As expected, tests using 10 mM $CaCl_2$ have higher *k* values than tests using DI water as the permeant liquid (Figure 7). This is consistent with numerous previous studies (e.g., Stern & Shackelford, 1998). In addition, tests 10B-500-A and 15B-500-A have similar *k* to tests with less bentonite percent and a lower *I* permeant solution. As *I* of the permeant increases, the bentonite in the mixture swells less due to suppression of the diffuse double layer. Less swelling in the bentonite results in higher *k* due to larger pathways for fluid flow.

3.1.4 Effect of Adding Rock Flour

Most mixtures in this study aimed to fill 100% of pores in a sand matrix for each mixture using rock flour, bentonite, or both. As such, as rock flour percentage increases the amount of bentonite needed to completely fill the remaining pores of the sand matrix decreases. However, bentonite content was not held constant while increasing rock flour, limiting the number of conclusions that can be drawn from adding rock flour to the mixtures.

Tests 4B-0-H and 4B-10-H were created to fill 50% of the pore space in the matrix only using bentonite. Tests 4B7R-0-H, 4B7R-0-A and 4B7R-10-H, 4B7R-10-A fill 100% of the pore space using bentonite plus rock flour. Each of these tests have about 3.5% bentonite by dry mass. For both the DI water tests and the 10 mM $CaCl_2$ tests, the specimens containing rock flour (7.3% by dry mass) have lower *k* by about two orders of magnitude. This data suggests that *k* can be lowered by adding an inert filler such as rock flour to a mixture already containing bentonite. Stern and Shackelford (1998) show that adding an inert filler like attapulgite clay to a sand-bentonite mixture will lower *k* when bentonite content is kept constant. However, this study only observed a 2-fold decrease when adding 10% attapulgite to 10% bentonite. Similarly, the study found that

going from a base mixture of 5% bentonite amended with 5% attapulgite to a mixture of 5% bentonite and 15% attapulgite results in a 50-fold decrease in k. These results can be generalized to show that adding an inert filler has a greater effect at decreasing *k* at lower bentonite contents.

3.2 Direct Shear

Shear stress versus deformation plots for three selected specimens at different bentonite contents are shown in Figure 9, with all plots being shown in Appendices D and E (35 and 825 kPa, respectively). Peak friction angles are calculated using the peak shear stress from each test after the 20-point moving average was applied. Ultimate strengths were determined as: (1) strength dropped after reaching a peak, and shear stress remained relatively constant; (2) vertical displacement remained relatively constant. Friction angles reported in this study are secant friction angles because a single effective stress was used to calculate each value.

Specimens with a lower percentage of fines reach a peak strength at lower relative horizontal displacement (relative horizontal displacement = horizontal displacement / original specimen length) than specimens with more fines (Figure 9). The sand specimens reach a peak strength at 3% relative horizontal displacement at both 35 and 825 kPa. Test 2B11R-0-A reaches a peak strength at 6% relative horizontal displacement for both 35 and 825 kPa. Specimen 30B-0-A reaches peak strengths at 20% and 13% relative horizontal displacement for 35 and 825 kPa, respectively. However, unlike the other two specimens shown in Figure 9, there is little drop in strength post-peak for specimen 30B-0-A indicating that the mixture is behaving in a ductile manner.

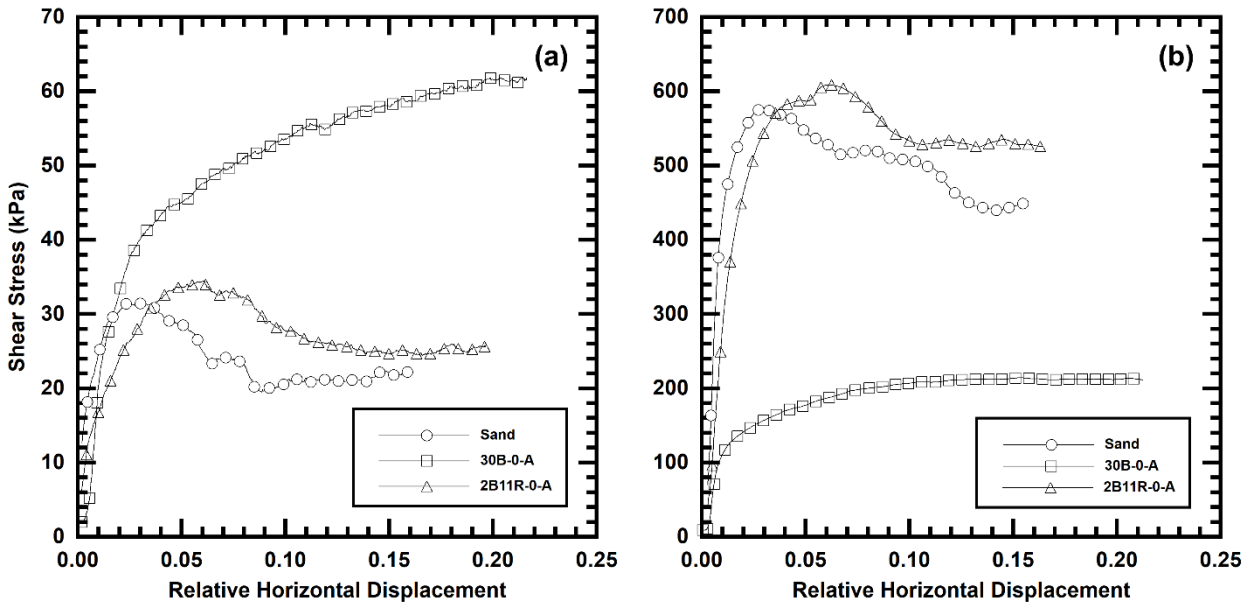

Figure 9. Shear stress versus relative horizontal displacement for selected specimens at (a) 35 kPa and (b) 825 kPa. Five percent of collected data points are shown and a line is used to connect data points to better display changes in shear strength. The magnitude of the vertical axis is different for plots (a) and (b) to better display trends in the data.

Mixtures in this study were made using combinations of sand, rock flour, and bentonite. In a sand-bentonite-rock flour mixture, the bentonite percentage will have much greater impact on the bulk mixture strength properties than rock flour. This is because bentonite has greater swell characteristics, higher liquid and plastic limits, and lower shear strength.

To normalize the fines percentage in each mixture, an equivalent fines fraction is used to display direct shear results. Tiwari & Marui (2003) measured the residual shear strength of bentonite-kaolin-Toyoura sand mixtures using ring-shear and use a 20% equivalent weight of kaolin versus bentonite, where the following equation determines the equivalent clay percentage:

$$Equivalent\ Clay\ \% = (0.20 * kaolin\ \%) + bentonite\ \%$$

This relationship was developed based on the observation that the residual strength of bentonite $\varphi_{r,bentonite} = 0.2\ \varphi_{r,kaolin}$. While the present study primarily uses rock flour instead of

kaolinite, the similar properties between the two allows the following equation to be used for equivalent fines percentage:

$$Equivalent\ Fines\ \% = (0.20 * rock\ flour\ \%) + bentonite\ \%$$

Equivalent fines percentage is used as opposed to equivalent clay percentage due to rock flour containing both silt and clay sized particles. The two tests using kaolinite (15K-0-H and 15K-10-H) also use the equation above for calculating equivalent fines percentage with the rock flour percentage being replaced by kaolinite in the calculation.

3.2.1 Increasing Fines Content

Figure 10 shows the peak friction angles (φ'_{peak}) and ultimate friction angles (φ'_{u}) measured during direct shear testing. At 35 kPa normal stress, φ'_{peak} increases from 45 degrees at 0% equivalent fines to almost 70 degrees at 15% equivalent fines. Percentages greater than 15 equivalent fines result in slightly lower φ'_{peak}. At 825 kPa normal stress, φ'_{peak} remains relatively constant between 35 and 40 degrees for an equivalent fines percentage between 0 and 15. Above 15% equivalent fines, φ'_{peak} decreases to an average of 19 degrees at 20% and 12 degrees at 30 percent.

At 35 kPa effective stress, φ'_{u} increases from about 35 degrees at 0-5% equivalent fines to greater than 60 degrees at 15% equivalent fines. At values greater than 15% equivalent fines there is no noticeable increase or decrease in φ'_{u}. At 825 kPa, φ'_{u} values generally vary between 30 and 35 degrees below 15% equivalent fines. Greater than 15% equivalent fines results in a substantial drop in φ'_{u}, with an average φ'_{u} = 19.0 degrees at 20% and φ'_{u} =11.7 degrees at 30% equivalent fines.

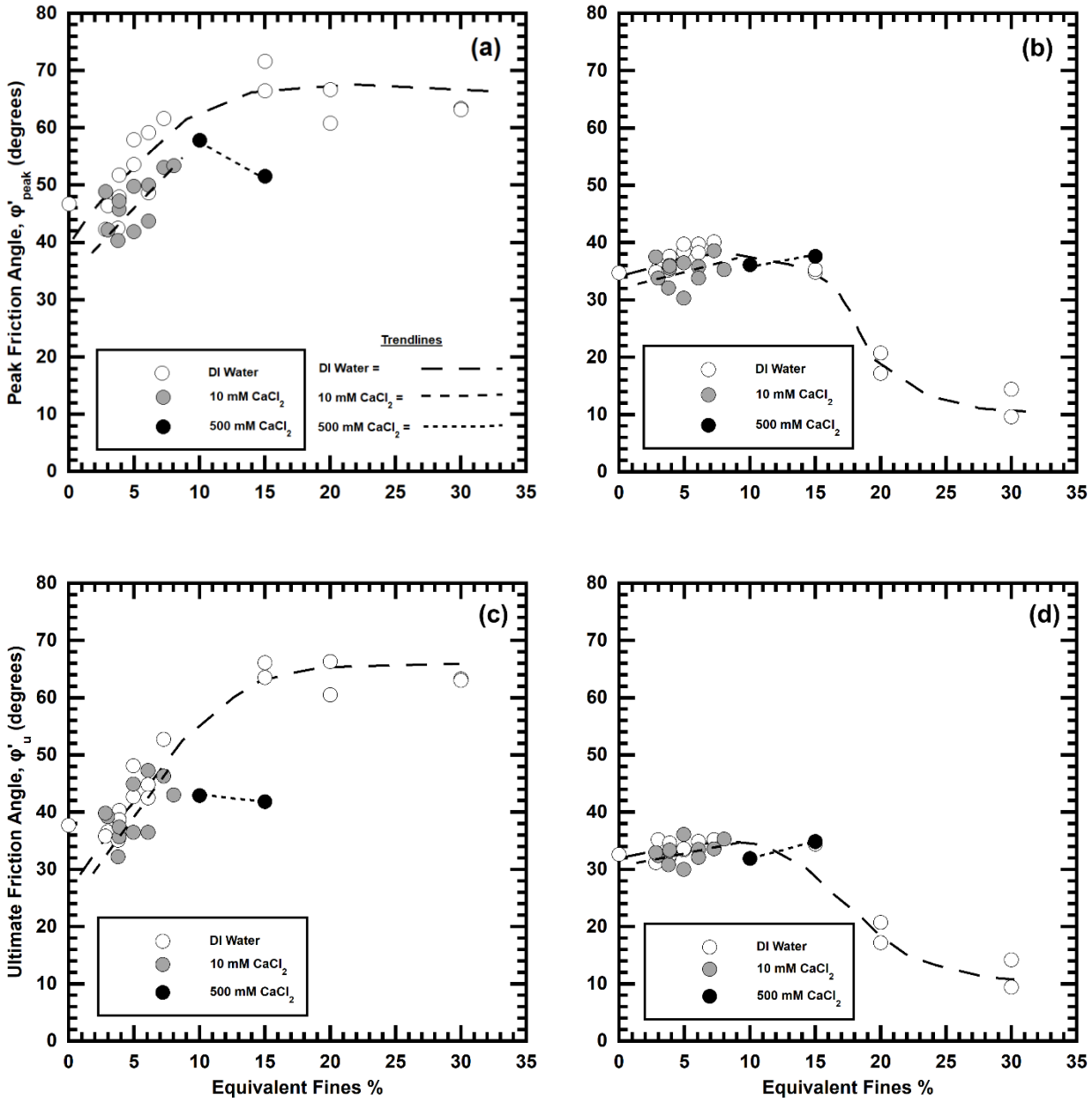

Figure 10. Peak friction angles (a,b) and ultimate friction angles (c,d) at 35 kPa (a,c) and 825 kPa (b,d) normal stress measured from direct shear testing. The data points at zero equivalent fines percentage are sand. Dashed lines are drawn to show general trends for each permeant solution.

Results from Tiwari & Marui (2003) show drop in φ'_u with increasing equivalent clay percentage. Between 0 and 10 equivalent clay percentage, φ'_u decreases moderately from about 30 degrees to 27 degrees. From 10 to 20 percent, φ'_u decreases from 27 to about 15 degrees. Ultimate

shear strength continues to decrease until about 40% equivalent clay is present in the mixture. At this equivalent clay percentage, φ'_u equals 3.5 degrees. The greatest change in φ'_u occurs between 15% and 25% equivalent clay. These results generally agree with the current study as φ'_u is significantly reduced between 15% and 25% equivalent fines at 825 kPa. While φ'_u of specimens with a bentonite content greater than 30% were not measured in this study, φ'_u is expected to become relatively constant with increasing fines in mixtures with greater than 30% bentonite because the matrix of specimens will be dominated by swollen bentonite with minimal sand-to-sand grain contacts.

In this study, measured friction angle increased between 0% and 15% equivalent fines at 35 kPa. As stated above, Tiwari & Marui (2003) observe a decrease in φ'_u with increasing clay. However, Mollins et al. (1999) observe an increase in strength up to about 5-10% bentonite with peak friction angles decreasing at clay contents greater than 10%. The increase in strength observed in Mollins et al. (1999) is attributed to the specimens between 5-10% bentonite having the highest dilatancy indices in their study.

To the author's knowledge, no study reports sand-bentonite mixtures with friction angles greater than 70 degrees. The φ'_u values from Tiwari & Marui (2003) are all lower than 30 degrees. However, the specimens in Tiwari & Marui (2003) were prepared to a $\gamma_d = 15$ kN/m^3 ($\approx$1.53 g/cm^3), and φ'_u values were obtained from residual shear strength envelopes using effective normal stresses between 10 kPa and 250 kPa. Excluding cohesion, Chalermyanont & Arrykul (2005) observed a secant friction angle of 55 degrees at a bentonite content of 9% (γ_d not specified). The failure envelope in Gueddouda (2008) for a 15% sand-bentonite provides a secant friction angle of 55 degrees at a $\gamma_d = 1.73$ g/cm^3.

The tests with friction angles larger than 60 degrees at 35 kPa are possibly due to several factors. The minimum prepared γ_d in the current study is 1.64 g/cm^3 before permeation, with the average γ_d =1.81 g/cm^3. The high γ_d in this study compared to other studies could account for the greater measured φ'_u values. In addition, the Mohr-Coulomb failure envelope is likely curved at very low effective stresses. Day (1992) measured the shear strength of unsupported compacted clay specimens (zero effective stress) at γ_d of approximately 1.65 g/cm^3. At this stress, Day (1992) concluded that the inclination of the Coulomb failure plane could be as high as 84 degrees. In addition, Day (1992) observed a 6-fold strength increase when letting specimens cure for 21 days rather than 1 day, which the author attributed to development of bonds forming over time (an increase in effective cohesion). Similarly, Lessard & Mitchell (1985) found that the remolded strength of quick clays increased with aging over time, where greater than 10-fold increases in strength were observed for both waxed and unwaxed specimens that aged for 12 months. In the present study, all specimens were allowed to age for at least 30 days before undergoing shear strength testing, with some aging for over 12 months during *k* testing. The combination of the aging time, the curved failure envelope at low effective stress, and the high γ_d, all possibly contributed to the high friction angles observed at 35 kPa.

Another possible cause for the extremely high friction angles at 35 kPa is the development of negative excess pore water pressure during shear. While the procedures in ASTM D3080-98 were followed by measuring t_{50} to ensure that the shear rate was slow enough to prevent excess pore water pressures from developing for the specimen, it is possible that the shear rate of 0.25 mm/min was too fast. Further investigation is required to explore this possibility.

3.2.2 Effect of Increasing Permeant Concentration

Between 0% and 10% equivalent fines, DI water specimens tend to have higher peak friction angles than the 10 mM $CaCl_2$ specimens (e.g. 7B-0-H vs. 7B-10-H). This trend is more apparent at 35 kPa than at 825 kPa. Specimens permeated with 10 mM $CaCl_2$ solution were expected to have a greater friction angle than specimens permeated with DI water because calcium bentonite has a higher friction angle than sodium bentonite, and the reduced swell of calcium bentonite will allow more sand grain contacts.

For each of the 10 sand-bentonite-rock flour combinations in which a DI water and a 10 mM $CaCl_2$ specimen were permeated from the same mixture, the initial γ_d before permeation is greater in the DI water specimen. In every case, the DI water specimen has a greater observed peak friction angle at both 35 kPa and 825 kPa effective normal stress. The exceptions to this are tests 14R-0-H and 14R-10-H. Test 14R-10-H has a greater initial γ_d than 14-0-H. Test 14R-10-H also has a greater observed peak friction angle at both 35 kPa and 825 kPa than 14-0-H. The DI water specimens most likely have greater initial γ_d values because they were extruded from the bottom of the mold after compaction, resulting in somewhat higher density which will increase shear strength (Ladd, 1978). No post-permeation 10 mM $CaCl_2$ specimens have lower e_i than DI water specimens that were created from the same mixture. The 10 mM $CaCl_2$ samples were always extruded from the top half of the compacted sample.

3.2.3 Peak vs. Ultimate Strengths

Figure 11 provides a comparison of the relationship between the ratio of peak to ultimate friction angle ($\varphi'_{peak} / \varphi'_{u)}$ and equivalent fines percentage measured in direct shear testing. At 35 kPa normal stress, $\varphi'_{peak} / \varphi'_{u}$ values range between 1.05 and 1.35 for equivalent fines between 0%

and 10%. Equivalent fines from 15% to 30% show a reduction in $\varphi'_{peak} / \varphi'_{u}$ with values ranging between 1.00 and 1.25. At 20% and 30% equivalent fines, φ'_{peak} is near the ultimate friction angle.

At 825 kPa normal stress, $\varphi'_{peak} / \varphi'_{u}$ varies between 1.00 and 1.25 from 0% to 10% equivalent fines. Like the 35 kPa normal stress tests, $\varphi'_{peak} / \varphi'_{u}$ tends to decrease with increasing fines. Equivalent fines values of 20% and 30% have average $\varphi'_{peak} / \varphi'_{u}$ values of 1.00 and 1.02, respectively.

A high $\varphi'_{peak} / \varphi'_{u}$ indicates strain softening behavior where there is a drop in shear strength at critical state compared to φ'_{peak}. A lower $\varphi'_{peak} / \varphi'_{u}$ suggests less strain hardening is occurring where peak strengths are similar to ultimate strength and there is little drop in shear strength at high strain. In general, at low equivalent fines percentages the 825 kPa direct shear tests have lower $\varphi'_{peak} / \varphi'_{u}$ than the 35 kPa tests, which suggests that sand-bentonite mixtures will have less strain softening than at lower stresses.

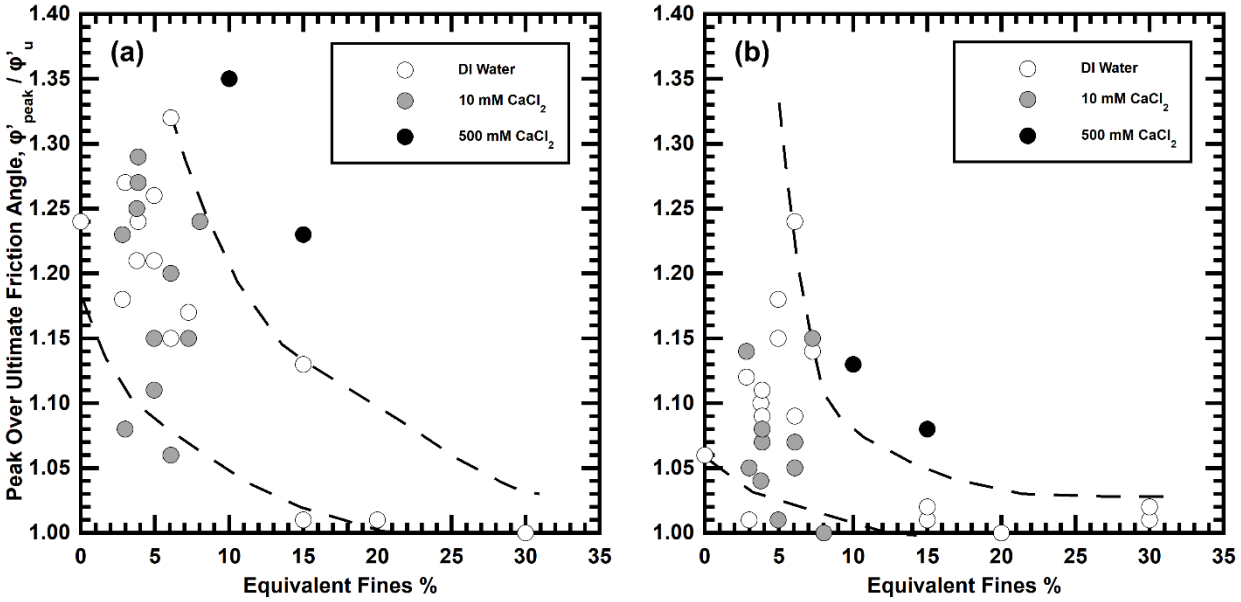

Figure 11. Peak friction angle divided by ultimate friction angle vs. equivalent fines percentage for (a) 35 kPa and (b) 825 kPa effective normal stress. Dashed lines are drawn to show the general trend of DI water specimens.

Ductility can be evaluated by quantifying the displacement at which a sample reaches peak strength. Figure 12 compares the relative horizontal displacement at φ'_{peak} to equivalent fines percentage. In Figure 12a, relative horizontal displacements at peak shear strength generally fall between the values of 0.04 and 0.10 below 10% equivalent fines. In Figure 12b, for the same equivalent fines percentage range, relative horizontal displacements at peak shear strength are between 0.05 and 0.15. The increase in effective stress results in a higher relative horizontal displacement at peak strength, suggesting less brittle behavior.

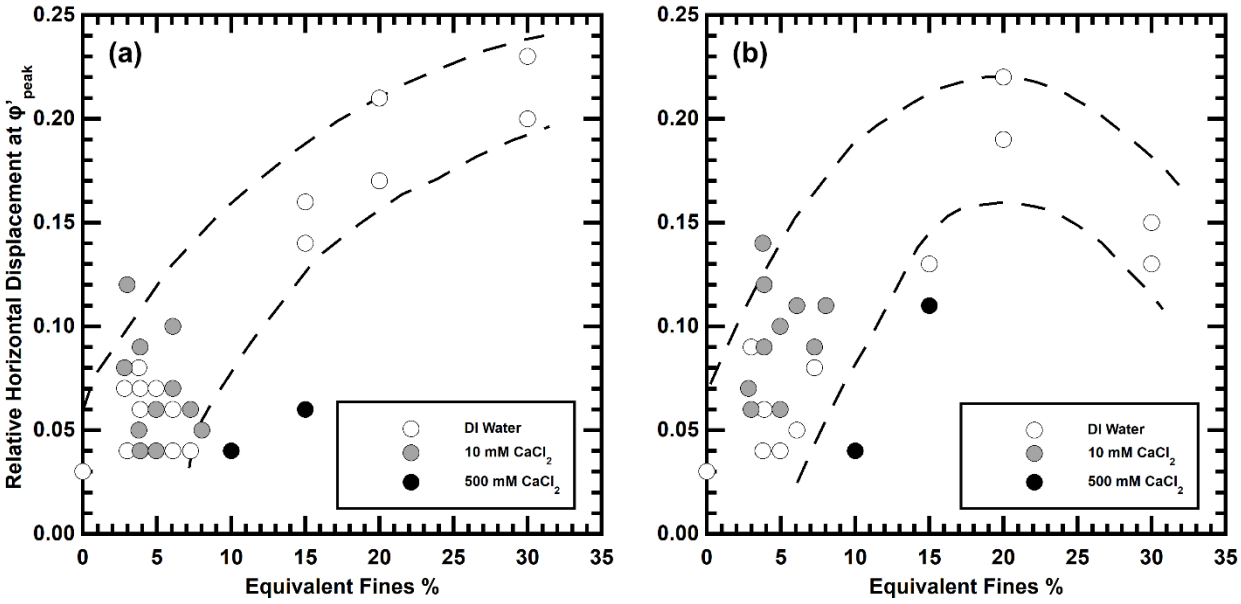

Figure 12. Relative horizontal displacement vs. equivalent fines percentage at (a) 35 kPa and (b) 825 kPa effective stress. Relative horizontal displacement is used rather than strain due to the displacement not being a true strain in direct shear testing. Dashed lines are drawn to show the general trend of DI water specimens.

In addition, for both low and high effective stresses, Figure 12 shows that a higher equivalent fines percentage results in an increase in ductile behavior. Although not fitting this trend, the data points at 30% equivalent fines in Figure 12b reach a peak strength at a relatively low relative horizontal displacement that did not decrease greatly at higher displacements (average

$\varphi'_{peak} / \varphi'_{u} = 1.02$ for the two tests). These findings are consistent with Mollins et al. (1999) who found that increasing bentonite content resulted in a higher axial strain at peak strength in sand-bentonite mixtures during direct shear testing.

3.2.4 Dilative vs. Contractive Behavior

Figure 13 shows the change in e of specimens during direct shear testing. At 35 kPa effective stress, none of the tests exhibit contractive behavior. For equivalent fines percentage values lower than 10, most specimens have a final void ratio (e_{final}) that is between 0.00 and 0.05 greater than initial void ratio ($e_{initial}$). For specimens greater than 10% equivalent fines, e_{final} is generally between 0.05 and 0.15 greater than $e_{initial}$. As equivalent fines percentage increases, more dilation occurs.

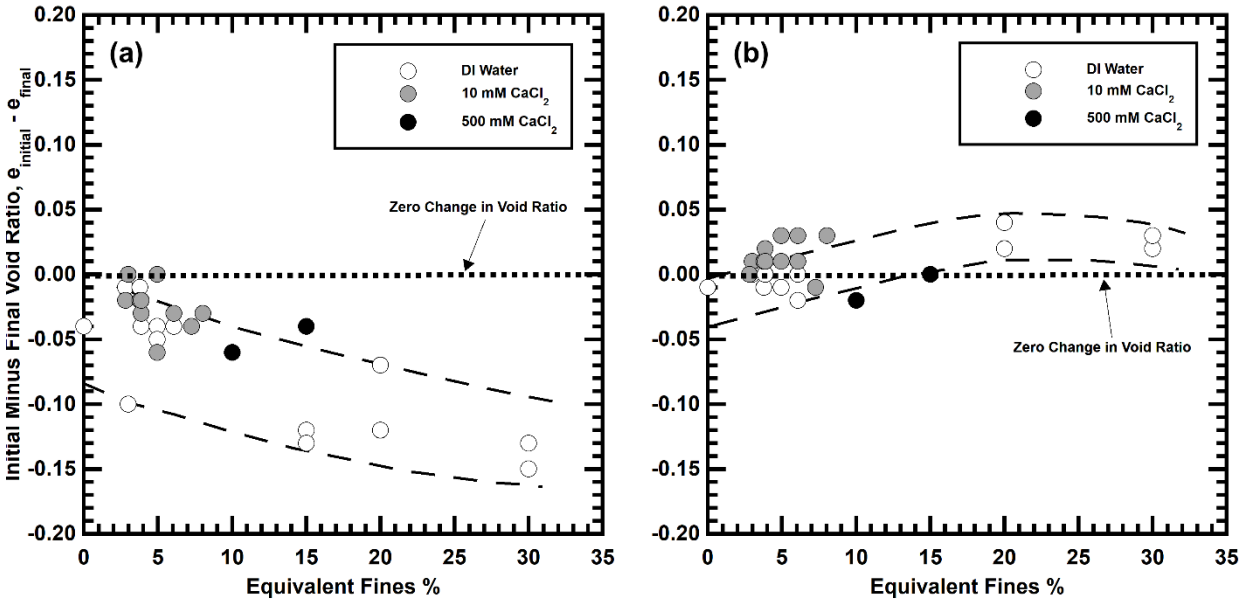

Figure 13. Dilative or contractive tendencies of specimens during direct shear testing for (a) 35 kPa and (b) 825 kPa effective normal stress. The initial e is the e before the specimen begins shearing while the final e is the e at ultimate strength. Negative values indicate that e_{final} is greater than $e_{initial}$ due to dilation. Positive values indicate e_{final} is less than $e_{initial}$ because of contraction. Dashed lines are drawn to show the general trend of DI water specimens.

At 825 kPa, more specimens exhibit contraction than dilation. All specimens that are dilative are at or below a 10% equivalent fine. Below 10% equivalent fines, only 1 of 10 of the 10 mM $CaCl_2$ specimens exhibit dilative behavior while 5 of the 10 DI water specimens are dilative. This could be attributed to the greater initial γ_d of DI water specimens discussed previously. No specimen at 825 kPa had an $e_{final} \pm 0.05\ e_{initial}$.

Dilation is expected to occur for dense specimens at low effective stresses because there are few pore spaces available for grains to fill when being sheared. As effective stress increases, dilation is suppressed because grains need to overcome a greater force when moving up and over other grains. In general, dilation at low stress and contraction at high stress are observed with this data. Suppressed dilation at high confining pressures is well documented in the literature (e.g., Lee, 1965; Lee & Seed, 1967).

Samples with the greatest equivalent fines percentage (30B-0-A and 30B-0-dup-A) are the most dilative specimens at 35 kPa even though they had some of the highest $e_{initial}$ in the study before shearing (0.67 and 0.75, respectively). While it is not fully understood why this is, all specimens consolidated before being sheared after the 35 kPa load was applied in the direct shear apparatus (e went from 0.78 to 0.67 for 30B-0-A; 0.80 to 0.75 for 30B-0-dup-A). This consolidation would be reversible to an extent when dilating during shear.

3.2.5 Displacement of Sand

To quantify the packing of the sand grains, the following equation is used to calculate the void ratio of the sand grains, e_{sand}, in a saturated sand-bentonite-rock flour specimen:

$$e_{sand} = \frac{V_{fines} + V_{water}}{V_{sand}}$$

where V_{fines} is the volume of bentonite plus the volume of rock flour. Figure 14 shows the relationship between true fines percentage and e_{sand} before undergoing shear. In Figure 14a, the values of e_{sand} reach 0.76 at approximately 15% fines. Above this value, the sand grains will begin to lose contact with each other due to displacement by rock flour and bentonite. While shear strength values do not substantially drop off at fines percentages greater than 15% for 35 kPa effective stress, the greatest observed friction angles were recorded at 15% equivalent fines. The low effective stress allows the fines to add to shear strength while the sand grains are still in contact.

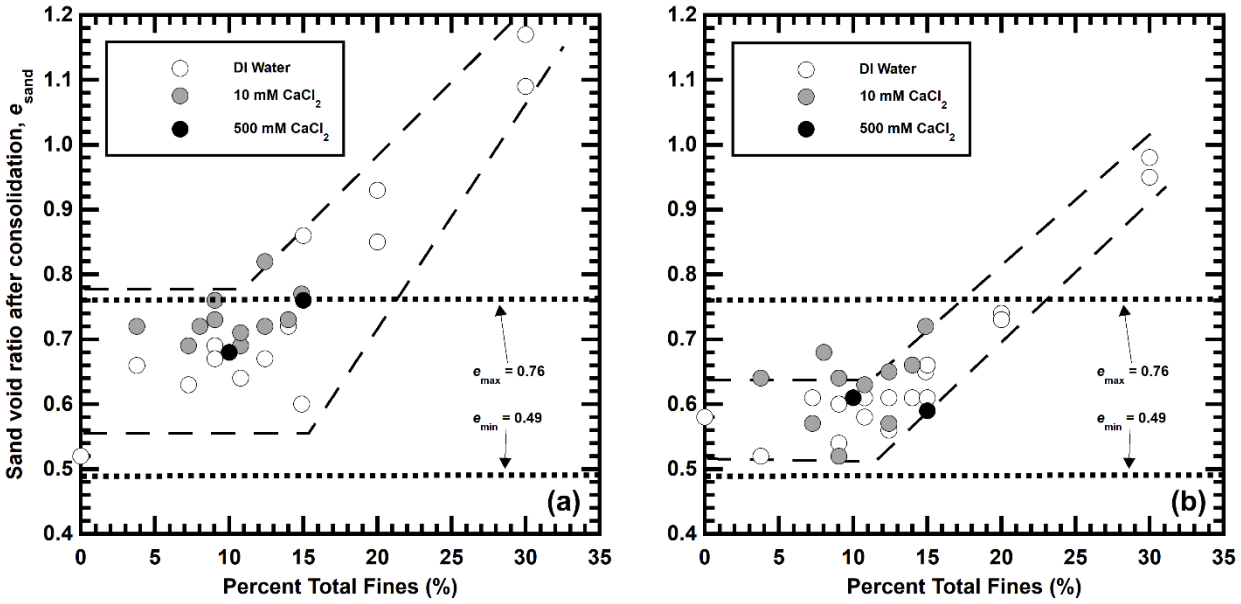

Figure 14. Sand void ratio, e_{sand}, before shear vs. percent total fines by dry mass at (a) 35 kPa and (b) 825 kPa effective stress. The dotted lines show the minimum and maximum void ratios of the sand. Dashed lines are drawn to show the general trend of DI water specimens.

At 825 kPa, e_{sand} do not exceed 0.76 until greater than 20% fines. Specimens at this stress consolidate when loaded due to the dissipation of water while the volume of sand solids concurrently remains the same. Due to consolidation under the load, the calculated e_{sand} decreases,

explaining why e_{sand} observed in Figure 14b are lower than those in Figure 14a. Nonetheless, shear strength decreases substantially once e_{sand} is approximately 0.76 at 825 kPa.

Figure 15 shows the relationship between φ'_{peak} and e_{sand} and highlights the drop in strength at 825 kPa once e_{sand} exceeds 0.76. In addition, e_{sand} is lowest at approximately 10% total fines (Figure 14). This is consistent with Mollins et al. (1999) in which e_{sand} were lowest in sand-bentonite mixtures for specimens containing 5-10% total fines (Mollins et al., 1999). In Mollins et al. (1999), mixtures containing greater than 10% fines had greater initial e_{sand}.

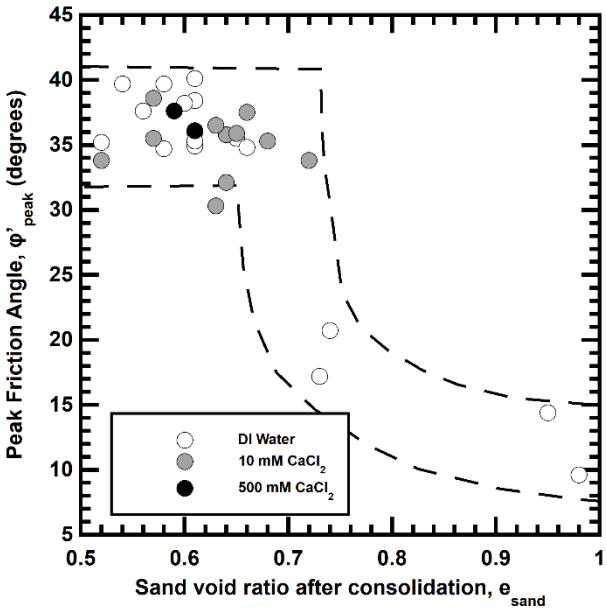

Figure 15. Peak friction angle vs. e_{sand} for direct shear testing at 825 kPa. Peak friction angle decreases substantially at e_{sand} > 0.76. Dashed lines are drawn to show the general trend of DI water specimens.

4. SUMMARY AND CONCLUSIONS

The objective of this study was to evaluate the potential of constructed mineral-bentonite barriers yielding concurrent low *k* and high shear strength to be used in mining and other containment applications. Mixtures containing sand, rock flour, and bentonite were created and permeated in a flexible-wall permeameter using a range of *I* solutions. Sub-samples were extracted from the permeated specimens and were subsequently tested for strength using direct shear testing. Key findings include:

- Hydraulic conductivity tended to decrease with increasing bentonite content.
- Specimens permeated with 10 mM $CaCl_2$ typically had higher final equilibrium *k* than specimens with the same mixture components of sand, rock flour, and bentonite than specimens permeated with DI water.
- Rock flour alone was not a suitable replacement for bentonite at the same percentages by mass and percentages up to 14.9% did not lower *k* below 10^{-9} m/s.
- At 35 kPa effective stress, shear strength increased with increasing fines until 15% equivalent fines percentage. At 825 kPa, shear strength remained relatively constant until 15% equivalent fines percentage followed by a substantial drop in strength for mixtures with greater than 15% equivalent fines percentage.
- Specimens were more ductile at higher equivalent fines percentages due to higher relative horizontal displacements at φ'_{peak}.

- The highest percentage sand-bentonite specimens (30% bentonite by mass) were the most dilative samples at 35 kPa. More specimens were contractive than dilative at 825 kPa with dilation decreasing with increasing equivalent fines percentage.

- At 825 kPa, φ'_{peak} substantially dropped when the e_{sand} exceeded the maximum void ratio of the sand matrix of $e_{max} = 0.76$.

The results from this study suggest that designing a mineral-bentonite barrier with a low hydraulic conductivity and a high shear strength across a range of effective stresses is attainable. However, there is a relatively narrow range of bentonite contents that will allow for such a barrier to be constructed. At 15% bentonite content, a sand-bentonite barrier can provide an ultimate shear strength of greater than 30 degrees and a low *k*. However, both shear strength and *k* are dependent on numerous variables that can change the performance of the barrier. These are highlighted in Table 2. This list is not exhaustive but highlights the key contributing variables to mineral-bentonite barrier performance. As seen in Table 2, many factors can alter the performance of a mineral-bentonite barrier. In addition, the variables listed in Table 2 are likely to change over the lifespan of a liner used in mining applications. For example, a mineral-bentonite liner used under a heap leach pad will initially have relatively low effective stress due to the low height of ore placed on top. As the heap pile height increases, the effective stress will also increase. The increase in effective stress will cause densification of the liner due to consolidation. Consolidation of the liner will decrease the volume of void space and make pathways for fluid flow more tortuous. Increased densification in a mineral-bentonite will also result in a barrier with a higher shear strength if contacts are maintained in the coarse-grained matrix. Also, the permeant liquid in the liner might change over time due to changes in the lixiviant used to extract ore from the heap leach. A change in permeant liquid will affect the long-term hydraulic performance of the barrier.

Table 2. Variables affecting performance in a mineral-bentonite barrier.

Variable	Hydraulic conductivity (*k*)	Shear Strength (φ′)
Bentonite content	↑ bentonite = ↓ *k*	↑ bentonite = ↓ φ′
Dry density (γ_d)	↑ γ_d = ↓ *k*	↑ γ_d = ↑ φ′
Effective stress (σ′)	↑ σ′ = ↓ *k*	↑ σ′ = ↓ φ′ *
Permeant ionic strength (*I*)	↑ *I* = ↑ *k*	↑ *I* = ↑ φ′ †
Fines Percentage	↑ fines = ↓ *k*	↑ fines = ↓ φ′

* Friction angle decreases when σ′ increases, but strength at failure increases with increased σ′. The curved nature of the failure envelope is more apparent at very low σ′. At high σ′, the failure envelope is linear for small changes in σ′.

† The research directly addressing this topic only examines bentonite contents greater than 30%. While this current study reports slightly higher φ′ for higher *I* solutions, more research is needed to examine this relationship at low bentonite percentages.

To construct a sand-bentonite barrier optimized for both fluid flow and strength, extensive field and laboratory testing should be done to capture the range and evolution of conditions that might exist during the life of the barrier. At a minimum, the following should be completed before construction of the barrier:

- Obtain a thorough understanding of the anticipated stress conditions that will be placed on the liner and the identify permeant solution(s) that will be contained.
- Identify a source for a granular material that will constitute the matrix of the mineral-bentonite barrier. Determine the minimum and maximum void ratios of the granular

material to know the value at which the grains begin to be displaced with increasing fines content.

- Create mixtures using different quantities of the source granular material, bentonite, and other potential fine-grained amendments, such as tailings. Aim to fill the void space between the coarse-grained matrix without decreasing contact between the grains.
- Measure *k* of each mixture using a flexible-wall permeameter at both the minimum and the maximum anticipated effective stresses to know how *k* will change with increasing stress. Evaluate *k* using the anticipated permeant solution that the barrier will be containing.
- Measure φ´ of each mixture at multiple effective stresses in the range of anticipated stresses the barrier will be subject to. Utilize a triaxial testing setup so that pore pressures are recorded, and deformation behavior is better captured than in direct shear testing.
- Analyze the results of both *k* and strength testing to begin to conceptualize an initial design for a barrier.

One of the primary objectives of this study was to create an engineered barrier with similar hydraulic and strength properties to a glacial till. While *k* of 10^{-12} was not achieved, friction angles greater than 35 degrees were measured at an effective stress of 825 kPa. Creating an engineered barrier that is compacted to the same degree as a glacial till is extremely difficult. Past consolidation pressures in some tills are on the order of tens of thousands of kPa due to ice thicknesses of 1000 m or more. The extreme stresses that some tills have undergone can result in void ratios lower than 0.20 (Easterbrook, 1964). The current next best alternative is to use combinations of sand, bentonite, and fine-grained inert fillers such as tailings or rock flour. If carefully designed and constructed, a mineral-bentonite barrier may provide, in perpetuity, the

necessary low k and high shear strength required for liners in many waste containment applications.

5. REFERENCES

Abichou, T., Benson, C. H., & Edil, T. B. (2002). Micro-structure and hydraulic conductivity of simulated sand-bentonite mixtures. *Clays and Clay Minerals*, *50*(5), 537–545. https://doi.org/10.1346/000986002320679422

Alston, C., Daniel, D. E., & Devroy, D. J. (1997). *Design and construction of sand–bentonite liner for effluent treatment lagoon, Marathon, Ontario*. *34*, 12.

ASTM D1557-12. Standard Test Methods for Laboratory Compaction Characteristics of Soil Using Modified Effort (56,000 ft-lbf/ft3 (2,700 kN-m/m3).pdf. (2012). ASTM International. https://doi.org/10.1520/D1557-12R21

ASTM D2453-16. Test Methods for Maximum Index Density and Unit Weight of Soils Using a Vibratory Table. (2016). ASTM International. https://doi.org/10.1520/D4253-16E01

ASTM D2454-16. Test Methods for Minimum Index Density and Unit Weight of Soils and Calculation of Relative Density. (2016). ASTM International. https://doi.org/10.1520/D4254-16

ASTM D2487-17. Practice for Classification of Soils for Engineering Purposes (Unified Soil Classification System). (2017). ASTM International. https://doi.org/10.1520/D2487-17E01

ASTM D3080-98. Standard Test Method for Direct Shear Test of Soils Under Consolidated Drained Conditions. (2022). ASTM International.

ASTM D4318-17. Standard Test Methods for Liquid Limit, Plastic Limit, and Plasticity Index of Soils. (2017). ASTM International.

ASTM D7100-11. Test Method for Hydraulic Conductivity Compatibility Testing of Soils with Aqueous Solutions. (2011). ASTM International. http://www.astm.org/cgi-bin/resolver.cgi?D7100-11R20

Bareither, C. A., Edil, T. B., Benson, C. H., & Mickelson, D. M. (2008). Geological and Physical Factors Affecting the Friction Angle of Compacted Sands. *Journal of Geotechnical and Geoenvironmental Engineering*, *134*(10), 1476–1489. https://doi.org/10.1061/(ASCE)1090-0241(2008)134:10(1476)

Bareither, C. A., Ghazi Zadeh, S., Conzelmann, J., Scalia, J., & Shackelford, C. D. (2017). Evaluation of mechanical and hydraulic properties of geosynthetic clay liners for mining applications. *Tailings and Mine Waste*.

Cao, L., Peaker, S. M., & Ahmad, S. (2015). *Engineering characteristic of glacial tills in GTA*.

Chalermyanont, T., & Arrykul, S. (2005). *Compacted sand-bentonite mixtures for hydraulic containment liners*. 11.

Chapuis, R. P. (2002). The 2000 R.M. Hardy Lecture: Full-scale hydraulic performance of soil-bentonite and compacted clay liners. *Canadian Geotechnical Journal*, *39*(2), 417–439. https://doi.org/10.1139/t01-092

Chapuis, R. P., Lavoie, J., & Girard, D. (1992). *Design, construction, performance, and repair of the soil–bentonite liners of two lagoons*. *29*, 12.

Clark, B. G. (2018). The engineering properties of glacial tills. In *Geotechnical Research* (Vol. 5, pp. 262–277). ICE. https://doi.org/10.1680/jgere.18.00020

Daniel, D. E., Koerner, R. M., Bonaparte, R., Landreth, R. E., Carson, D. A., & Scranton, H. B. (1998). Slope Stability of Geosynthetic Clay Liner Test Plots. *Journal of Geotechnical and Geoenvironmental Engineering*, *124*(7), 628–637. https://doi.org/10.1061/(ASCE)1090-0241(1998)124:7(628)

Day, R. W. (1992). Effective Cohesion for Compacted Clay. *Journal of Geotechnical Engineering*, *118*(4), 611–619.

Easterbrook, D. J. (1964). Void Ratios and Bulk Densities as Means of Identifying Pleistocene Tills. *Geological Society of America Bulletin*, *75*(8), 745.

Eid, H. T., & Stark, T. D. (1997). Eid and Stark Shear Behavior of an Unreinforced Geosynthetic Clay Liner.pdf. *Geosynthetics International*, *4*(6), 645–659.

Essington, M. E. (2021). *Soil and water chemistry: An integrative approach* (Second). CRC Press, Taylor & Francis Group.

Ghazizadeh, S., & Bareither, C. A. (2016). Critical Evaluation of the Long-Term Shear Strength of Geosynthetic Clay Liners. *Geo-Chicago 2016*, 11–23. https://doi.org/10.1061/9780784480144.002

Ghazizadeh, S., & Bareither, C. A. (2019). Evaluation of GCL and Geomembrane Characteristics on Failure Modes and Critical Shear Strength of GCL/Geomembrane Composite Systems. *Geo-Congress 2019*, 344–353. https://doi.org/10.1061/9780784482087.032

Ghazizadeh, S., Bareither, C. A., Scalia, J., & Shackelford, C. D. (2018). Synthetic Mining Solutions for Laboratory Testing of Geosynthetic Clay Liners. *Journal of Geotechnical and Geoenvironmental Engineering*, *144*(10), 06018011. https://doi.org/10.1061/(ASCE)GT.1943-5606.0001953

Gipson, A. H. (1985). Permeability Testing on Clayey Soil and Silty Sand-Bentonite Mixture Using Acid Liquor. In *Hydraulic Barriers in Soil and Rock* (pp. 140–154). ASTM International.

Gueddouda, M. K., Lamara, M., Aboubaker, N., & Taibi, S. (2008). *Hydraulic Conductivity and Shear Strength of Dune Sand–Bentonite Mixtures*. *13*, 15.

Haug, M. D., Barbour, S. L., & Longval, P. (1988). Design and construction of a prehydrated sand–bentonite liner to contain brine. *Canadian Journal of Civil Engineering*, *15*(6), 955–963. https://doi.org/10.1139/l88-127

Hojka, K., Allan, A., Cotta, G., Bynski, D., MacGarvie, A., & Bou-Karam, L. (2019). Encapsulation of Mine Waste with Geomembrane as the Preferred Closure Option for Gordon Lake Sites in NWT. *TAILINGS AND MINE WASTE*.

Jo, H. Y., Benson, C. H., & Edil, T. B. (2006). Rate-limited cation exchange in thin bentonitic barrier layers. *Canadian Geotechnical Journal*, *43*(4), 370–391. https://doi.org/10.1139/t06-014

Kenney, T. C., van Veen, W. A., Swallow, M. A., & Sungaila, M. A. (1992). *Hydraulic conductivity of compacted bentonite–sand mixtures*. *29*.

Koerner, R. M. (2012). *Designing with Geosynthetics* (6th ed., Vol. 2).

Kolstad, D. C., Benson, C. H., Edil, T. B., & Jo, H. Y. (2004). Hydraulic conductivity of a dense prehydrated GCL permeated with aggressive inorganic solutions. *Geosynthetics International*, *11*(3), 233–241. https://doi.org/10.1680/gein.11.3.209.44488

Komine, H., & Ogata, N. (1999). Experimental Study on Swelling Characteristics of Sand-Bentonite Mixture for Nuclear Waste Disposal. *Soils and Foundations*, *39*(2), 83–97.

Koutsourais, M. M., Sprague, C. J., & Pucetas, R. C. (1991). Interfacial Friction Study of Cap and Liner Components for Landfill Design. *Geotextiles and Geomembranes*, 531–548.

Ladd, R. S. (1978). Preparing Test Specimens Using Undercompaction. *Geotechnical Testing Journal*, *Vol. 1*(No. 1).

Lee, J.-M., & Shackelford, C. D. (2005a). Impact of Bentonite Quality on Hydraulic Conductivity of Geosynthetic Clay Liners. *Journal of Geotechnical and Geoenvironmental Engineering*, *131*(1), 64–77. https://doi.org/10.1061/(ASCE)1090-0241(2005)131:1(64)

Lee, J.-M., & Shackelford, C. D. (2005b). Solution Retention Capacity as an Alternative to the Swell Index Test for Sodium Bentonite. *Geotechnical Testing Journal*, *28*(1), 12520. https://doi.org/10.1520/GTJ12520

Lee, J.-M., Shackelford, C. D., Benson, C. H., Jo, H.-Y., & Edil, T. B. (2005). Correlating Index Properties and Hydraulic Conductivity of Geosynthetic Clay Liners. *Journal of Geotechnical and Geoenvironmental Engineering*, *131*(11), 1319–1329. https://doi.org/10.1061/(ASCE)1090-0241(2005)131:11(1319)

Lee, K. L. (1965). *Triaxial Compressive Strength of Saturated Sand Under Seismic Loading Conditions*. University of California, Berkeley.

Lee, K. L., & Seed, H. B. (1967). Drained Strength Characteristics of Sands. *Journal of the Soil Mechanics and Foundations Division*, *SM6*, 117–141.

Lessard, G., & Mitchell, J. K. (1985). The causes and effects of aging in quick clays. *Canadian Geotechnical Journal*, *22*(3), 335–346. https://doi.org/10.1139/t85-046

Lupo, J. F., & Morrison, K. F. (2007). Geosynthetic design and construction approaches in the mining industry. *Geotextiles and Geomembranes*, *25*(2), 96–108. https://doi.org/10.1016/j.geotexmem.2006.07.003

Meer, S. R., & Benson, C. H. (2007). Hydraulic Conductivity of Geosynthetic Clay Liners Exhumed from Landfill Final Covers. *Journal of Geotechnical and Geoenvironmental Engineering*, *133*(5), 550–563. https://doi.org/10.1061/(ASCE)1090-0241(2007)133:5(550)

Mishra, A. K., Ohtsubo, M., Li, L. Y., Higashi, T., & Park, J. (2009). Effect of salt of various concentrations on liquid limit, and hydraulic conductivity of different soil-bentonite mixtures. *Environmental Geology*, *57*(5), 1145–1153. https://doi.org/10.1007/s00254-008-1411-0

Mitchell, J. K., & Soga, K. (2005). *Fundamentals of Soil Behavior* (Third). John Wiley & Sons, Inc.

Mollins, L. H., Stewart, D. I., & Cousens, T. W. (1996). Predicting the properties of bentonite-sand mixtures. *Clay Minerals*, *31*(2), 243–252. https://doi.org/10.1180/claymin.1996.031.2.10

Mollins, L. H., Stewart, D. I., & Cousens, T. W. (1999). Drained strength of bentonite-enhanced sand. *Géotechnique*, *49*(4), 523–528. https://doi.org/10.1680/geot.1999.49.4.523

Petrov, R. J., & Rowe, R. K. (1997). *Geosynthetic clay liner (GCL) – chemical compatibility by hydraulic conductivity testing and factors impacting its performance*. *34*, 23.

Rowe, R. K. (2005). Long-term performance of contaminant barrier systems. *Géotechnique*, *55*(9), 631–678. https://doi.org/10.1680/geot.2005.55.9.631

Sample-Lord, K. M. (2015). *Membrane Behavior and Diffusion in Unsaturated Sodium Bentonite*. Colorado State University.

Scalia, J. (2012). *Bentonite-Polymer Composites for Containment Applications*. University of Wisconsin-Madison.

Scalia, J., & Benson, C. H. (2010a). Effect of Permeant Water on the Hydraulic Conductivity of Exhumed GCLs. *Geotechnical Testing Journal*, *33*(3), 102609. https://doi.org/10.1520/GTJ102609

Scalia, J., & Benson, C. H. (2010b). Preferential flow in geosynthetic clay liners exhumed from final covers with composite barriers. *Canadian Geotechnical Journal*, *47*(10), 1101–1111. https://doi.org/10.1139/T10-018

Scalia, J., Benson, C. H., Bohnhoff, G. L., Edil, T. B., & Shackelford, C. D. (2014). Long-Term Hydraulic Conductivity of a Bentonite-Polymer Composite Permeated with Aggressive Inorganic Solutions. *Journal of Geotechnical and Geoenvironmental Engineering*, *140*(3), 04013025. https://doi.org/10.1061/(ASCE)GT.1943-5606.0001040

Shackelford, C. D., Benson, C. H., Katsumi, T., Edil, T. B., & Lin, L. (2000). Evaluating the hydraulic conductivity of GCLs permeated with non-standard liquids. *Geotextiles and Geomembranes*, *18*(2–4), 133–161. https://doi.org/10.1016/S0266-1144(99)00024-2

Shackelford, C. D., Sevick, G. W., & Eykholt, G. R. (2010). Hydraulic conductivity of geosynthetic clay liners to tailings impoundment solutions. *Geotextiles and Geomembranes*, *28*(2), 149–162. https://doi.org/10.1016/j.geotexmem.2009.10.005

Sharma, H. D., & Kozicki, P. (1988). *The Use of Synthetic Liner and/or Soil-Bentonite Liner for Groundwater Protection*. 10.

Stark, T. D., & Eid, H. T. (1996). Shear Behavior of Reinforced Geosynthetic Clay Liners. *Geosynthetics International*, *3*(6), 771–786. https://doi.org/10.1680/gein.3.0084

Stern, R. T., & Shackelford, C. D. (1998). Permeation of Sand-Processed Clay Mixtures with Calcium Chloride Solutions. *Journal of Geotechnical and Geoenvironmental Engineering*, *124*(3), 231–241. https://doi.org/10.1061/(ASCE)1090-0241(1998)124:3(231)

Thiel, R., & Smith, M. E. (2004). State of the practice review of heap leach pad design issues. *Geotextiles and Geomembranes*, *22*(6), 555–568. https://doi.org/10.1016/j.geotexmem.2004.05.002

Thielmann, S. S., Fox, P. J., & Athanassopoulos, C. (2013). Interface Shear Testing of GCL Liner Systems for Very High Normal Stress Conditions. *Geo-Congress 2013*, 63–71. https://doi.org/10.1061/9780784412787.007

Tiwari, B., & Marui, H. (2003). Estimation of residual shear strength for bentonite-kaolin-Toyoura sand mixture. *Journal of the Japan Landslide Society*, *40*(No. 2), 124–133.

Triplett, E. J., & Fox, P. J. (2001). Shear Strength of HDPE Geomembrane/Geosynthetic Clay Liner Interfaces. *Journal of Geotechnical and Geoenvironmental Engineering*, *127*(6), 543–552. https://doi.org/10.1061/(ASCE)1090-0241(2001)127:6(543)

Xiang, G., Ye, W., & Jalal, F. E. (2021). Shear strength of bentonite–sand mixture saturated with saline solution. *Environmental Earth Sciences*, *80*(23), 770. https://doi.org/10.1007/s12665-021-10044-7

Zanzinger, H., & Alexiew, N. (2000, January 1). *Prediction of long term shear strength of geosynthetic clay liners with shear creep tests*. 2nd European Geosynthetic Conference, Bologna.

Zanzinger, H., & Saathoff, F. (2012). Long-term internal shear strength of a reinforced GCL based on shear creep rupture tests. *Geotextiles and Geomembranes*, *33*, 43–50. https://doi.org/10.1016/j.geotexmem.2012.02.007

Zhang, L., Sun, D., & Jia, D. (2016). Shear strength of GMZ07 bentonite and its mixture with sand saturated with saline solution. *Applied Clay Science*, *132–133*, 24–32. https://doi.org/10.1016/j.clay.2016.08.004

APPENDIX A – LABORATORY PHOTOGRAPH LOG

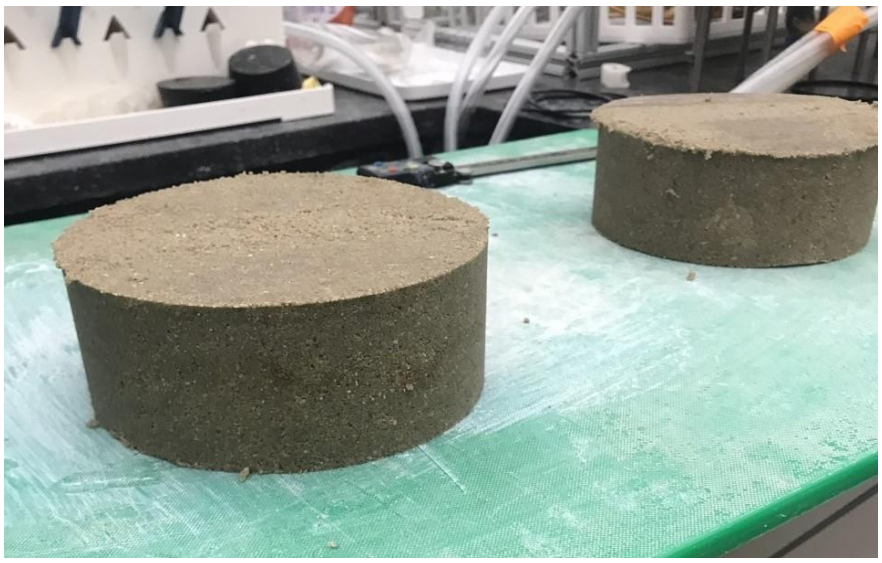

Figure A1. Example specimens after compaction in modified Proctor mold and cutting in half. Each specimen is about 6 cm in height.

Figure A2. Example specimen post-permeation. The dark color on the specimen is likely due to bacterial growth that occurred during permeation.

Figure A3. Specimen before using cutting-rings to extract sub-specimens. Sub-specimens were cut side by side on permeated specimens.

Figure A4. Hydraulic conductivity specimen being cut using cutting ring. Two sub-specimens were obtained from each hydraulic conductivity test.

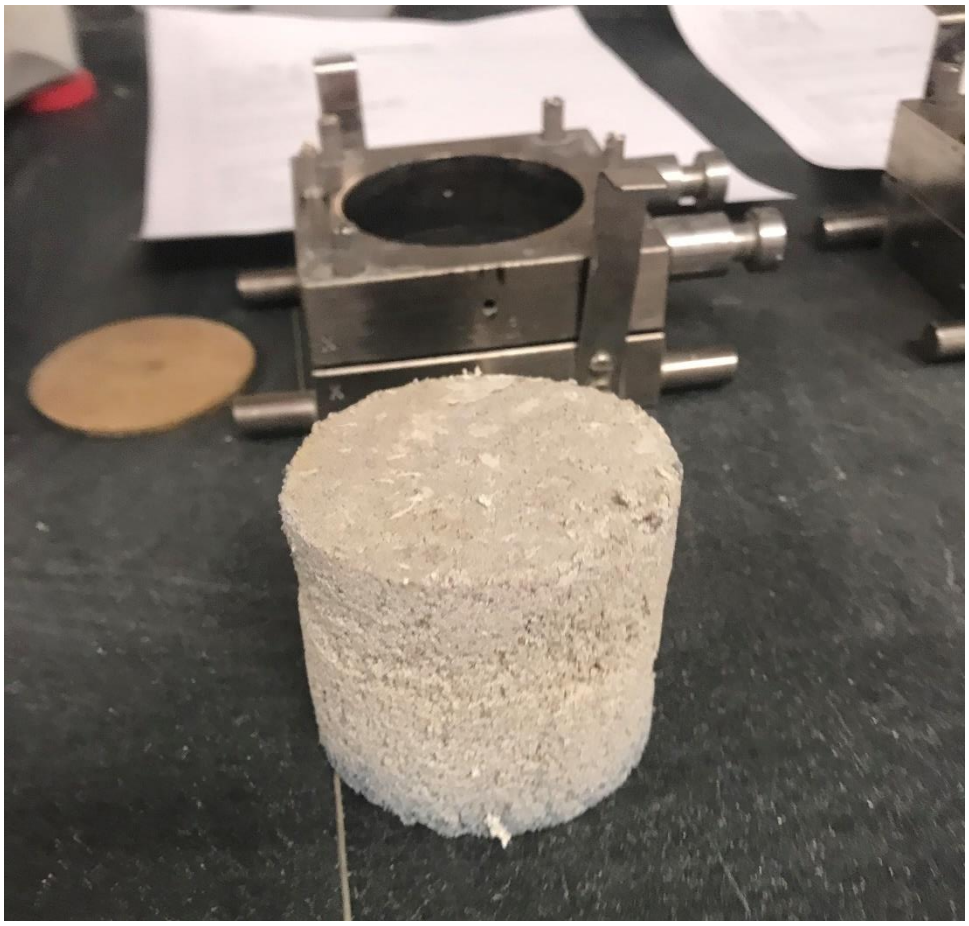

Figure A5. Sub-specimen after being cut from permeated specimen. The sub-specimen will be trimmed to a height of approximately 23 mm.

APPENDIX B – TABULATED HYDRAULIC CONDUCTIVITY AND DIRECT SHEAR DATA

Table B1. Hydraulic conductivity test results.

Test ID	Permeant Liquid	% Bentonite by Dry Mass	% Kaolinite by Dry Mass	% Rock Flour by Dry Mass	PVF	Final k (m/s)
7B-0-H	DI Water	7.26	0	0	0.6	4.2×10^{-11}
7B-10-H	10 mM CaCl2	7.26	0	0	8.5	1.0×10^{-8}
15K-0-H	DI Water	0	14.90	0	3.5	1.0×10^{-7}
15K-10-H	10 mM CaCl2	0	14.90	0	3.0	6.1×10^{-7}
14R-0-H	DI Water	0	0	14.00	2.5	1.7×10^{-7}
14R-10-H	10 mM CaCl2	0	0	14.00	2.7	4.6×10^{-7}
4B-0-H	DI Water	3.77	0	0	2.3	4.3×10^{-7}
4B-10-H	10 mM CaCl2	3.77	0	0	2.3	1.8×10^{-6}
4B7R-0-H	DI Water	3.50	0	7.27	2.2	5.3×10^{-11}
4B7R-10-H	10 mM CaCl2	3.50	0	7.27	4.3	2.8×10^{-8}
2B11R-0-H	DI Water	1.72	0	10.70	4.5	2.2×10^{-8}
2B11R-10-H	10 mM CaCl2	1.72	0	10.70	7.3	8.6×10^{-8}
5B4R-0-H	DI Water	5.34	0	3.70	1.9	9.1×10^{-11}
5B4R-10-H	10 mM CaCl2	5.34	0	3.70	11.1	2.9×10^{-7}
2B11R-0-A	DI Water	1.72	0	10.70	2.9	7.7×10^{-8}
2B11R-10-A	10 mM CaCl2	1.72	0	10.70	3.9	2.9×10^{-7}
4B7R-0-A	DI Water	3.50	0	7.27	1.9	5.0×10^{-9}
4B7R-10-A	10 mM CaCl2	3.50	0	7.27	3.8	1.4×10^{-8}
5B4R-0-A	DI Water	5.34	0	3.70	0.8	1.9×10^{-11}
5B4R-10-A	10 mM CaCl2	5.34	0	3.70	2.9	7.5×10^{-10}
8B-10-A	10 mM CaCl2	8.02	0	0	5.0	8.5×10^{-11}
10B-500-A	500 mM CaCl2	10.00	0	0	2.8	7.4×10^{-8}
15B-500-A	500 mM CaCl2	15.00	0	0	2.6	2.7×10^{-7}

Table B2. Direct shear test results for 35 kPa effective stress.

Test ID	Permeant Liquid	Equivalent Fines Percentage	φ'_{peak}	φ'_{u}	$e_{initial}$	$e_{ultimate}$	Rel. Horz. Disp. at φ'_{peak}
Sand	-	-	46.8	37.7	0.52	0.56	0.03
7B-0-H	DI Water	7.26	61.7	52.7	0.56	0.60	0.04
7B-10-H	10 mM CaCl2	7.26	53.1	46.3	0.61	0.66	0.06
15K-0-H	DI Water	2.98	46.4	36.6	0.37	0.46	0.04
15K-10-H	10 mM CaCl2	2.98	42.2	39.2	0.51	0.51	0.12
14R-0-H	DI Water	2.80	42.3	35.8	0.48	0.49	0.07
14R-10-H	10 mM CaCl2	2.80	48.9	39.8	0.49	0.51	0.08
4B-0-H	DI Water	3.77	42.5	35.1	0.63	0.64	0.08
4B-10-H	10 mM CaCl2	3.77	40.4	32.2	0.68	0.70	0.05
4B7R-0-H	DI Water	4.95	58.0	48.1	0.55	0.59	0.04
4B7R-10-H	10 mM CaCl2	4.95	41.9	36.5	0.53	0.53	0.04
2B11R-0-H	DI Water	3.86	51.8	40.3	0.52	0.56	0.07
2B11R-10-H	10 mM CaCl2	3.86	45.8	35.7	0.52	0.55	0.04
5B4R-0-H	DI Water	6.08	59.2	44.8	0.57	0.61	0.04
5B4R-10-H	10 mM CaCl2	6.08	50.0	47.3	0.61	0.63	0.07
2B11R-0-A	DI Water	3.86	48.0	38.7	0.47	0.50	0.06
2B11R-10-A	10 mM CaCl2	3.86	47.3	37.4	0.61	0.63	0.09
4B7R-0-A	DI Water	4.95	53.7	42.7	0.48	0.53	0.07
4B7R-10-A	10 mM CaCl2	4.95	49.9	44.9	0.54	0.60	0.06
5B4R-0-A	DI Water	6.08	48.7	42.5	0.55	0.58	0.06
5B4R-10-A	10 mM CaCl2	6.08	43.8	36.5	0.63	0.66	0.10
8B-10-A	10 mM CaCl2	8.02	53.4	43.0	0.63	0.67	0.05
10B-500-A	500 mM CaCl2	10.00	57.9	42.9	0.58	0.63	0.04
15B-500-A	500 mM CaCl2	15.00	51.6	41.8	0.59	0.63	0.06
15B-0-A	DI Water	15.00	71.7	63.5	0.68	0.80	0.14
15B-0-dup-A	DI Water	15.00	66.5	66.1	0.69	0.82	0.16
20B-0-A	DI Water	20.00	60.8	60.5	0.69	0.76	0.17
20B-0-dup-A	DI Water	20.00	66.7	66.3	0.61	0.73	0.21
30B-0-A	DI Water	30.00	63.4	63.3	0.67	0.80	0.20
30B-0-dup-A	DI Water	30.00	63.2	63.0	0.75	0.90	0.23

Table B3. Direct shear test results for 825 kPa effective stress.

Test ID	Permeant Liquid	Equivalent Fines Percentage	φ'_{peak}	φ'_{u}	$e_{initial}$	$e_{ultimate}$	Rel. Horz. Disp. at φ'_{peak}
Sand	-	-	34.7	32.6	0.58	0.59	0.03
7B-0-H	DI Water	7.26	40.1	35.2	0.53	0.54	0.08
7B-10-H	10 mM CaCl2	7.26	38.6	33.6	0.49	0.50	0.09
15K-0-H	DI Water	2.98	35.5	35.2	0.41	0.40	0.09
15K-10-H	10 mM CaCl2	2.98	33.8	32.4	0.46	0.45	0.06
14R-0-H	DI Water	2.80	34.9	31.2	0.39	0.39	0.07
14R-10-H	10 mM CaCl2	2.80	37.5	32.9	0.42	0.42	0.07
4B-0-H	DI Water	3.77	35.2	31.8	0.48	0.49	0.04
4B-10-H	10 mM CaCl2	3.77	32.1	30.8	0.60	0.59	0.14
4B7R-0-H	DI Water	4.95	38.4	33.4	0.45	0.46	0.04
4B7R-10-H	10 mM CaCl2	4.95	30.3	30.0	0.47	0.44	0.06
2B11R-0-H	DI Water	3.86	37.6	34.6	0.38	0.37	0.09
2B11R-10-H	10 mM CaCl2	3.86	35.5	33.2	0.38	0.37	0.09
5B4R-0-H	DI Water	6.08	39.7	32.1	0.43	0.45	0.05
5B4R-10-H	10 mM CaCl2	6.08	35.8	33.5	0.52	0.51	0.11
2B11R-0-A	DI Water	3.86	36.0	32.5	0.41	0.42	0.06
2B11R-10-A	10 mM CaCl2	3.86	35.9	33.4	0.45	0.45	0.12
4B7R-0-A	DI Water	4.95	39.7	33.6	0.42	0.44	0.06
4B7R-10-A	10 mM CaCl2	4.95	36.5	36.1	0.47	0.45	0.10
5B4R-0-A	DI Water	6.08	38.2	34.9	0.48	0.49	0.11
5B4R-10-A	10 mM CaCl2	6.08	33.8	32.1	0.40	0.38	0.11
8B-10-A	10 mM CaCl2	8.02	35.3	35.3	0.60	0.56	0.11
10B-500-A	500 mM CaCl2	10.00	36.1	31.9	0.50	0.52	0.04
15B-500-A	500 mM CaCl2	15.00	37.6	34.9	0.42	0.42	0.11
15B-0-A	DI Water	15.00	34.8	34.4	0.48	0.49	0.13
15B-0-dup-A	DI Water	15.00	35.3	34.8	0.44	0.43	0.11
20B-0-A	DI Water	20.00	20.7	20.7	0.50	0.48	0.19
20B-0-dup-A	DI Water	20.00	17.2	17.2	0.48	0.45	0.22
30B-0-A	DI Water	30.00	14.4	14.2	0.53	0.51	0.15
30B-0-dup-A	DI Water	30.00	9.6	9.4	0.56	0.53	0.13

APPENDIX C – HYDRAULIC CONDUCTIVITY TEST RESULTS

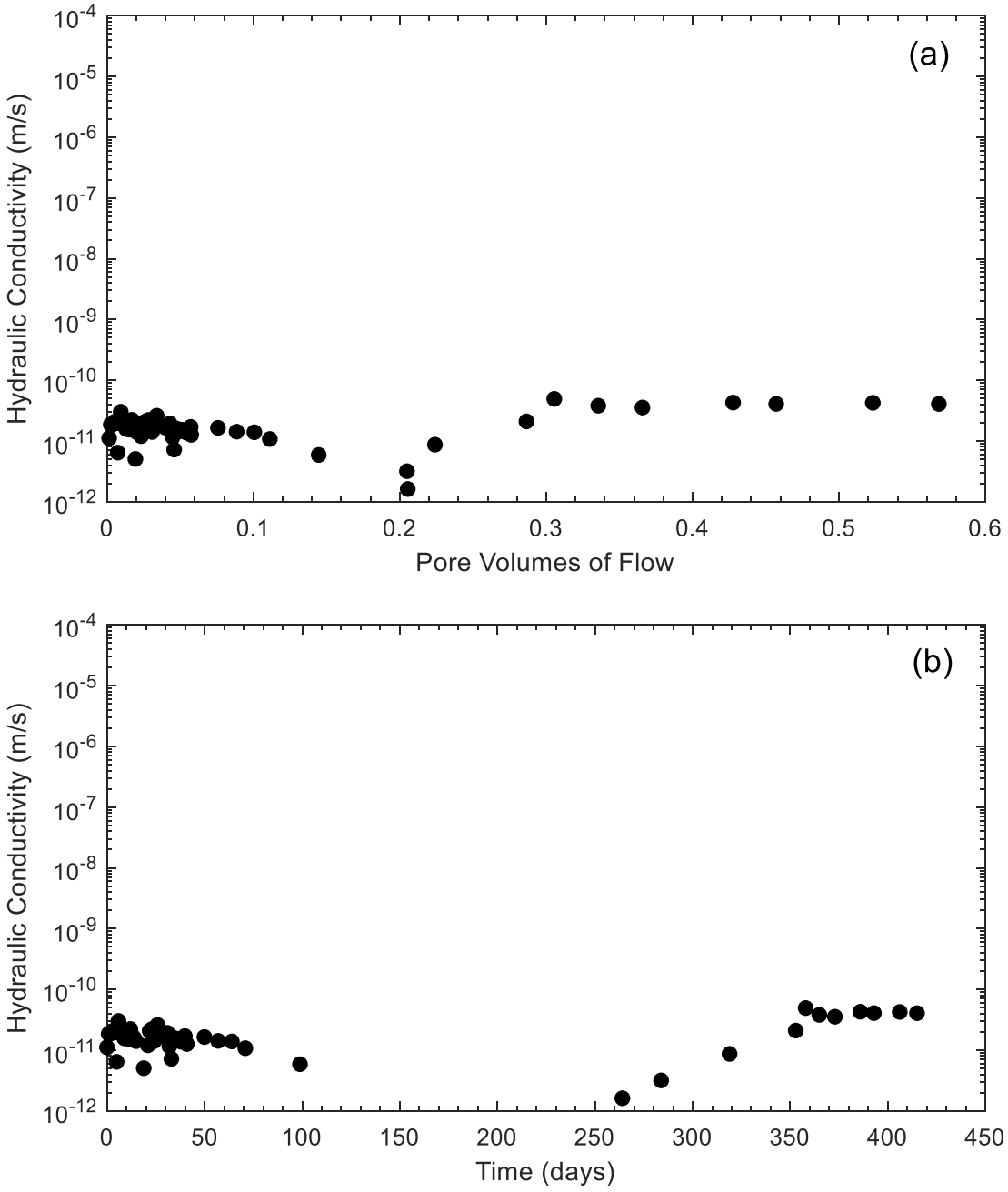

Figure C1. Hydraulic conductivity versus: (a) Pore volumes of flow; (b) time for test 7B-0-H.

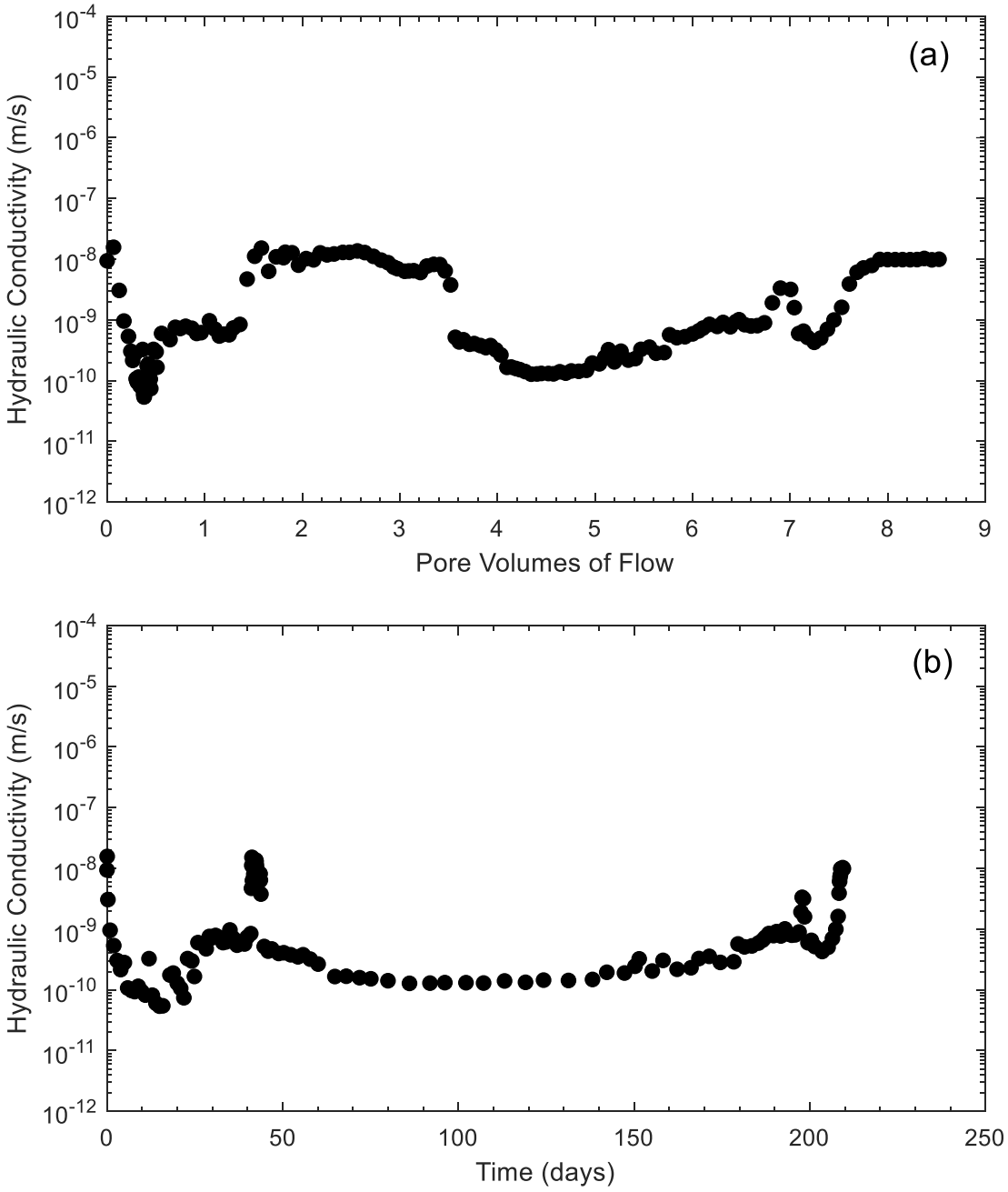

Figure C2. Hydraulic conductivity versus: (a) Pore volumes of flow; (b) time for test 7B-10-H.

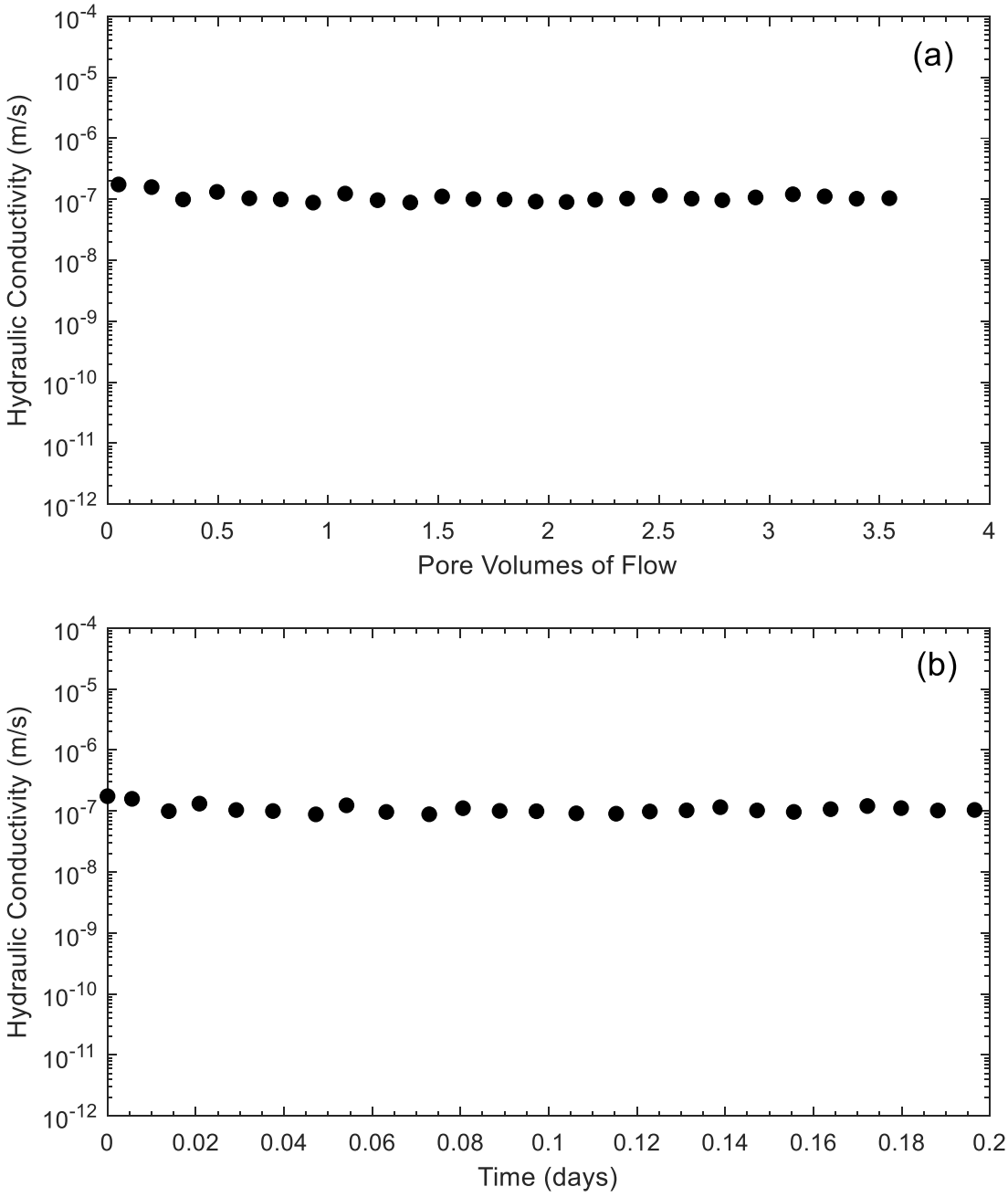

Figure C3. Hydraulic conductivity versus: (a) Pore volumes of flow; (b) time for test 15K-0-H.

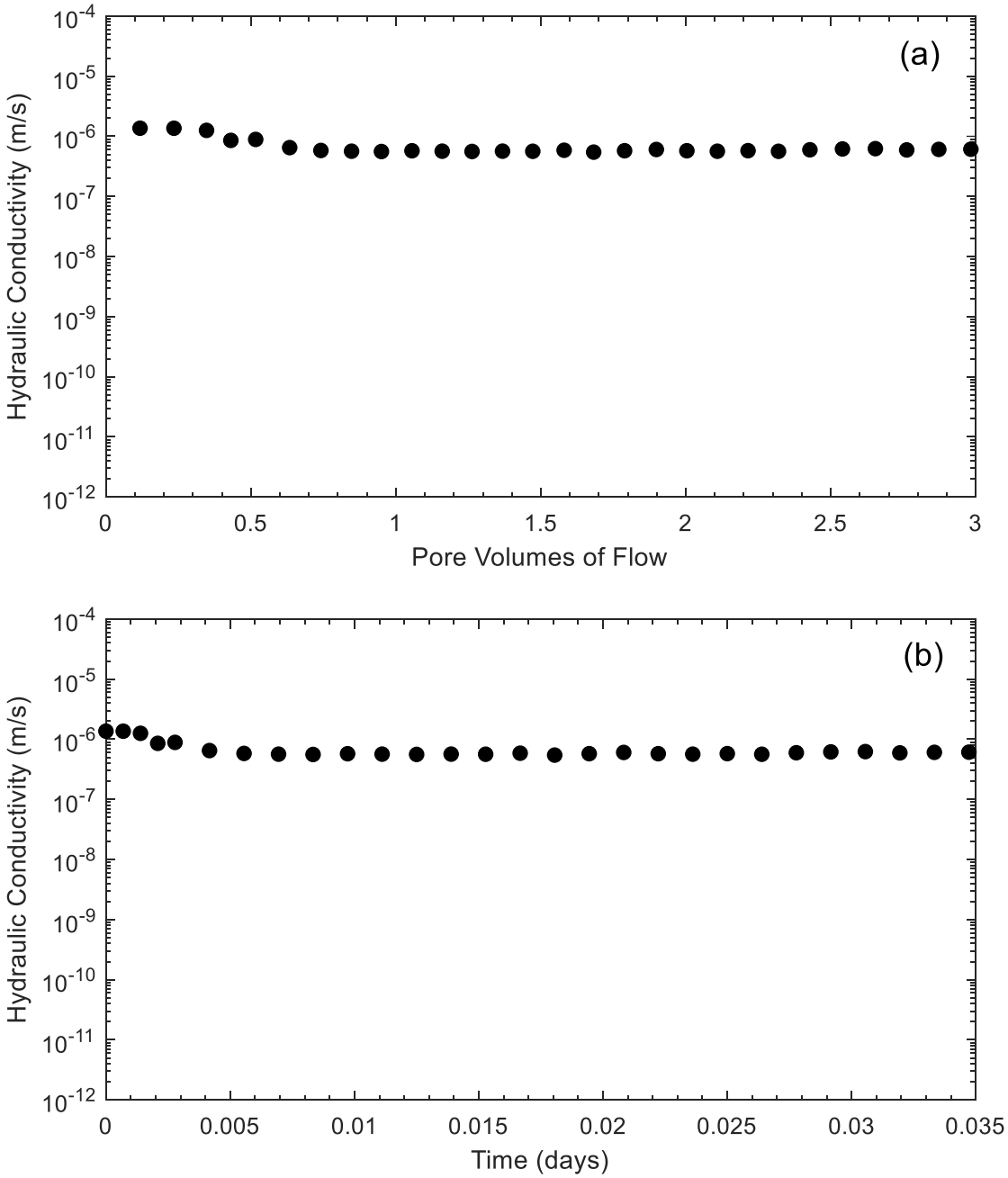

Figure C4. Hydraulic conductivity versus: (a) Pore volumes of flow; (b) time for test 15K-10-H.

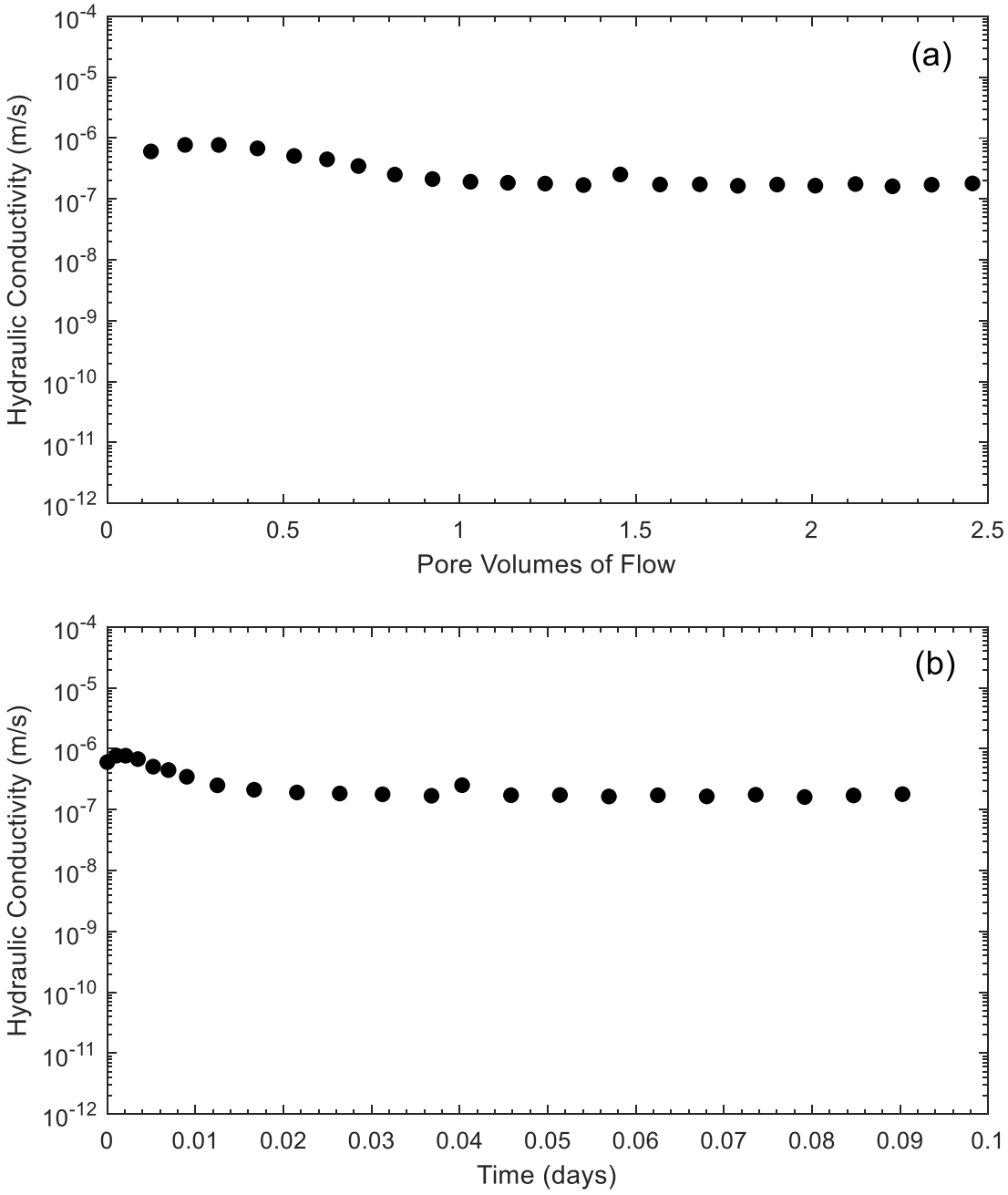

Figure C5. Hydraulic conductivity versus: (a) Pore volumes of flow; (b) time for test 14R-0-H.

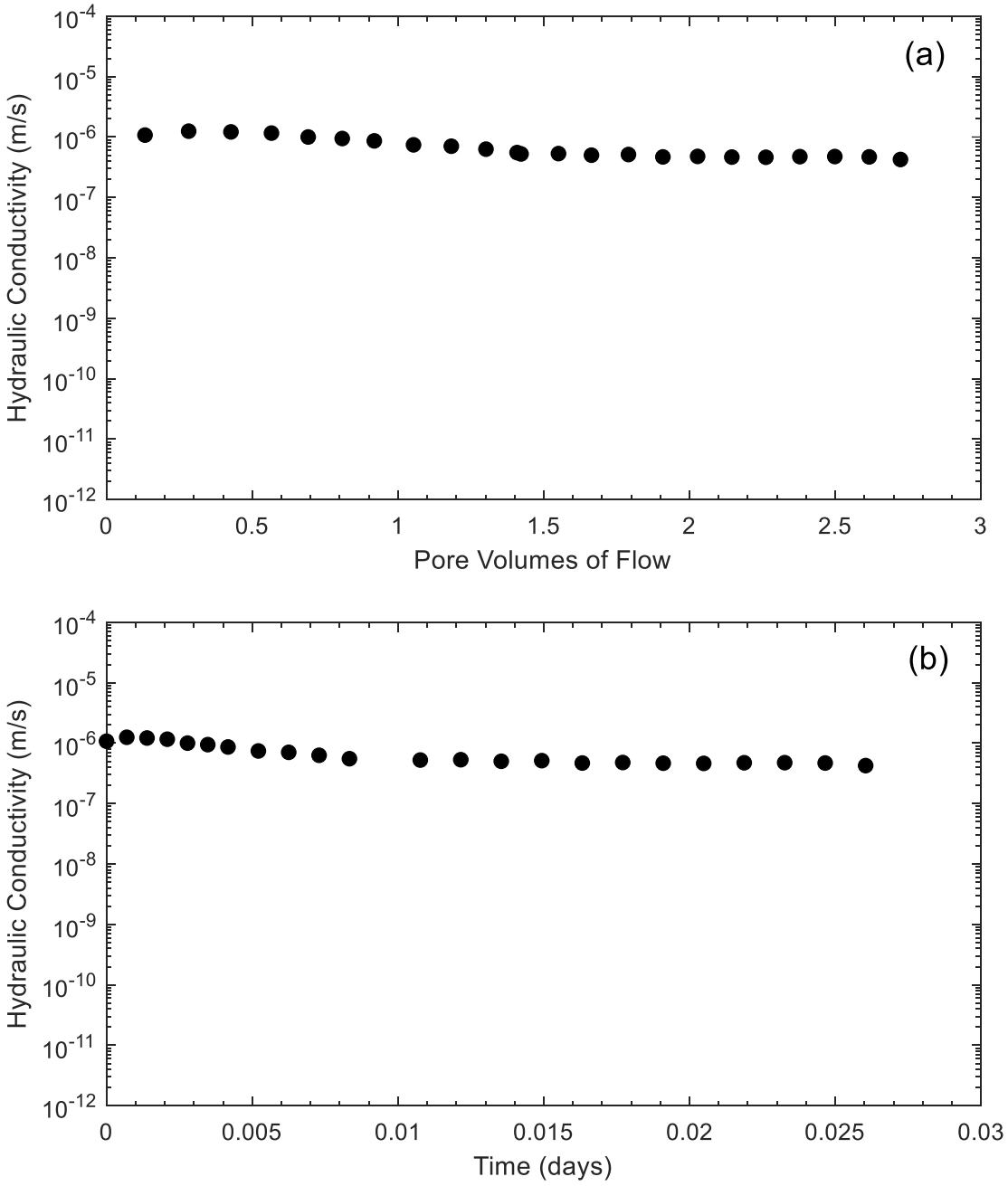

Figure C6. Hydraulic conductivity versus: (a) Pore volumes of flow; (b) time for test 14R-10-H.

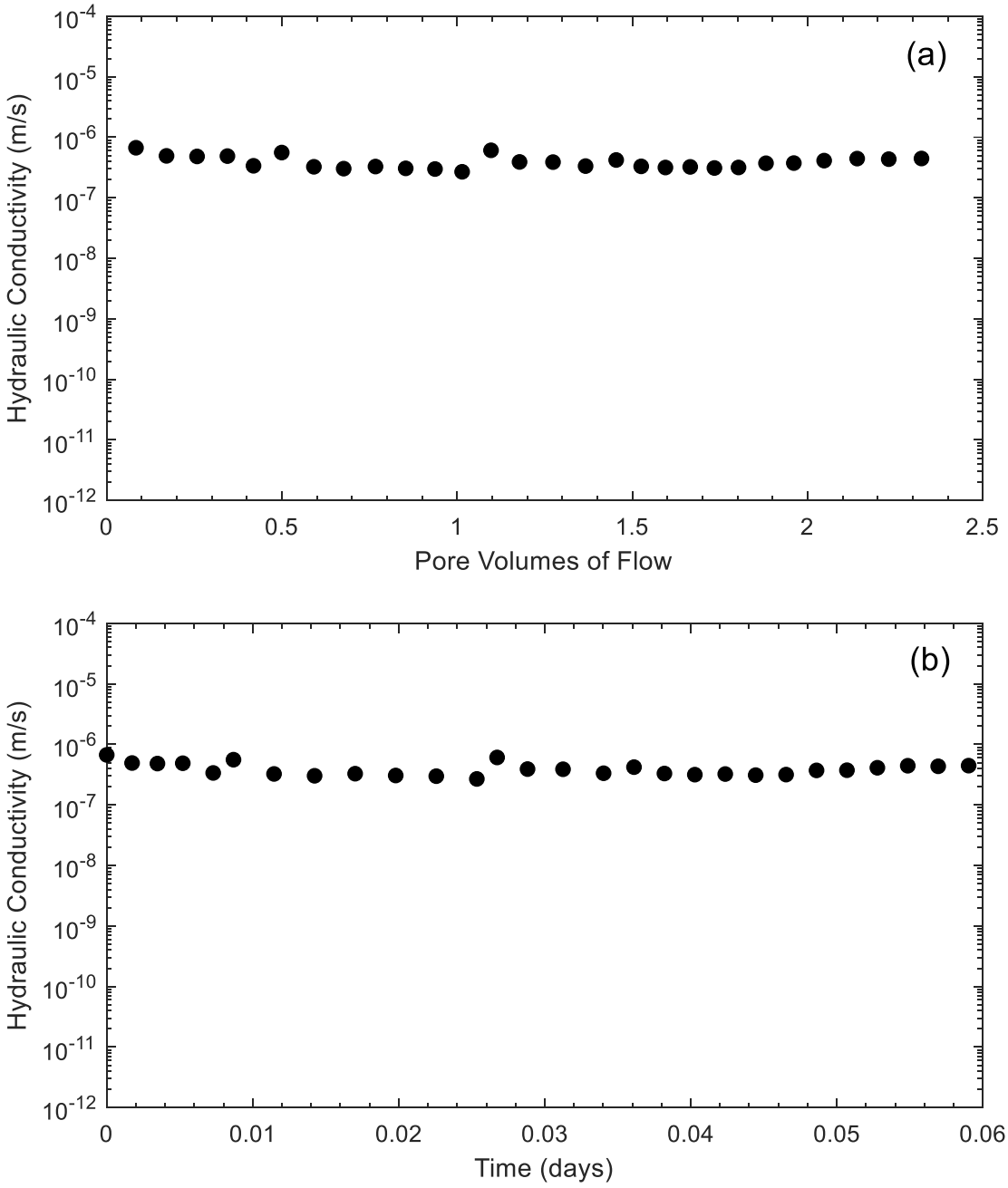

Figure C7. Hydraulic conductivity versus: (a) Pore volumes of flow; (b) time for test 4B-0-H.

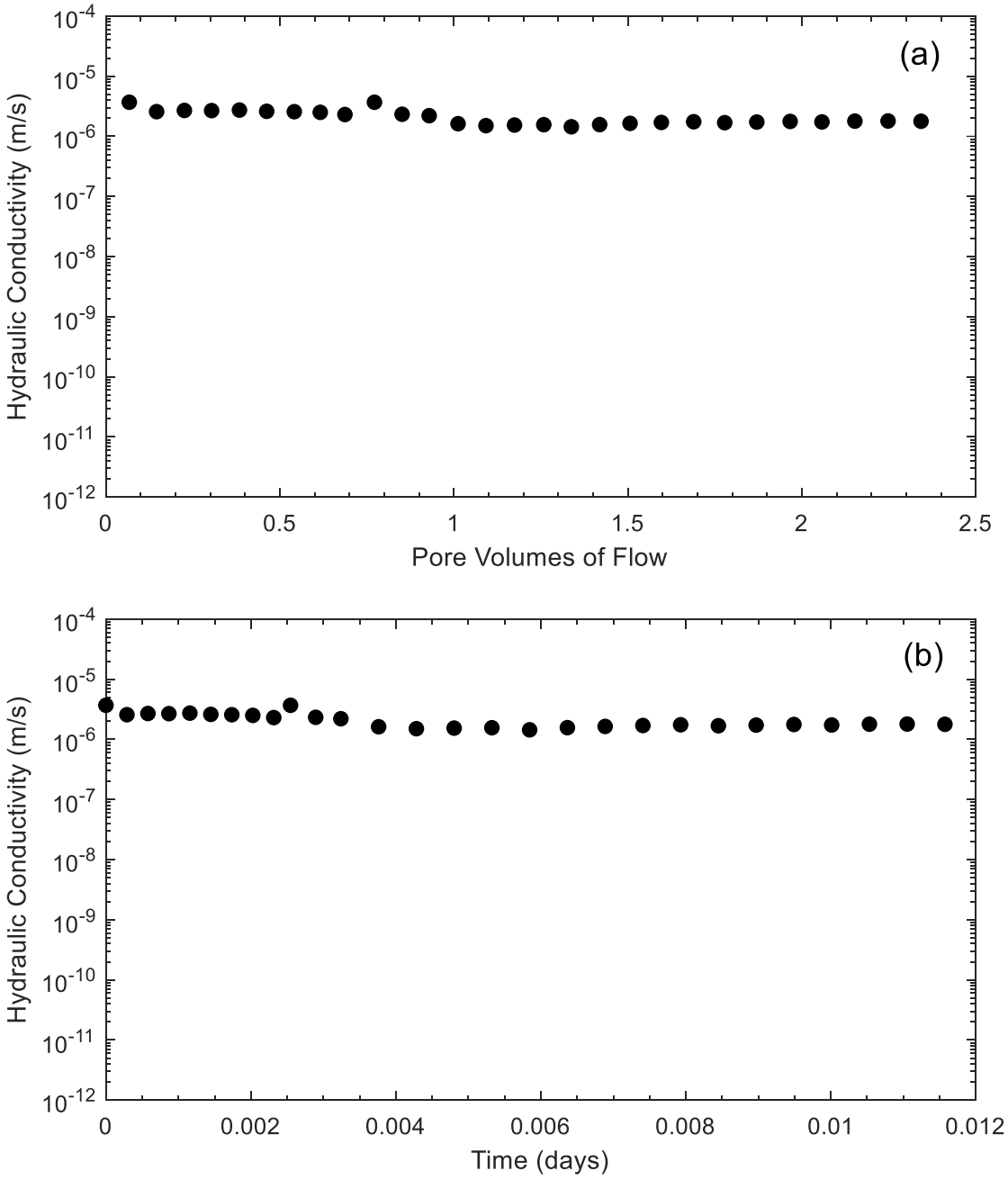

Figure C8. Hydraulic conductivity versus: (a) Pore volumes of flow; (b) time for test 4B-10-H.

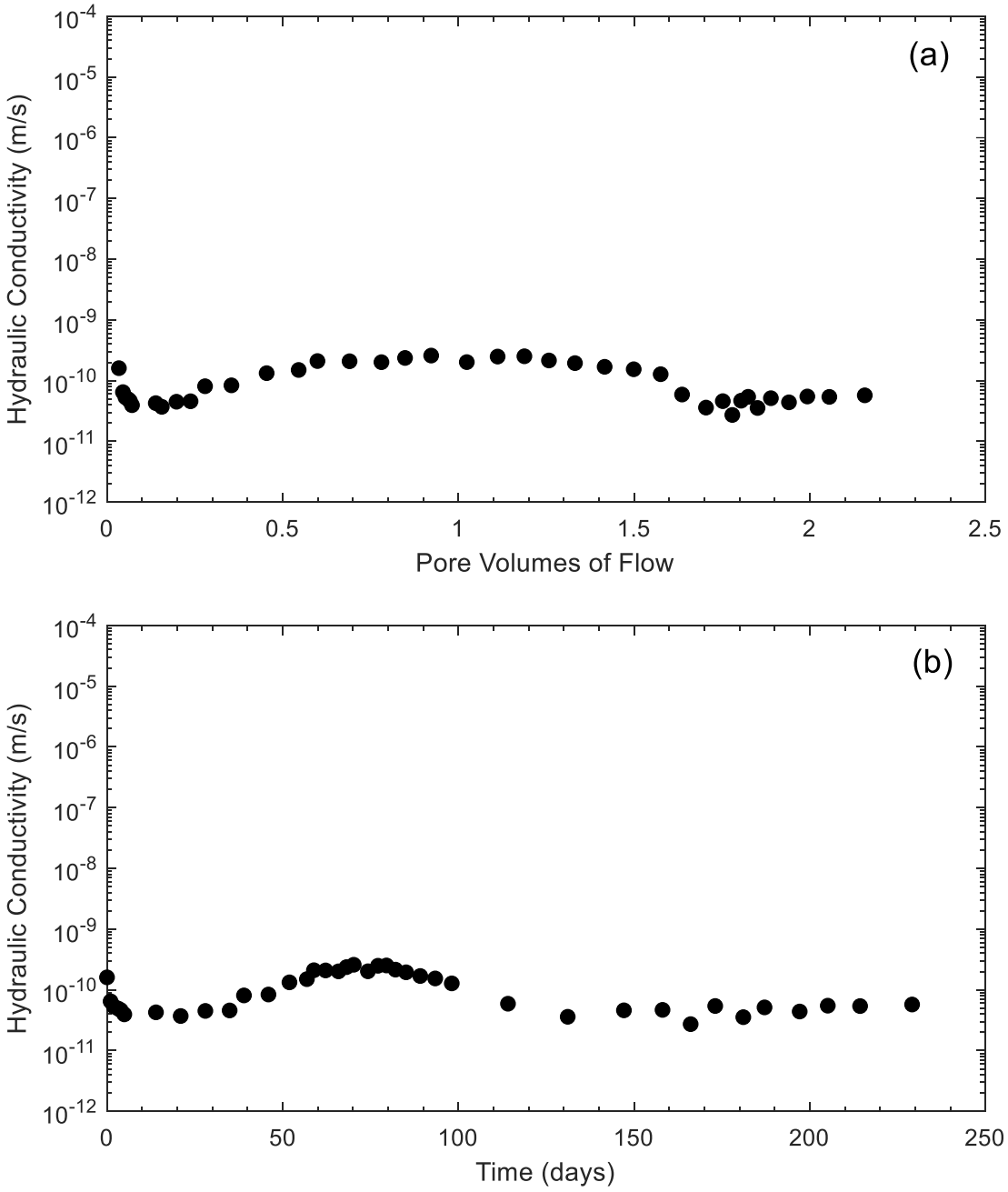

Figure C9. Hydraulic conductivity versus: (a) Pore volumes of flow; (b) time for test 4B7R-0-H.

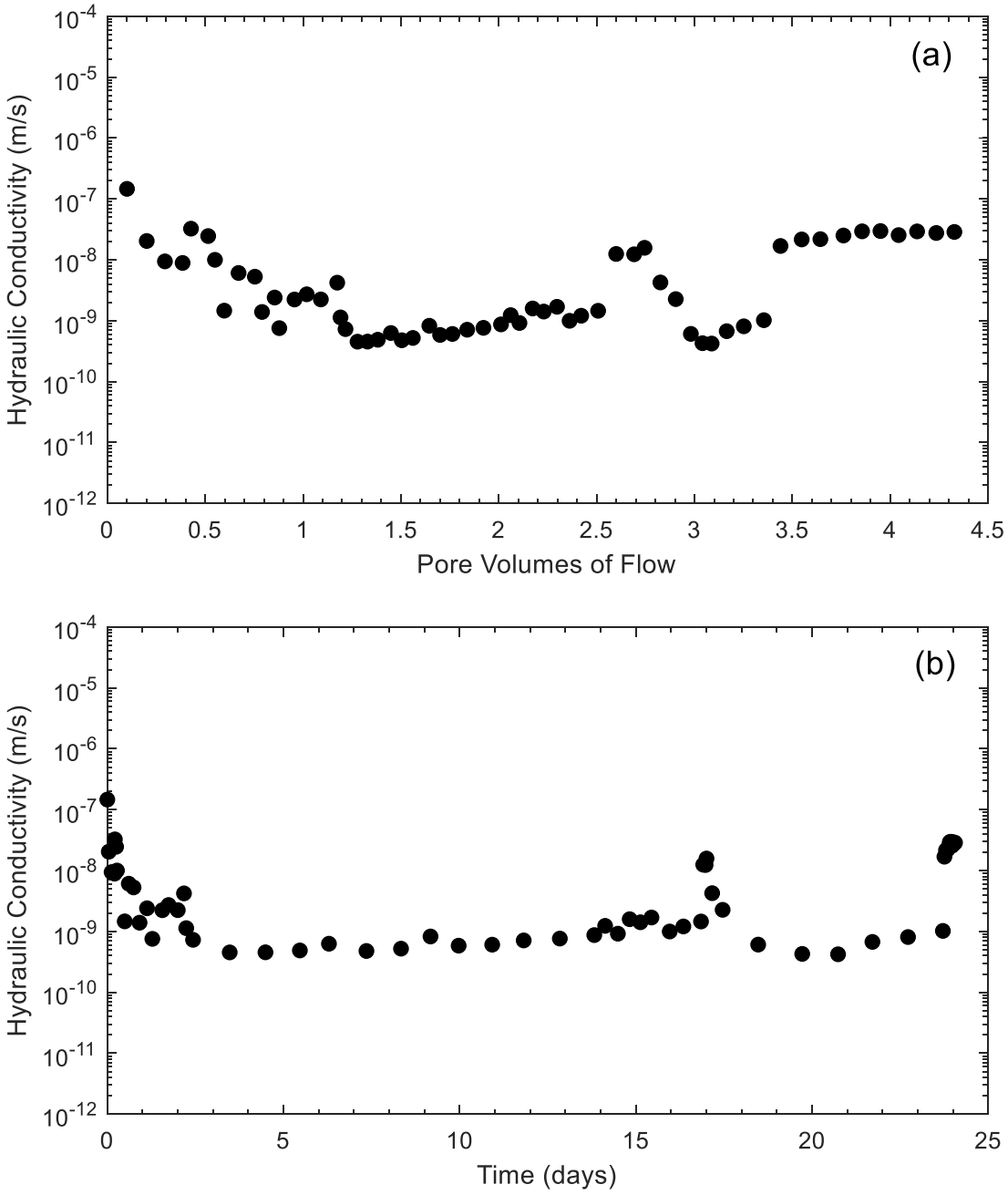

Figure C10. Hydraulic conductivity versus: (a) Pore volumes of flow; (b) time for test 4B7R-10-H.

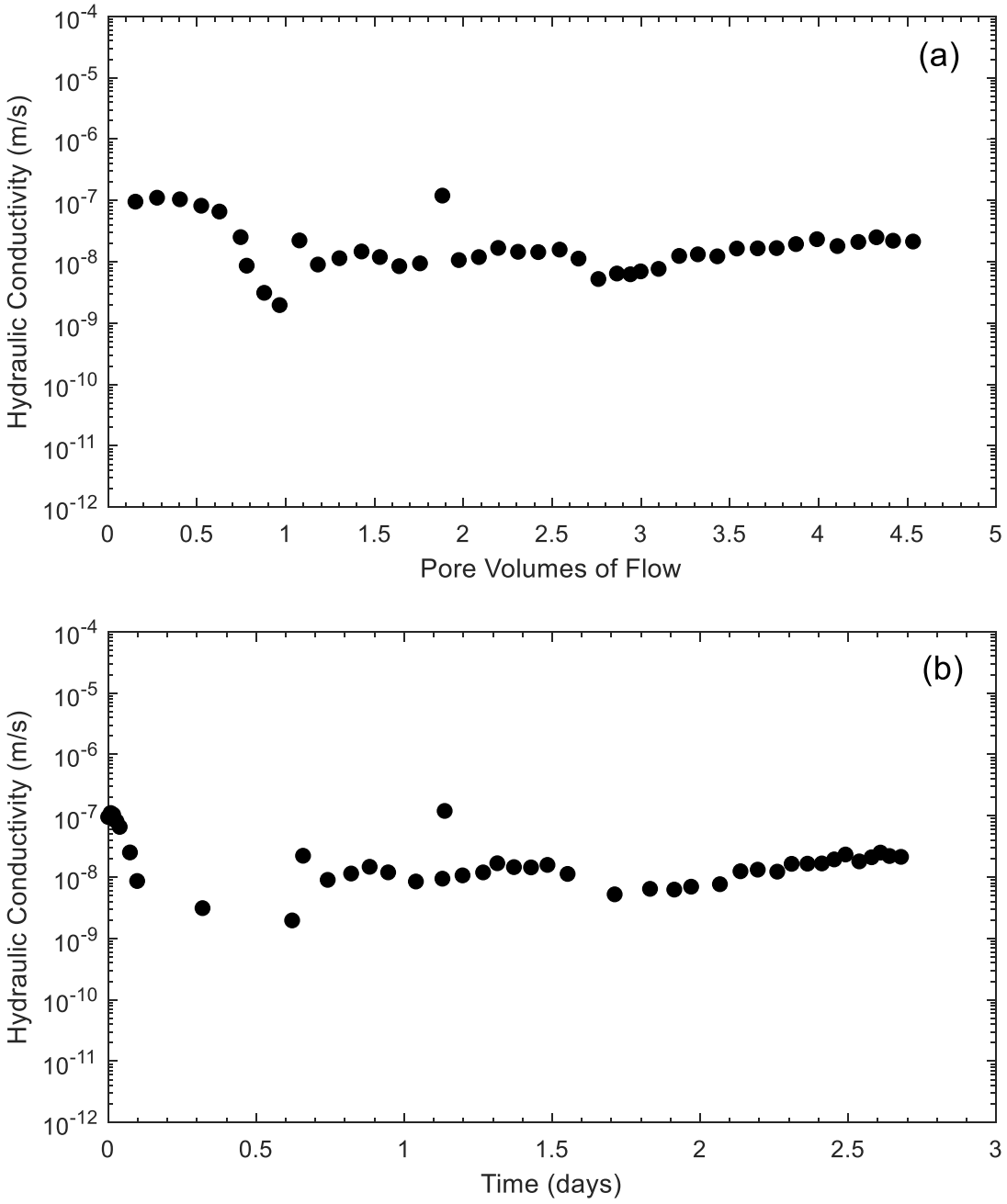

Figure C11. Hydraulic conductivity versus: (a) Pore volumes of flow; (b) time for test 2B11R-0-H.

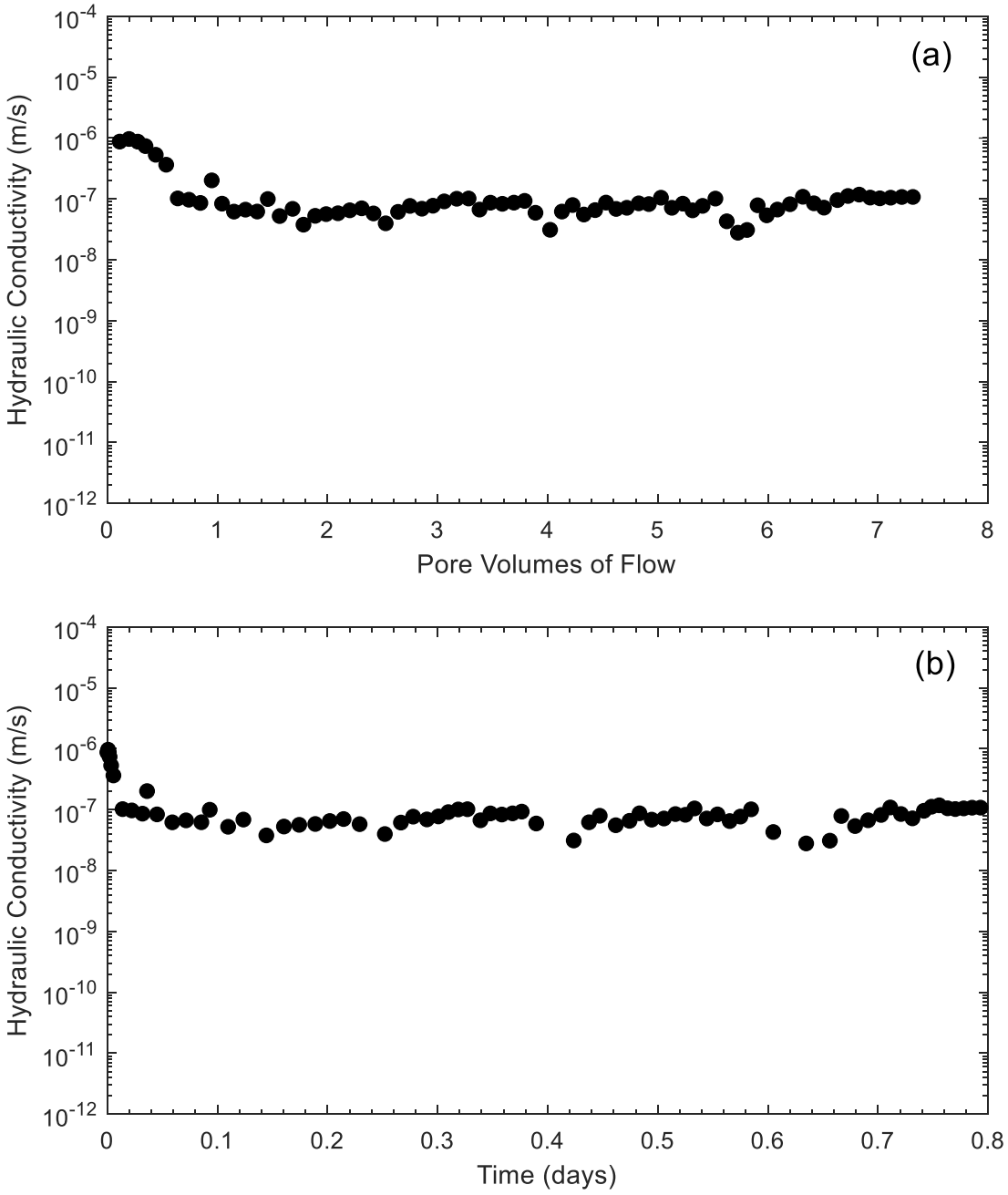

Figure C12. Hydraulic conductivity versus: (a) Pore volumes of flow; (b) time for test 2B11R-10-H.

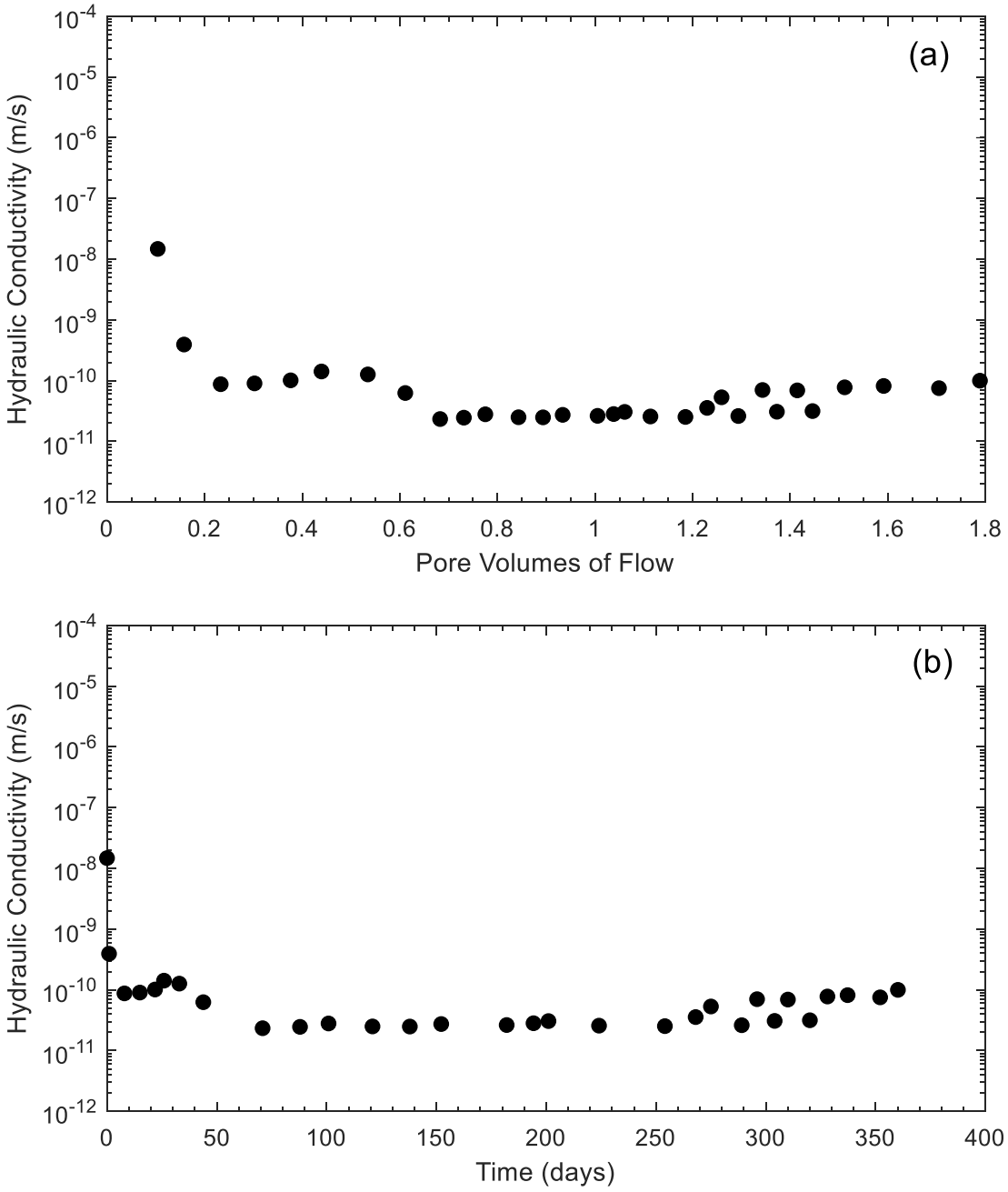

Figure C13. Hydraulic conductivity versus: (a) Pore volumes of flow; (b) time for test 5B4R-0-H.

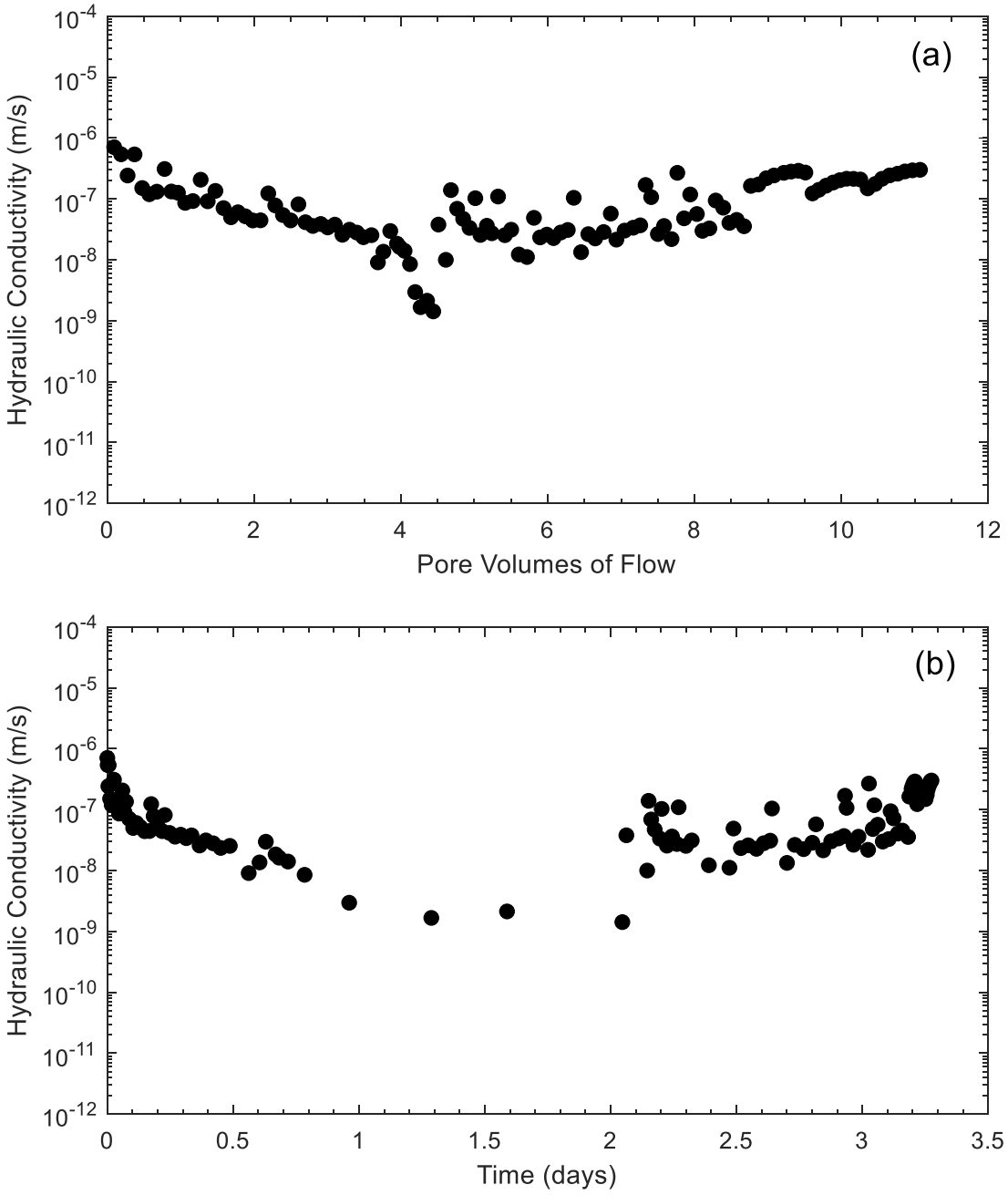

Figure C14. Hydraulic conductivity versus: (a) Pore volumes of flow; (b) time for test 5B4R-10-H.

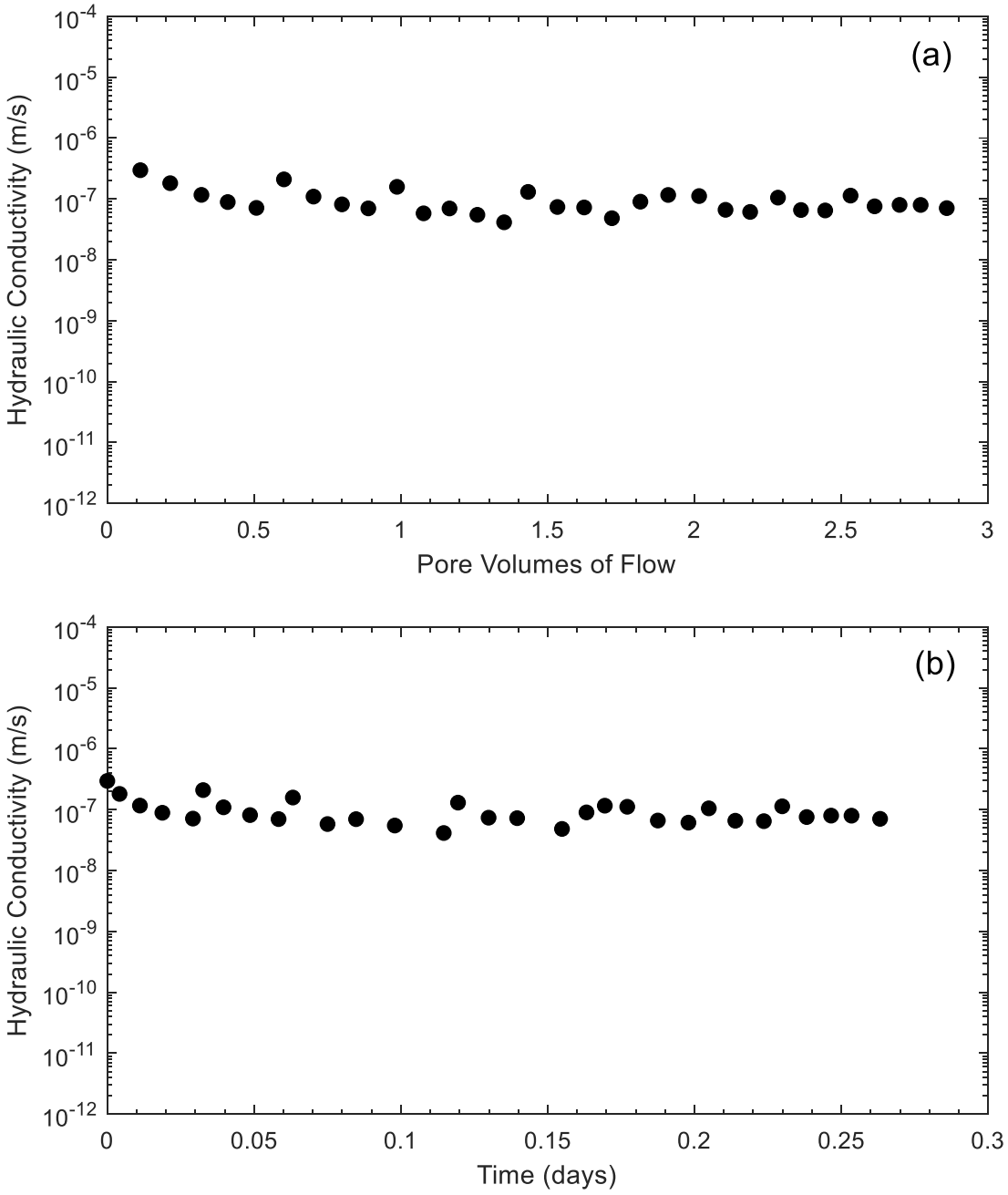

Figure C15. Hydraulic conductivity versus: (a) Pore volumes of flow; (b) time for test 2B11R-0-A.

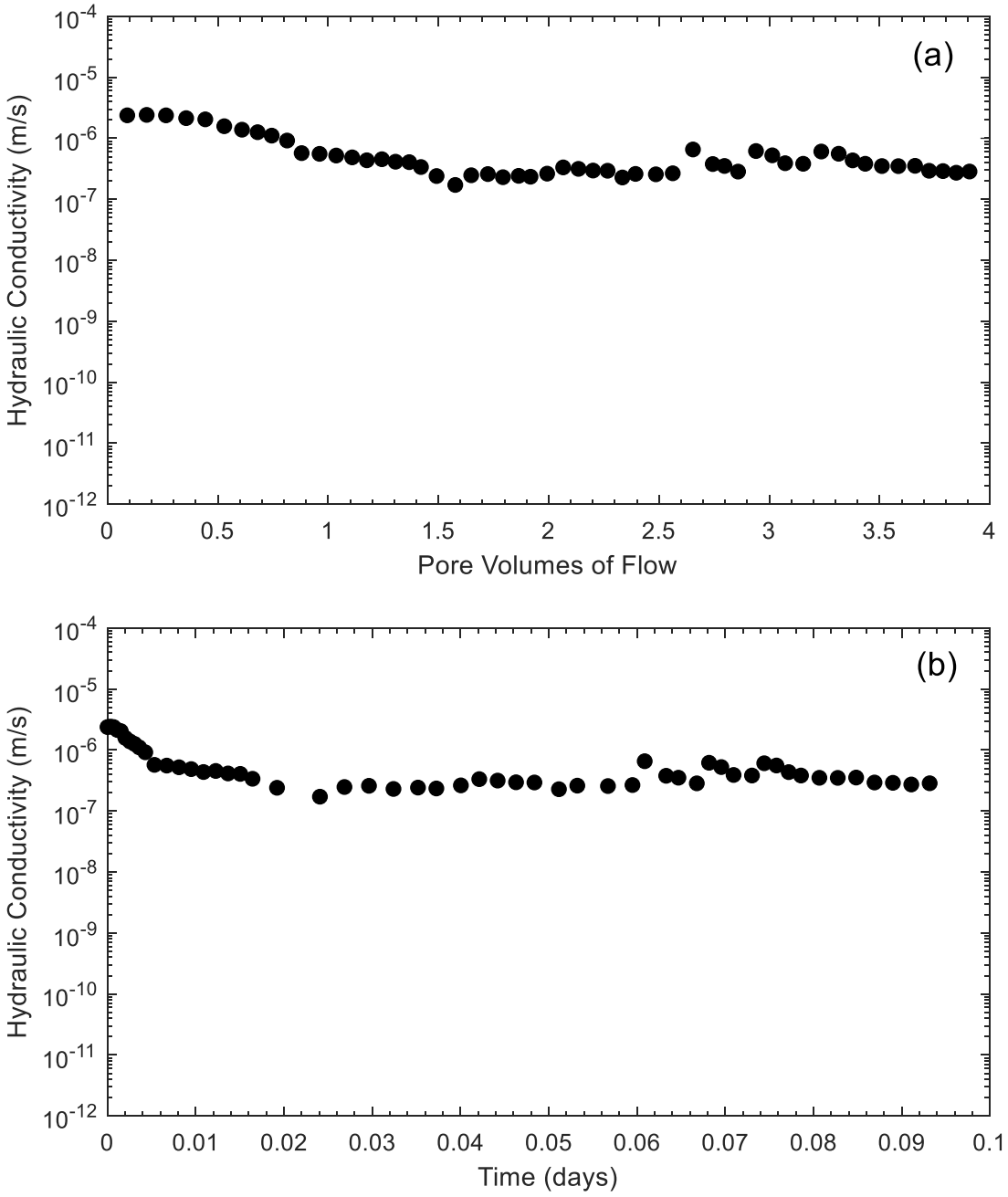

Figure C16. Hydraulic conductivity versus: (a) Pore volumes of flow; (b) time for test 2B11R-10-A.

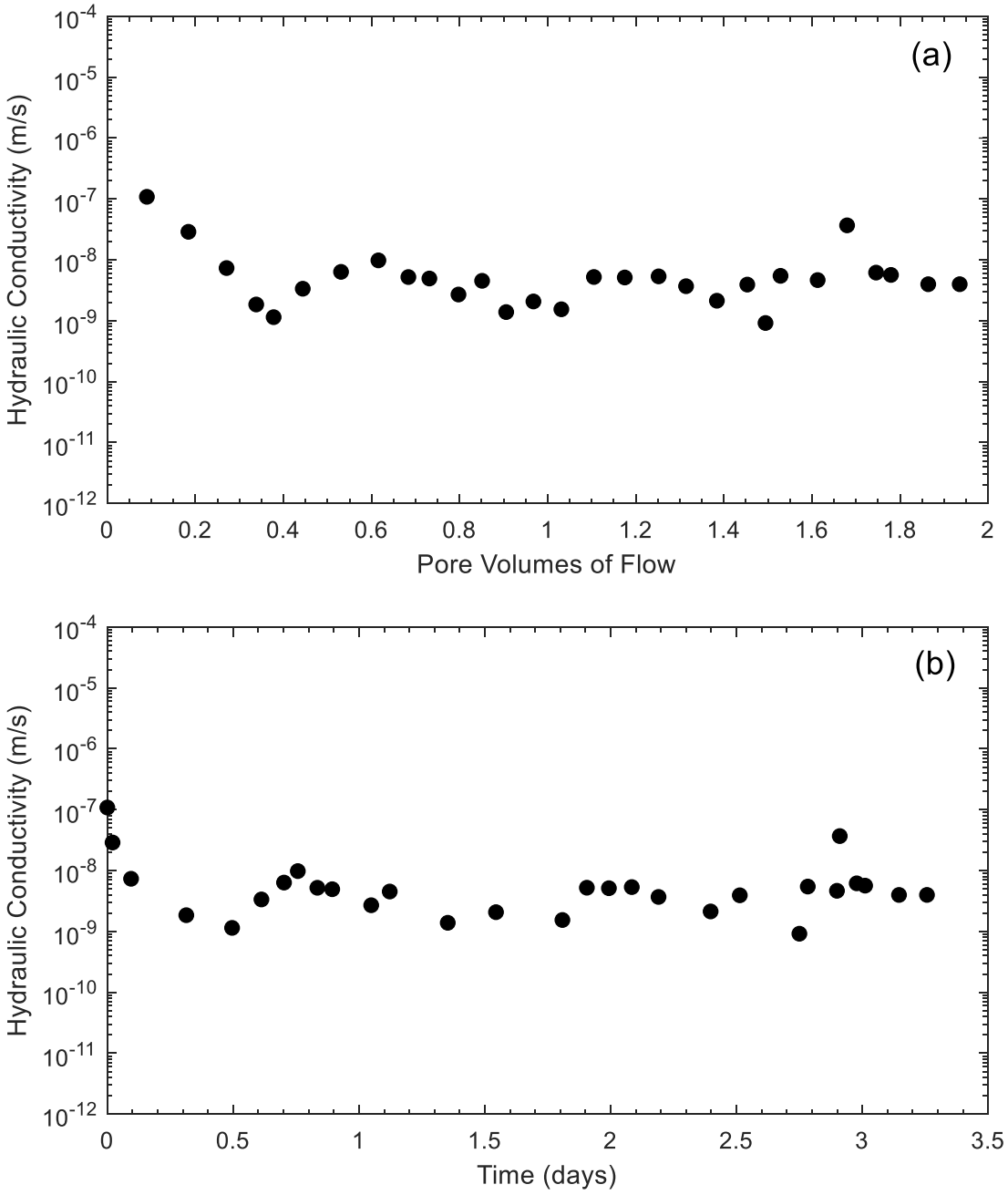

Figure C17. Hydraulic conductivity versus: (a) Pore volumes of flow; (b) time for test 4B7R-0-A.

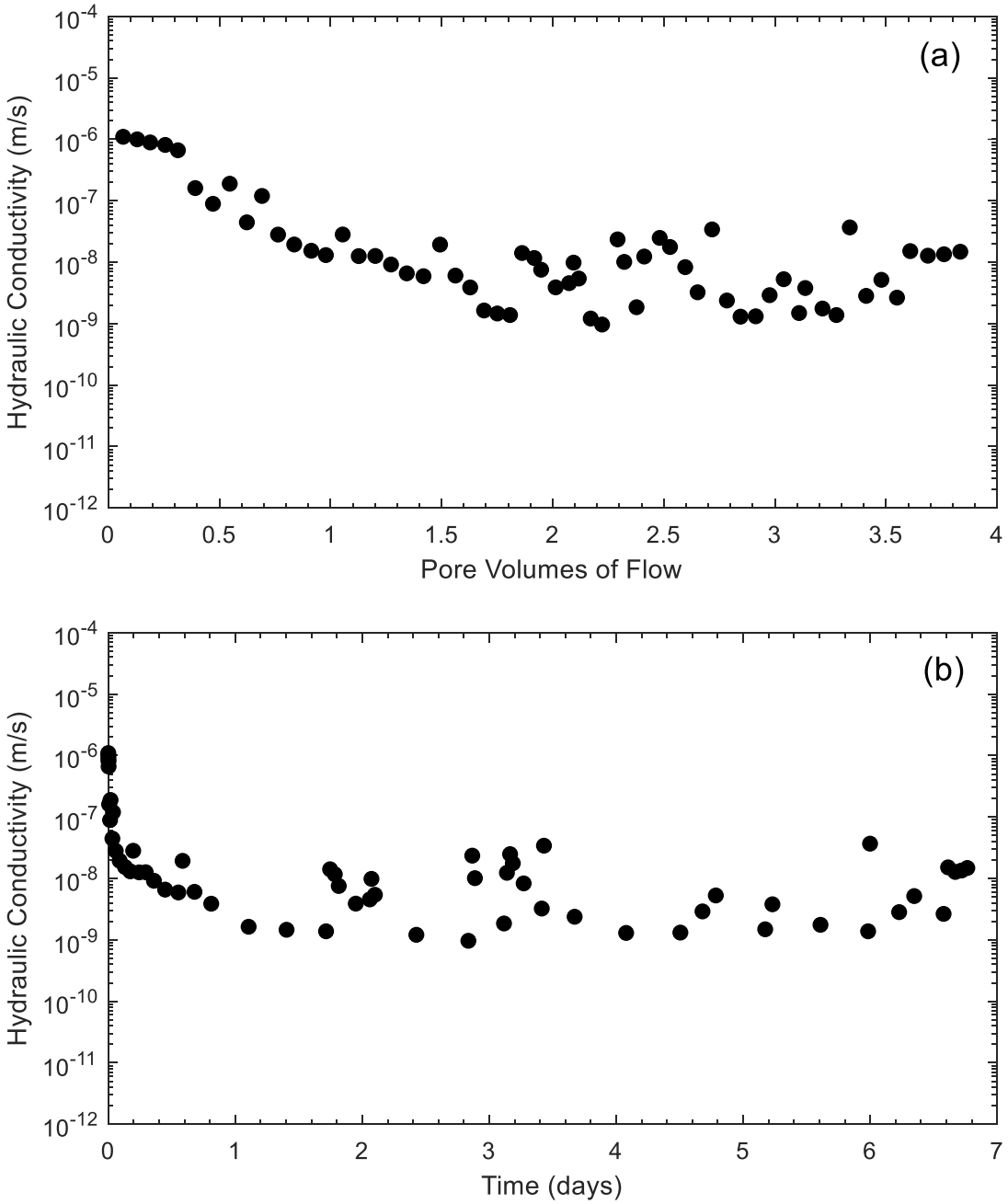

Figure C18. Hydraulic conductivity versus: (a) Pore volumes of flow; (b) time for test 4B7R-10-A.

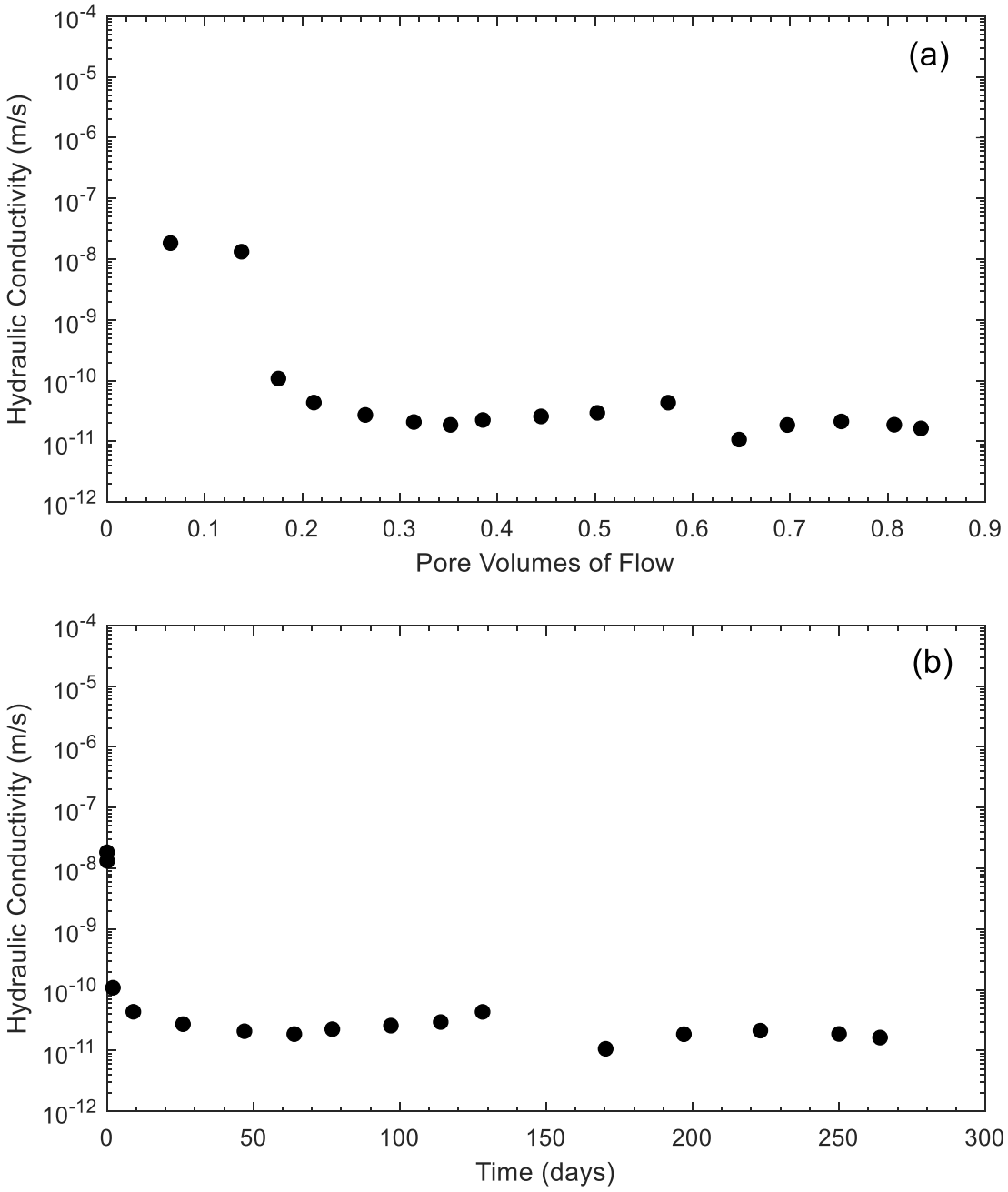

Figure C19. Hydraulic conductivity versus: (a) Pore volumes of flow; (b) time for test 5B4R-0-A.

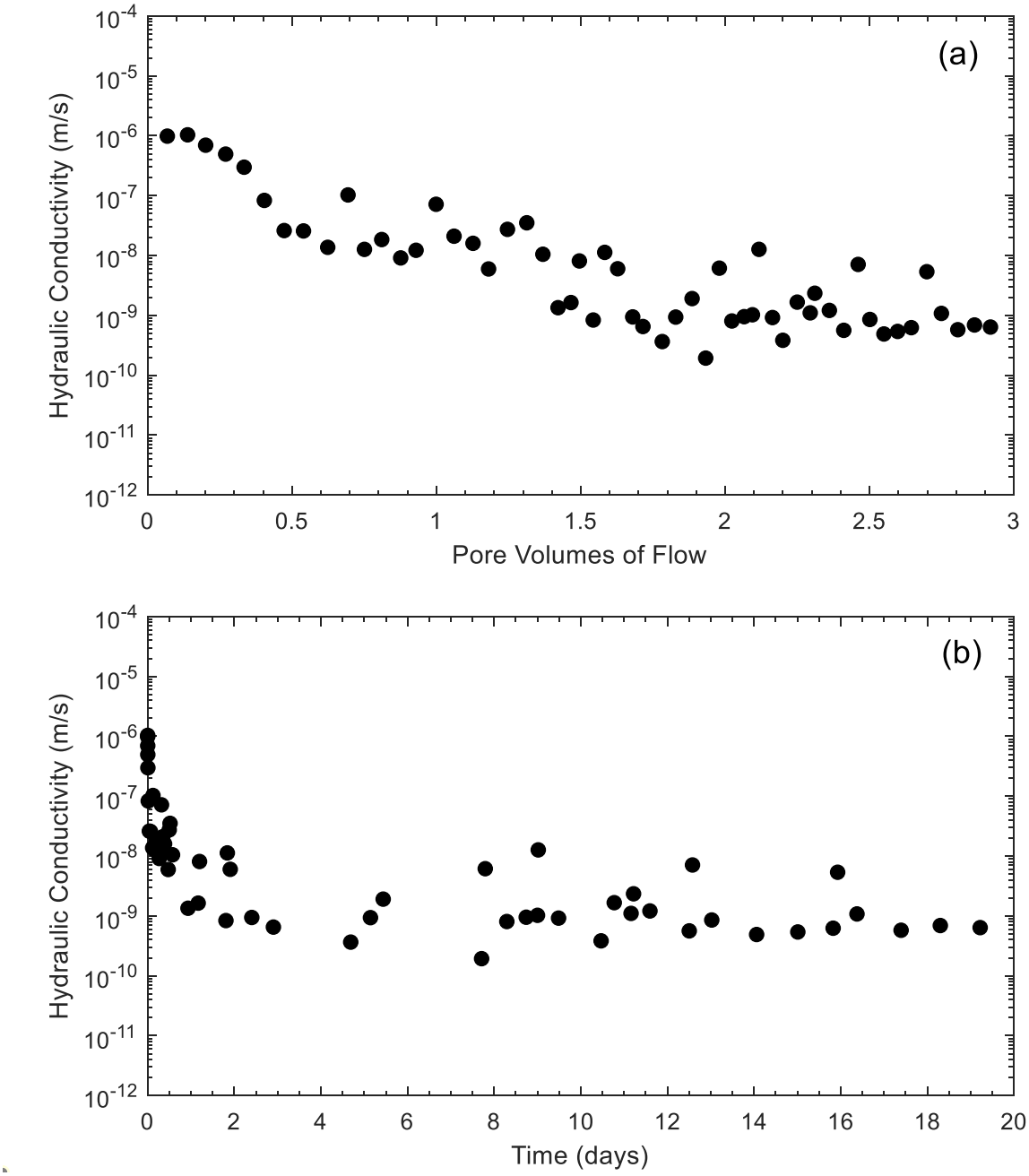

Figure C20. Hydraulic conductivity versus: (a) Pore volumes of flow; (b) time for test 5B4R-10-A.

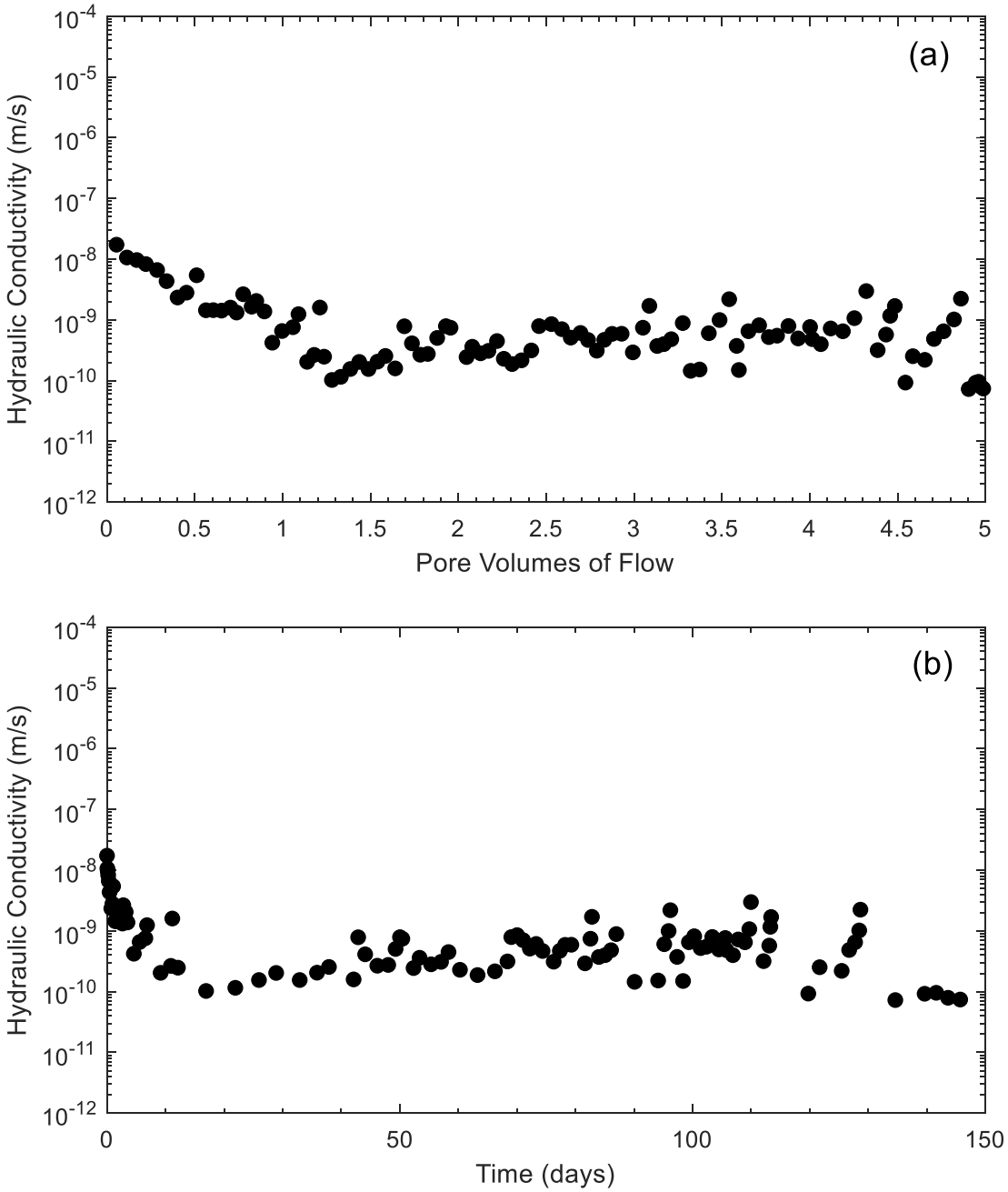

Figure C21. Hydraulic conductivity versus: (a) Pore volumes of flow; (b) time for test 8B-10-A.

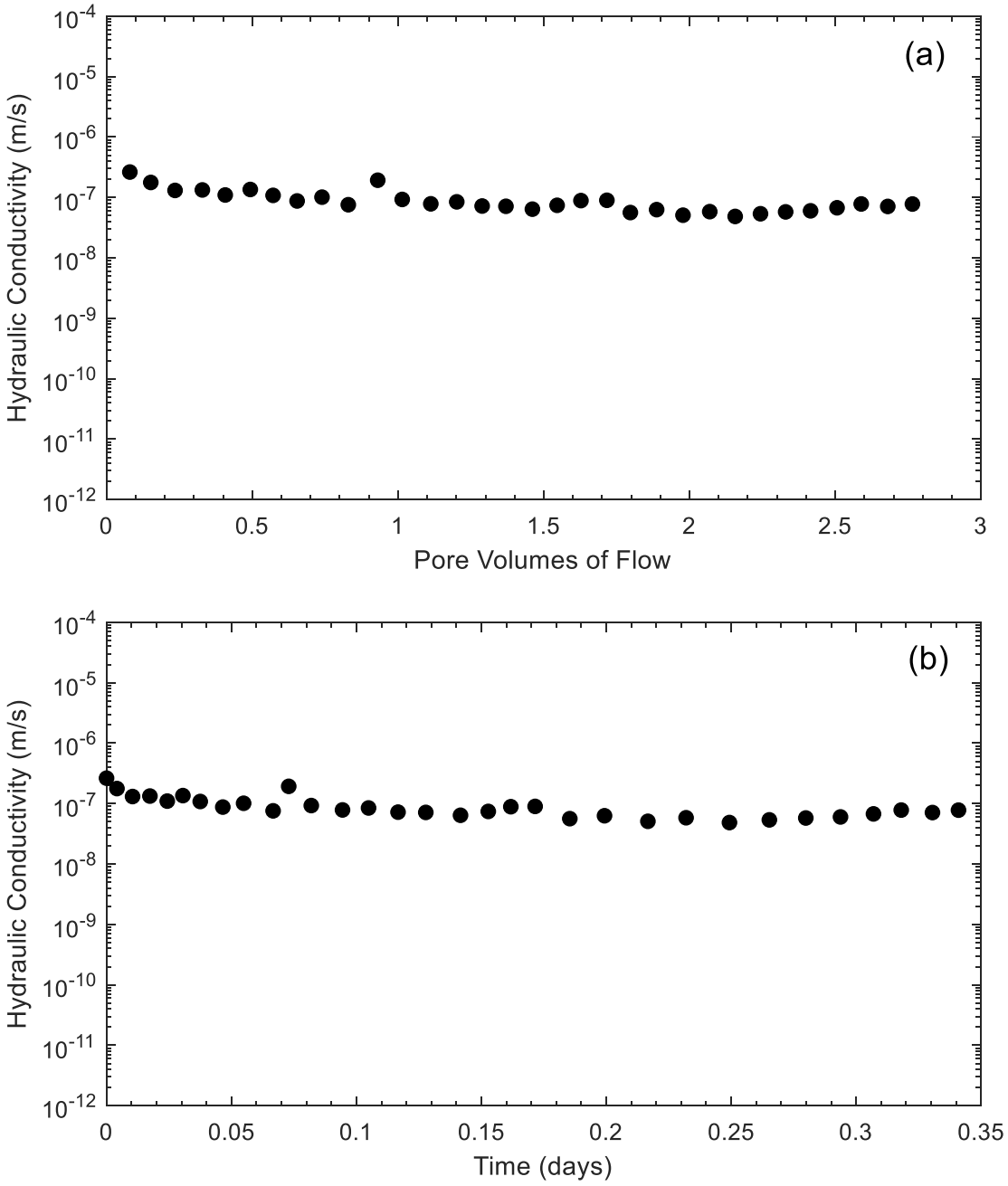

Figure C22. Hydraulic conductivity versus: (a) Pore volumes of flow; (b) time for test 10B-500-A.

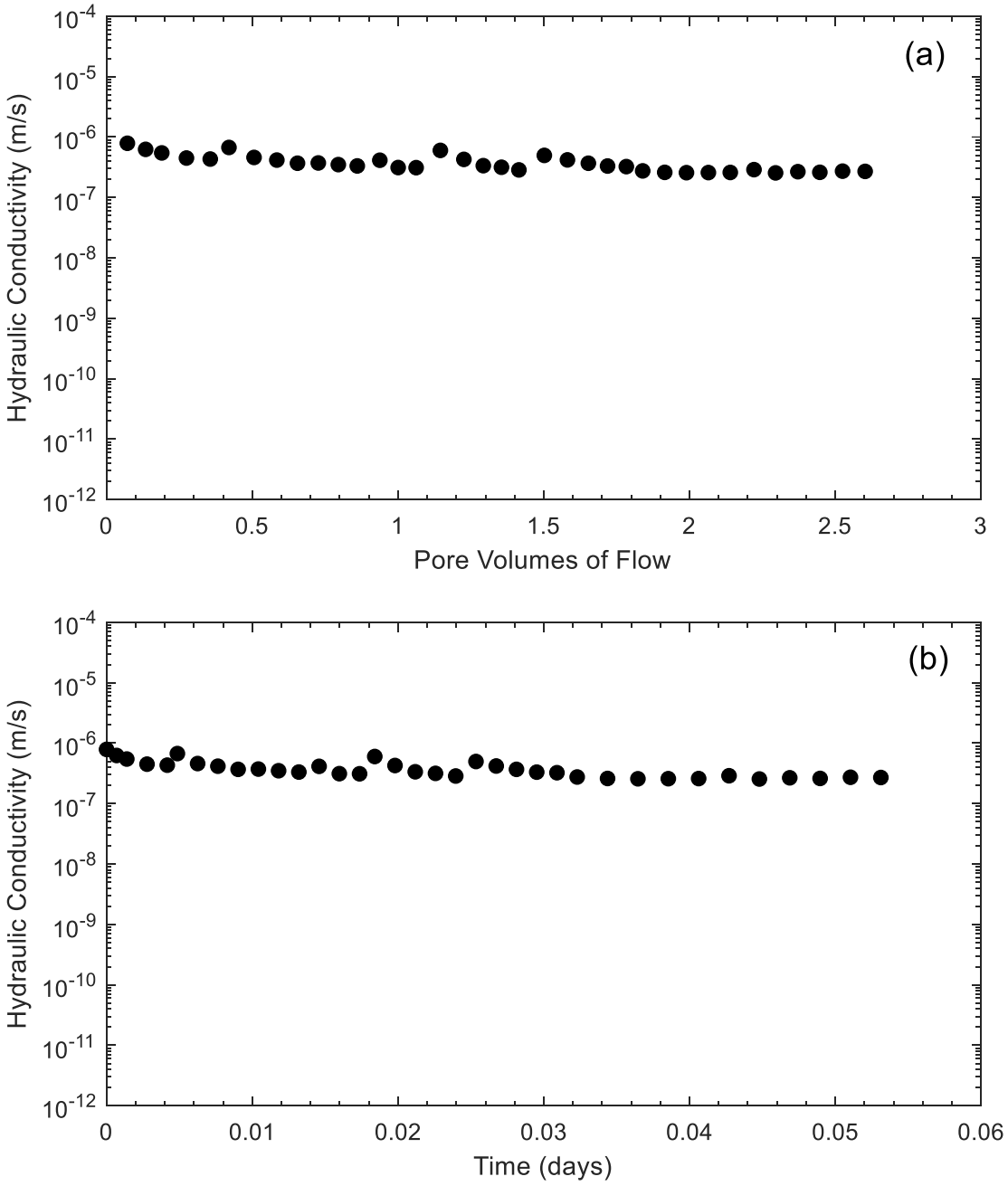

Figure C23. Hydraulic conductivity versus: (a) Pore volumes of flow; (b) time for test 15B-500-A.

APPENDIX D – DIRECT SHEAR TEST RESULTS – 35 KPA

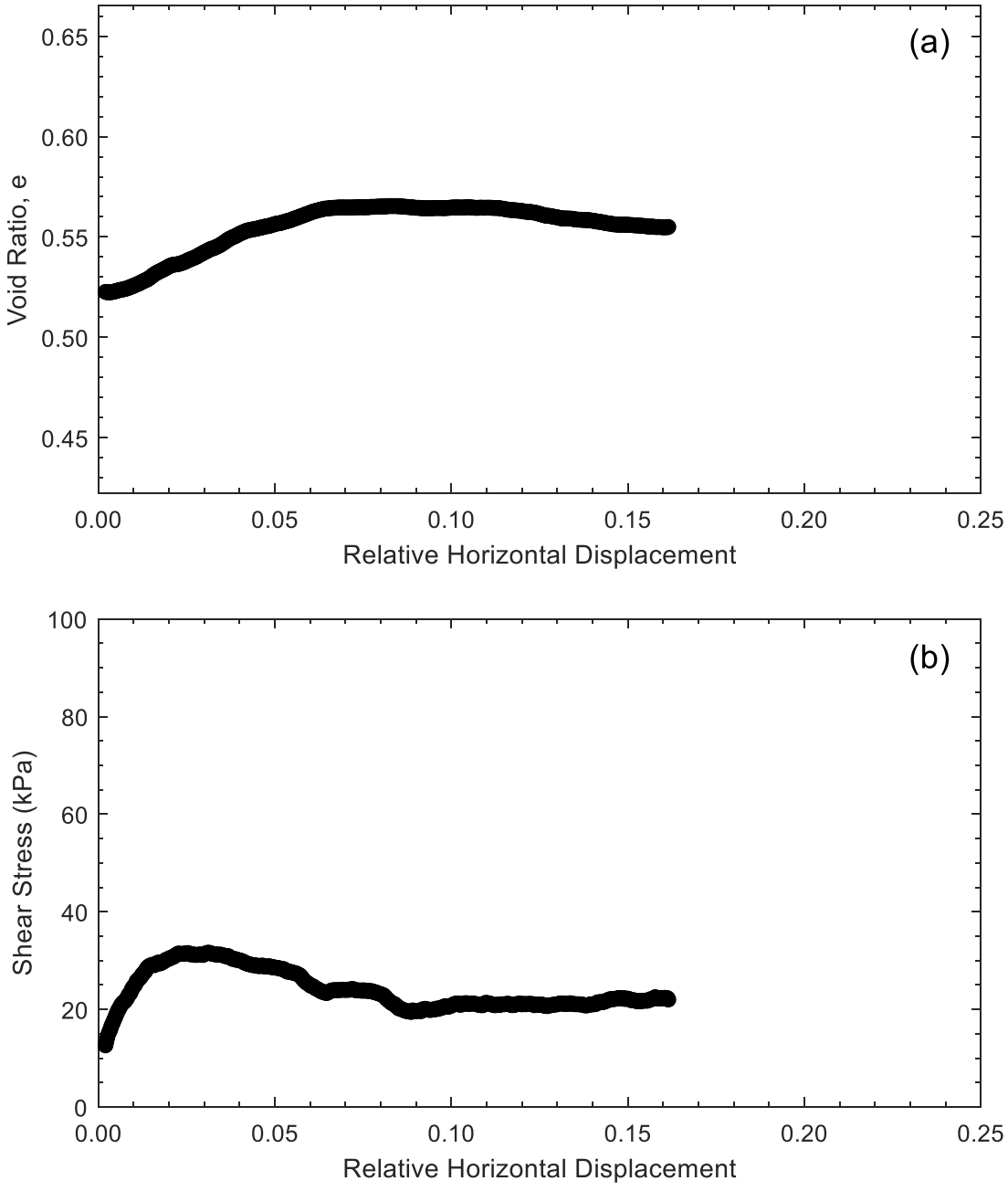

Figure D1. Direct shear test results for sand at 35 kPa effective stress: (a) Void ratio, e, versus relative horizontal displacement; (b) Shear stress (kPa) versus relative horizontal displacement.

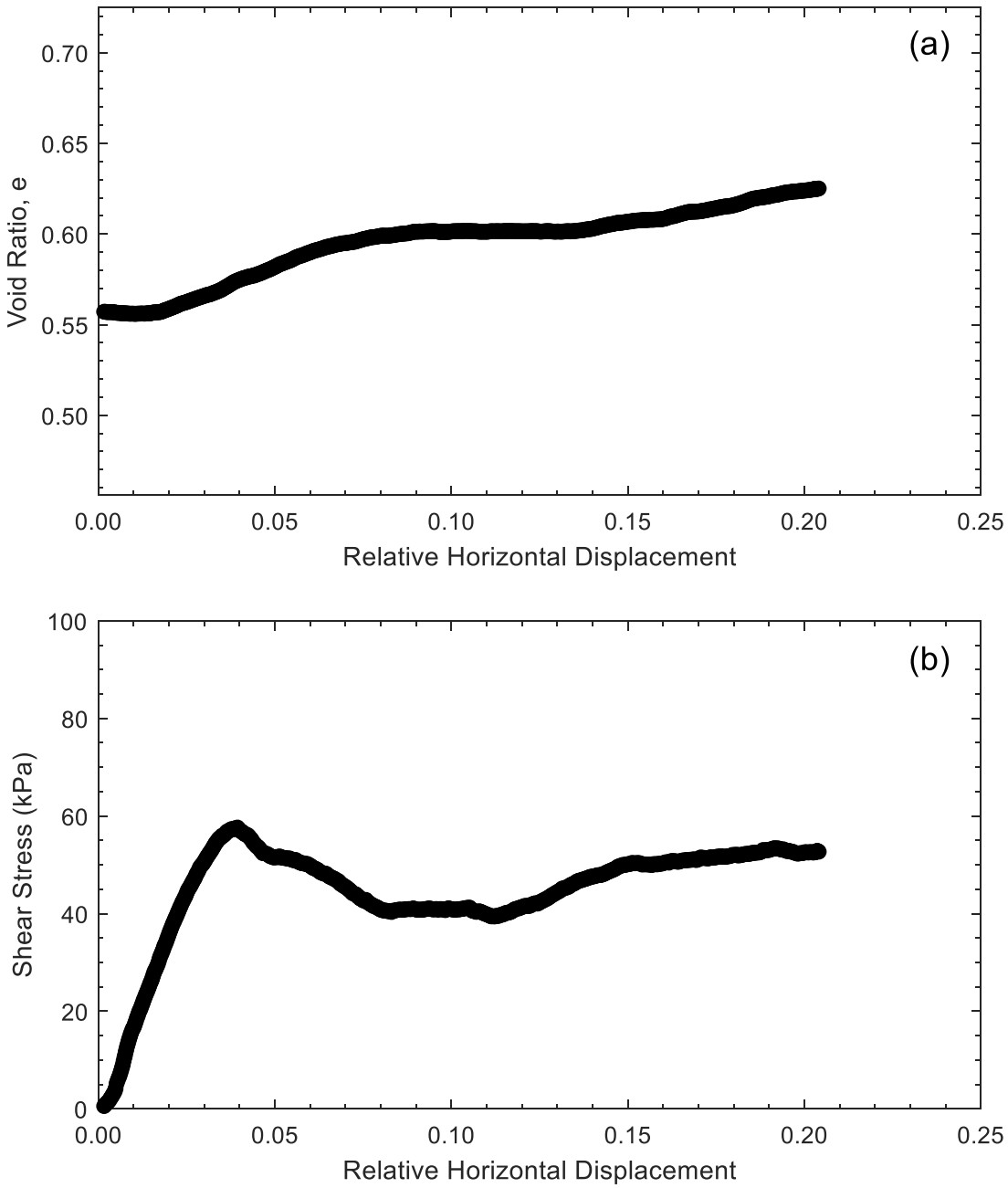

Figure D2. Direct shear test results for specimen 7B-0-H at 35 kPa effective stress: (a) Void ratio, e, versus relative horizontal displacement; (b) Shear stress (kPa) versus relative horizontal displacement.

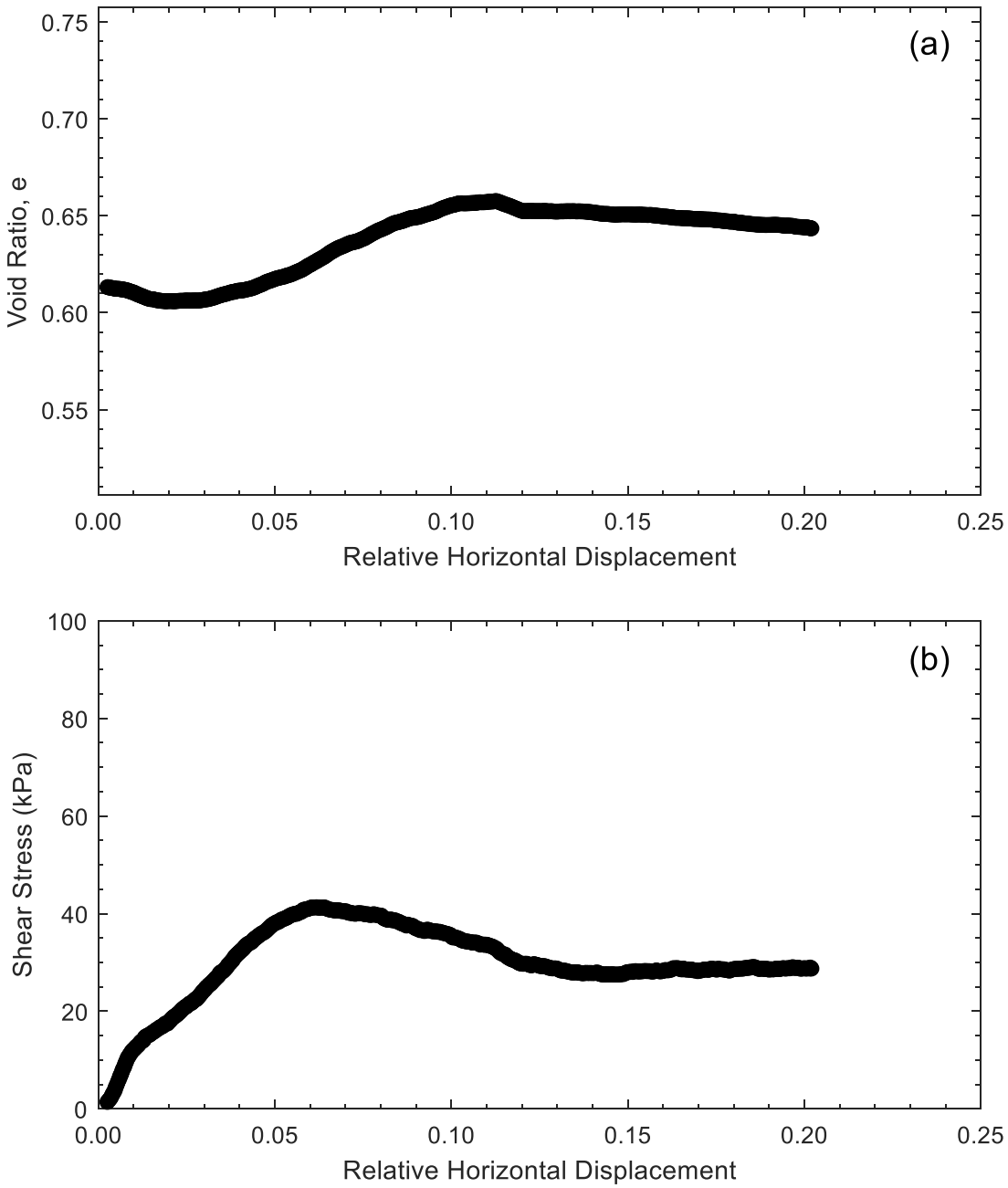

Figure D3. Direct shear test results for specimen 7B-10-H at 35 kPa effective stress: (a) Void ratio, e, versus relative horizontal displacement; (b) Shear stress (kPa) versus relative horizontal displacement.

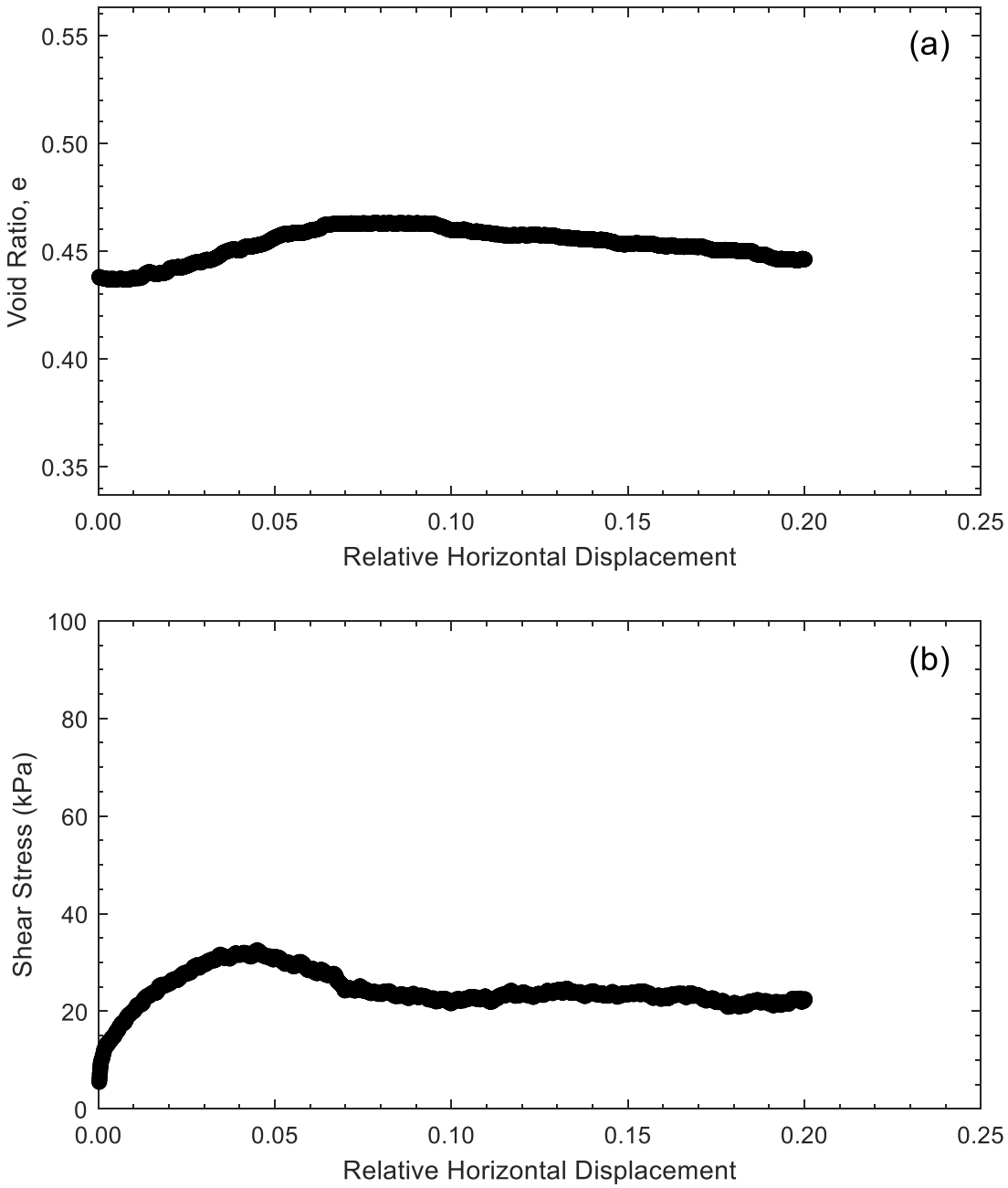

Figure D4. Direct shear test results for specimen 15K-0-H at 35 kPa effective stress: (a) Void ratio, e, versus relative horizontal displacement; (b) Shear stress (kPa) versus relative horizontal displacement.

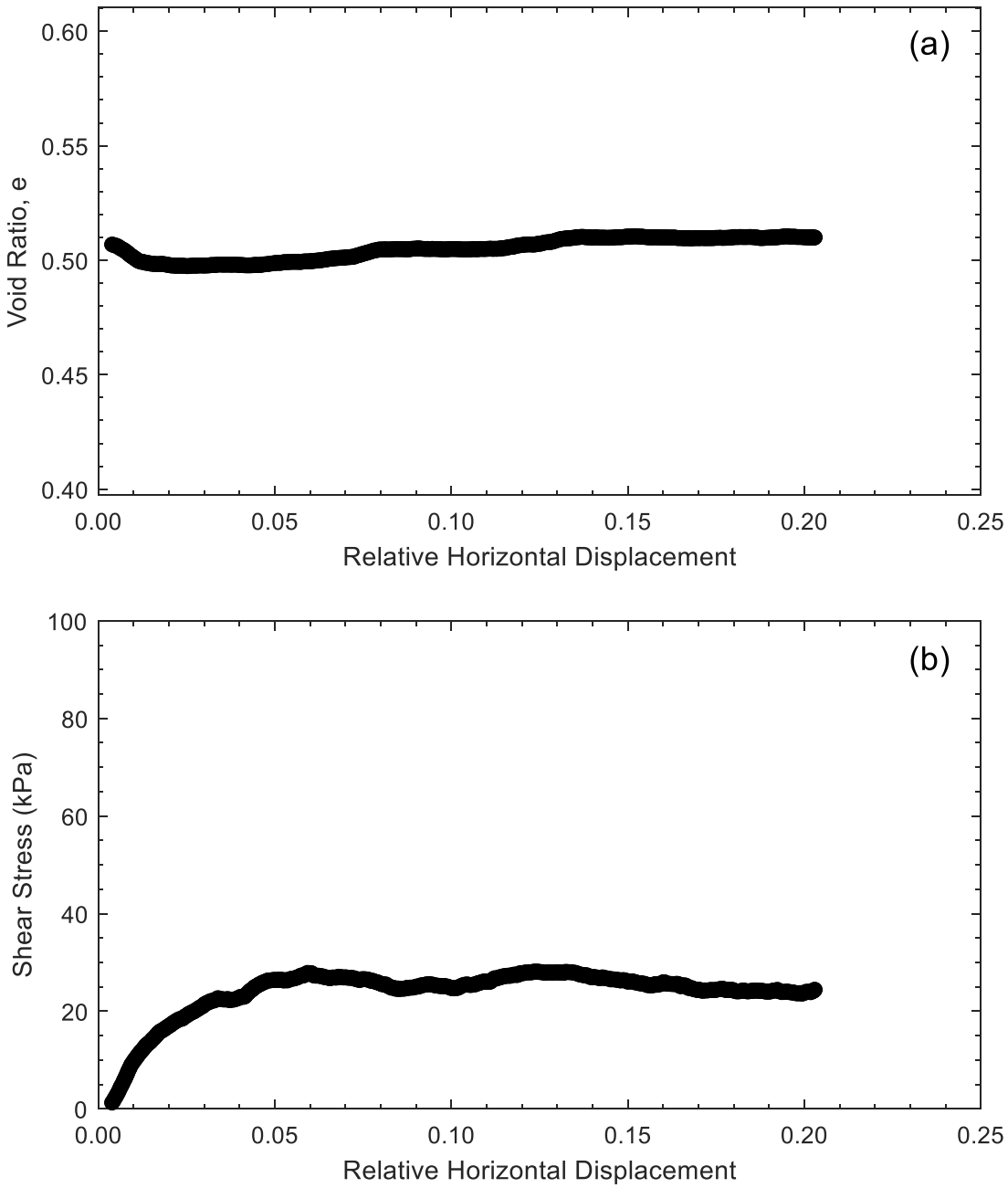

Figure D5. Direct shear test results for specimen 15k-10-H at 35 kPa effective stress: (a) Void ratio, e, versus relative horizontal displacement; (b) Shear stress (kPa) versus relative horizontal displacement.

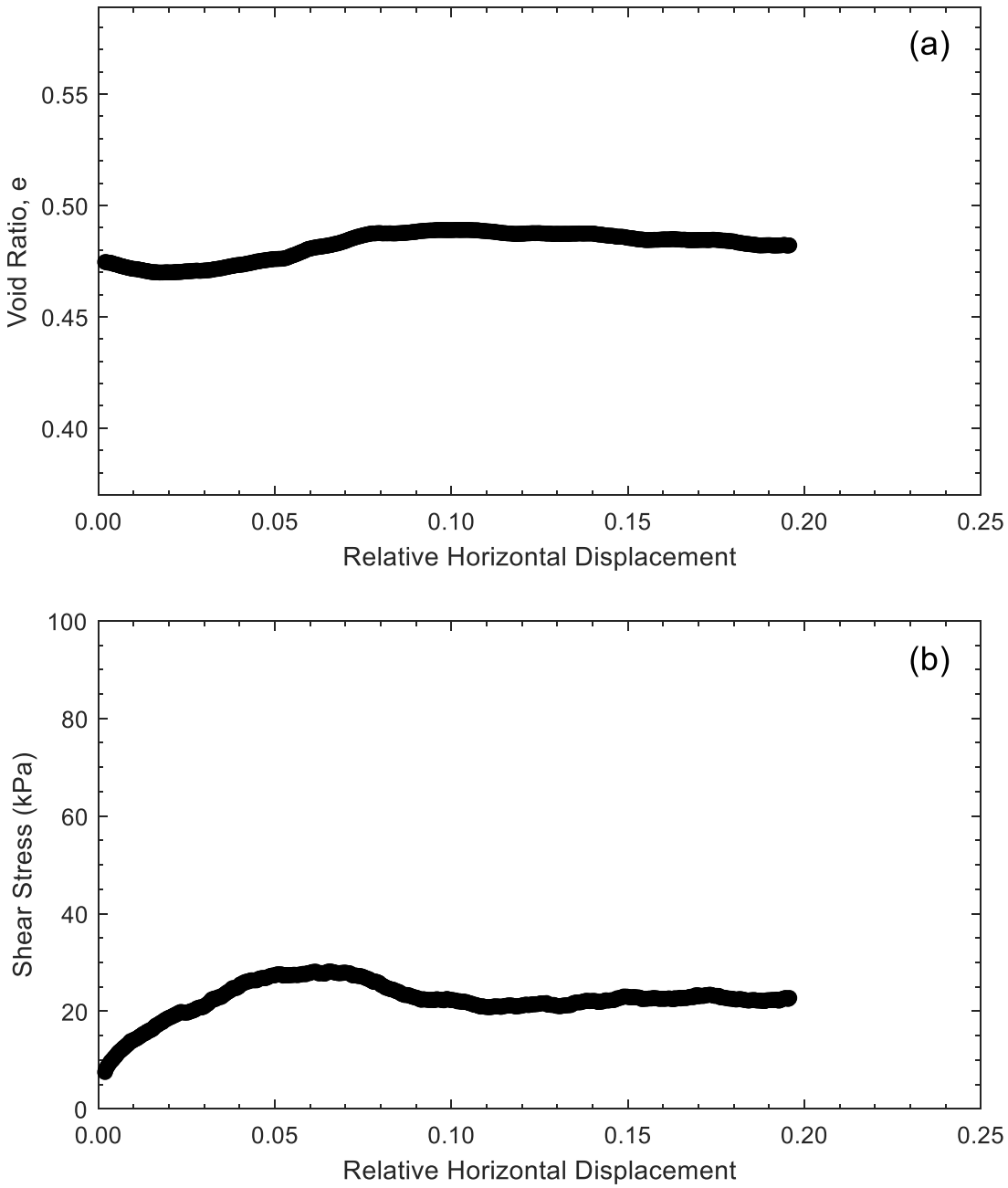

Figure D6. Direct shear test results for specimen 14R-0-H at 35 kPa effective stress: (a) Void ratio, e, versus relative horizontal displacement; (b) Shear stress (kPa) versus relative horizontal displacement.

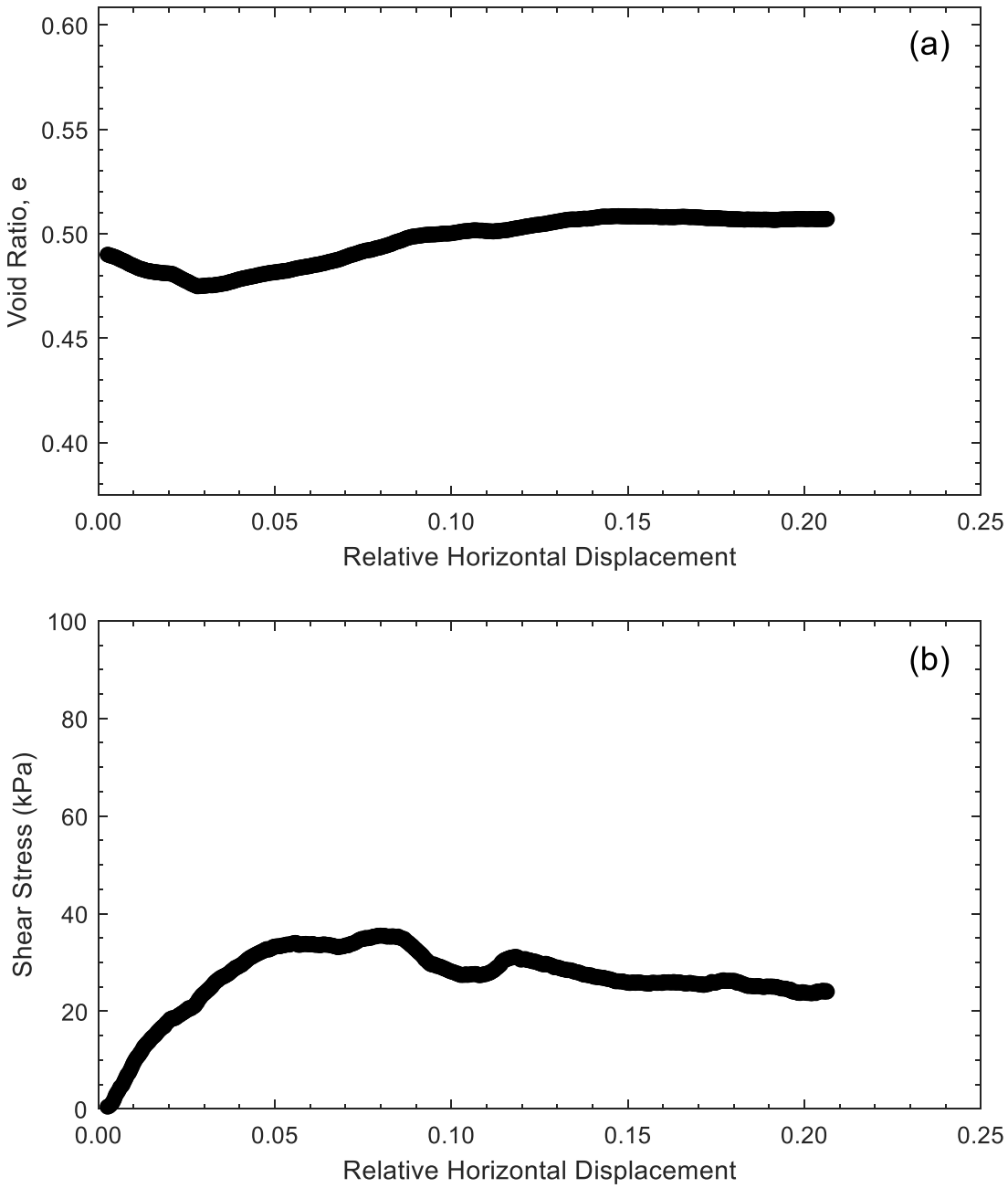

Figure D7. Direct shear test results for specimen 14R-10-H at 35 kPa effective stress: (a) Void ratio, e, versus relative horizontal displacement; (b) Shear stress (kPa) versus relative horizontal displacement.

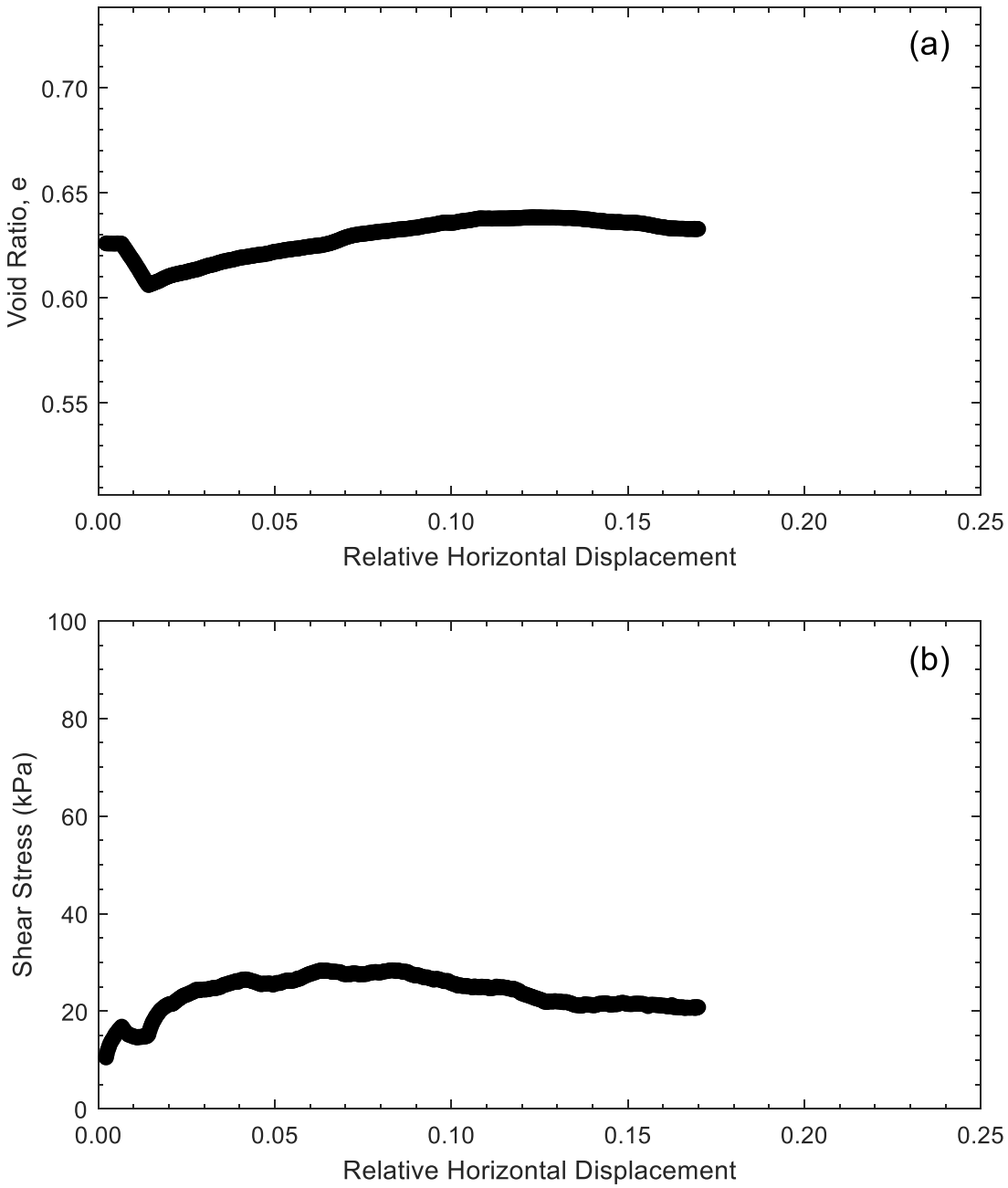

Figure D8. Direct shear test results for specimen 4B-0-H at 35 kPa effective stress: (a) Void ratio, e, versus relative horizontal displacement; (b) Shear stress (kPa) versus relative horizontal displacement.

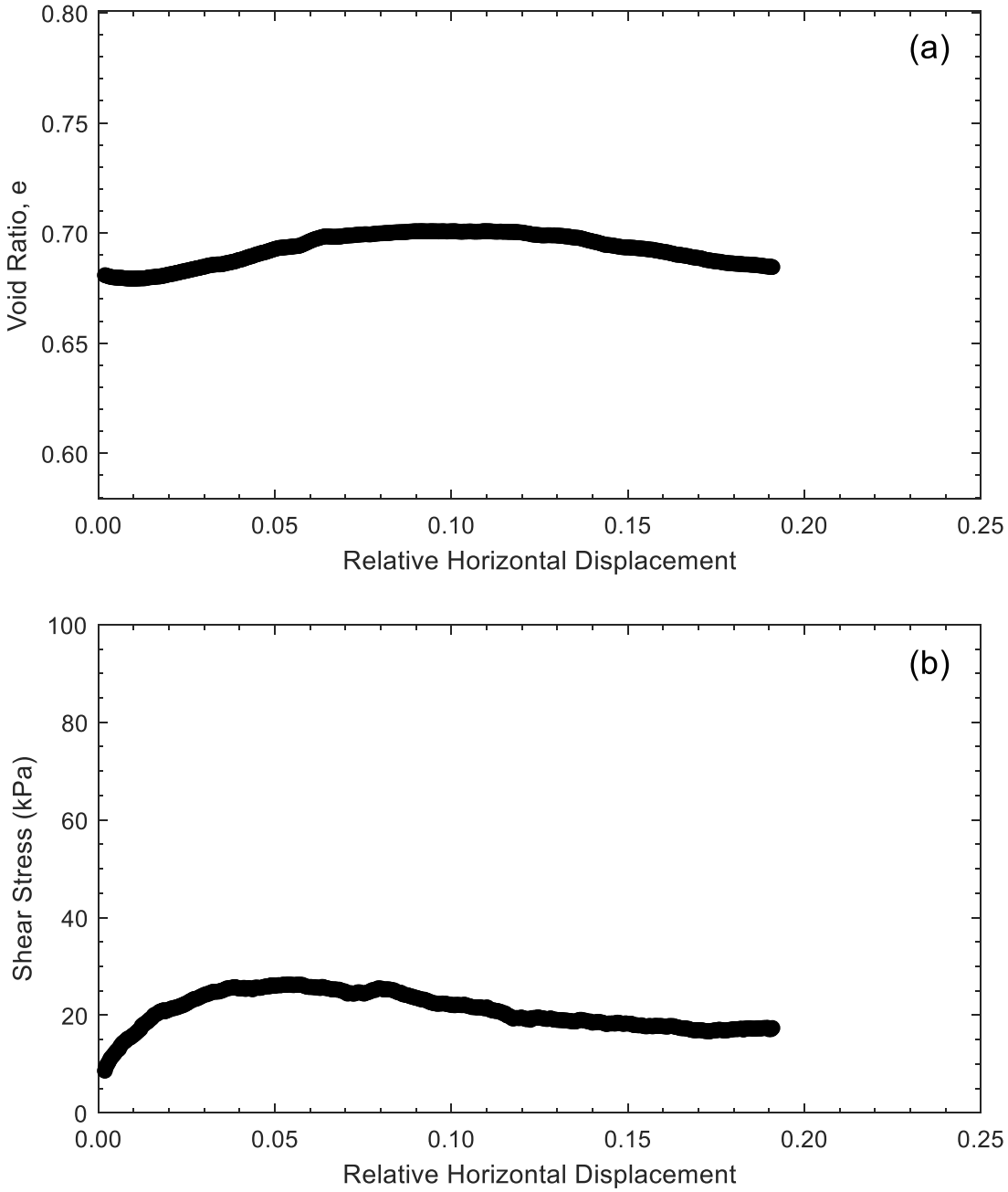

Figure D9. Direct shear test results for specimen 4B-10-H at 35 kPa effective stress: (a) Void ratio, e, versus relative horizontal displacement; (b) Shear stress (kPa) versus relative horizontal displacement.

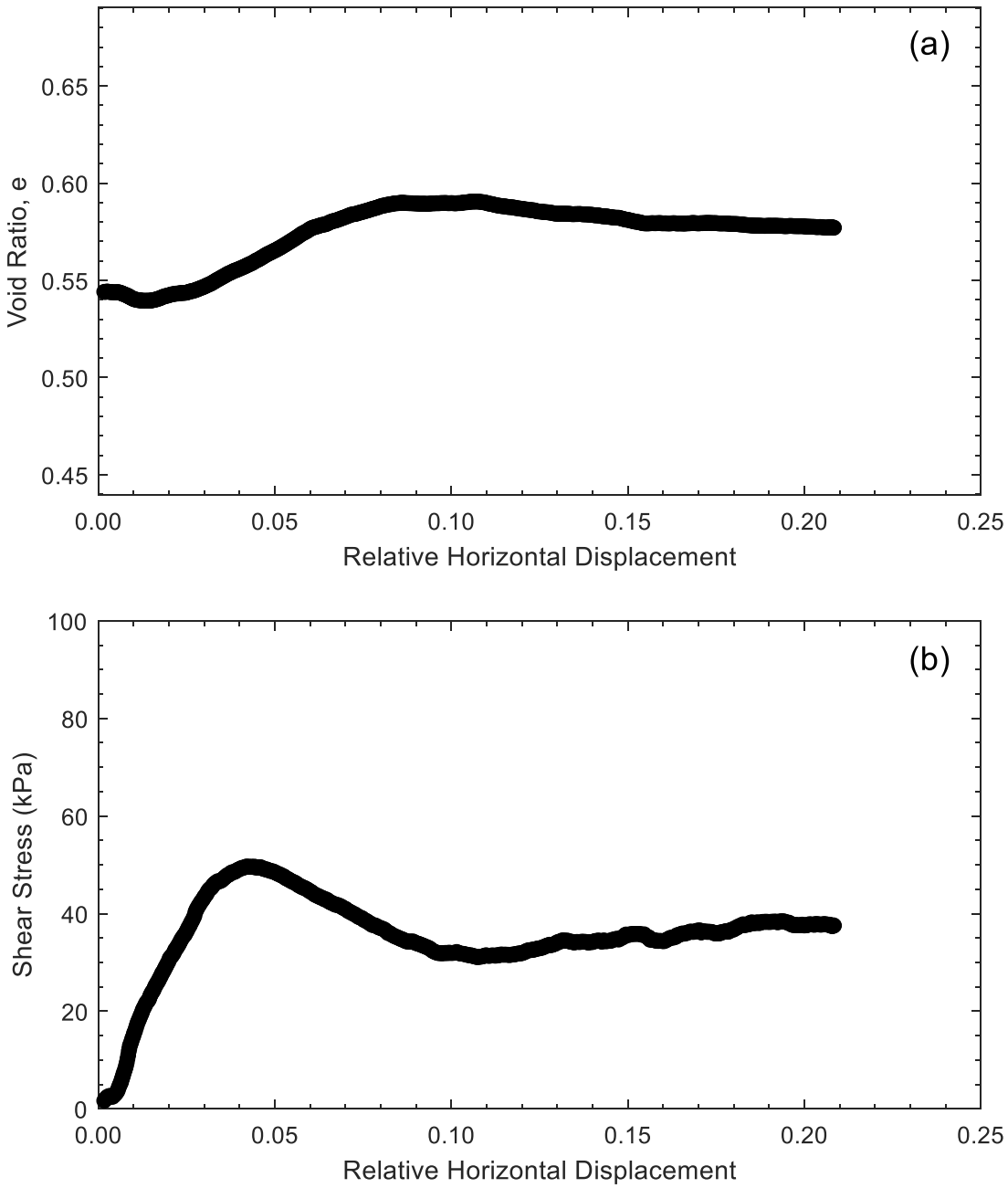

Figure D10. Direct shear test results for specimen 4B7R-0-H at 35 kPa effective stress: (a) Void ratio, e, versus relative horizontal displacement; (b) Shear stress (kPa) versus relative horizontal displacement.

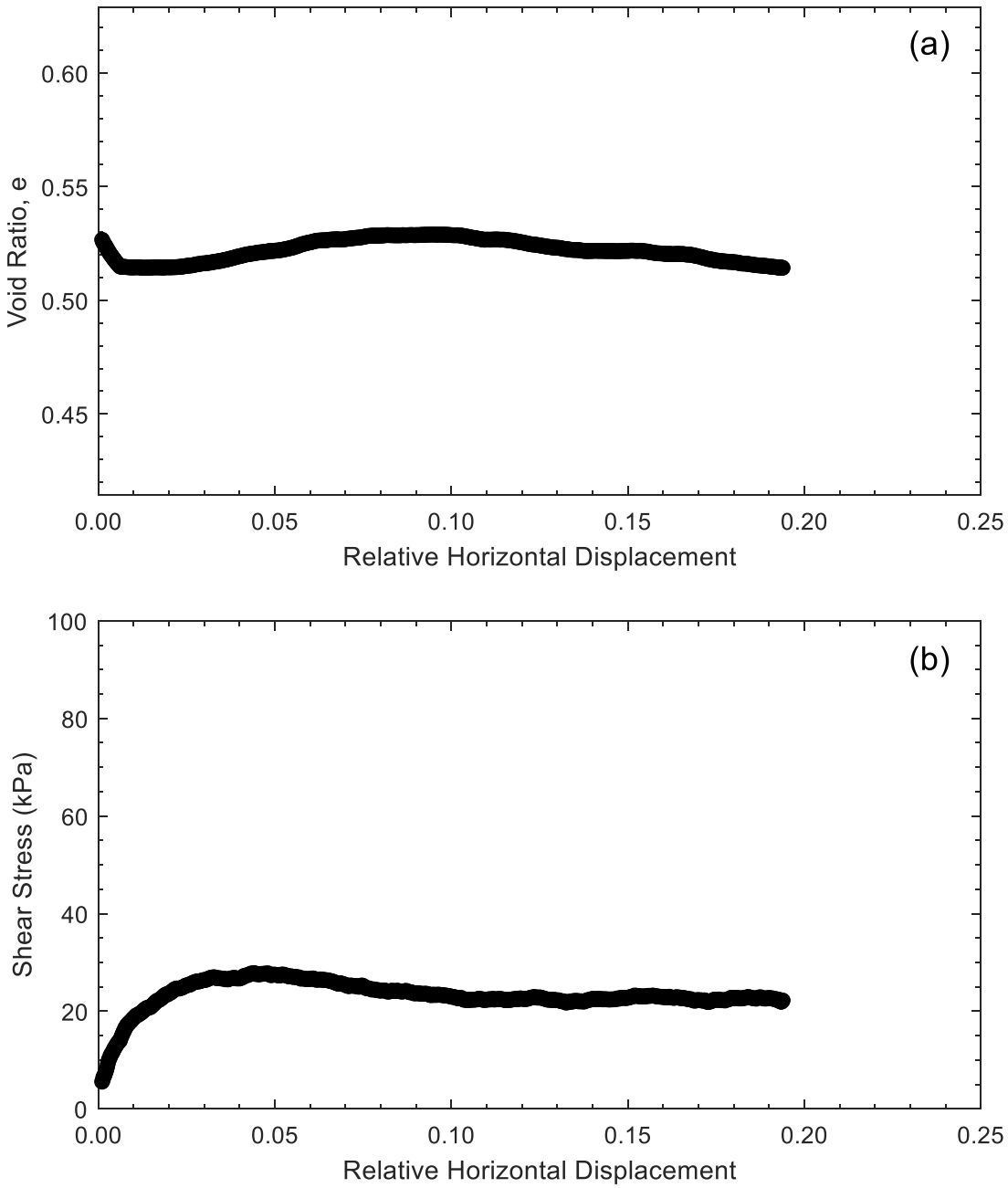

Figure D11. Direct shear test results for specimen 4B7R-10-H at 35 kPa effective stress: (a) Void ratio, e, versus relative horizontal displacement; (b) Shear stress (kPa) versus relative horizontal displacement.

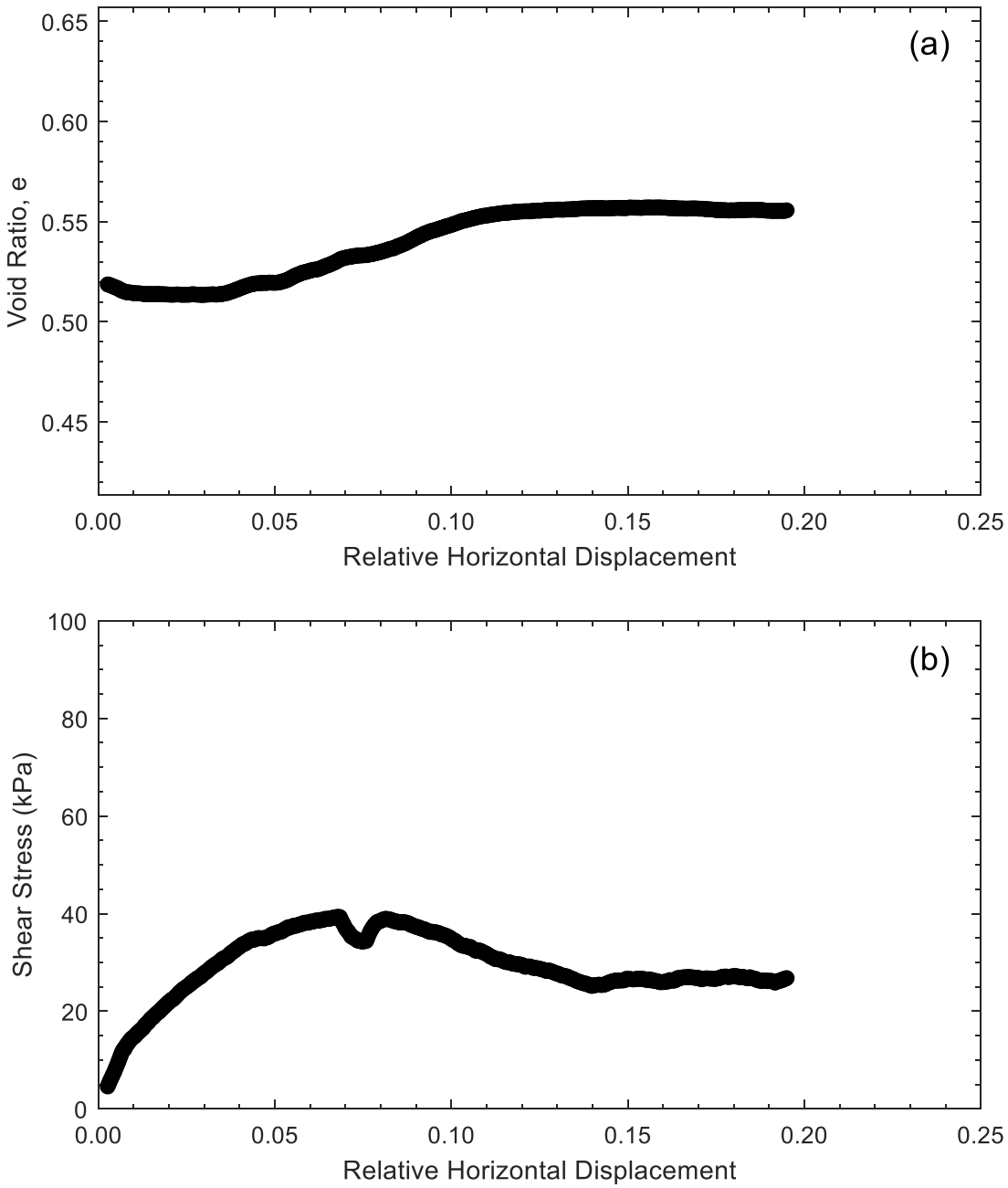

Figure D12. Direct shear test results for specimen 2B11R-0-H at 35 kPa effective stress: (a) Void ratio, e, versus relative horizontal displacement; (b) Shear stress (kPa) versus relative horizontal displacement.

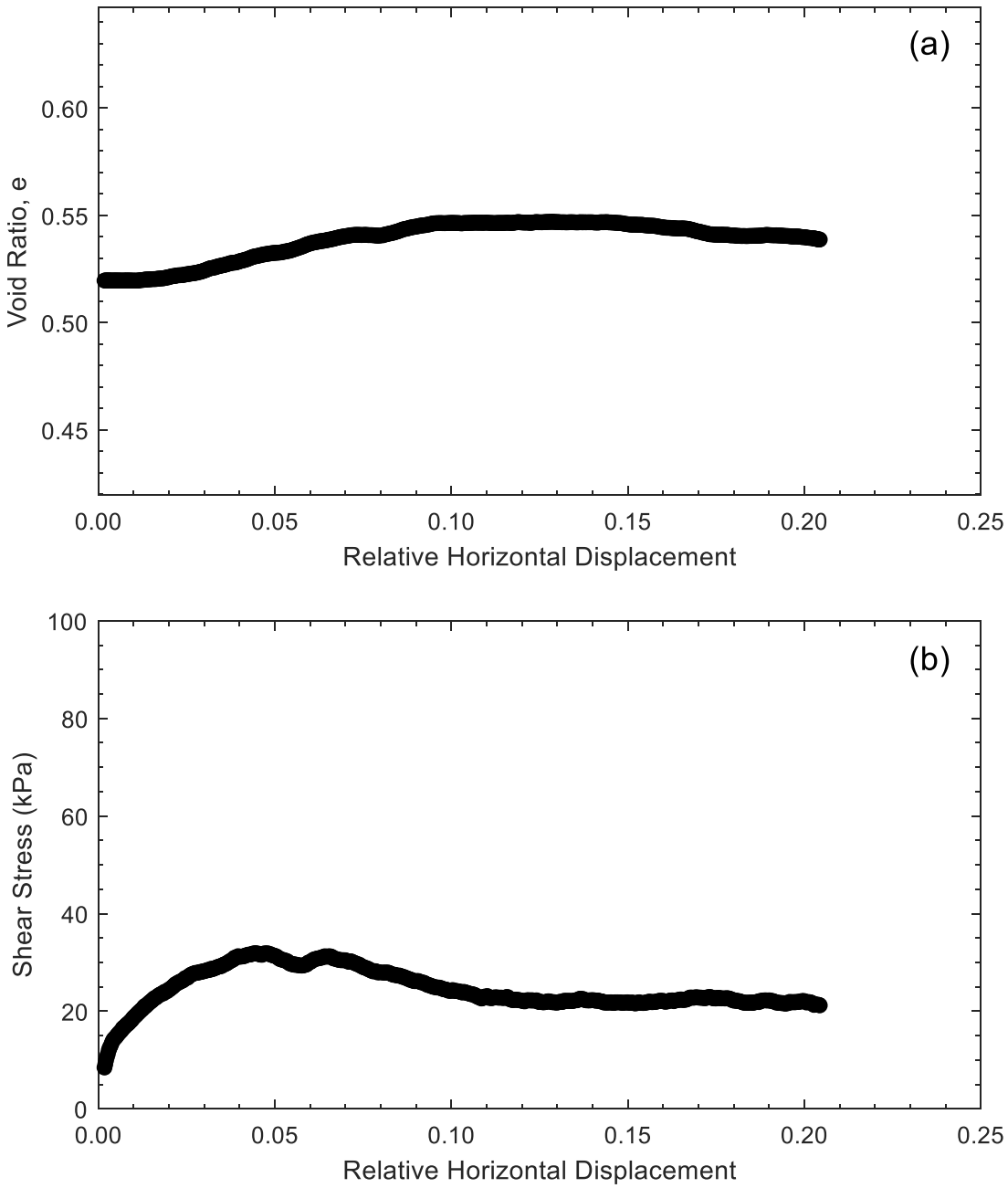

Figure D13. Direct shear test results for specimen 2B11R-10-H at 35 kPa effective stress: (a) Void ratio, e, versus relative horizontal displacement; (b) Shear stress (kPa) versus relative horizontal displacement.

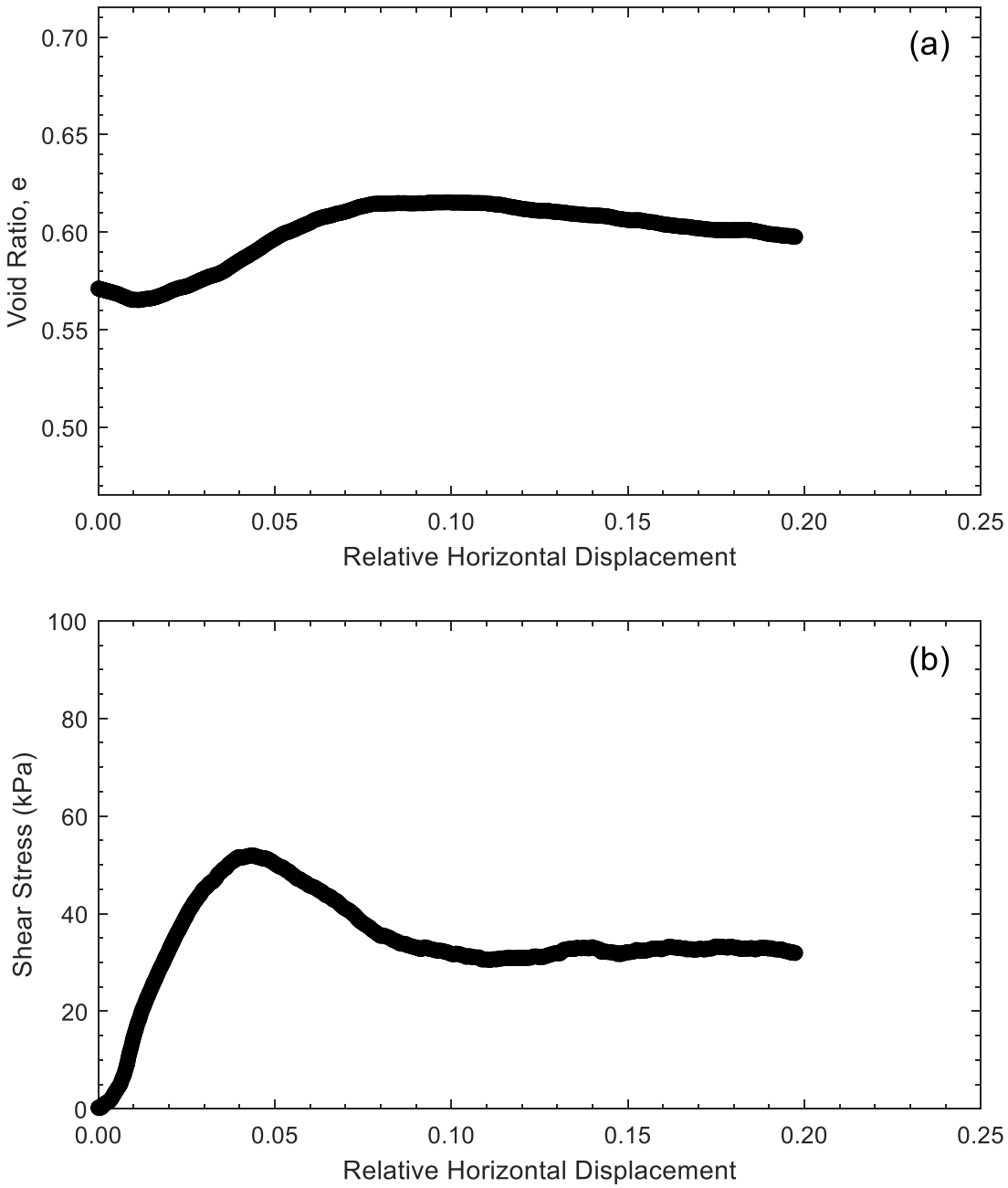

Figure D14. Direct shear test results for specimen 5B4R-0-H at 35 kPa effective stress: (a) Void ratio, e, versus relative horizontal displacement; (b) Shear stress (kPa) versus relative horizontal displacement.

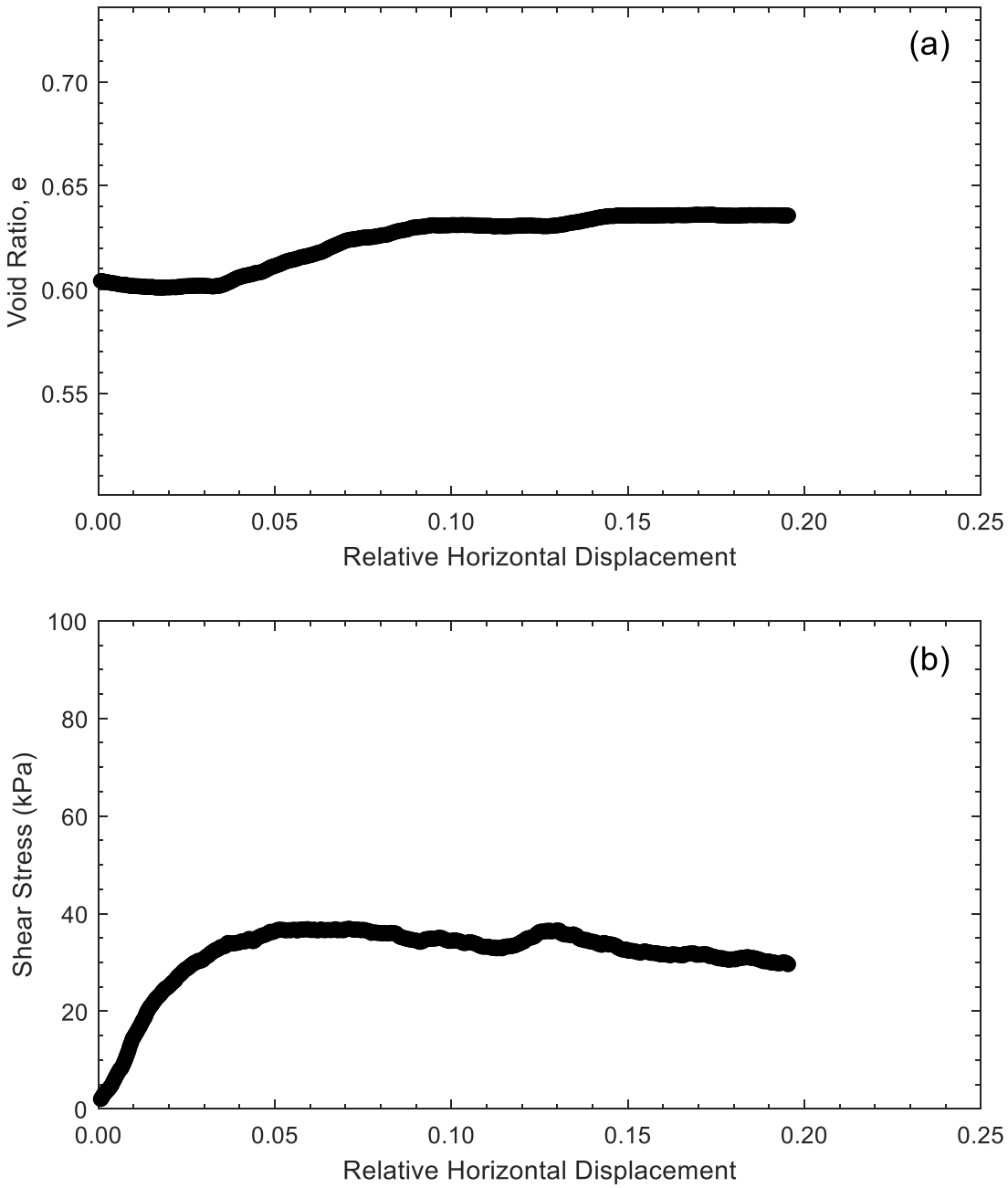

Figure D15. Direct shear test results for specimen 5B4R-10-H at 35 kPa effective stress: (a) Void ratio, e, versus relative horizontal displacement; (b) Shear stress (kPa) versus relative horizontal displacement.

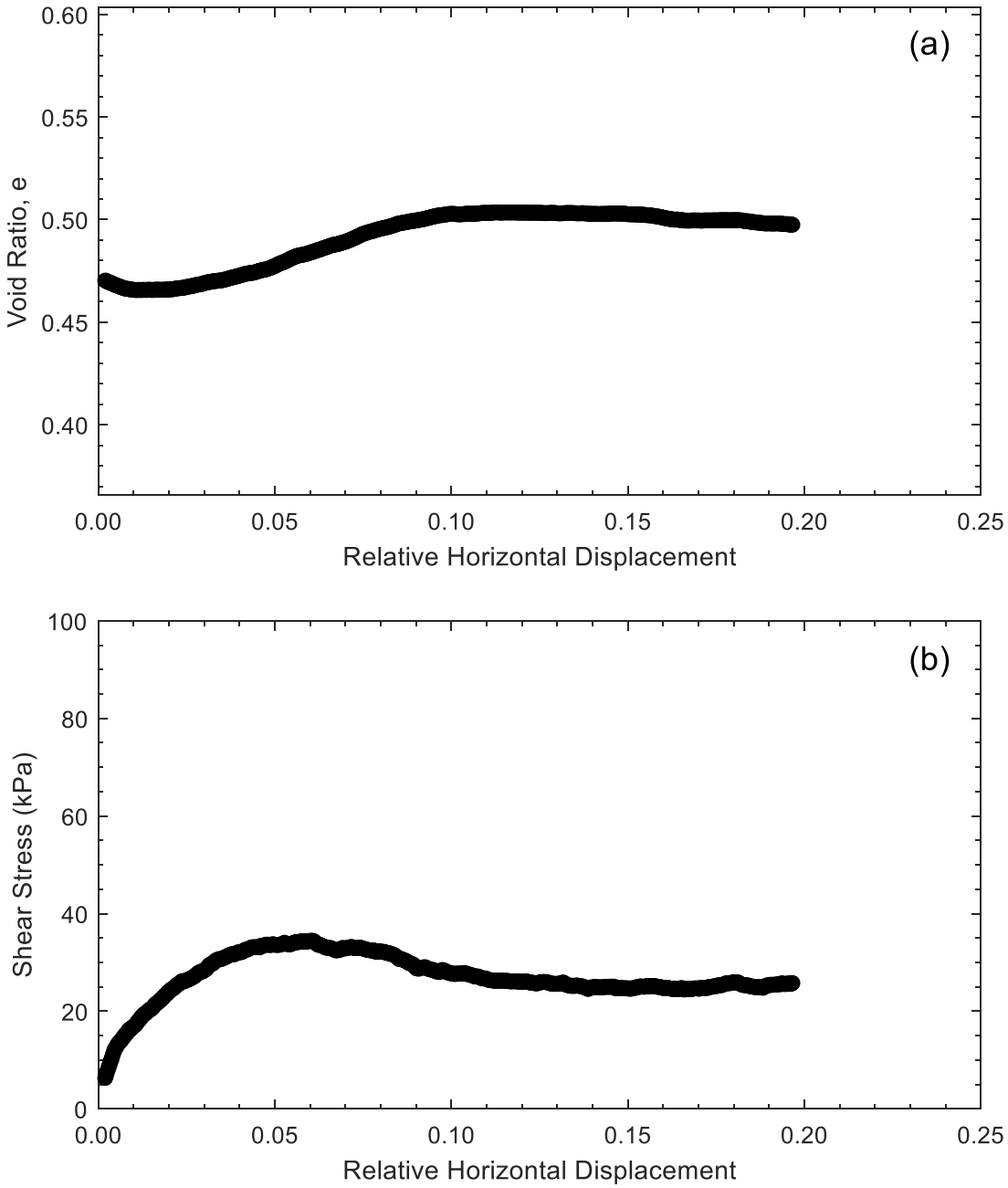

Figure D16. Direct shear test results for specimen 2B11R-0-A at 35 kPa effective stress: (a) Void ratio, e, versus relative horizontal displacement; (b) Shear stress (kPa) versus relative horizontal displacement.

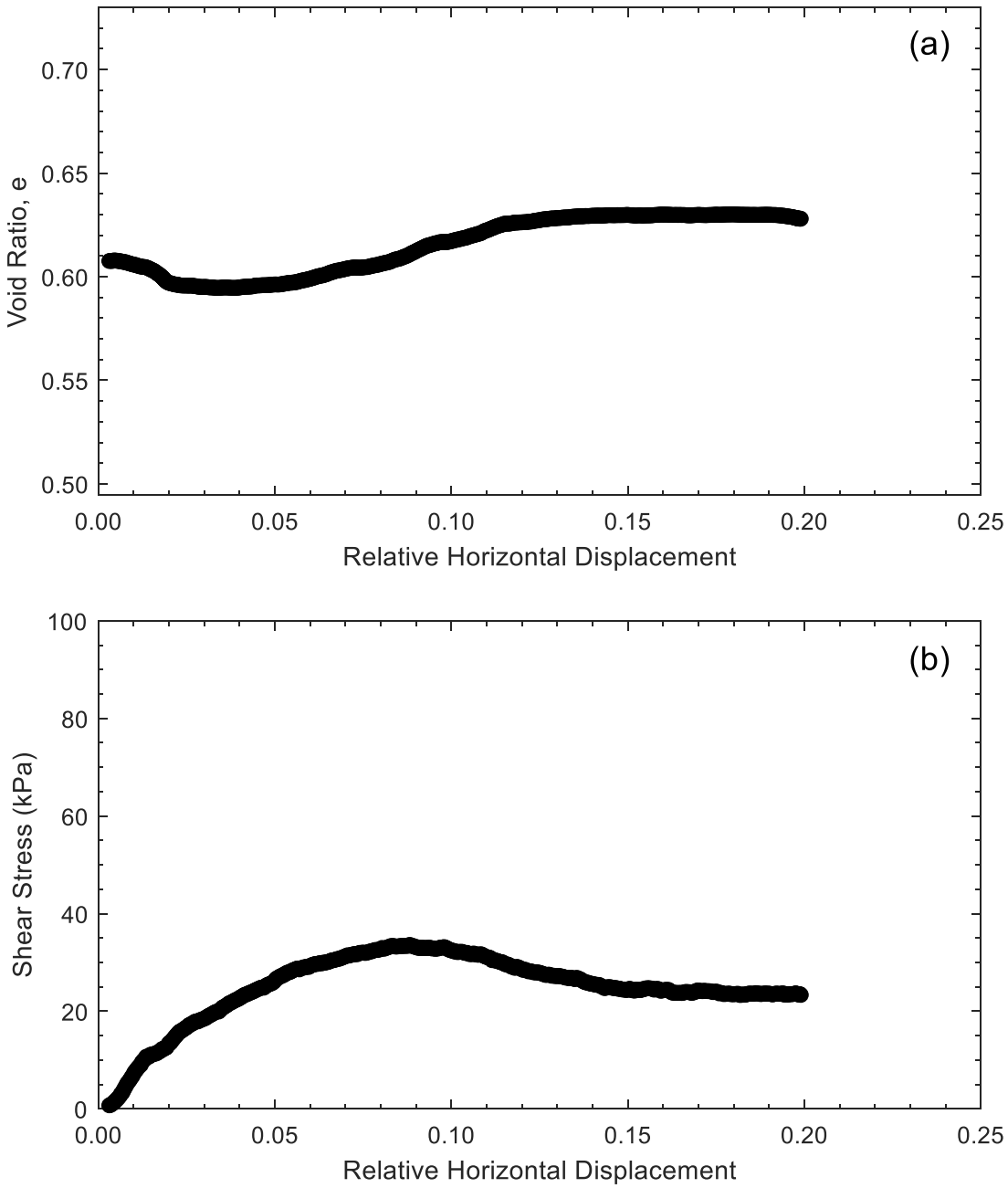

Figure D17. Direct shear test results for specimen 2B11R-10-A at 35 kPa effective stress: (a) Void ratio, e, versus relative horizontal displacement; (b) Shear stress (kPa) versus relative horizontal displacement.

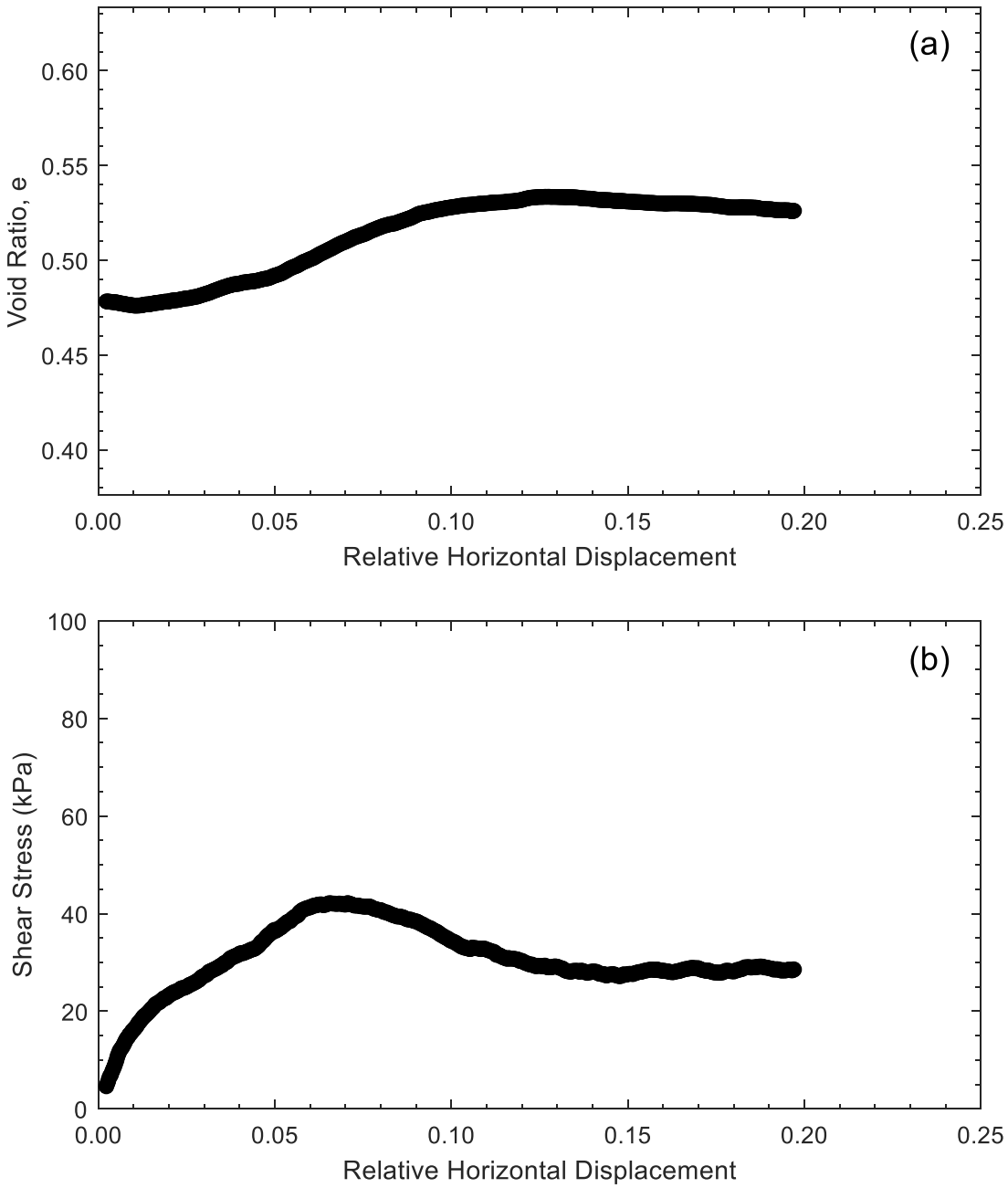

Figure D18. Direct shear test results for specimen 4B7R-0-A at 35 kPa effective stress: (a) Void ratio, e, versus relative horizontal displacement; (b) Shear stress (kPa) versus relative horizontal displacement.

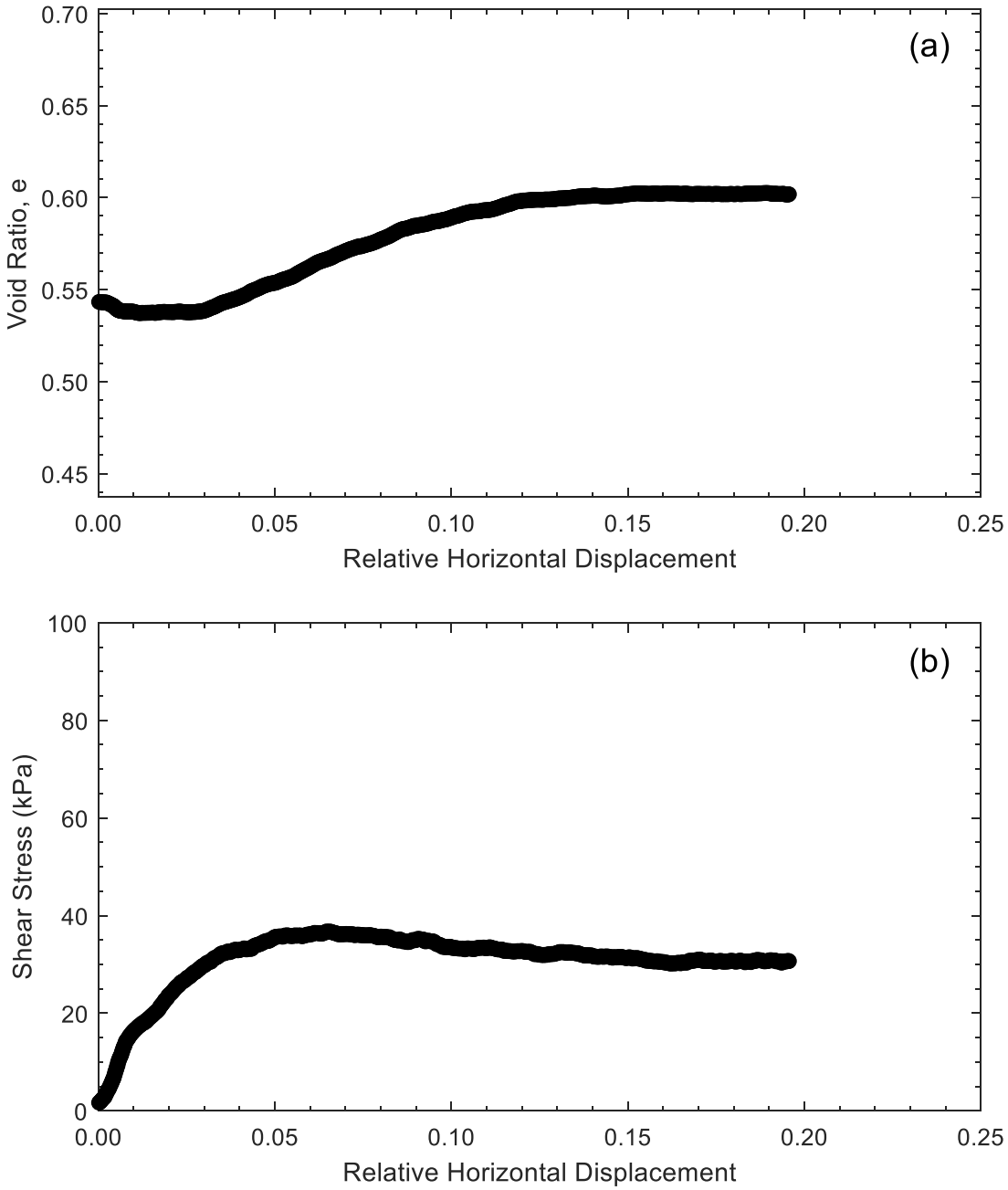

Figure D19. Direct shear test results for specimen 4B7R-10-A at 35 kPa effective stress: (a) Void ratio, e, versus relative horizontal displacement; (b) Shear stress (kPa) versus relative horizontal displacement.

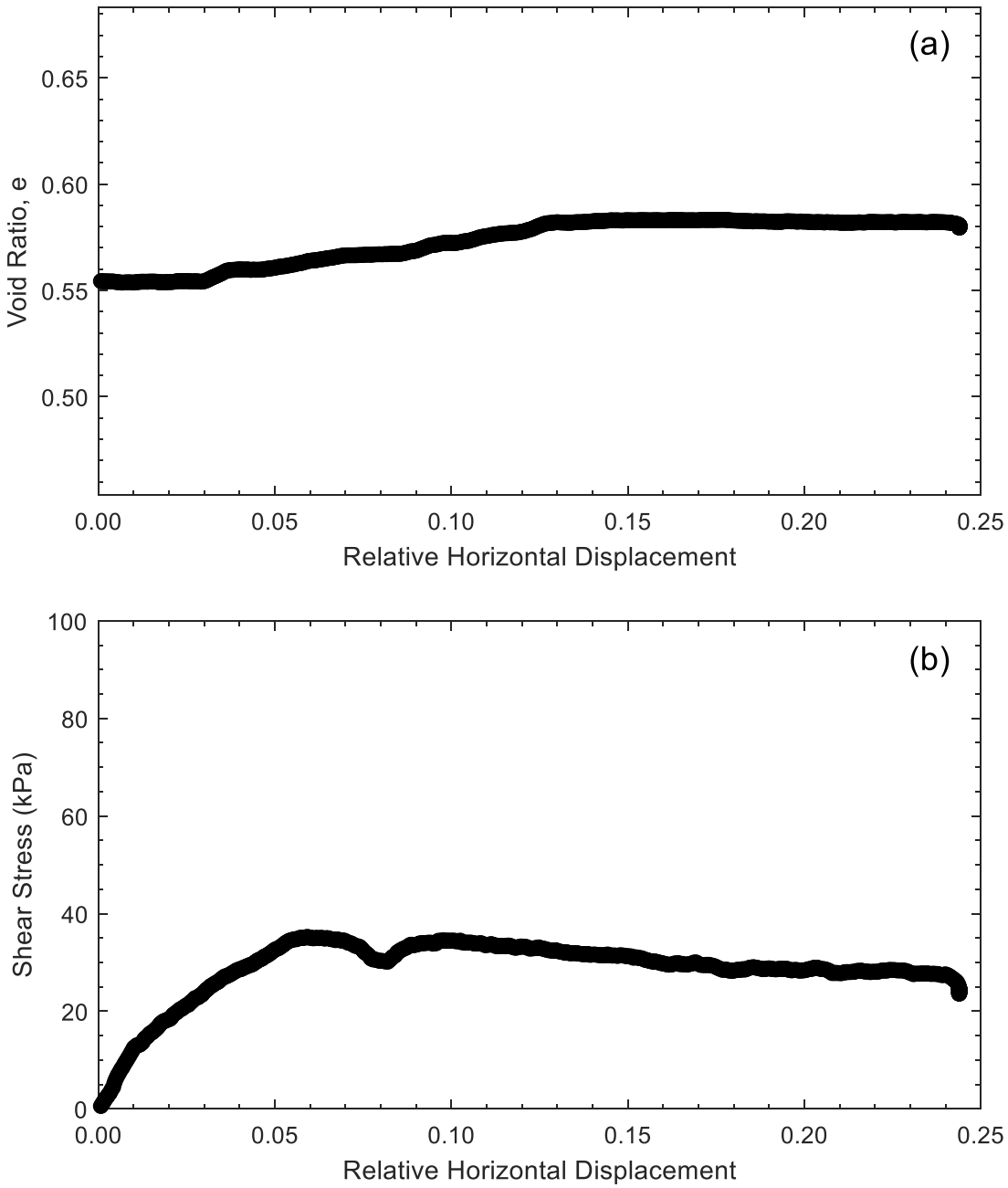

Figure D20. Direct shear test results for specimen 5B4R-0-A at 35 kPa effective stress: (a) Void ratio, e, versus relative horizontal displacement; (b) Shear stress (kPa) versus relative horizontal displacement.

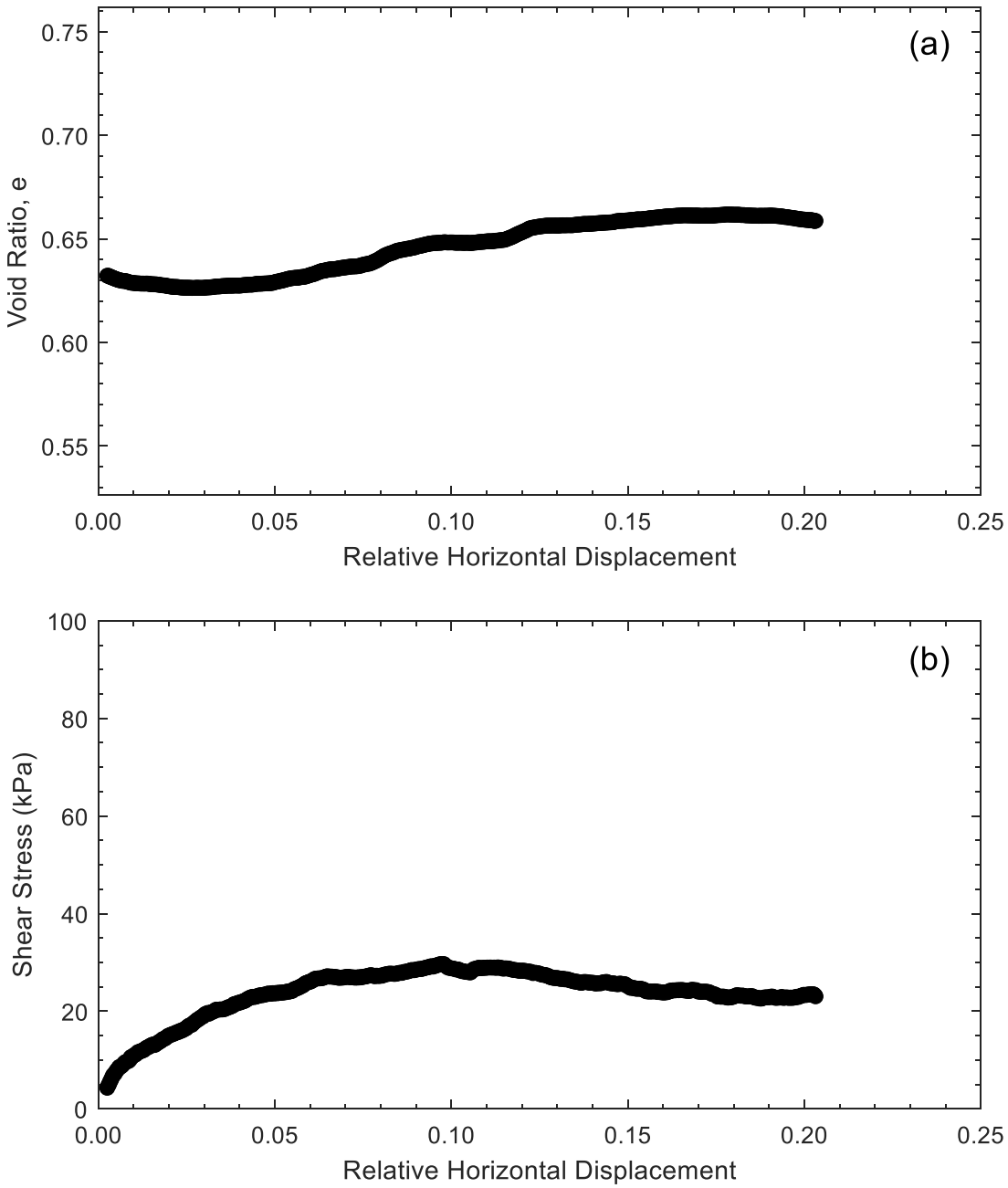

Figure D21. Direct shear test results for specimen 5B4R-10-A at 35 kPa effective stress: (a) Void ratio, e, versus relative horizontal displacement; (b) Shear stress (kPa) versus relative horizontal displacement.

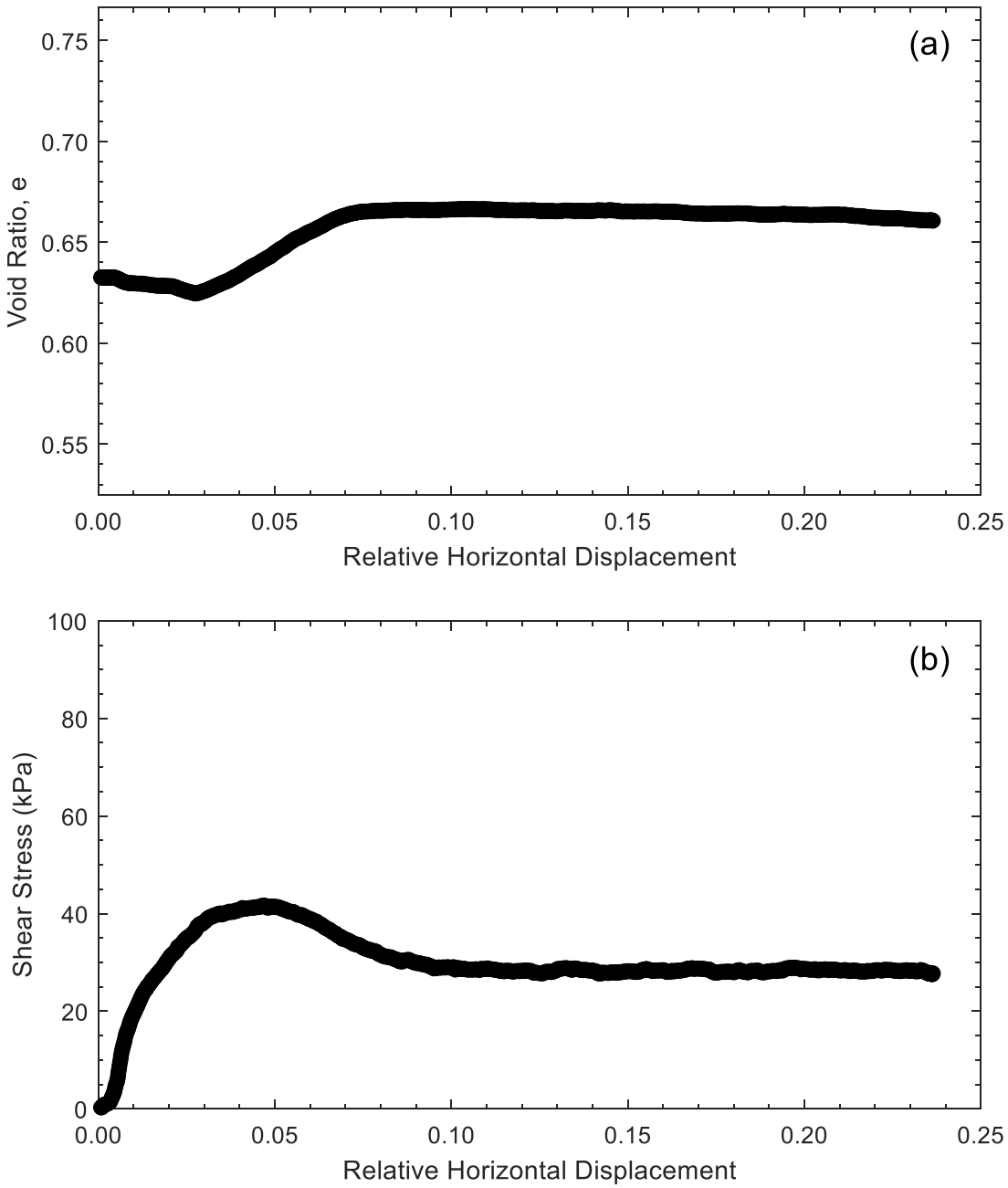

Figure D22. Direct shear test results for specimen 8B-10-A at 35 kPa effective stress: (a) Void ratio, e, versus relative horizontal displacement; (b) Shear stress (kPa) versus relative horizontal displacement.

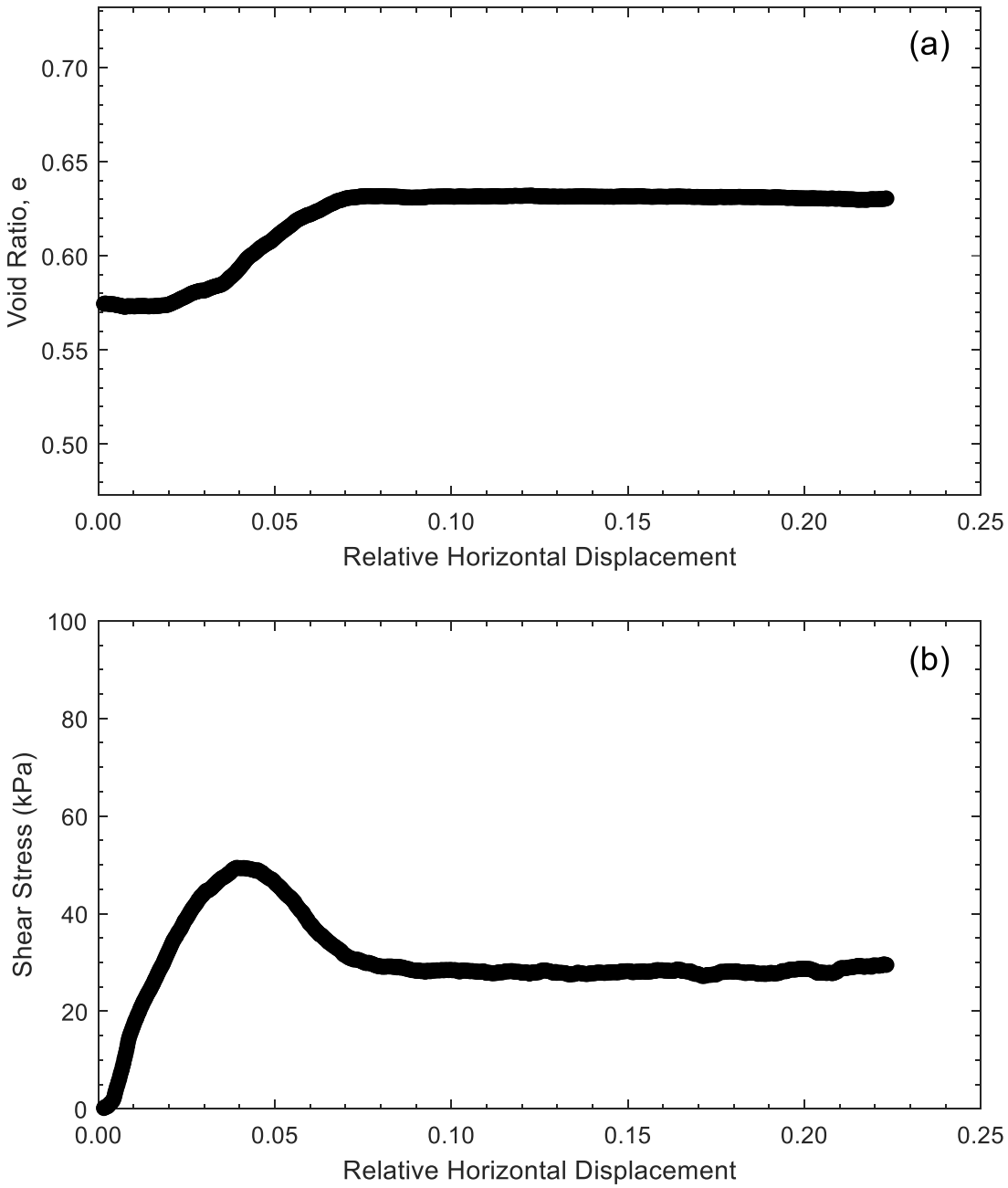

Figure D23. Direct shear test results for specimen 10B-500-A at 35 kPa effective stress: (a) Void ratio, e, versus relative horizontal displacement; (b) Shear stress (kPa) versus relative horizontal displacement.

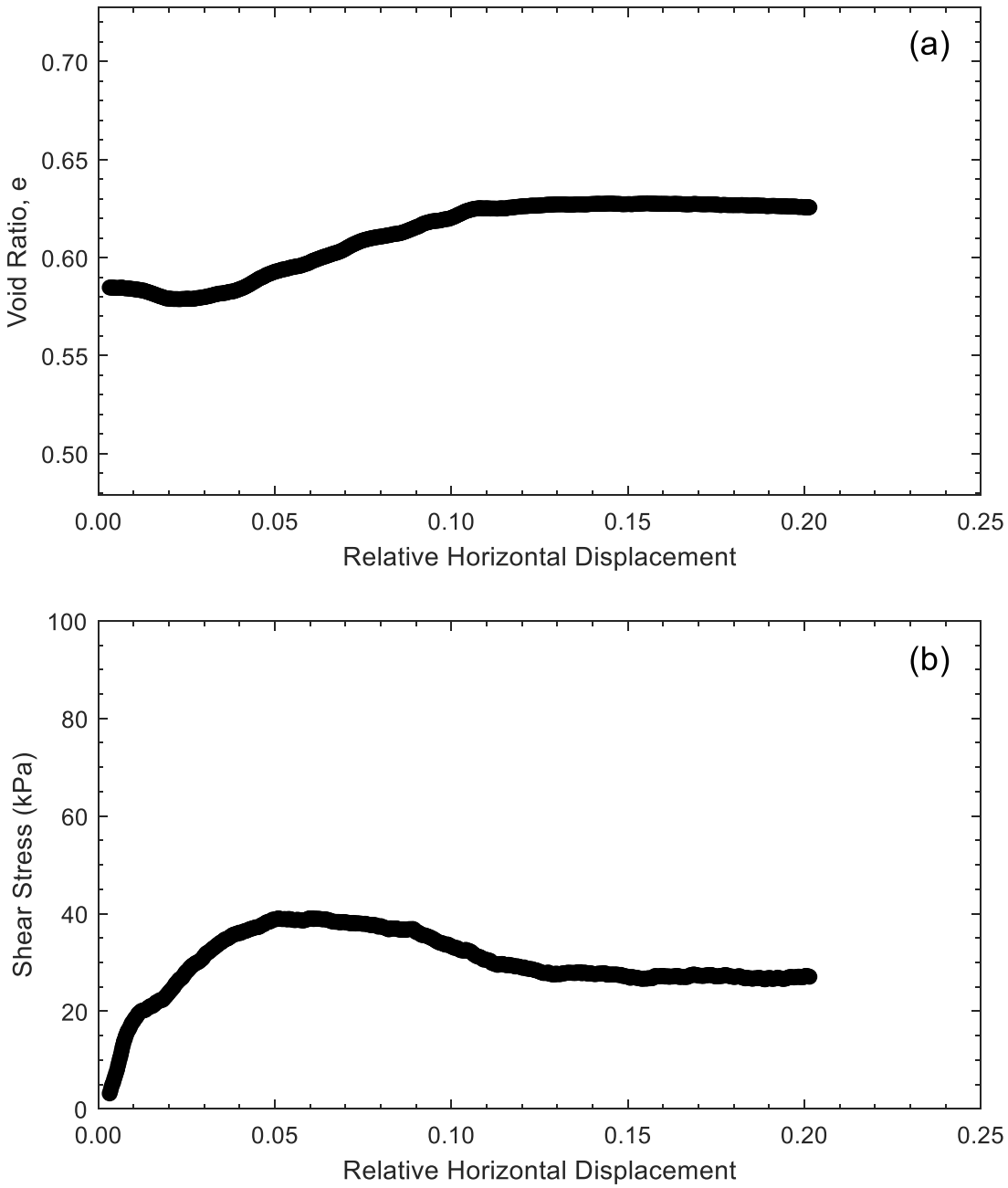

Figure D24. Direct shear test results for specimen 15B-500-A at 35 kPa effective stress: (a) Void ratio, e, versus relative horizontal displacement; (b) Shear stress (kPa) versus relative horizontal displacement.

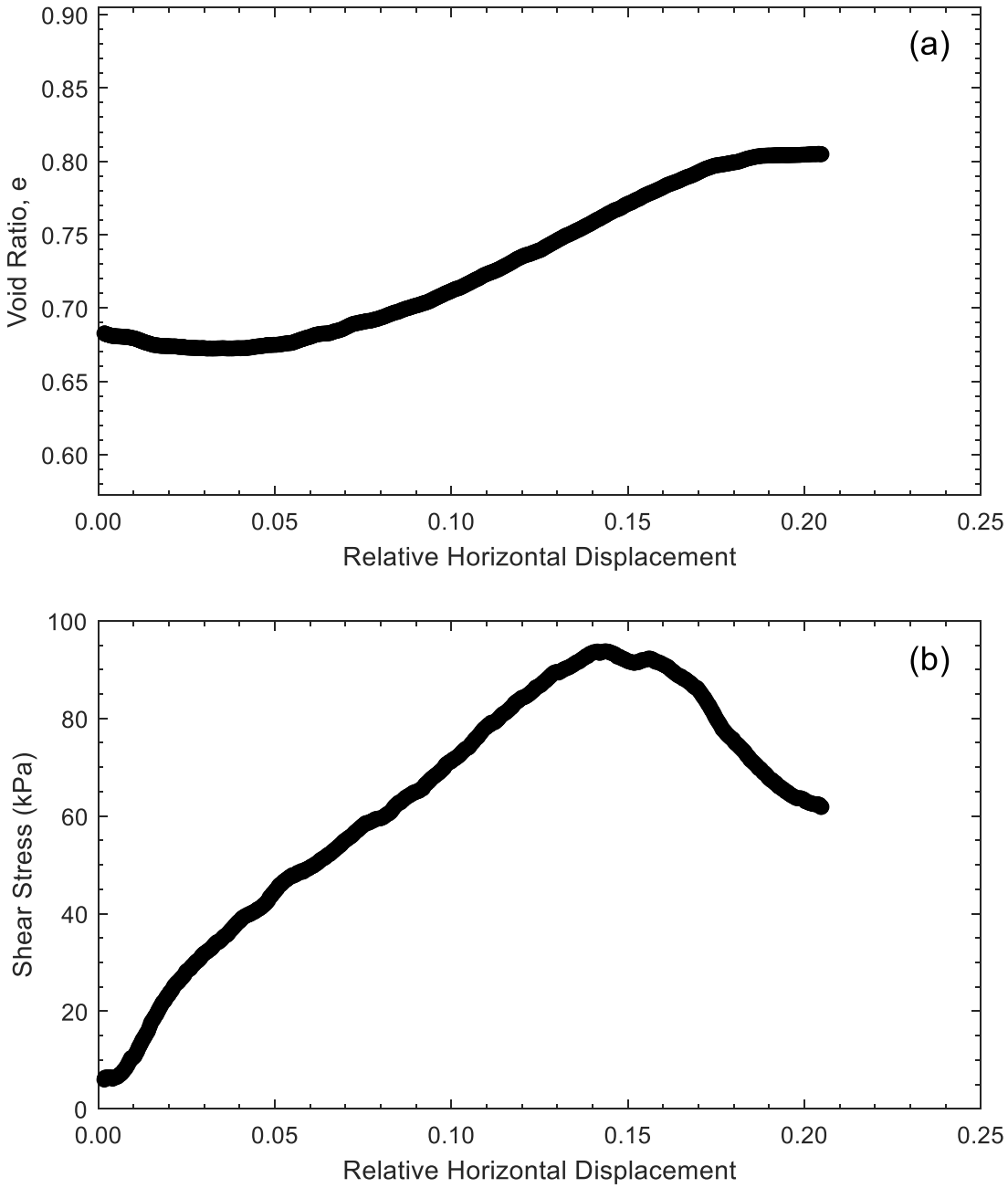

Figure D25. Direct shear test results for specimen 15B-0-A at 35 kPa effective stress: (a) Void ratio, e, versus relative horizontal displacement; (b) Shear stress (kPa) versus relative horizontal displacement.

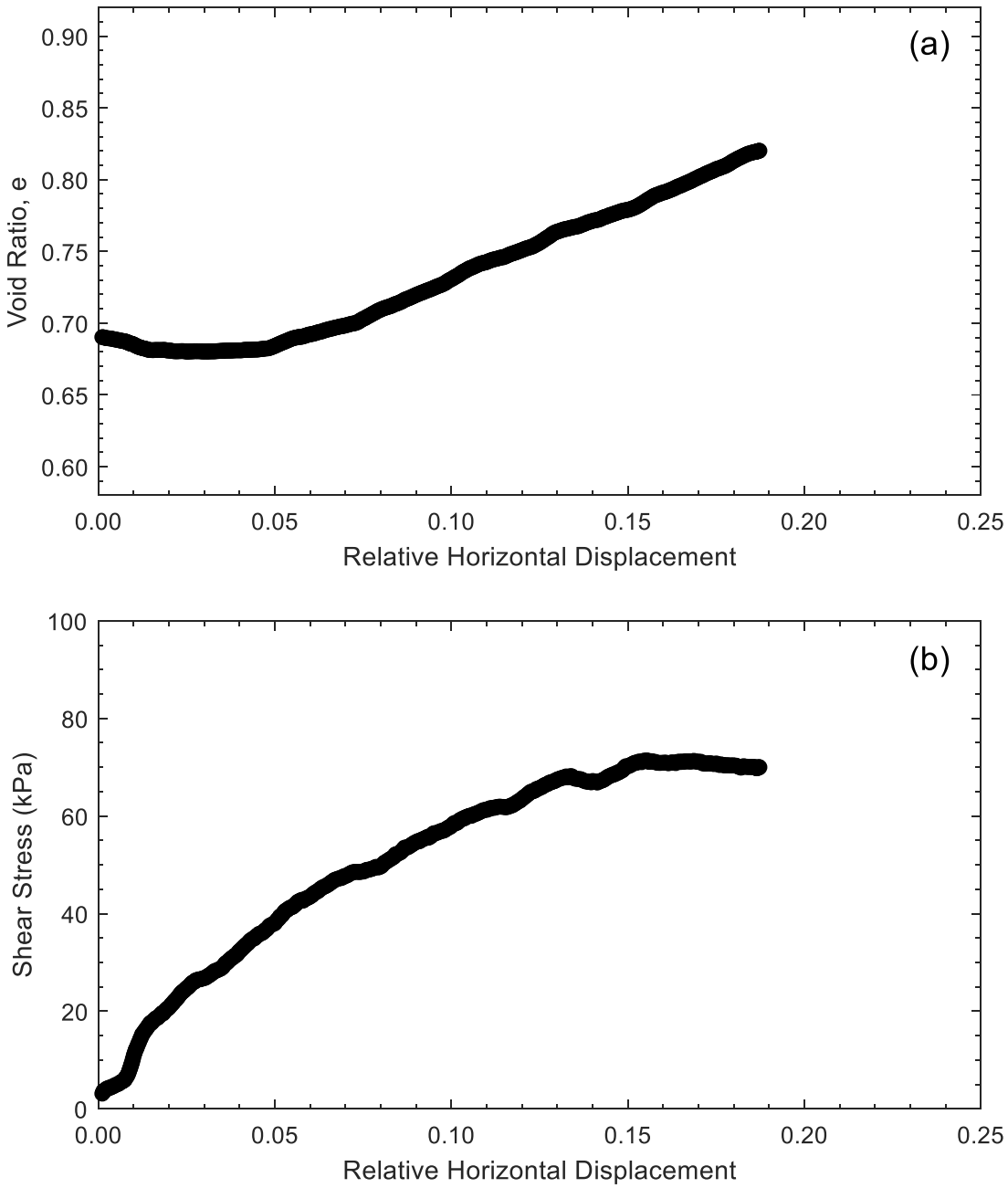

Figure D26. Direct shear test results for specimen 15B-0-dup-A at 35 kPa effective stress: (a) Void ratio, e, versus relative horizontal displacement; (b) Shear stress (kPa) versus relative horizontal displacement.

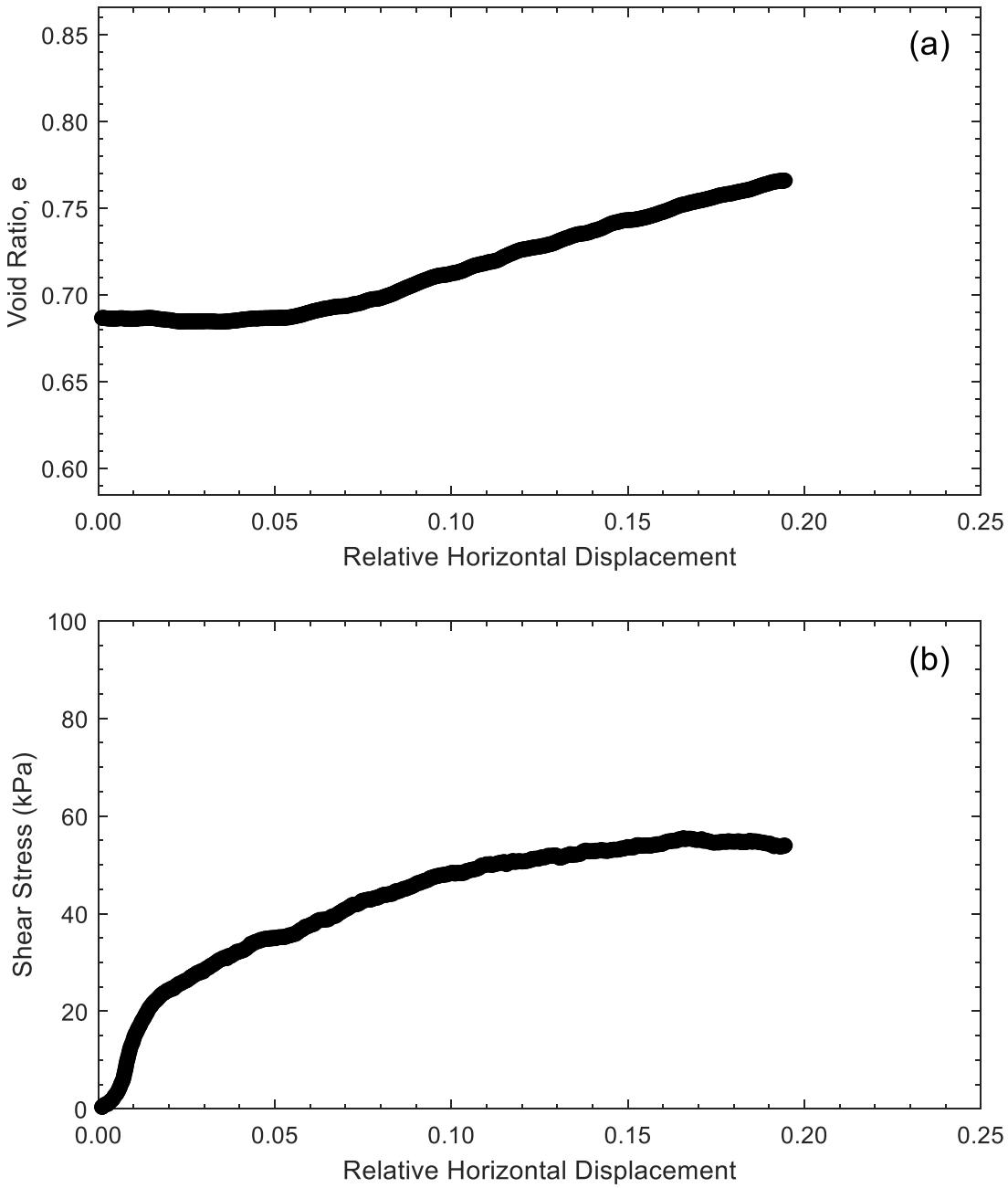

Figure D27. Direct shear test results for specimen 20B-0-A at 35 kPa effective stress: (a) Void ratio, e, versus relative horizontal displacement; (b) Shear stress (kPa) versus relative horizontal displacement.

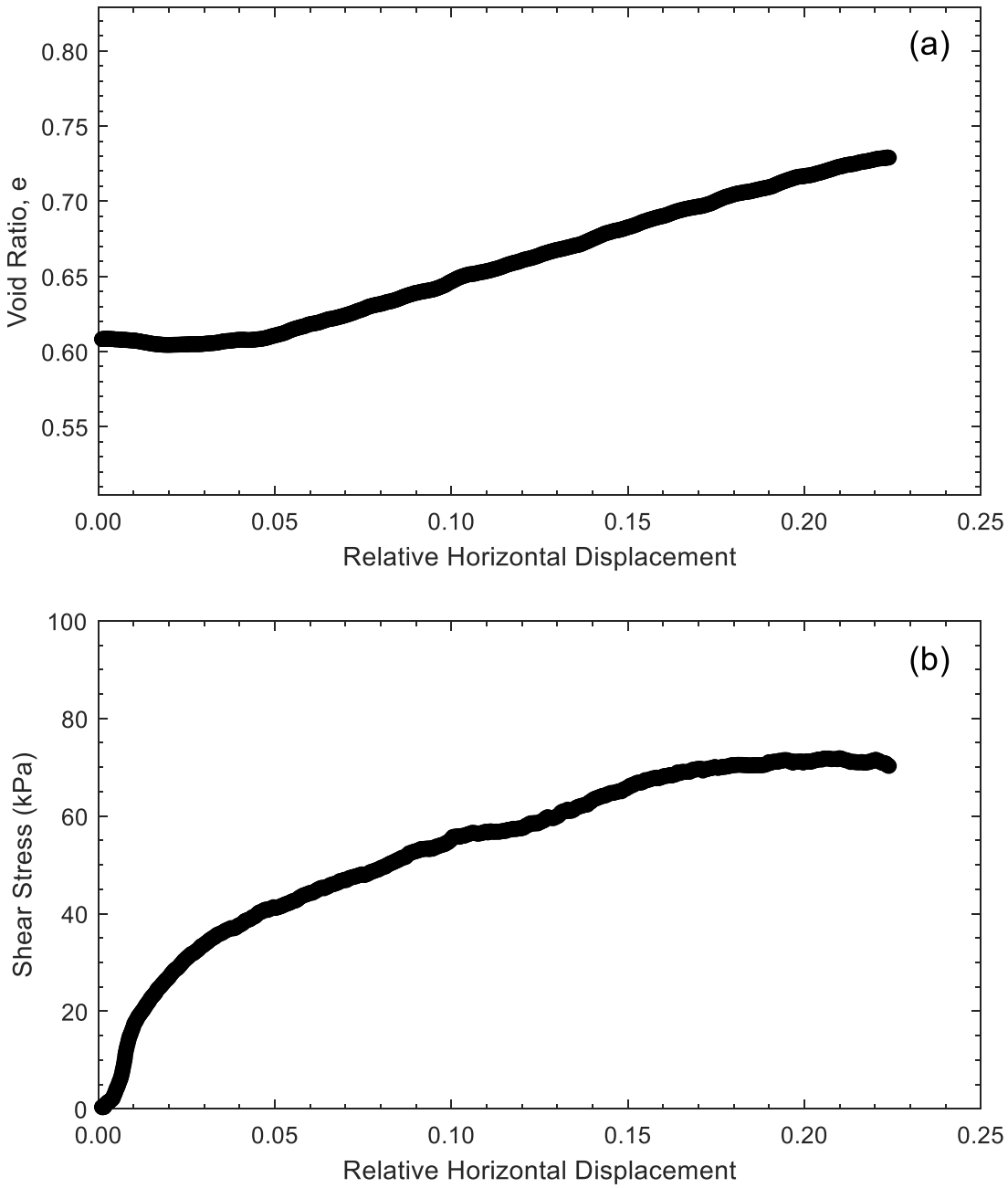

Figure D28. Direct shear test results for specimen 20B-0-dup-A at 35 kPa effective stress: (a) Void ratio, e, versus relative horizontal displacement; (b) Shear stress (kPa) versus relative horizontal displacement.

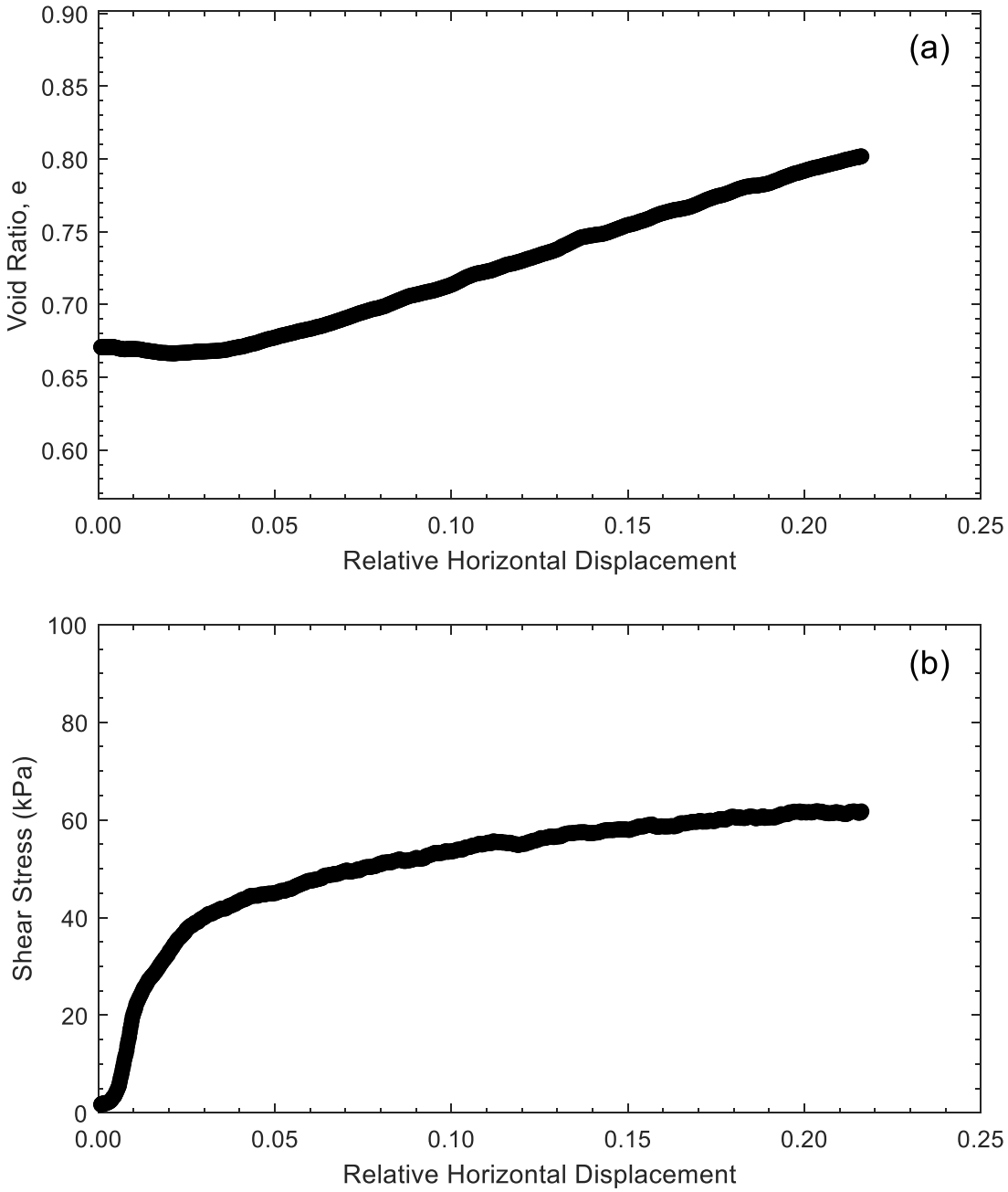

Figure D29. Direct shear test results for specimen 30B-0-A at 35 kPa effective stress: (a) Void ratio, e, versus relative horizontal displacement; (b) Shear stress (kPa) versus relative horizontal displacement.

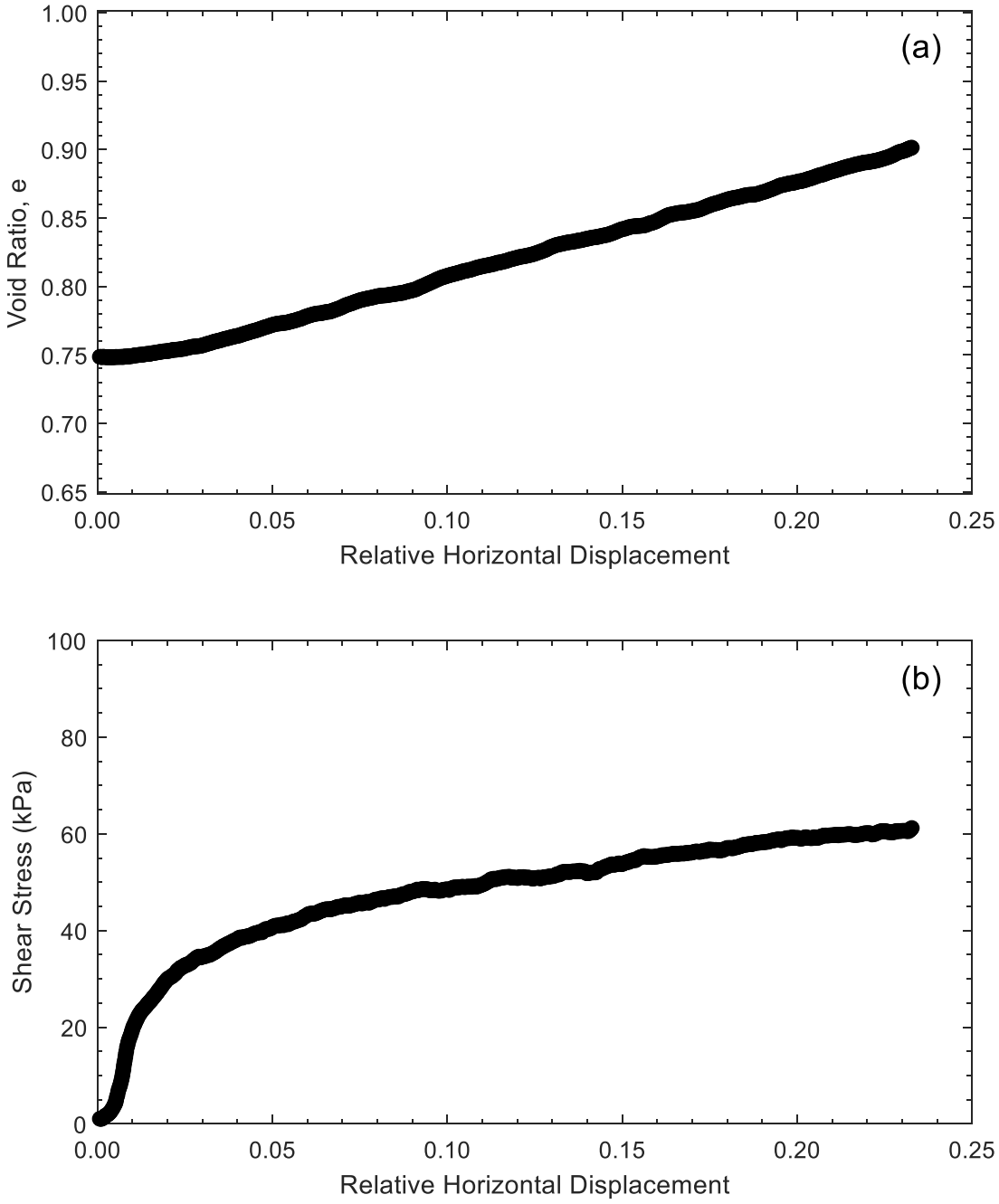

Figure D30. Direct shear test results for specimen 30B-0-dup-A at 35 kPa effective stress: (a) Void ratio, e, versus relative horizontal displacement; (b) Shear stress (kPa) versus relative horizontal displacement.

APPENDIX E – DIRECT SHEAR TEST RESULTS – 825 KPA

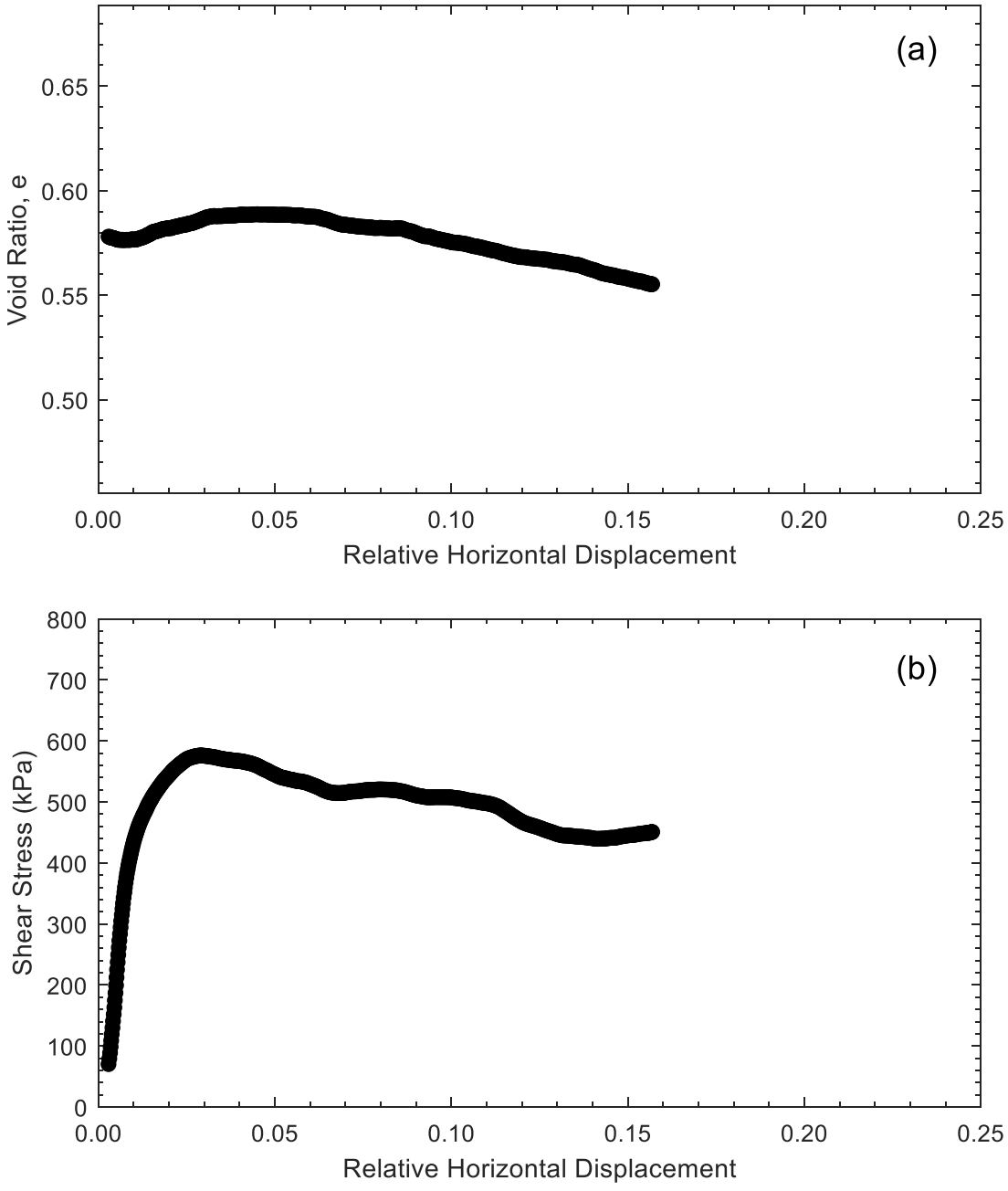

Figure E1. Direct shear test results for sand at 825 kPa effective stress: (a) Void ratio, e, versus relative horizontal displacement; (b) Shear stress (kPa) versus relative horizontal displacement.

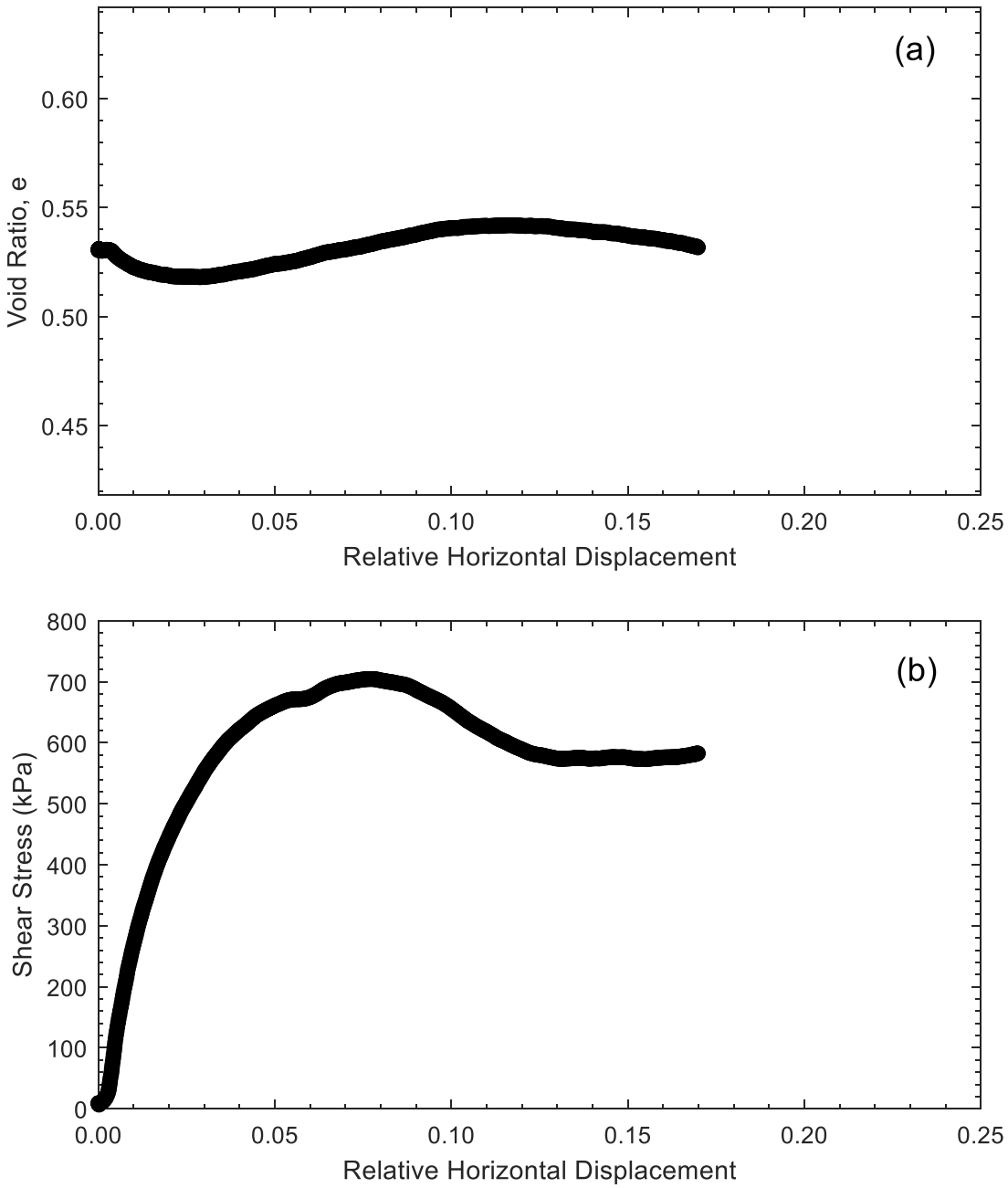

Figure E2. Direct shear test results for specimen 7B-0-H at 825 kPa effective stress: (a) Void ratio, e, versus relative horizontal displacement; (b) Shear stress (kPa) versus relative horizontal displacement.

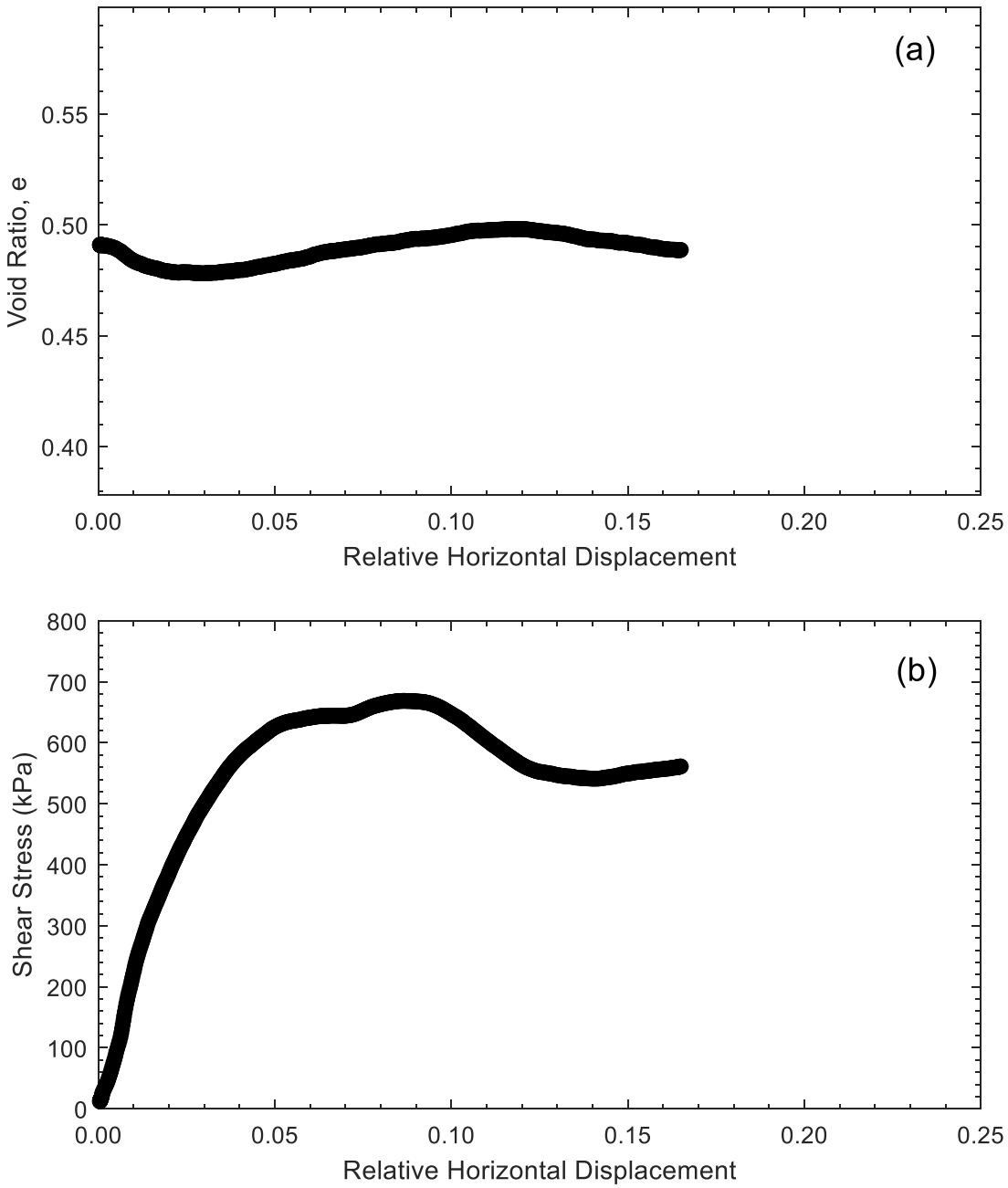

Figure E3. Direct shear test results for specimen 7B-10-H at 825 kPa effective stress: (a) Void ratio, e, versus relative horizontal displacement; (b) Shear stress (kPa) versus relative horizontal displacement.

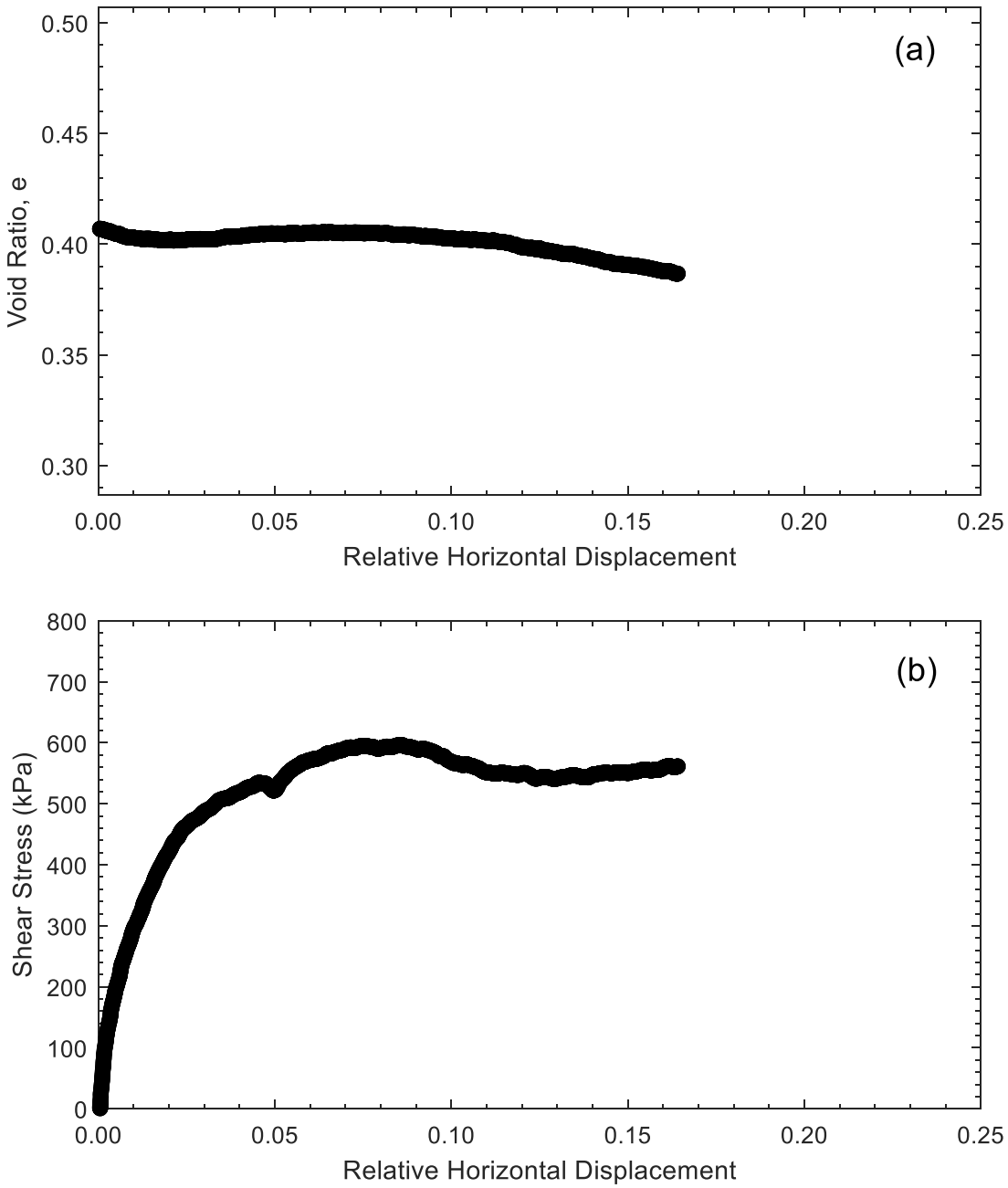

Figure E4. Direct shear test results for specimen 15K-0-H at 825 kPa effective stress: (a) Void ratio, e, versus relative horizontal displacement; (b) Shear stress (kPa) versus relative horizontal displacement.

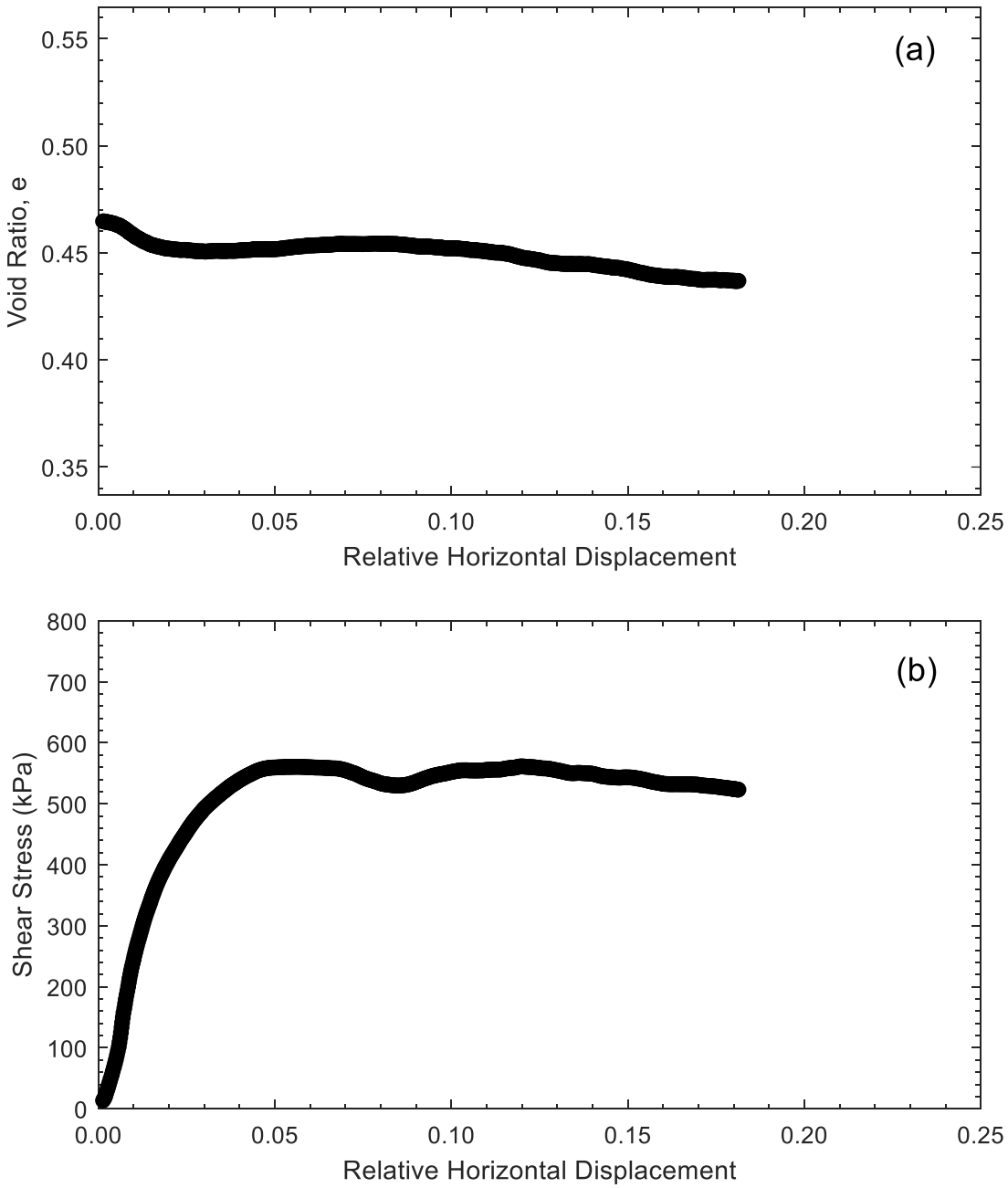

Figure E5. Direct shear test results for specimen 15K-10-H at 825 kPa effective stress: (a) Void ratio, e, versus relative horizontal displacement; (b) Shear stress (kPa) versus relative horizontal displacement.

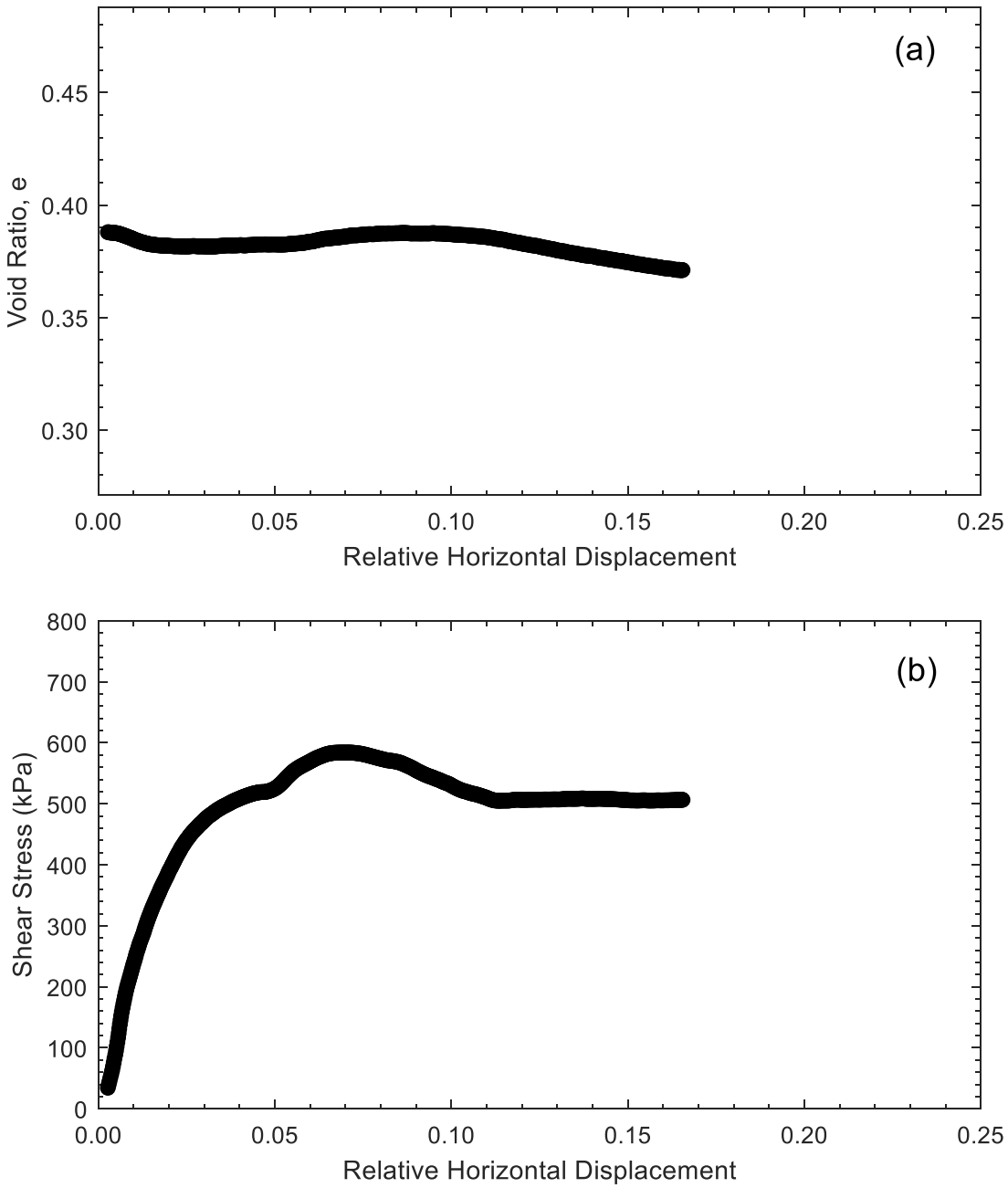

Figure E6. Direct shear test results for specimen 14R-0-H at 825 kPa effective stress: (a) Void ratio, e, versus relative horizontal displacement; (b) Shear stress (kPa) versus relative horizontal displacement.

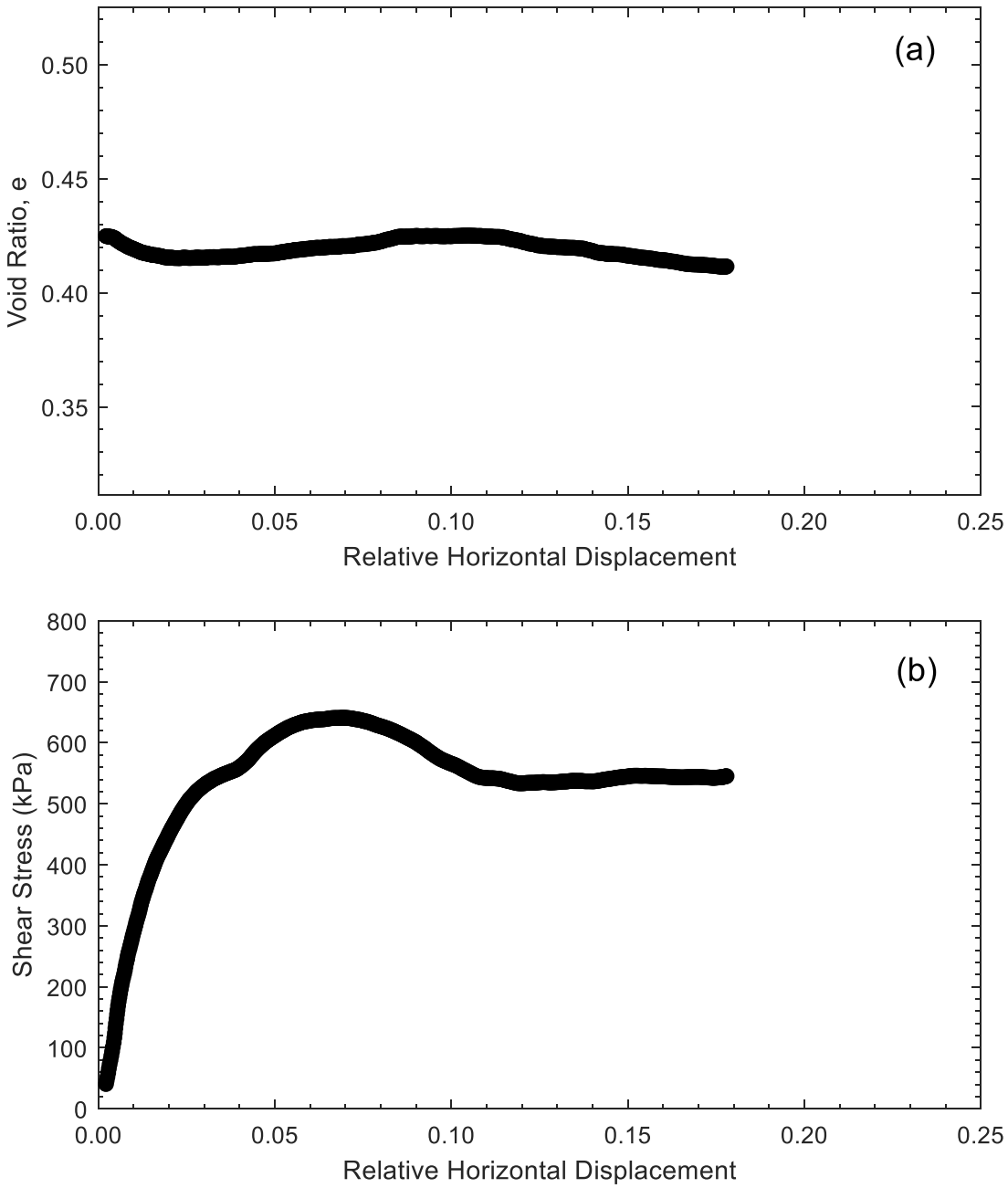

Figure E7. Direct shear test results for specimen 14R-10-H at 825 kPa effective stress: (a) Void ratio, e, versus relative horizontal displacement; (b) Shear stress (kPa) versus relative horizontal displacement.

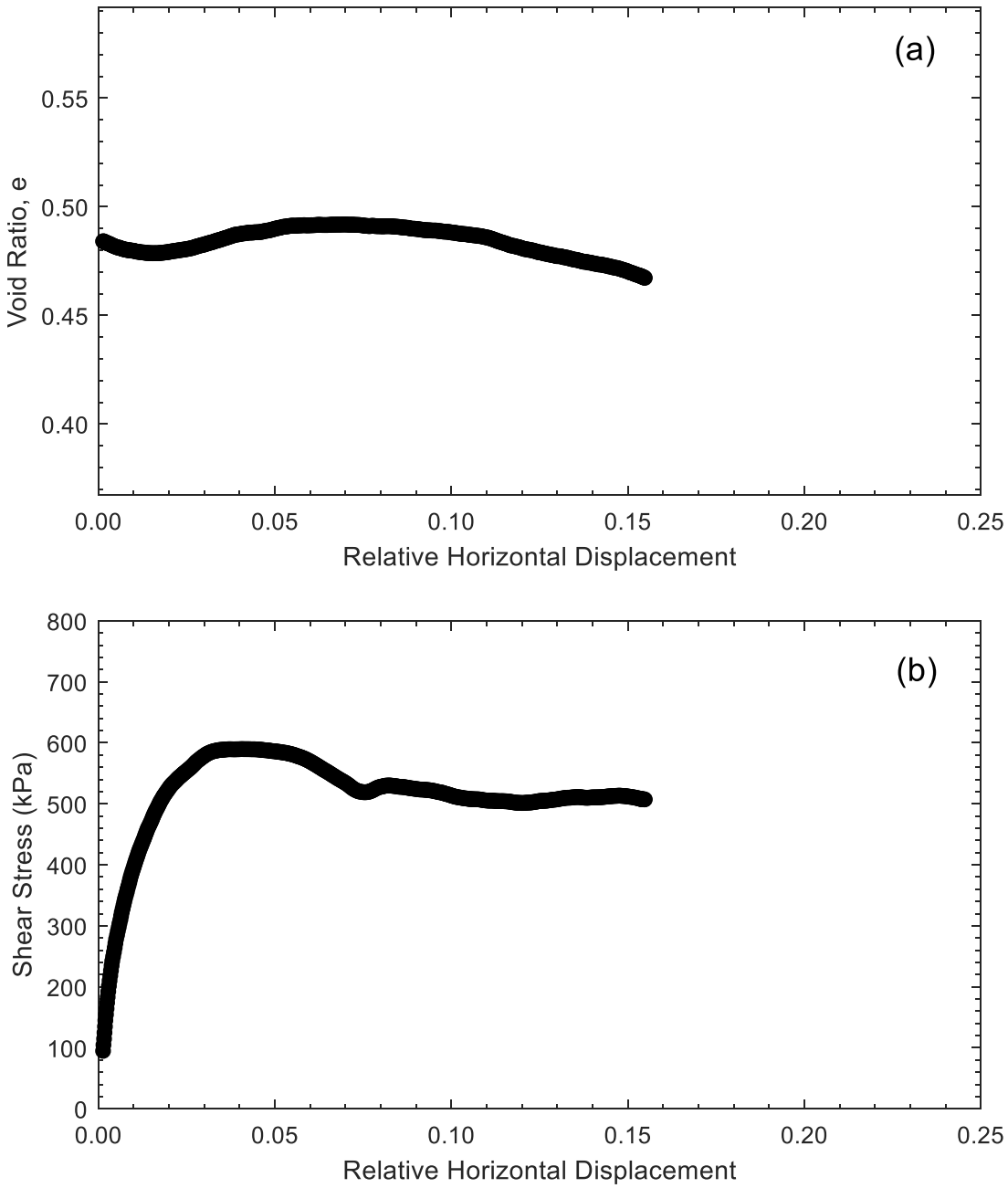

Figure E8. Direct shear test results for specimen 4B-0-H at 825 kPa effective stress: (a) Void ratio, e, versus relative horizontal displacement; (b) Shear stress (kPa) versus relative horizontal displacement.

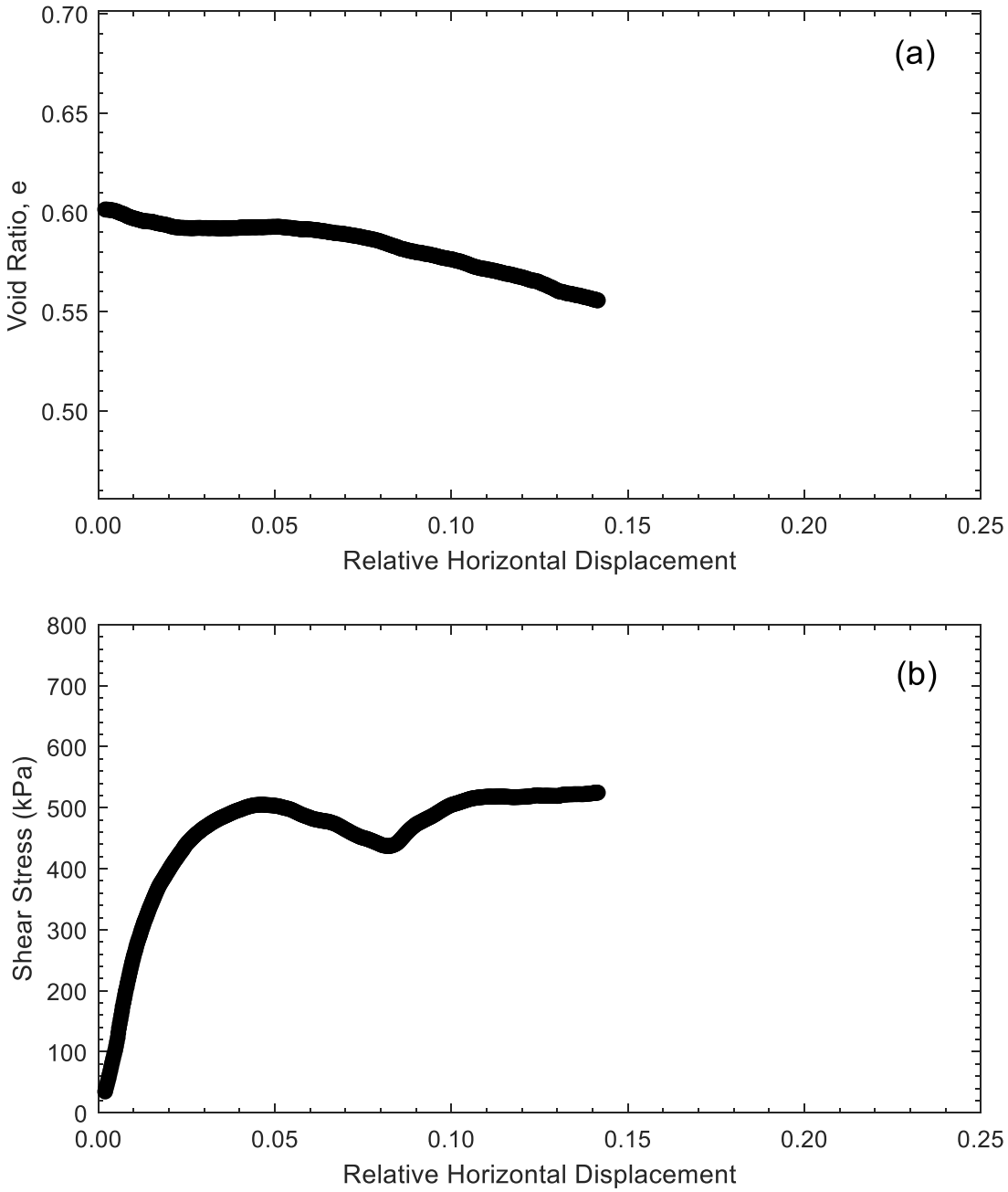

Figure E9. Direct shear test results for specimen 4B-10-H at 825 kPa effective stress: (a) Void ratio, e, versus relative horizontal displacement; (b) Shear stress (kPa) versus relative horizontal displacement.

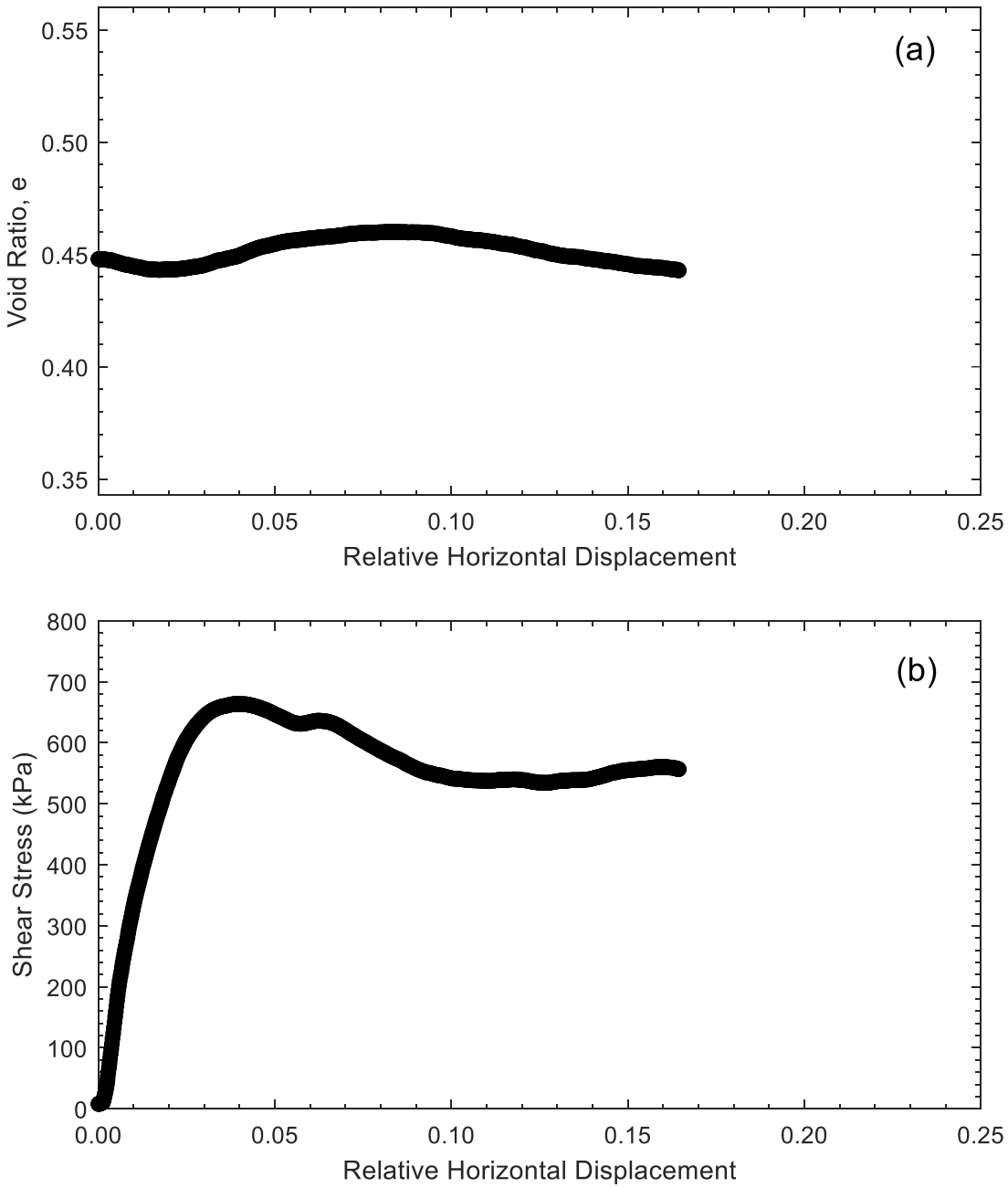

Figure E10. Direct shear test results for specimen 4B7R-0-H at 825 kPa effective stress: (a) Void ratio, e, versus relative horizontal displacement; (b) Shear stress (kPa) versus relative horizontal displacement.

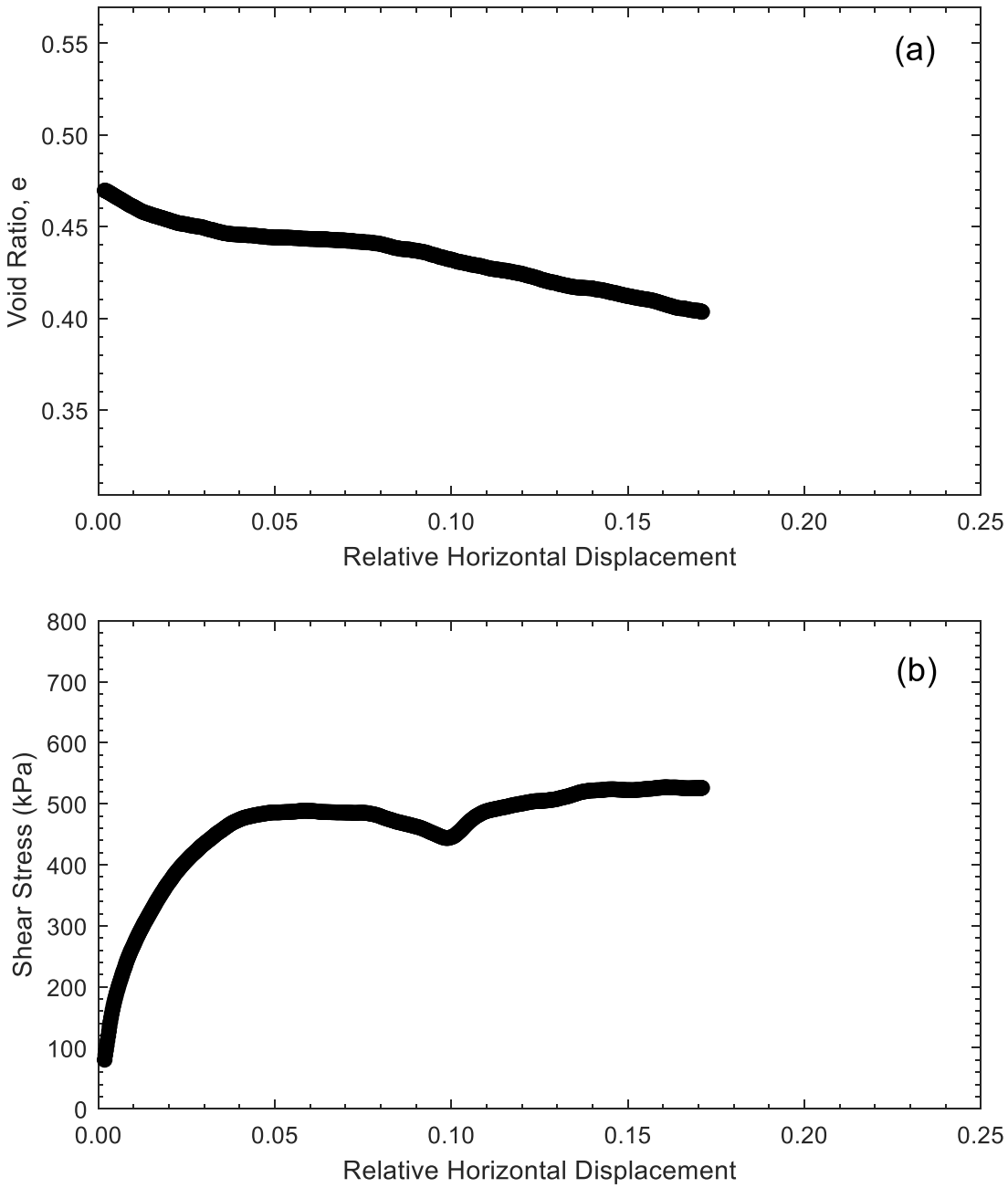

Figure E11. Direct shear test results for specimen 4B7R-10-H at 825 kPa effective stress: (a) Void ratio, e, versus relative horizontal displacement; (b) Shear stress (kPa) versus relative horizontal displacement.

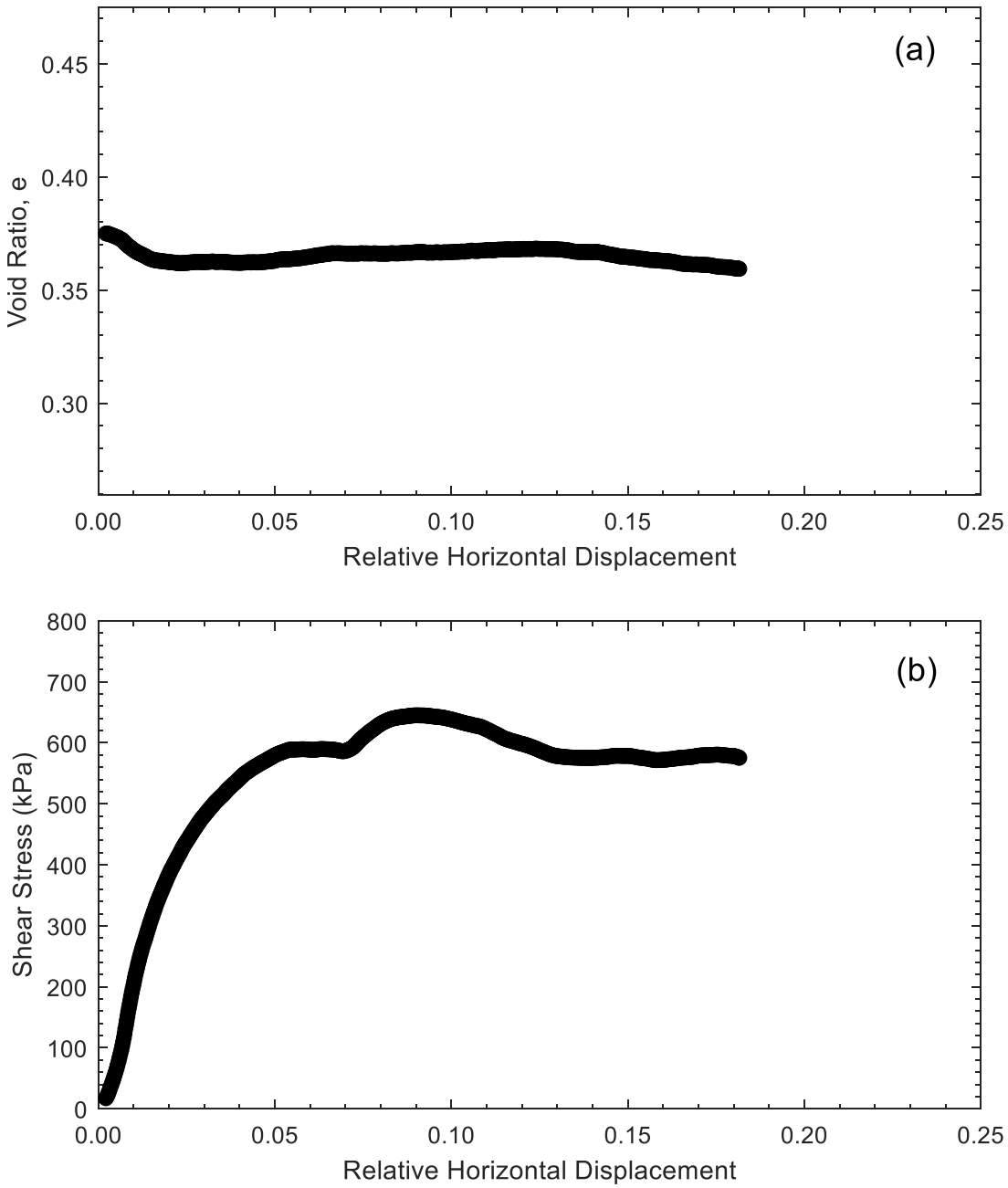

Figure E12. Direct shear test results for specimen 2B11R-0-H at 825 kPa effective stress: (a) Void ratio, e, versus relative horizontal displacement; (b) Shear stress (kPa) versus relative horizontal displacement.

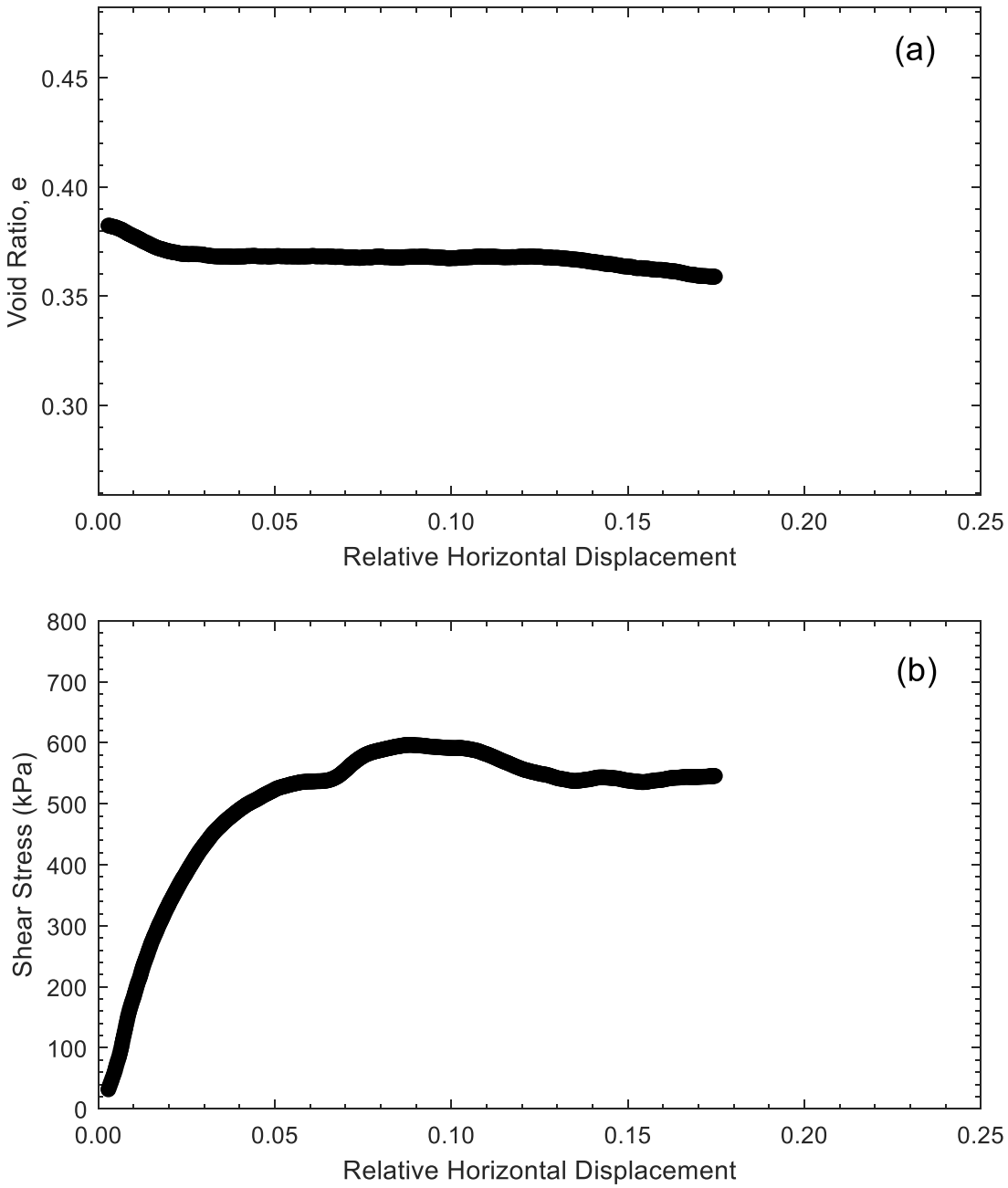

Figure E13. Direct shear test results for specimen 2B11R-10-H at 825 kPa effective stress: (a) Void ratio, e, versus relative horizontal displacement; (b) Shear stress (kPa) versus relative horizontal displacement.

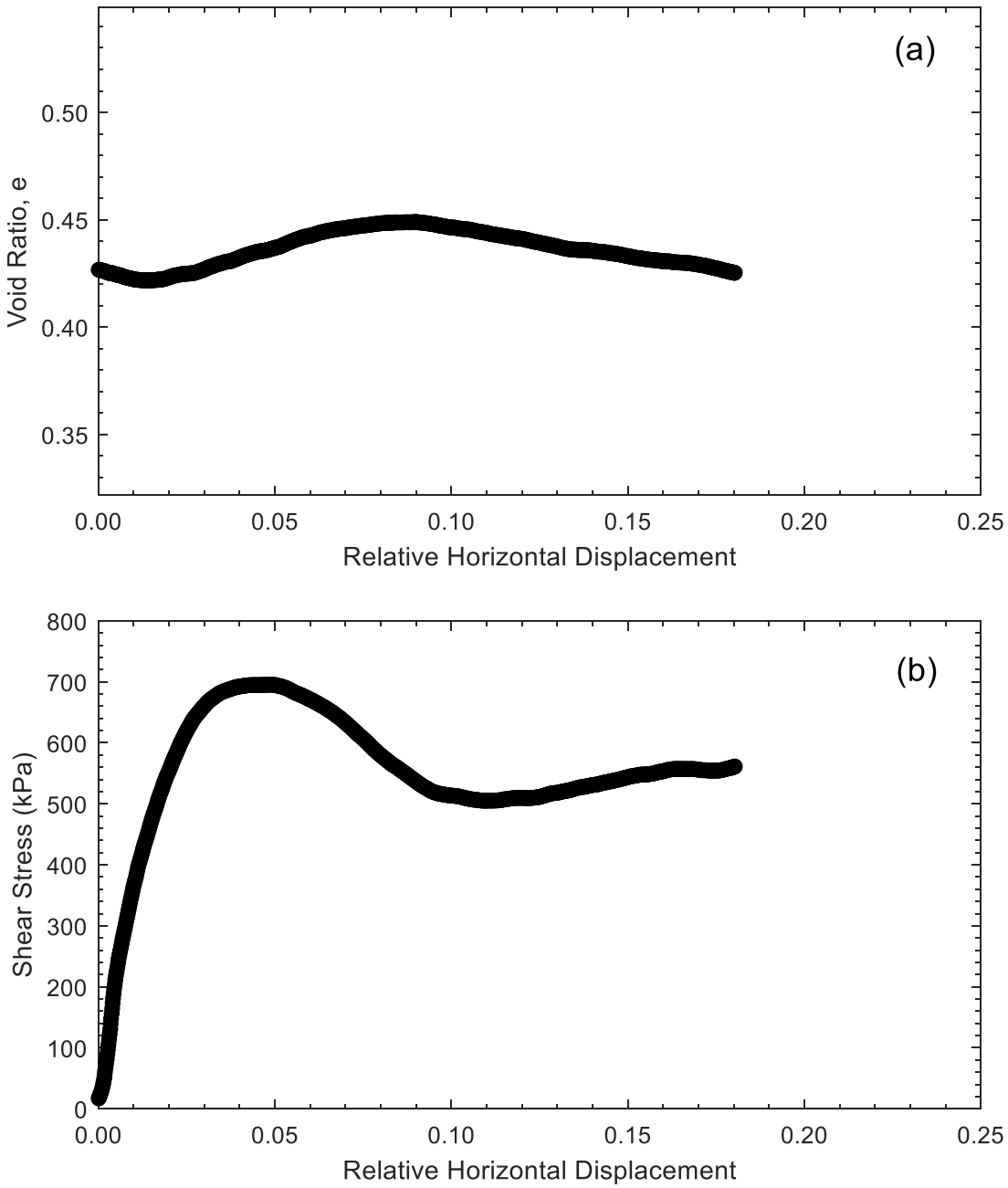

Figure E14. Direct shear test results for specimen 5B4R-0-H at 825 kPa effective stress: (a) Void ratio, e, versus relative horizontal displacement; (b) Shear stress (kPa) versus relative horizontal displacement.

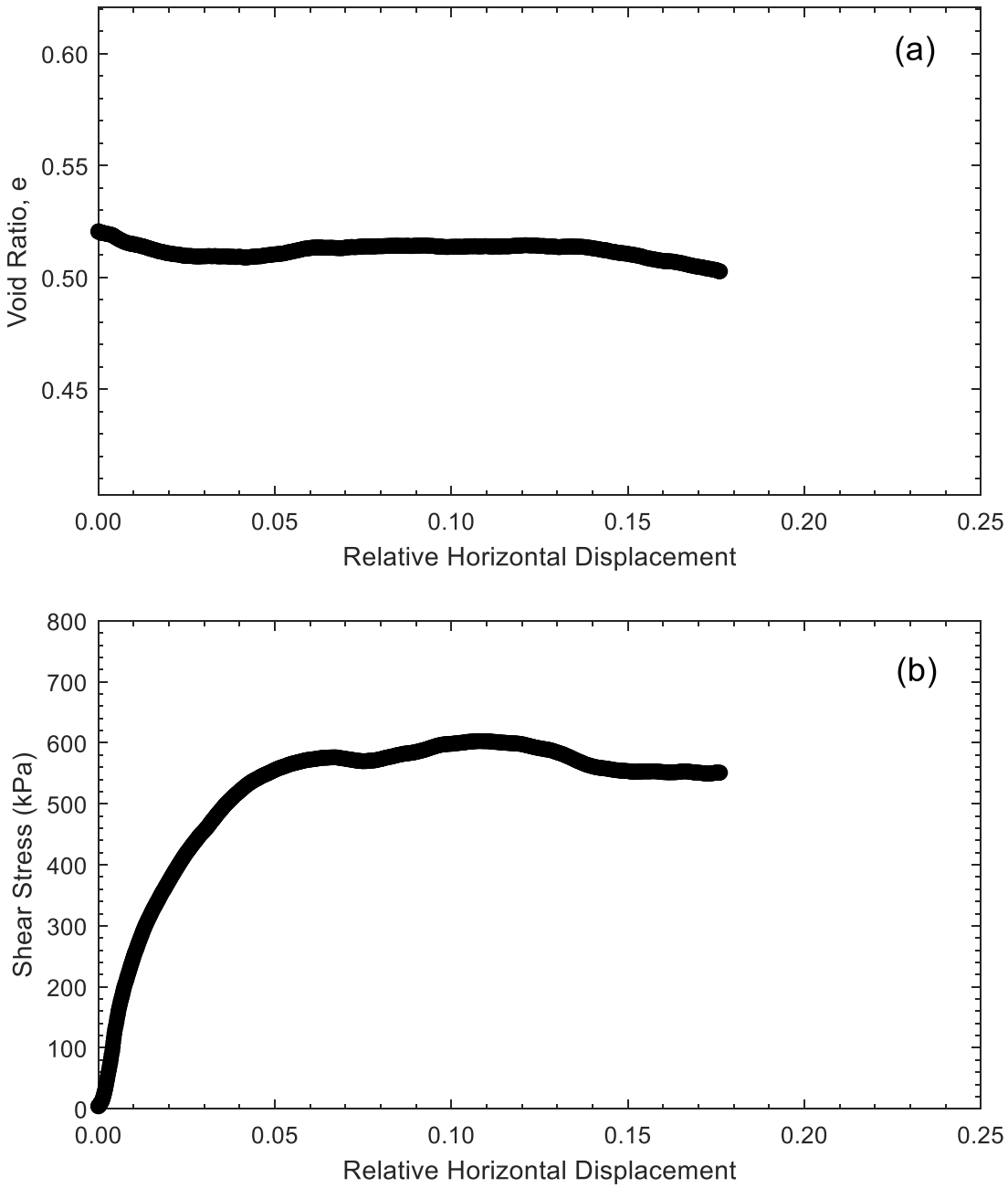

Figure E15. Direct shear test results for specimen 5B4R-10-H at 825 kPa effective stress: (a) Void ratio, e, versus relative horizontal displacement; (b) Shear stress (kPa) versus relative horizontal displacement.

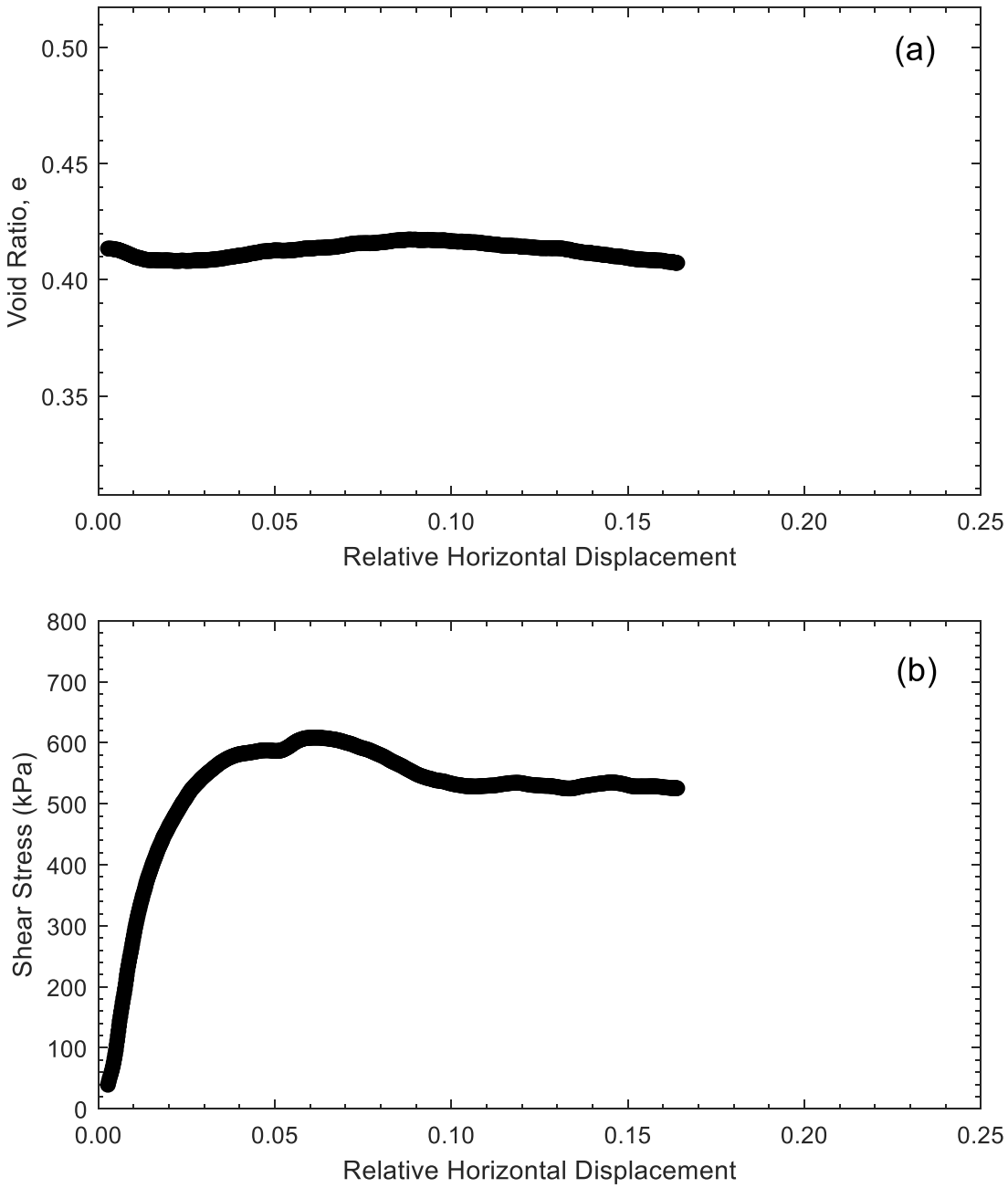

Figure E16. Direct shear test results for specimen 2B11R-0-A at 825 kPa effective stress: (a) Void ratio, e, versus relative horizontal displacement; (b) Shear stress (kPa) versus relative horizontal displacement.

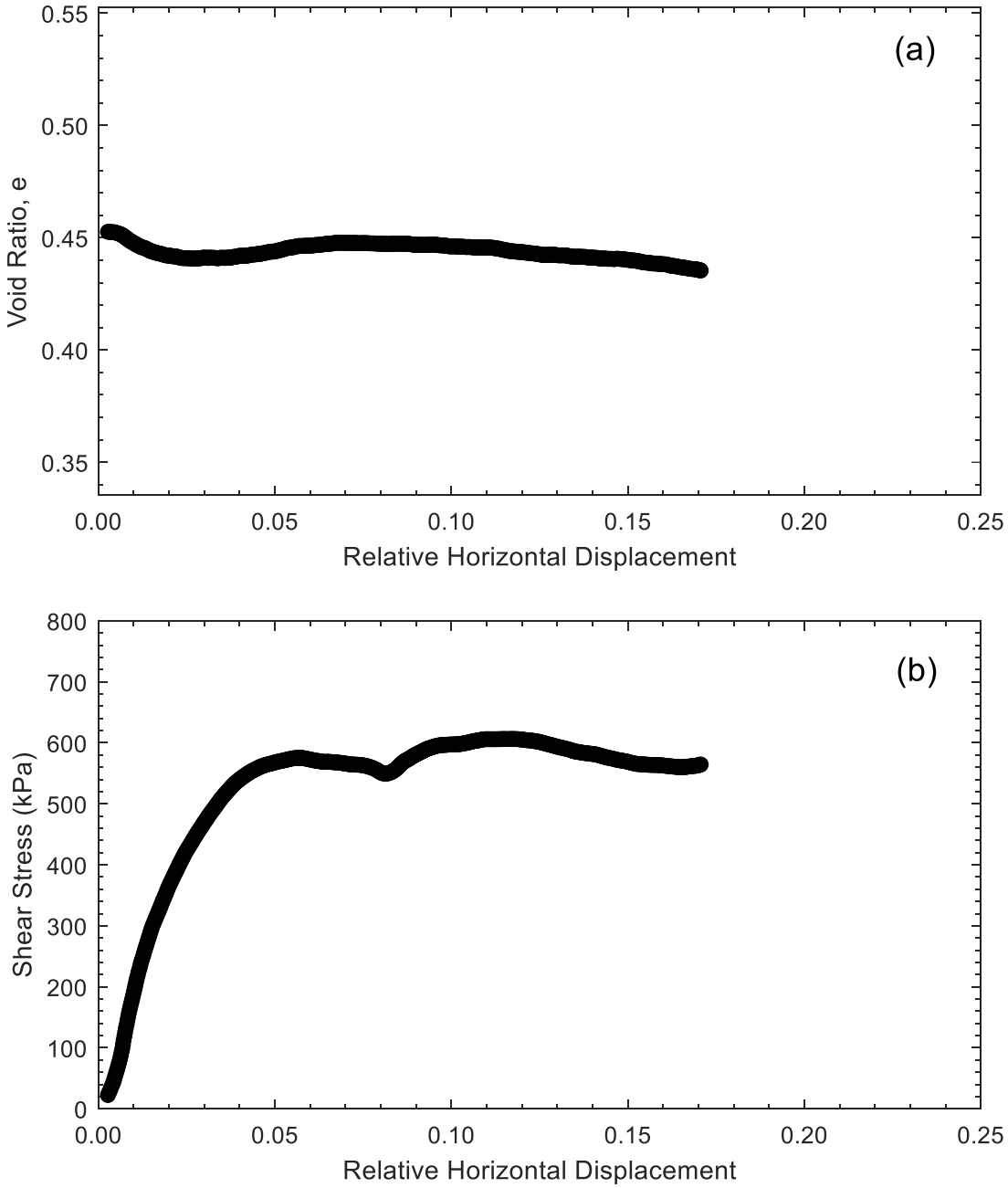

Figure E17. Direct shear test results for specimen 2B11R-10-A at 825 kPa effective stress: (a) Void ratio, e, versus relative horizontal displacement; (b) Shear stress (kPa) versus relative horizontal displacement.

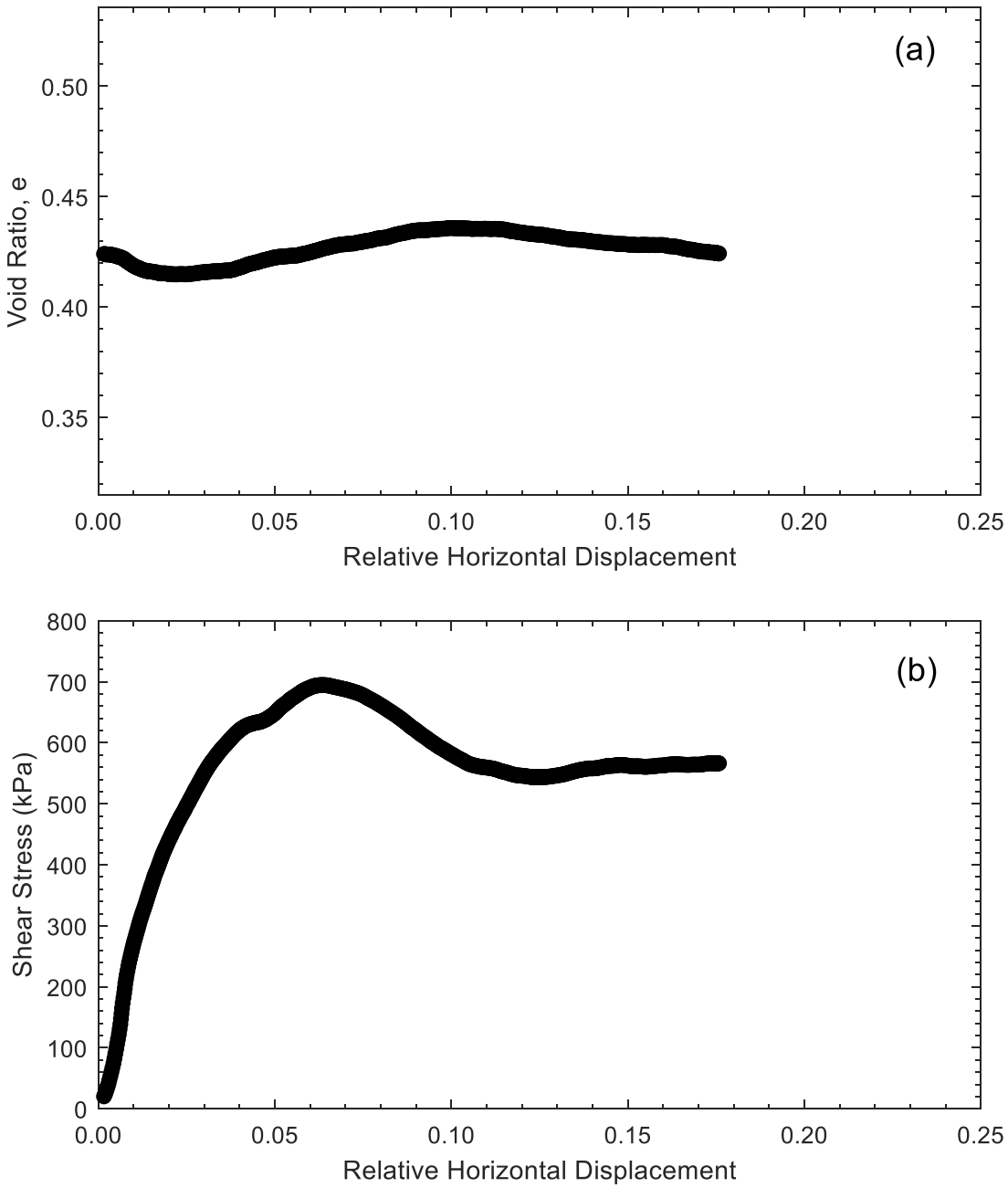

Figure E18. Direct shear test results for specimen 4B7R-0-A at 825 kPa effective stress: (a) Void ratio, e, versus relative horizontal displacement; (b) Shear stress (kPa) versus relative horizontal displacement.

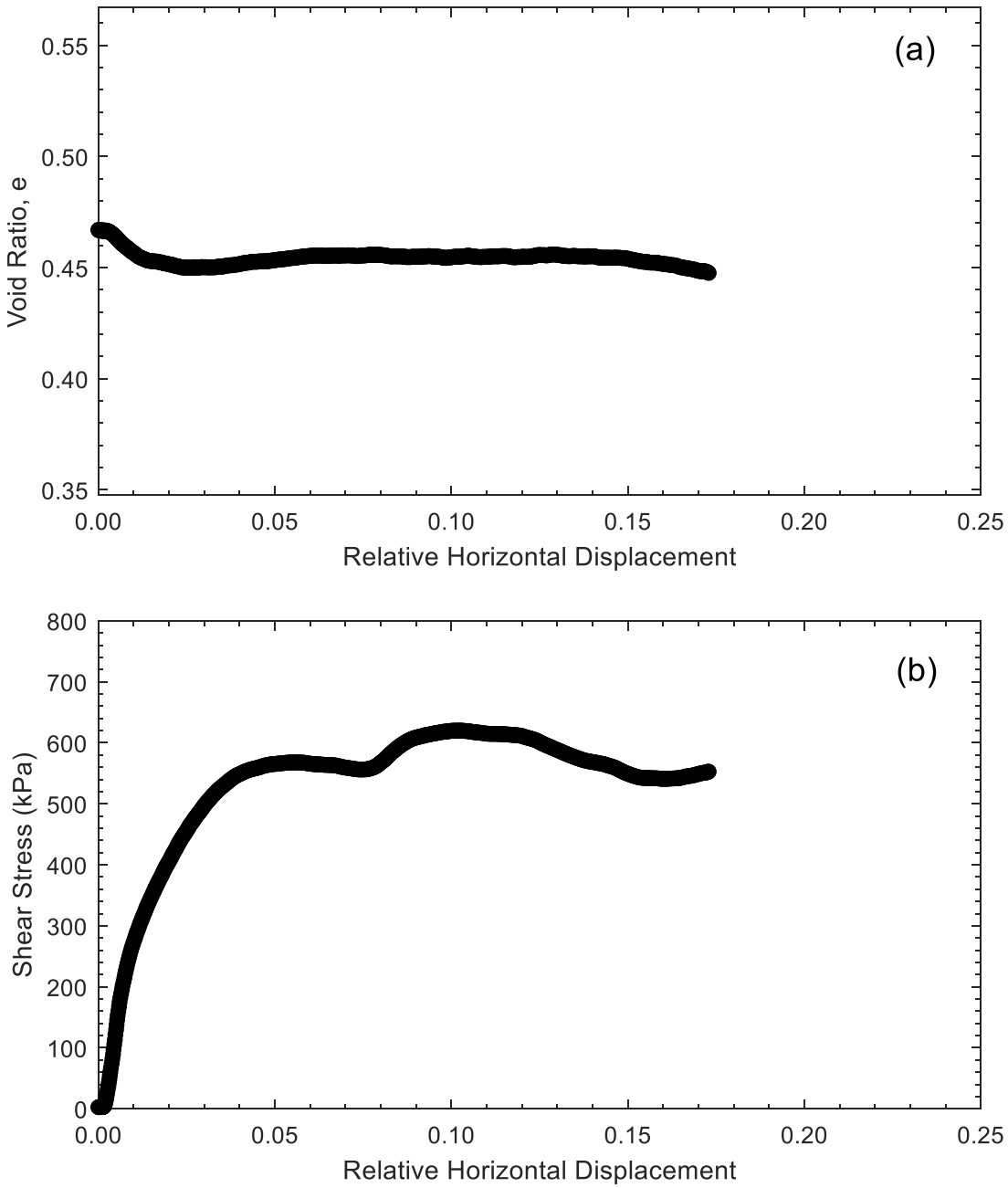

Figure E19. Direct shear test results for specimen 4B7R-10-A at 825 kPa effective stress: (a) Void ratio, e, versus relative horizontal displacement; (b) Shear stress (kPa) versus relative horizontal displacement.

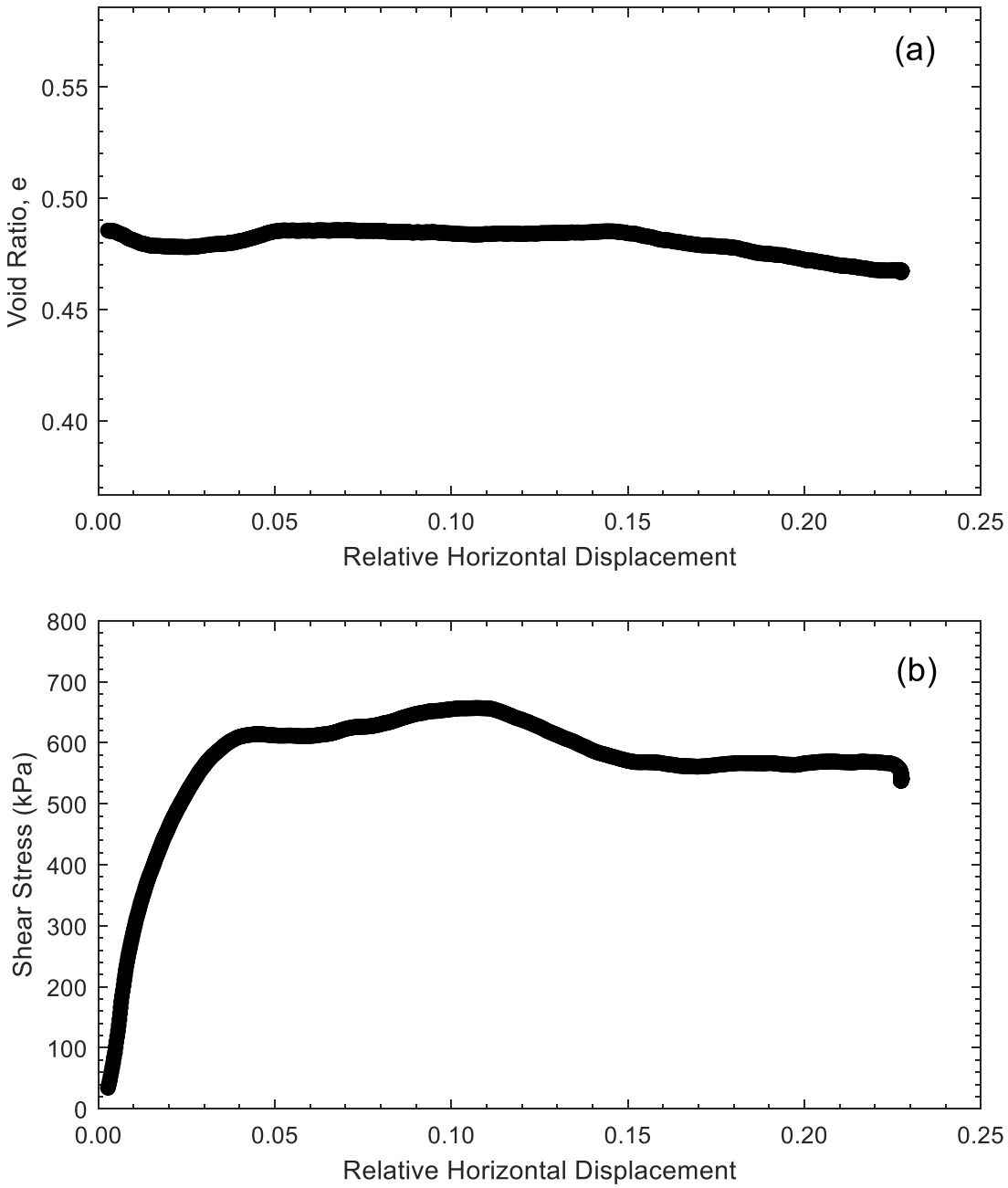

Figure E20. Direct shear test results for specimen 5B4R-0-A at 825 kPa effective stress: (a) Void ratio, e, versus relative horizontal displacement; (b) Shear stress (kPa) versus relative horizontal displacement.

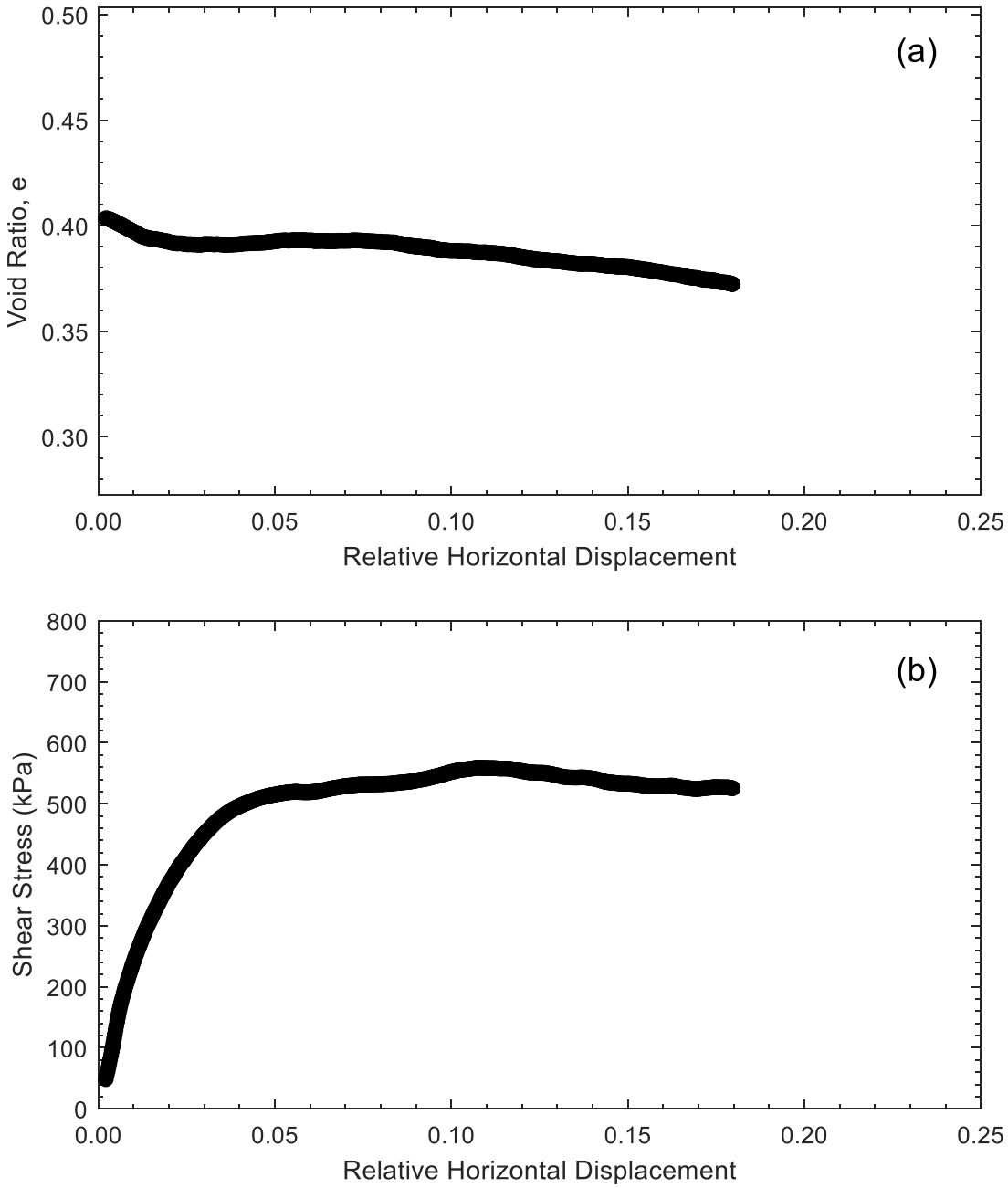

Figure E21. Direct shear test results for specimen 5B4R-10-A at 825 kPa effective stress: (a) Void ratio, e, versus relative horizontal displacement; (b) Shear stress (kPa) versus relative horizontal displacement.

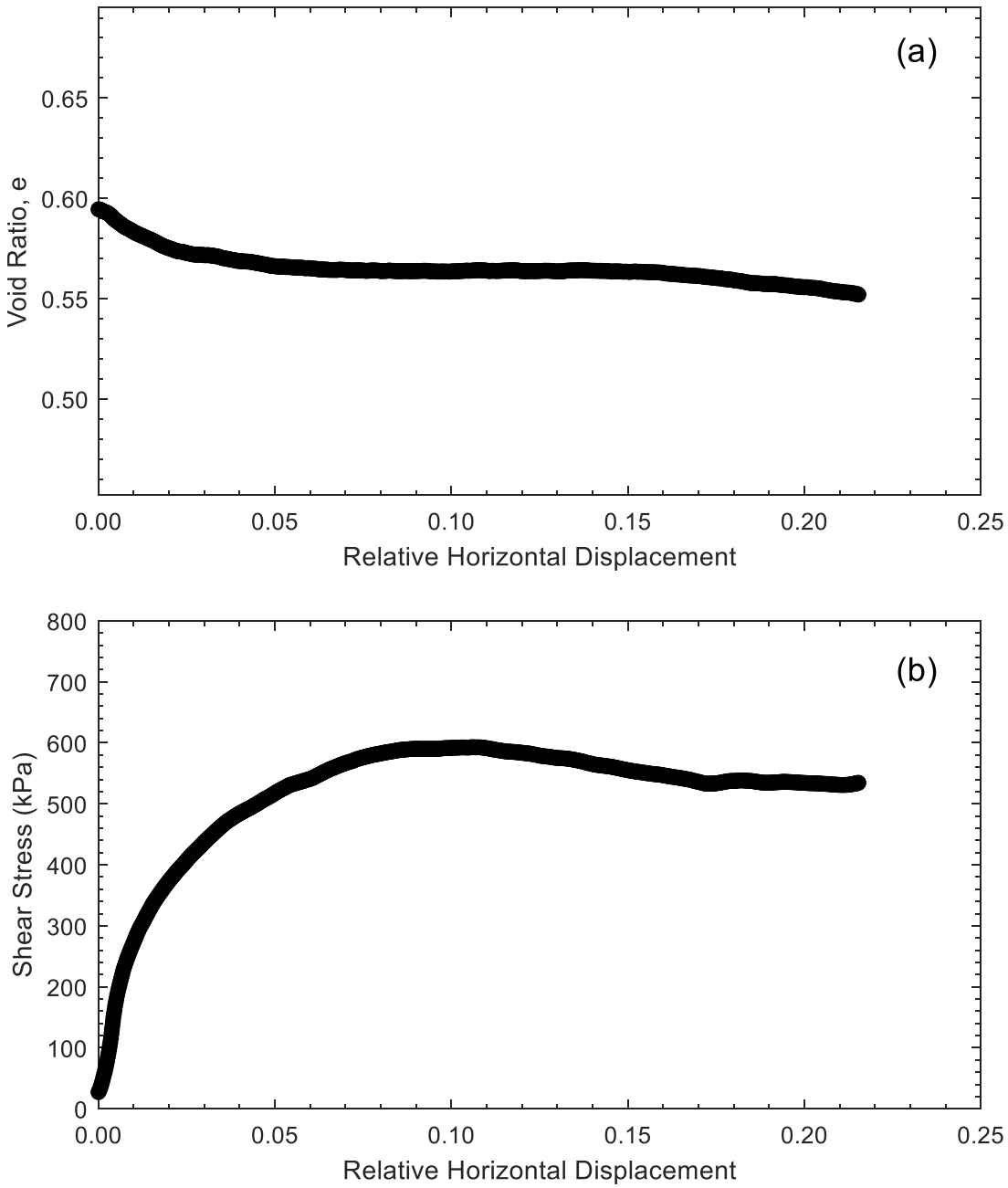

Figure E22. Direct shear test results for specimen 8B-10-A at 825 kPa effective stress: (a) Void ratio, e, versus relative horizontal displacement; (b) Shear stress (kPa) versus relative horizontal displacement.

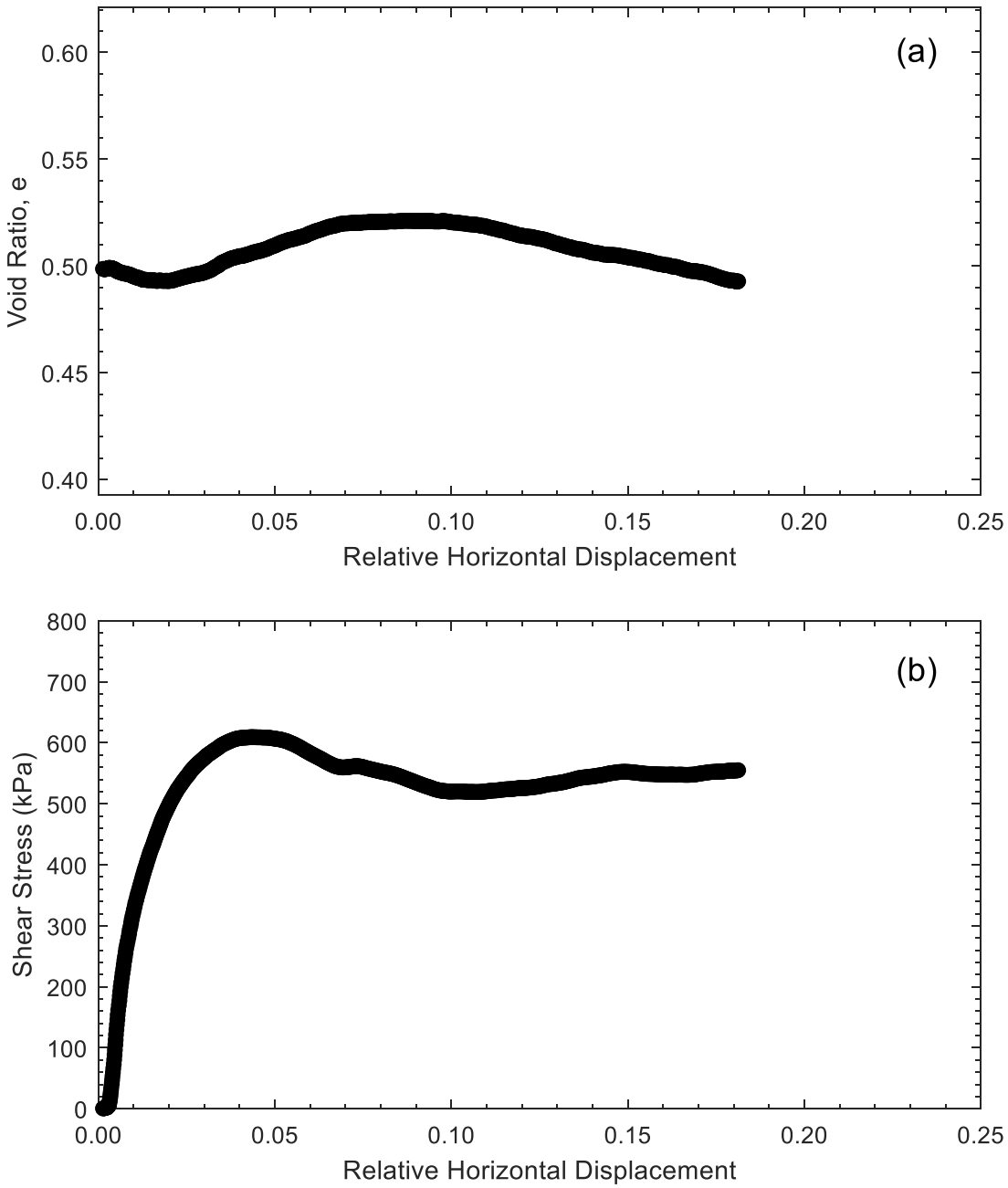

Figure E23. Direct shear test results for specimen 10B-500-A at 825 kPa effective stress: (a) Void ratio, e, versus relative horizontal displacement; (b) Shear stress (kPa) versus relative horizontal displacement.

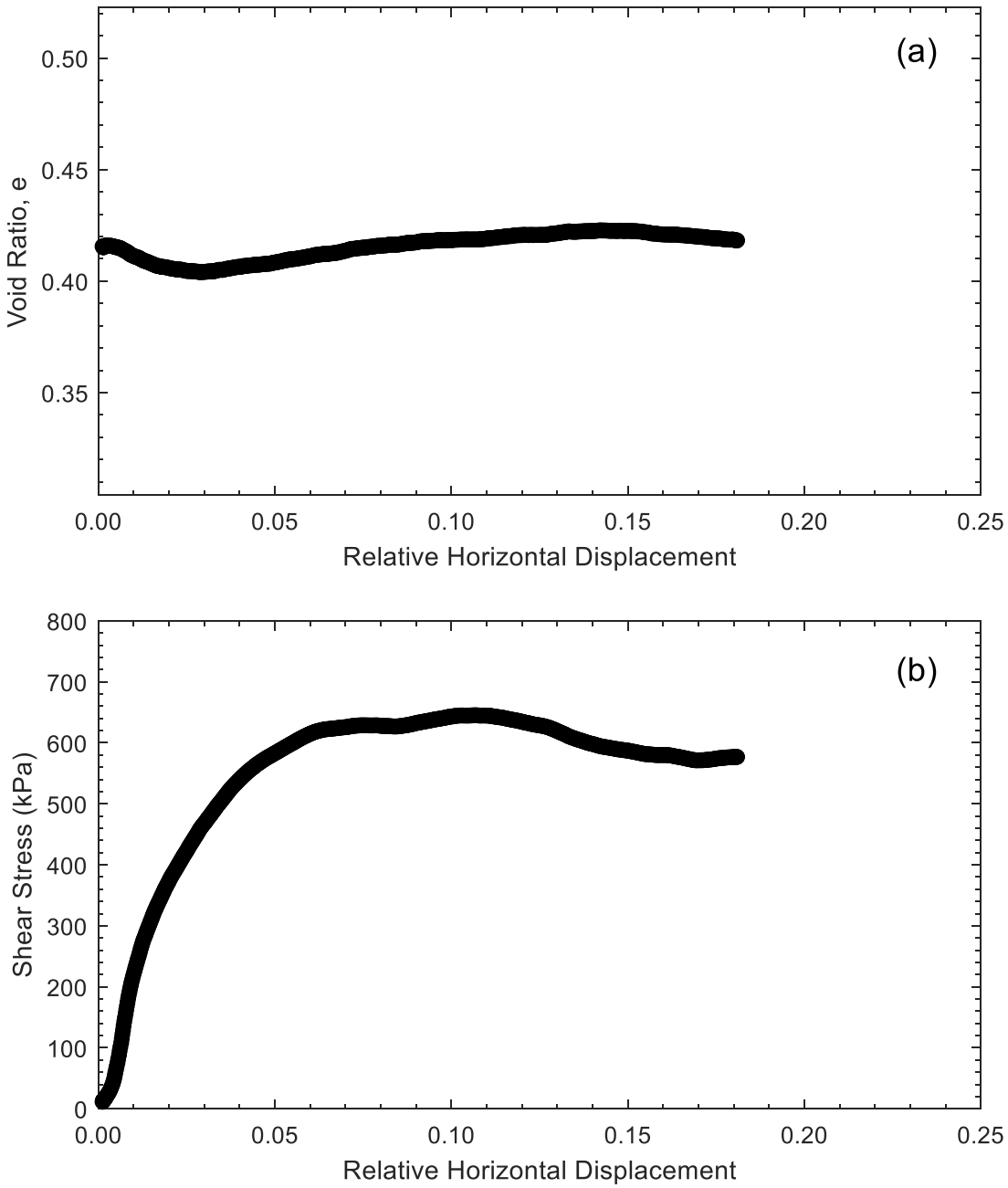

Figure E24. Direct shear test results for specimen 15B-500-A at 825 kPa effective stress: (a) Void ratio, e, versus relative horizontal displacement; (b) Shear stress (kPa) versus relative horizontal displacement.

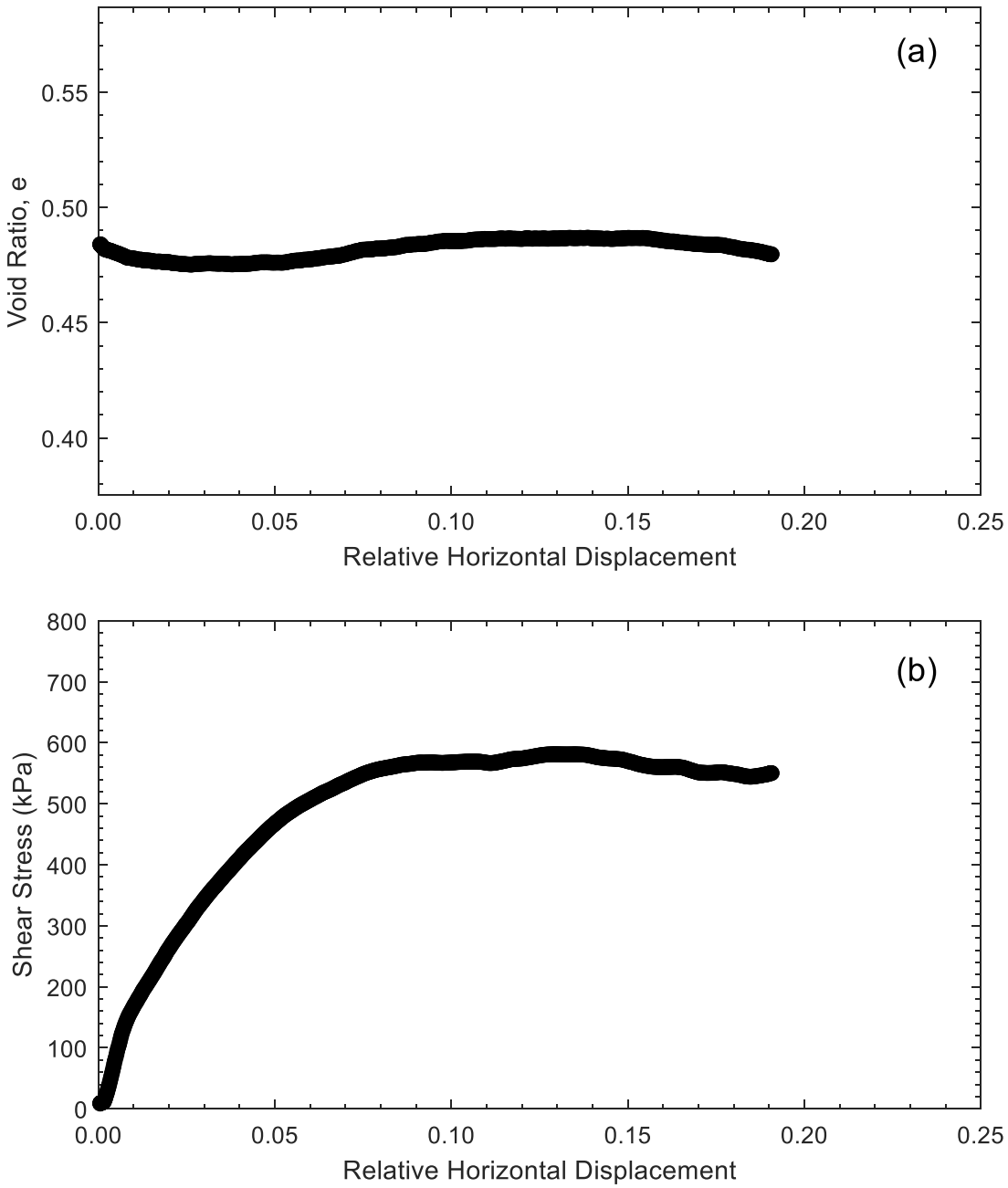

Figure E25. Direct shear test results for specimen 15B-0-A at 825 kPa effective stress: (a) Void ratio, e, versus relative horizontal displacement; (b) Shear stress (kPa) versus relative horizontal displacement.

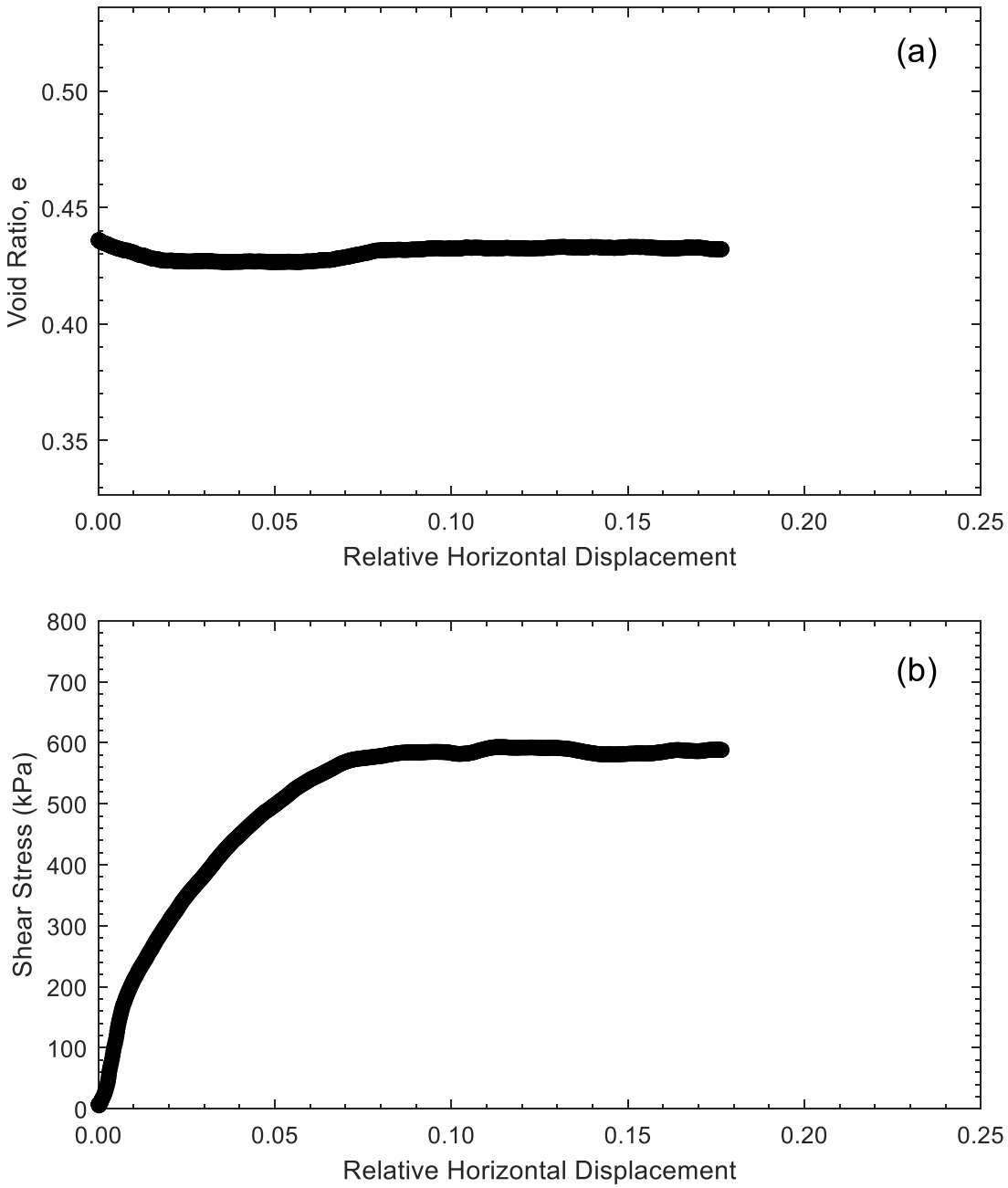

Figure E26. Direct shear test results for specimen 15B-0-dup-A at 825 kPa effective stress: (a) Void ratio, e, versus relative horizontal displacement; (b) Shear stress (kPa) versus relative horizontal displacement.

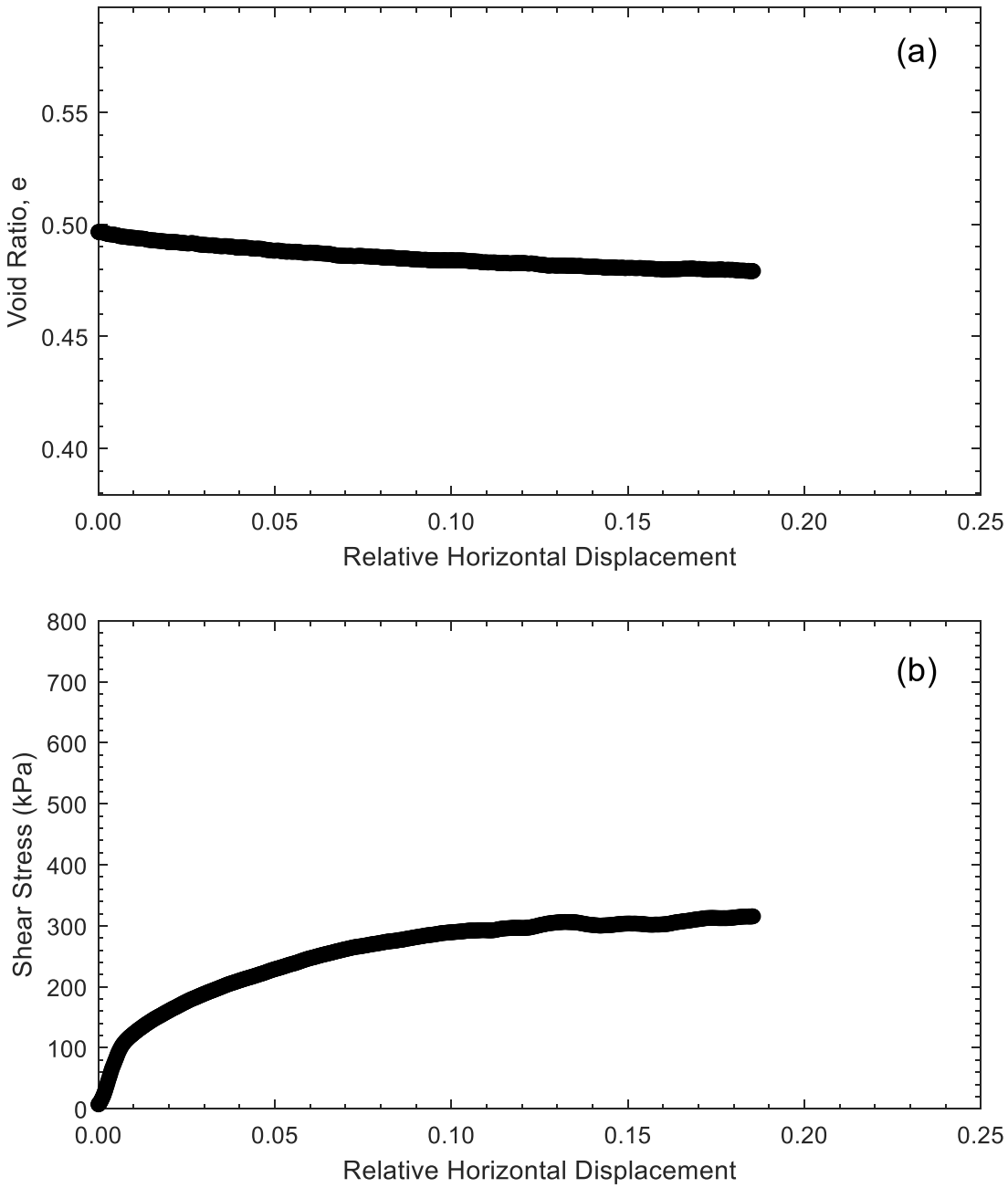

Figure E27. Direct shear test results for specimen 20B-0-A at 825 kPa effective stress: (a) Void ratio, e, versus relative horizontal displacement; (b) Shear stress (kPa) versus relative horizontal displacement.

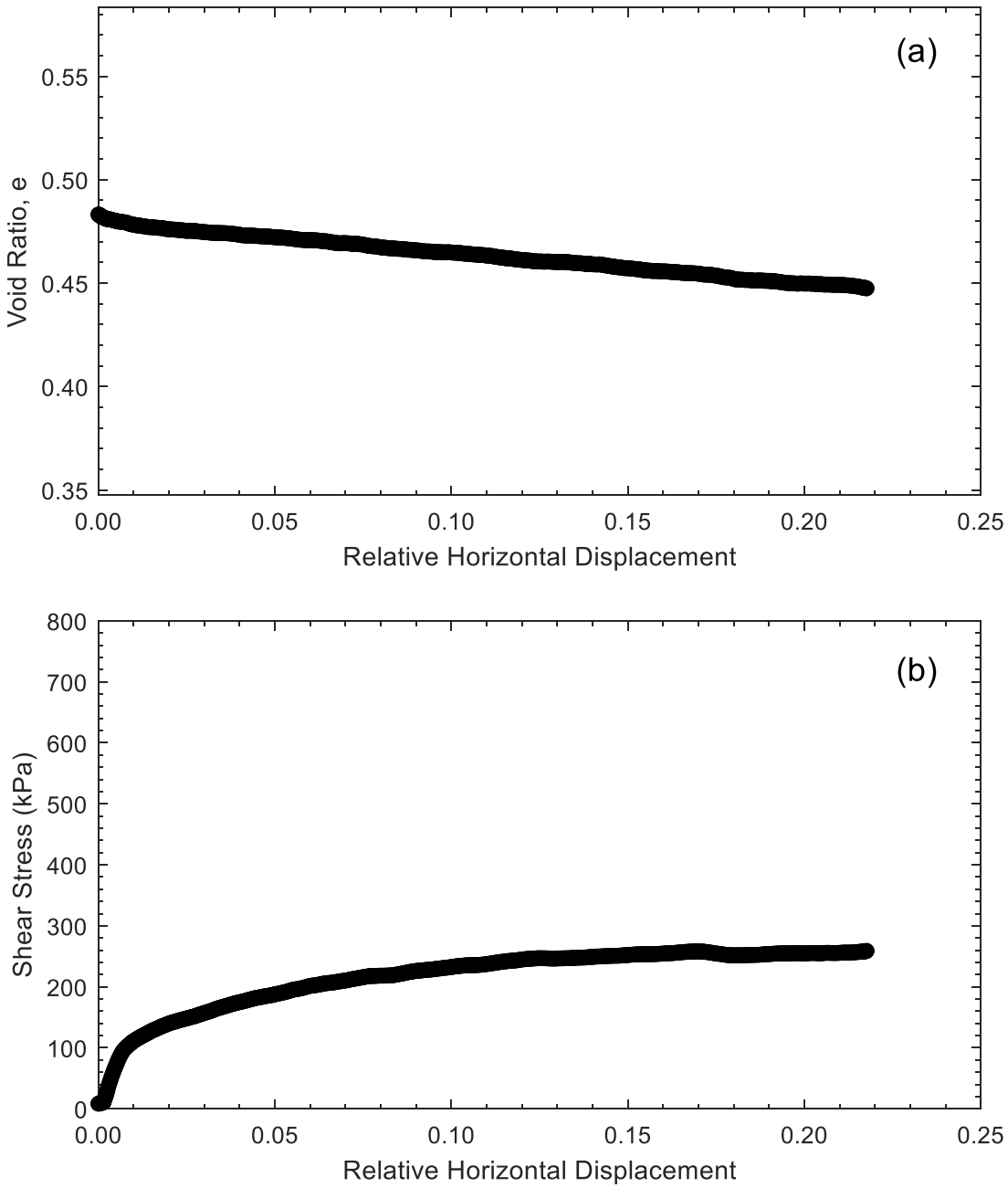

Figure E28. Direct shear test results for specimen 20B-0-dup-A at 825 kPa effective stress: (a) Void ratio, e, versus relative horizontal displacement; (b) Shear stress (kPa) versus relative horizontal displacement.

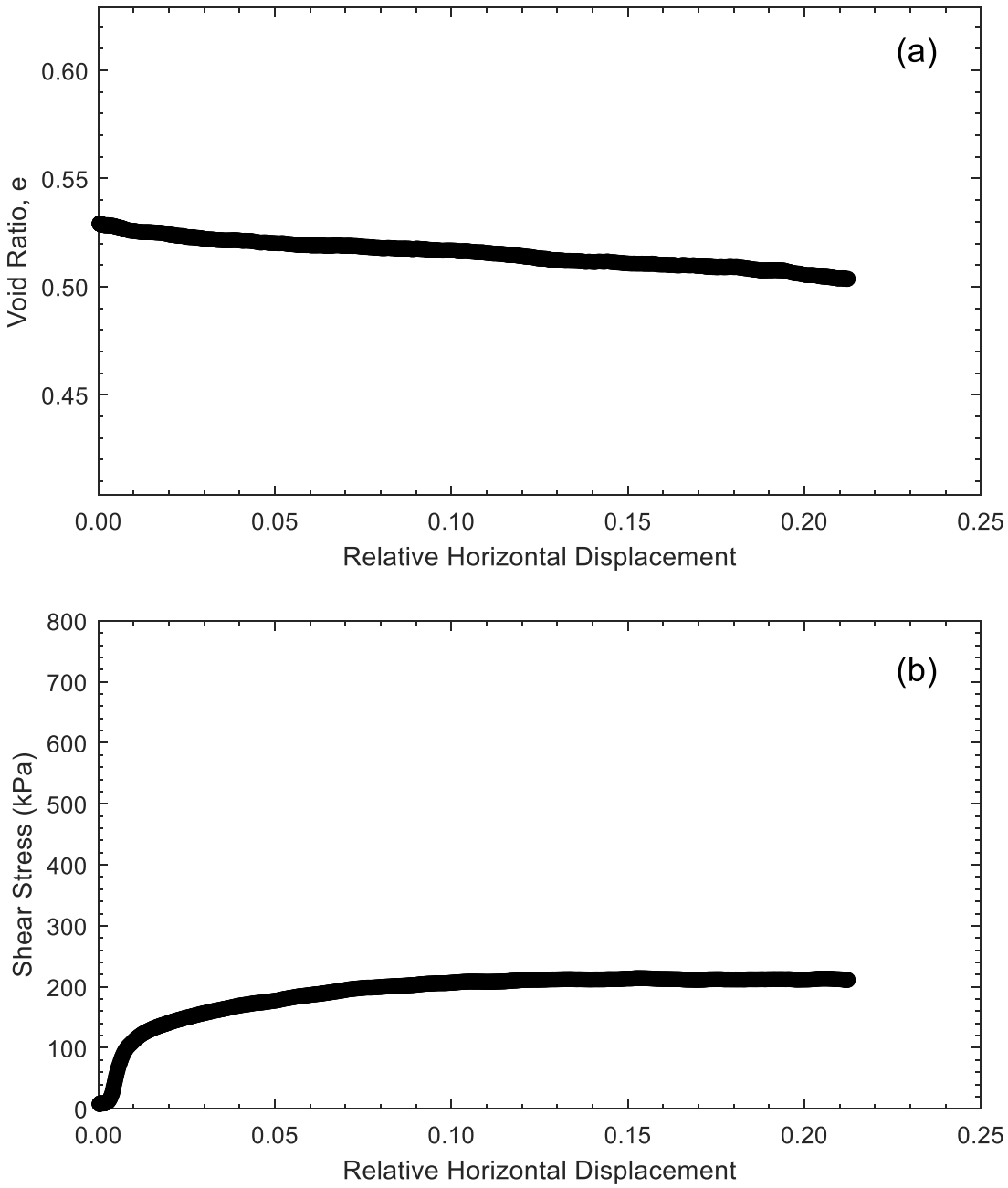

Figure E29. Direct shear test results for specimen 30B-0-A at 825 kPa effective stress: (a) Void ratio, e, versus relative horizontal displacement; (b) Shear stress (kPa) versus relative horizontal displacement.

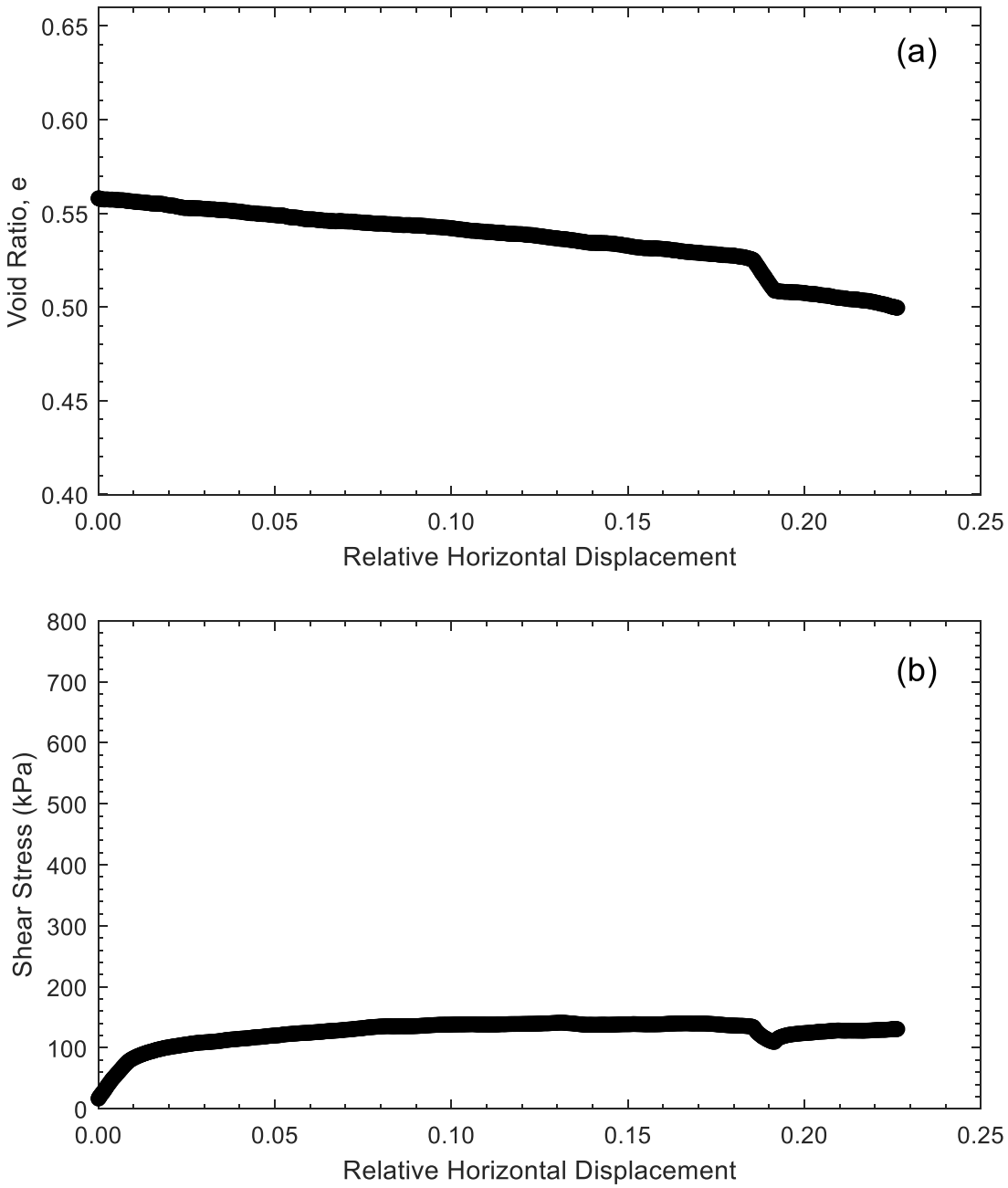

Figure E30. Direct shear test results for specimen 30B-0-dup-A at 825 kPa effective stress: (a) Void ratio, e, versus relative horizontal displacement; (b) Shear stress (kPa) versus relative horizontal displacement.